UNIVERSITÀ DEGLI STUDI DI ROMA
"LA SAPIENZA"

FACOLTÀ DI SCIENZE MATEMATICHE, FISICHE E NATURALI

A numerical approach to the kinetics of driven and cooling granular gases

Dottorato di Ricerca in Fisica
Ph.D. in Physics
XIV Ciclo – AA.AA. 1998-2001
Coordinatore: *Prof. Guido Martinelli*

Supervisor:
Prof. Angelo Vulpiani

Candidato:
Dott. Andrea Puglisi

In girum imus nocte et consumimur igni

Contents

Introduction

Granular Materials are a new frontier in Statistical Mechanics.

Being inspired to a long history of problems in engineer and industrial application, with roots in the 19th century, a large and heterogeneous family of experiments has demonstrated the richness of granular phenomenology. Moreover, the fundamental properties of granular media (mainly inelasticity of collisions and macroscopicity of grains) have motivated the born of an entire new branch of theoretical physics with its zoo of minimal models, the so-called *granular gases*, displaying an intriguing behavior in spite of their simplicity. The speculative spirit of this branch of theoretical granular physics must not be underestimated: often granular gases are very abstract models that can be observed only in the silicon cage of a computer simulation, but their importance for a substantial criticism of the basic assumptions (and limits) of Kinetic Theory, Hydrodynamics and general non-equilibrium Statistical Mechanics, is widely recognized. This thesis focuses on the particular subject of Kinetic Theory of Granular Gases and is devoted to two main tasks:

- a tentative review of recognized fundamental problems (experiments and theories);
- a study, by means of numerical and analytical tools, of some basic models.

In this introduction we give a brief presentation of granular materials and anticipate the content of the five chapters of this thesis.

What are granular materials?

A granular material is a substance made of grains, i.e. macroscopic particles with a spatial extension (average diameter) that ranges from the microns to the centimeters. In line of principle the size of grains is not limited as far as their behavior can be described by classical mechanics. For example, the physics of planetary rings (made of objects with a diameter far larger than centimeters) is sometimes approached using models of granular media. More often the term "granular" applies to industrial powders: in chemical or pharmaceutical industries the problem of mixing or separating different kinds of powders is well known; the problem of the transport of pills, seeds, concretes, etc. is also widely studied by engineers; the prevention of avalanches or the study of formation and motion of desert dunes are the subject of important studies all around the world, often involving granular theories; silos containing granular food sometimes undergo to dramatic breakages, or more often their content become irreversibly stuck in the inside, because of huge internal force chains; the problem of diffusion of fluids through densely packed granular materials (earths) is vital for the industry of natural combustibles; the study of ripples formations in the sand under shallow sea waters can solve important emergencies on many coasts of the world. Rough estimates of the losses suffered in the U.S. economy due to "granular problems" amount to ... billions of dollars a year.

The physicists usually have reduced the complexity of real situations, performing experiments to probe the fundamental behavior of granular media. The models proposed by theoretical physicists are even more idealized, in order to catch the essential ingredients of single phenomena. Therefore, in an experiment the grains are often all smooth spheres with the same size, same restitution coefficient, perfectly dry, in the void, and so on. In a numerical simulation the grains can become rods moving on a segment or disks without rotational freedom. However some ingredients are common in all the approaches to granular systems and, in some sense, can be considered the very definition (from the point of view of Physics) of the granular state of matter.

What are the basic properties of granular materials?

In the study of granular physics the properties that are usually shared by different models are the following:

- the grains are **macroscopic**: they are described by rules of classical mechanics and, moreover, the volume occupied by a grain is excluded by the volume available for the motion of all the other grains; the last property seems trivial but has many non-trivial consequences: mainly geometrical frustration, strong spatial correlations, relevance of collisional transport versus streaming transport, enhancement of re-collisions in the kinetic equations (breakdown of molecular chaos), in a

few words: a failure of mean field approximations; of course these consequences are observables when the excluded volume is a relevant percentage of the total volume, otherwise they can be neglected;

- as a consequence of macroscopicity, the grains interact (with each other as well as with the boundaries) by means of **dissipative interactions**: this means that static and dynamic friction is always at work and that collisions are inelastic; the energy lost is transferred to internal degrees of freedom, i.e. heat, and subsequently dispersed to the environment;

- the environmental thermal temperature plays no role in the dynamics of the grains, i.e. they are almost always considered at $T = 0$; this is due again to the macroscopic nature of grains and in particular to their masses, which are usually of the order of an Avogadro number of molecular masses: the kinetic or potential energy of a grain is therefore many orders of magnitude larger than the thermal energy conserved in the internal degrees of freedom; in the kinetic theory of granular gases the role of "microscopic degrees" is played by the grains themselves, so that a **granular temperature** can be introduced in terms of the random motion of grains.

What are the open problems in the physics of granular materials?

It is useful to stress here the existence of a main division between two different "states" in which the granular materials can be, depending upon the external conditions (available volume, intensity of the driving, degree of inelasticity of the collisions, presence of fluids, and so on):

- Stable or metastable granular systems: this family of problems comprehends the study of the distribution and the analysis of correlations in the internal forces in a pile or silo of grains, the characterization of the propagation of mechanical perturbations (sound) inside densely packed arrays of grains, the very slow compaction dynamics observed when a box full of grains is vibrated (the grains can rest in a metastable state, in the absence of vibration, which is far from the minimum packing fraction attainable), the study of time and size distributions of avalanches in a pile which has reached its critical slope.

- Flowing granular systems: this set of problems is instead composed of all the situations where an uninterrupted flow is present. Typically granular flows are divided in slow dense flows and rapid dilute flows. When the stationary velocity of the flow increases (due to an increase of external driving forces) the shear work induced by internal friction generates granular temperature and granular pressure, which in exchange produces a decrease of volume fraction occupied by grains [52]. This ensures that, almost always, a rapid flow is also dilute and that theoretical methods belonging to kinetic theory, as well as a hydrodynamic description, can be tried and are sometimes successful. Every kind of typical fluid experiment has been performed on granular systems: from Couette cells to inclined channels to rotating drums, finding non-linear constitutive relations. High amplitude vibrations can generate interesting convection phenomena in a box containing grains, always associated to size and density segregation (apparently violating entropic principles). Patterns (two dimensional standing waves) can form on the free surface of a vibrated granular layer. The study of simulated models have arisen new questions on the constitutive behavior in rapid flows, and recently new experiments have focused on this subject, measuring the velocity probability distribution functions and finding that in a wide set of situations this distribution is not Gaussian. The study of internal stress fluctuations and of velocity structure factors has given further elements to the investigation of kinetics of granular flows. A strong debate is still alive, on the limits of application of hydrodynamic formalism (and on the possibility of its derivation through kinetic theory).

What are granular gases?

In a word, they are "ideal" inelastic gases. The paradigm of inelastic gases is the gas of **smooth hard spheres** with restitution coefficient $r < 1$. They are often considered in two and even in one

dimension. It could be said that a simple change in a parameter (r, from $r = 1$ to $r < 1$) has awakened again the interest in hard spheres gases, which were deeply investigated in their elastic form in the 60's and 70's. The interest on granular gases is born from the necessity of probing granular kinetics theories elaborated in the 80's (for a review see [52]): this program was begun by means of simple simulations (the first simulation of granular materials are described in [52]). As long as new phenomena were observed (clustering [96], inelastic collapse [157], breakdown of equipartition [77], and so on) the interest increased and a better and better formalization of the theory was achieved.

The attention has been initially directed toward **cooling** granular gases, that is inelastic gases without external energy sources. A cooling granular gas starts from an initial state which is usually homogeneous in density and has some kind of distribution of velocities (for example Gaussian). After a number of collisions of the order of the size (number of particles) of the system, the effects of inelasticity begin to appear: the total kinetic energy (that, if calculated in the center of mass frame, is equivalent to the global granular temperature) decreases as an inverse power of the time $E(t) \sim t^{-2}$ and the distribution of velocities, even if scaled with its variance, is no more the initial distribution. After some time, if the system is large enough, velocity correlations start to appear: in fact two particles exit from an inelastic collision with a reduction of their relative velocity in the direction perpendicular to their distance, i.e. they travel more parallel than before the collision. This velocity correlations appear, for example, as vortices. When this happens the decay of the energy with time changes, in particular the energy decays more slowly, because collisions among such correlated particles dissipate less energy. Furtherly, some time later, correlations in the density emerge, the particles clusterize and the energy decay changes again. A numerical study of these late stages of the cooling gas evolution usually requires good resources and optimization of the algorithms (these instabilities appear at large scale and at late times, furtherly the aging of the system prevents from accumulating statistics over time), but also special regularizations for the collision rules: in a cluster of particles, in fact, the time between collisions may reduce to zero (numerical zero), that is the collision rate may diverge. This situation is known as *inelastic collapse* and usually prevents the simulation from going on. A restitution coefficient that depends on the relative velocity of the colliding particles is commonly used to circumvent the problem.

After the seminal paper of Du, Li, and Kadanoff [77], part of the effort has been devoted to understand the problem of **driven** granular gases. Different models have been proposed, in order to reproduce realistic situations. The driving can be in-homogeneous, for example a vibrating wall, leading to an in-homogeneous stationary state, or otherwise homogeneous, for example a vibrating plate under the layer of grains. A good success has been obtained by a class of idealized driven models, usually referred to as *homogeneously heated* granular gases: the velocities of the particles are periodically "kicked" by a random amount. A debate exists on the necessity of introducing also a systematic friction proportional to the velocities of the particle. If the friction is considered, the model can be modeled in terms of a Langevin equation for the velocity of each particle with the addition of inelastic collisions. The friction term regularizes the evolution of the system, which otherwise would present undesirable phenomena (very large fluctuations of the total momentum and, depending on the dimensionality, also an increase of total kinetic energy). The numerical and analytical study of homogeneously heated granular gases have demonstrated that the stationary granular state is usually very different from that of an ideal gas, with non-Gaussian distribution of velocities and stationary spatial correlations. These features have been recently confirmed by experiments which are reasonable realizations of the model (for example spheres traveling on the surface of a rapidly vibrating plate, considering only horizontal velocities).

What is the content of this thesis?

This thesis consists of a review of existing experiments and theories (Chapter 1, Chapter 2 and first section of Chapter 5), and of a presentation of results obtained by the author with his coworkers.

We anticipate that we have devoted a part of the review work (Chapter 2) to a very concise summary of kinetic theory, with the ambition of offering a survey of the logical path from the Newton laws of mechanics to the Navier-Stokes-like hydrodynamic theories, giving in parallel the "granular" (inelastic) version of the theory. This give us the possibility to stress the assumptions underlying the theories

of ordinary fluids, in order to better evaluate the limits of existing granular kinetic and hydrodynamic models.

This thesis is organized as follows:

- The **First Chapter** concerns recent experiments on granular matter. It focuses on the difference between granular statics (or quasi-statics) and granular dynamics. In particular many experimental results on the rapid flow of dilute granular systems are reviewed.

- The **Second Chapter**, as already stated, contains a review of kinetic theory of standard fluids and a comparison with the kinetic theory of granular fluids. It begins with a discussion of different binary interactions (central potentials, hard spheres, Maxwell molecules, inelasticity) and statistical tools (mean free path or time and differential cross section). The standard derivation of kinetic Boltzmann equation from Liouville equation follows, with a discussion of the H-theorem, of ring kinetics theories (for dense systems), Enskog corrections and of granular kinetic "Boltzmann" or "Boltzmann-Enskog" equations. The hydrodynamic limit is taken in the third section of the chapter, reviewing the Chapman-Enskog expansion and the Grad method of moments, obtaining general equations for the time evolution of conserved quantities (density, moment and energy) and showing the approximations needed to come to the well-known Navier-Stokes equations. A presentation of granular hydrodynamic theories (from the 80's first theories to the most recent ones) comes after, followed, in the last section, by a discussion of the main criticisms to these theories and their basic assumptions.

- The **Third Chapter** is devoted to the study of the Randomly Driven Granular Gas (or Homogeneously Heated Granular Gas) with friction, a model that we have introduced [183] and investigated. We have collected results from simulations and analysis of toy models [184]. The model has two parameters (the restitution coefficient and the ratio between collision time and heating time). In some particular limits the model reproduces the properties of an ideal gases, but in general it shows a more complex behavior: the velocity distributions are non-Gaussian and the particle clusterize in fractal stationary structures.

- The **Fourth Chapter** discusses non-homogeneous driving in the presence of gravity. Two model have been proposed [15] in order to reproduce typical experimental situations: the grains rolling on an inclined plane with a vibrating bottom side, and the grains rolling down an inclined channel with rough bottom. The profiles of coarse-grained fields (density, velocity, temperature) agree with the experiments, as well as the distribution of velocities and the density correlations. A solvable hydrodynamic theory is presented and the problems related to the boundary conditions are discussed.

- The **Fifth Chapter** is devoted to the study of cooling granular gases and in particular focuses on the velocity distributions and on the emergence of velocity correlations. This chapter takes into account three different models: a very simplified mean field kinetic model (an inelastic version of the Maxwell molecules) called pseudo-Maxwell model, the $1D$ gas of inelastic hard spheres, and finally a $1D$ and $2D$ lattice gas model wit inelastic interactions among sites. The study of the pseudo-Maxwell model has led to the discovery of an exact stationary solution of the kinetic equation in $1D$, which in turn appears to be very *different* from the velocity distribution observed in the simulations of inelastic hard spheres. The study of the lattice gas model instead is capable of reproduce some of the main features of the inelastic hard spheres, in the homogeneous as well as in the velocity-correlated regimes.

- The **Appendix A** concerns the Direct Simulation Monte Carlo algorithm (due to Bird [30]) which is used in many simulations in Chapter 3 and Chapter 4. The **Appendix B** contains the numerical coefficients needed in the granular hydrodynamics as formulated by Brey et al. [39].

Chapter 1

Experiments on granular materials

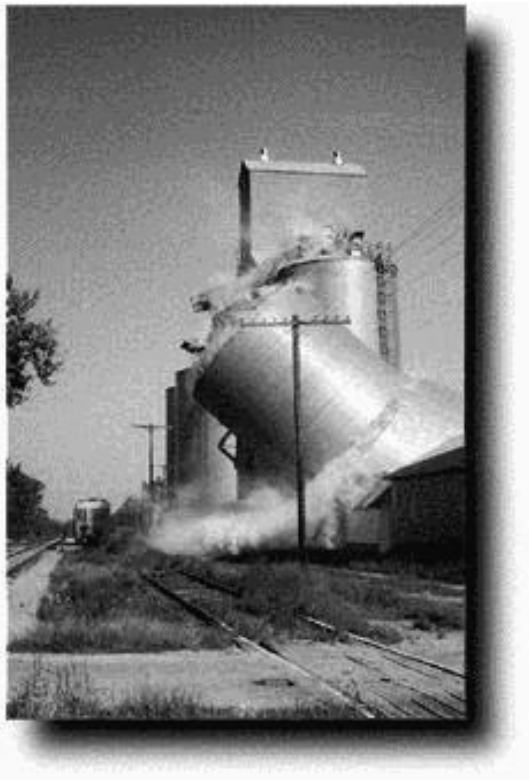

Even if the initial motivation for the study of granular materials was the large number of problems encountered in industrial processes, the experimental approach to the granular state has not been reduced to a mere reproduction of applicative situations: the strong theoretical questions arisen in the last two decades have guided the experiments toward more refined and often simpler, more essential, set-ups which could shed light on new fundamental mechanisms. Numerical work has been invaluable as a source of new problems and interesting questions (for example molecular dynamics simulations of diluted granulars systems have stimulated the measurement of velocity distributions, predicting a non-Maxwellian behavior), while at the same time some phenomena observed in experiments have led to the birth of new theoretical paradigms (e.g. sand-pile avalanches have inspired the debate on *self organized criticality*).

For a long time the term *granular materials* has designed anything similar to sand, so that in all workshops and conferences this subject was treated as a coherent field of study with its coherent scientific community and its coherent set of questions and possible answers. This was not true and it is now recognized: there is nothing like a Universal Granular Behavior, there is probably nothing similar to a Granular Equation of State and, above all, the mechanisms that must be taken into account in order to explain *some* typical granular phenomena are often useless in the study of *other* typical granular phenomena. This means that the study and the modeling of internal stress propagation in grain silos is of little help for the investigation of surface waves or for the pattern formation in rotating drums, as well as the hydrodynamic description of dilute and quasi-elastic granular flows cannot work in more dense and inelastic situations (this fact can be less obvious). As a consequence of this, it has grown the necessity of more specialized workshops and of a better definition of granular sub-topics. One important example has been the large increase of interest in the physics of **Granular Gases** [182], i.e. assemblies of grains in dilute packing, characterized by the high ratio between the number of binary interactions (inelastic collisions) and that of non-binary interactions (frequent in more dense situations). Many new phenomena in this context (cluster and shear instabilities, non-Maxwellian velocities, and much more) have made their first appearance in computer simulations and then have been observed in real experiments. It must be finally underlined that also a too specialistic approach can be dangerous. An essential feature of granular systems is the strong enhancement of fluctuations and therefore their non-equilibrium character: this means for example that, even in a dilute experimental set-up, regions with very high density can appear, leading to a dramatic failure of the assumption of "gas-like" behavior.

In the first section we review a number of real and numerical experiments performed on granulars that come to rest in a metastable equilibrium, e.g. studies on the Janssen effect and on the distribution of internal stresses, measures of the slow compaction under vibration and finally observation of avalanches in sand piles. The second section focuses on experiments concerning the fundamental physics of granular flows, taking into account systems subject to different kinds of external driving: shear (by means of Couette rheometers, inclined channel and so on), vibration and air fluidizing are the most common setups used to study granular dynamics.

1.1 Metastable granular materials

In this section we briefly review some of the experiments performed with granular materials which come to rest (in a metastable equilibrium) for a variable fraction of the whole experimental time. The study of internal stresses in grain silos requires that the material is always at rest. The study of compaction requires some form of periodic excitation (i.e. tapping from the bottom) and subsequent rest. The study of sandpiles, finally, can be performed in almost continuously driven granular materials, but the definition of *avalanche* requires a (possibly very brief) interruption of the flow.

1.1.1 Janssen effect and the distribution of internal stresses

In 1895 H. A. Janssen [118] discovered that in a vertical cylinder the pressure measured at the bottom does not depend upon the height of the filling, i.e. it does not follow the Stevin law which is valid for Newtonian fluids at rest [137]:

$$p_v(h) = \rho g h \tag{1.1}$$

where p_v is the vertical pressure, ρ the density of the fluid, g the gravity acceleration and h the height of the column of fluid above the level of measurement. The pressure in the granular material follows instead a different law, which accounts for saturation:

$$p_v(h) = \Lambda\rho g - (\Lambda\rho g - p_v(0))\exp(-h/\Lambda) \tag{1.2}$$

where Λ is of the order of the radius R of the cylinder. This guarantees the flow rate in a hourglass to be constant. Moreover, this law is very important in the framework of silos building, as the difference between ordinary hydrostatic and granular hydrostatic is mainly due to the presence of anomalous side pressure, i.e. force exerted against the walls of the cylinder. It happens that the use of a fluid-like estimate of the horizontal and vertical pressure leads to an underestimating of the side pressure and, consequently, to unexpected (and dramatic) explosions of silos [128].

The first interpretation of the law has been given by Janssen in his paper, in terms of a simplified model with the following assumptions:

1. The vertical pressure p_v is constant in the horizontal plane.
2. The horizontal pressure p_h is proportional to the vertical pressure p_v where $K = p_h/p_v$ is constant in space.
3. The wall friction $f = \mu p_h$ (where μ is the static friction coefficient) sustains the vertical load at contact with the wall.
4. The density ρ of the material is constant over all depths.

In particular the first assumption is not true (the pressure depends also upon the distance from the central axis of the cylinder) but is not essential in this model (as it is formulated as a one-dimensional problem), while the second assumption should be obtained by means of constitutive relations, i.e. it requires a microscopic justification.

Imposing the mechanical equilibrium of a disk of granular material of height dh and radius R (the radius of the container) the following equation is obtained:

$$\pi R^2 \frac{dp_v}{dh} dh + 2\pi R\mu K p_v dh = \pi R^2 \rho g dh \tag{1.3}$$

which becomes:

$$\frac{dp_v}{dh} + \frac{p_v}{\Lambda} = \rho g \tag{1.4}$$

where $\Lambda = \frac{R}{2\mu K}$. This equation is exactly solved by the function (1.2).

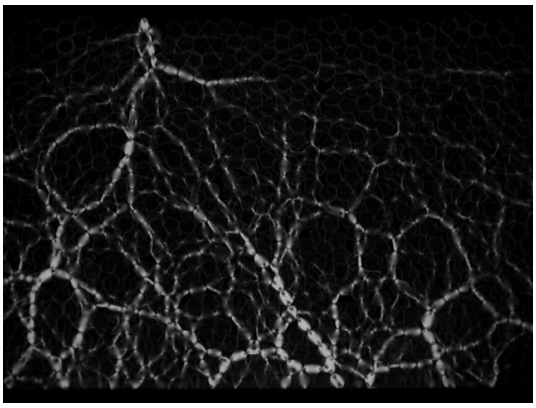

Figure 1.1: Force chains generated after a localized (on top) perturbation

The particular behavior of the vertical pressure in granular materials is mainly due to the anomalies in the *stress propagation*. The configuration of the grains in the container is random and the weight can be sustained in many different ways: every grain discharges its load to other grains underlying it or at its sides, creating big arches and therefore propagating the stress in unexpected directions. Moreover, arching is not only a source of randomness, but also of strong fluctuations, i.e. disorder: in a granular assembly some force chains can be very long and span the size of the entire system, posing doubts on the validity of (local) mean field modeling.

Further interesting phenomena have been experimentally observed in the statics of granular materials:

- the fluctuations of the pressure at the bottom of a silo are large, they can change of more than 20% in repeated pouring of grains in the same container [48], and in a single pouring the distribution of stresses, measured deep inside or at the bottom of the silo, show an exponential tail [141, 168, 46].
- the vertical pressure below conical sandpiles does not follow the height of the material, but rather has a *minimum* underneath the apex of the pile [217]

Different models have been proposed and debated in the last years, in order to understand the problem of the distribution of forces in a silo or in a granular heap.

The *q-model* has been introduced in 1995 (remarkably a century after the work of Janssen) by Liu et al. [141, 66] in order to reproduce the stress probability distribution observed in experiments. The model consists of a regular lattice of sites each with a particle of mass unity. Each site i in layer D is connected to exactly N sites j in layer $D+1$. Only the vertical components of the forces $w = \sigma_{zz}$ are considered explicitly: a random fraction $q_{ij}(D)$ of the total weight supported by particle i in layer D is transmitted to particle j in layer $D+1$. Thus the weight supported by the particle in layer D at the i-th site, $w(D,i)$, satisfies a stochastic equation:

$$w(D+1,j) = 1 + \sum_i q_{ij}(D) w(D,i) \tag{1.5}$$

The random variables $q_{ij}(D)$ are taken independent except for the constraint

$$\sum_j q_{ij} = 1 \tag{1.6}$$

which enforces the condition of force balance on each particle. Given a distribution of q's, it can be obtained the probability distribution $Q_D(w)$ of finding a site that bears a weight w on layer D. By means of mean field calculations, exact calculations and numerical solutions, the authors conclude that (apart of some limiting cases) a generic continuous distributions of q's lead to a distribution of weights

that, normalized to the mean, is independent of depth at large D and which decays exponentially at large weights. They find also a good agreement with molecular dynamics simulations of the packing of hard spheres. The q-model has many limits:

- it is a scalar model, i.e. it takes into account only one component of the internal stress (this was solved by P. G. de Gennes [72] who introduced a vectorial version of the q-model, obtaining a more realistic propagation of forces)
- it does not reproduce the minimum (the "dip") of the pressure measured under central axis at the bottom of a sand heap
- it does not reproduce the Janssen law [154]; this problem appears as a consequence of the diffusive nature of the q-model solution: the saturation depth D_s where the stress distribution becomes independent of depth scales with the silo width R as $D_s \sim R^2$, at odds with the Janssen observation that predicts $D_s \equiv \Lambda \sim R$.

A more refined version of the Janssen model has been introduced by Bouchaud et al. [36]: the authors have considered a local version of the Janssen assumption on the proportionality between horizontal and vertical stresses:

$$\sigma_{xx} = k\sigma_{zz} \tag{1.7a}$$
$$\sigma_{yy} = k\sigma_{zz} \tag{1.7b}$$
$$\sigma_{xy} = 0 \tag{1.7c}$$

which lead to the linear equation:

$$\frac{\partial^2 \sigma_{zz}}{\partial z^2} - k\left(\frac{\partial^2}{\partial x^2} + \frac{\partial^2}{\partial y^2}\right)\sigma_z z = 0 \tag{1.8}$$

This equation for the vertical stress is hyperbolic and therefore differs from the equivalent equation for an elastic medium, which is elliptic [136], and from the q-model equation that is parabolic (as a diffusion equation): it is equivalent to the equation for the wave propagation with z as the "time" variable and k as the inverse of the propagation velocity. This model well reproduces the dip in the measure of the pressure under the bottom of the conical heap [217]. A cellular automaton was introduced by Hemmingsson [106] which was capable of reproduce the dip under the heap as well as the correct Janssen law (with the linear scaling).

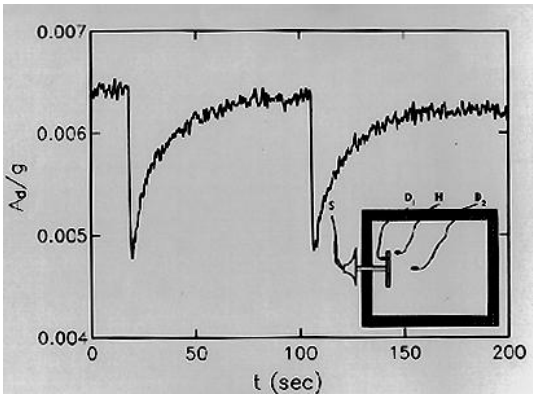

Figure 1.2: Propagation of sound

In the framework of the study of force networks in the bulk of a static arrangement of grains a key role was played by the experiments on the **propagation of sound**. The inhomogeneities present

inside a granular medium can drastically change the propagation of mechanical perturbations. Liu and Nagel [139, 140, 138] have addressed this issue in several experiments. They have discovered [139] that the in the bulk of a granular medium perturbed by a harmonic force (4 Hz) the fluctuations could be very large, measuring power-law spectra of the kind $1/f^{\alpha}$ with $\alpha = 2.2 \pm 0.05$. Then they have seen [140] that the sound group velocity can reach 5 times the phase velocity and that a change in the amplitude of vibration can result in a hysteretic behavior (due to a rearrangement of force chains). They have also measured [138] a 25% variation of the sound transmission as a consequence of a very small (compared to the size of the grains) thermal expansion of a little carbon resistor substituted to a grain of the granular medium. This sensitivity to perturbation is another signature of the strong disorder (arching and chain forces) in the bulk of the medium.

1.1.2 Vibration induced compaction and glassy granular systems

Another frontier of the experimental granular physics is the problem of *vibration induced compaction*: the granular material poured in a container (for example a simple box) quickly reaches the equilibrium, i.e. the balance of all internal and external forces. At that point one can measure the volume fraction, or packing fraction, i.e. the ratio:

$$\phi = \frac{\sum_i V_i}{V_{box}} \tag{1.9}$$

where the V_i are the volumes of the grains and V_{box} is the volume of the container measured up to the maximum (or average) height reached by the material. The packing fraction measured [174] at the end of the filling, for spheres, has been estimated to be bounded by the limiting values $\phi_{min} = 0.55$ and $\phi_{max} = 0.64$. After the initial filling, some external force, i.e. a vibration, can change the arrangement of grains and therefore its volume fraction, usually increasing it. S. F. Edwards and A. Mehta [160, 64] have proposed a new formalism that resembles thermodynamics and that describes the evolution of a granular system subject to slow vibration: in this formalism the energy is the occupied volume V and the Hamiltonian is a functional W that gives the occupied volume if applied to a certain configuration (spatial positions) of the grains. The granular system is assumed to evolve through states of equilibrium (in this new thermodynamics). The entropy S is defined as the logarithm of the number of possible configurations with the same occupied volume V, while the temperature is substituted by the "compactivity" X which is defined as

$$X = \frac{\partial V}{\partial S} \tag{1.10}$$

With this formalism, Barker and Mehta [17] have shown that the relaxation of the volume fraction in response to a continuous sequence of vibrations is fast exponential with two relaxation times associated with collective and individual modes. Another mechanism has been proposed to describe the vibration-induced compaction: in this theory the motion of the voids filling the space between the particles is effectively diffusive and as a result a power-law relaxation is predicted [55, 111].

The careful experiment of Knight et al. [126] demonstrated that the vibration-induced compaction (in a tube subject to tapping followed by long pauses) is governed by a logarithmically slow relaxation (see Fig. 1.3 on the facing page):

$$\phi(t) = \phi_f - \frac{\Delta\phi_\infty}{1 + B\ln(1 + t/\tau)} \tag{1.11}$$

where the parameters ϕ_f, $\Delta\phi_\infty$, B and τ depend only on the acceleration parameter Γ that is the ratio between the peak acceleration of a tap and the gravity acceleration g. The discover of this inverse logarithmic behavior (very slow with respect to previous predictions) has motivated the introduction of new models and has also attracted the interest of specialists of other fields: in particular the slow relaxation is a typical phenomenon observed in glassy states of matter, e.g. the aging in amorphous solids like glasses.

E. Ben-Naim et al. [23] have explained the slow relaxation law (1.11) in terms of a simple stochastic adsorption-desorption process: the desorption process is unrestricted and happens with a well defined

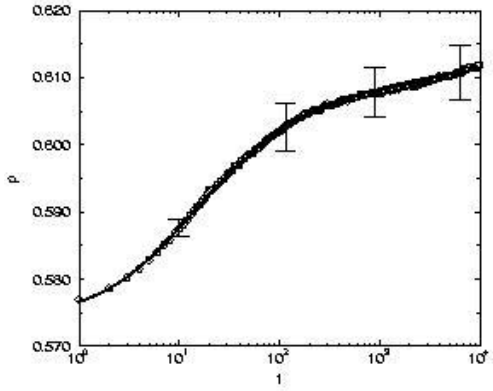

Figure 1.3: Slow Compaction: the packing fraction vs. time (in units of taps)

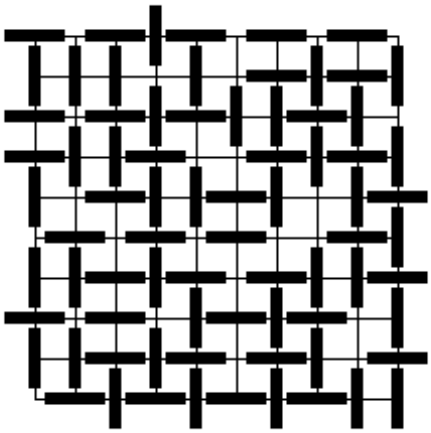

Figure 1.4: An example configuration of the Tetris-model

rate, while the adsorption process is restricted by the occupied volume, i.e. new particles cannot be adsorbed on top of previously adsorbed particles. This model has been also called *car parking model*, as it reproduces the increasing difficulty of parking a car in a parking lot as the number of parked cars get larger and larger. The inverse logarithmic law has been recovered solving this model.

Another way, perhaps more realistic, of recovering the inverse logarithmic relaxation, is described by Caglioti et al. [50, 49] by means of a "Tetris-like" model (displayed in Fig. 1.4 on the page before). In this model the grains are represented by objects disposed on a regular lattice: the different shapes of the objects induce geometrical frustration, i.e. some kinds of grains cannot stay near some other kinds of grains and therefore the equilibrium configuration of a filled box is disordered and present a random packing fraction: a computer simulation of the vibration dynamics (short periods of tapping followed by long periods of undriven rearrangement until the new equilibrium is reached) shows that this model reproduces the inverse logarithmic relaxation. The study of this model has shed light on many features of the dynamics of dense granular media, such as vibration-induced segregation, bubbling and avalanches. Moreover, the possibility of mapping the dynamics of the Tetris model onto that of a Ising-like spin system with vacancies has introduced a new bridge between the physics of granular media and that of disordered systems (like spin glasses and structural glasses). In particular the interest of researchers has focused on the following remarkable fact: spin glass models [164, 28] (such as the Sherrington- Kirkpatrick [200] model or the Edwards-Anderson model [78]) always contain a quenched (frozen) disorder, usually given by the set of J's that weight the interactions among spins. A dense granular media evolve without any frozen disorder, nevertheless its dynamics presents many "glassy" features (such as history dependence of the dynamics, hysteresis, frustration, metastable equilibria and so on) [170, 18]. This consideration is at the base of all the recent studies on spin lattice models *without* quenched disorder. It must be said that many of these models have little in common with the real granular materials and are often more useful tools in the study of the behavior of spin or structural glasses.

1.1.3 Sandpiles

When sand is added on the top of a sand heap (also known as sandpile problem) two phenomena are observed:

- the slope of the pile grows (with little flowing of sand on it) until a critical angle is reached; after that (if sand is still poured on the top) the slope stays almost constant and the sand flows along it;
- at the critical angle the flowing of sand is made of "avalanches" of different sizes and durations;

Starting from this qualitative observation, P. Bak et al. [9, 10] have introduced a cellular automaton model (see Fig. 1.5 on the facing page) where each site (for example in two dimensions (i, j)) of the lattice has associated a slope $z(i, j)$. If the slope exceeds a critical value z_c a rearrangement of the neighboring sites is performed, e.g. 4 is subtracted to the exceeded value and 1 is added to its 4 neighboring sites. The automaton may be executed in two different ways:

1. the field at time 0 has an average slope greater than z_c, and the system evolves freely;
2. the field at time 0 is everywhere equal to zero and at every step a randomly chosen site is incremented;

In both cases the systems reaches a stable configuration corresponding to the critical slope: every successive perturbation (i.e. increasing the field on some site) generates an avalanche that involves the rearrangement of a certain number of sites of the lattice. The authors show that the distribution of the extension of the avalanche follows a power law:

$$D(s) \sim s^{-\tau} \tag{1.12}$$

with $\tau \simeq 0.98$ for three or four logarithmic decades. In another work [206] the same authors define and study a set of critical exponents similar to those used in statistical mechanics of phase transitions.

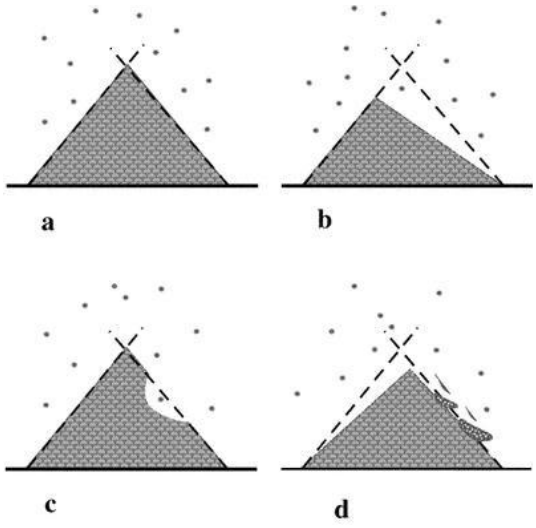

Figure 1.5: Possible configurations of a sandpile

The novelty of the work of Bak and coworkers is represented by the fact that a model was found that showed a critical behavior (i.e. power law relaxations, correlations at all sizes) without any fine tuning of the external parameter, whereas usual critical phase transitions need a precise tuning of the temperature to the critical temperature T_c. This self-organized critical behavior was intriguing as it seemed to be a key concept to understand the ubiquity of power laws in nature (e.g. $1/f$ noise, self-similar structures like fractals, turbulence and so on). The sandpile model is still studied, with all its variants (for a review see for example [101])), but it has been recognized to be not a good paradigm for the self-organized criticality: it was seen in fact [201, 216] that the driving rate (i.e. the rate of falling of grains on the top of the pile) acts exactly as a control parameter that has to be fine tuned to zero in order to observe criticality. However many important issues are still open: the interplay between the self-organization into a stationary state and the dynamical developing of correlations, the (numerical) measure of critical exponents, universality classes, upper critical dimensions and so on.

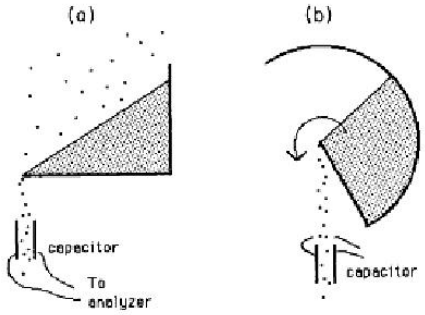

Figure 1.6: The experiment of Nagel and coworkers to measure avalanches in sandpiles

More remarkably, it has been pointed out that the sandpile model has little to do with sand (and granular matter) in general. In 1992 Nagel has published [169] the results of a series of experiments on sand in order to verify the predictions of Bak and coworkers. He has initially shown the difficulty of performing an exactly constant rate in the pouring of grains from above the top of a pile. Therefore he has introduced a different kind of experiment (see Fig. 1.6), where the sand fills partially a rotating drum: the constant angular velocity of the drum guarantees the constant driving needed to reach the critical slope and the avalanche regime. The statistical analysis of the avalanches has clearly

demonstrated that sand does not reproduce the critical behavior expected in self-organized criticality. The sandpile has *two* critical slopes: Θ_r is the rest angle (when the slope is less than Θ_r the pile is stable), Θ_m is maximum angle (when the slope is larger than Θ_m avalanches form and reduce the slope to an angle less than Θ_r). If the slope is comprised in between Θ_r and Θ_m there is *bistability*, i.e. the sand can rest or can produce avalanches, based on its previous history. The avalanches have a typical duration and the hysteretic cycle between the two angles has a well defined average frequency. No power laws have been observed.

1.2 Granular flows

In this section we review the typical experimental setups used in the investigation of the properties of flowing granular materials. We have chosen a subjective classification, whereas some setup could fall in a class as well as in another. Moreover, some phenomena (such as segregation or clustering) may be observed in more than one kind of setup.

1.2.1 *Slow* vs. *rapid* granular flows

If the motion of granular material occurs slowly, particles will stay in contact and interact frictionally with their neighbors over long periods of time. This is the "quasi-static" regime of granular flow and has been classically studied using modified plasticity models [21, 20, 34] based on a Coulomb friction criterion [68, 69].

At the other extreme is the rapid-flow regime which corresponds to high-speed flows [193, 52]. Instead of moving in many-particle blocks, each particle moves freely and "independently". In the rapid-flow regime, the velocity of each particle may be decomposed into a sum of the mean velocity of the bulk material and an apparently random component to describe the motion of the particle relative to the mean. The analogy between the random motion of the granular particles and the thermal motion of molecules in the kinetic-theory picture of gases is so strong that the mean-square value of the random velocities is commonly referred to as the "granular temperature" - a term first used by Ogawa [171]. As pointed out in the introduction, however, granular temperature has nothing to do with environmental thermal temperature, which usually plays no role in the dynamics of granular flows. Nevertheless, using this kinetic analogy, granular temperature generates pressure and governs the internal transport rates of mass, momentum and energy. Thus, while the term temperature sometimes leads to some semantical confusion for the uninitiated, the physical analogy between the two temperatures is so apt that its use has become standard throughout the field.

1.2.2 Couette cylinders

The first tentatives of studying granular media under the point of view of rheology, i.e. transport properties (discussed in more detail in section 2.4) have been performed using typical shear experiments used to probe ordinary fluids. In particular the Couette geometry has been largely used and is still now an important tool of investigation.

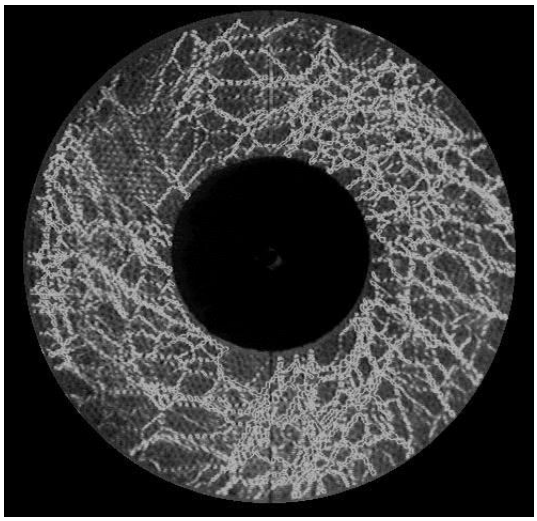

Figure 1.7: The experiment of Mueth and coworkers on a Couette cylinder: the paths of the internal forces are evidenced by means of non-invasive X-ray imaging

Even if there were earlier important experimental studies on the flow properties of granular materials (mainly initiated by Hagen [104] and Reynolds [187]), the modern pioneering work on the constitutive behavior of rapid granular flows was Bagnold's experimental study [8] of wax spheres, suspended in a glycerin-water-alcohol mixture and sheared in a coaxial cylinder rheometer (Couette experiment). His main finding was a constitutive relation between internal stresses and shear rate:

$$\mathcal{T}_{ij} = \rho_p \sigma^2 \gamma^2 \mathcal{G}_{ij}(n) \tag{1.13}$$

with ρ_p the particle density, σ the particle radius, γ the shear rate and $\mathcal{G}_{ij}$ a tensor-valued function of the solid fraction ϕ. This relation has been confirmed in shear-cell experiments with both wet or dry mixtures by Craig et al. [70], Hanes et al. [105], Savage et al. [195], and in many computer simulations [53, 54, 221].

Bagnold measured not only shear stresses (i.e. transversal components, say $i \neq j$ in $\mathcal{T}_{ij}$), but also normal stress ($i = j$), that is the analogous of pressure in gas kinetics: he referred to them as "dispersive stresses" as they tend to cause dilation of the material.

More recent experiments have focused on different phenomena observed in the Couette rheometer:

- **Fluctuations of stresses:** already in the experiments of Savage and Sayed [195] large fluctuations of internal (normal) stresses were observed; more recently Howell and Behringer [113] have seen that in a 2D Couette experiment the mean internal stress follows a continuous transition when the packing fraction of the granular material changes and passes through a critical value $\phi_c = 0.776$: when the packing fraction is above the critical threshold the material shows strong fluctuations of internal stress, while under the threshold the stresses are averagely zero and the system is highly compressible.

- **3d experiments:** Mueth et al. [167] have studied the formation of microstructures in the dense shearing regime in a 3D Couette rheometer, using non-invasive imaging by X-Ray microtomography (see Fig. 1.7 on the preceding page); they have found that the velocity parallel to the shear direction decays more rapidly than linear (from exponential to Gaussian-like decay, depending upon the regularity of the grains). A similar strong decay of the flow with the distance from the moving wall was observed in many experiments, for example recently by Losert et al. [145]

- **Diluted (air-fluidized) shear:** Losert et al. [143] have performed a Couette experiment with a flow of air coming from the bottom of the cylinder, in order to fluidize the material and obtaining smoother profiles. They have put in relation the RMS fluctuations of velocity and the shear forces, observing that $T^{1/2}(y) \sim \gamma(y)^\alpha$ with $\alpha = \simeq 0.4$, and suggesting a phenomenological model that explains the shear velocity profiles.

- **Size segregation:** Khosropour et al. [123] have observed convection patterns and size segregation in a Couette flow with spherical glass beads; they also checked the effect of interstitial fluids finding it irrelevant.

- **Planetary rings:** planetary rings (those of Saturn for example) have been sometime studied in the framework of granular rheology, whereas the "geometry" of the planetary experiment is similar to a Couette cell (grains are circularly sheared because the angular velocity depends upon the distance from the planet). A review of these study can be found in the work of Brahic [37].

1.2.3 Flow under gravity acceleration

Another way to probe hydrodynamic descriptions of rapid granular dynamics is the study of flows along inclined channels. In this kind of experiments the whole material is accelerated by gravity, but the friction with the plane induce shearing, so that measurements similar to the ones performed in Couette cells can be performed. The first experiments in this configuration were performed by Ridgway and Rupp [188], and reviews can be found in the works of Savage [192] and Drake [76]. Interest has focused on constitutive relations, as before, but also on the profiles of the hydrodynamic fields, mainly flow velocity and solid fraction: computer simulations (see for example Campbell and Brennen [53] and for an

exhaustive review the classical work of Campbell [52]) have allowed the measurement of the temperature field: this has confirmed the picture of a gas-like behavior, explaining the reduction of density (solid fraction) near the bottom by means of an increase of granular temperature, due to the shear work. In this framework the scheme representing the "mechanical energy path" sketched by Campbell in his review on rapid granular flow [52] is enlightening. The external driving force (i.e. gravity) induces mean motion (kinetic energy) which consequently generates friction with boundaries, that is shear work (granular temperature). The randomization represented by the granular temperature induces collisions among the grains, which are dissipative and therefore produce heat. Moreover, granular temperature generates internal (transversal as well as normal) stresses.

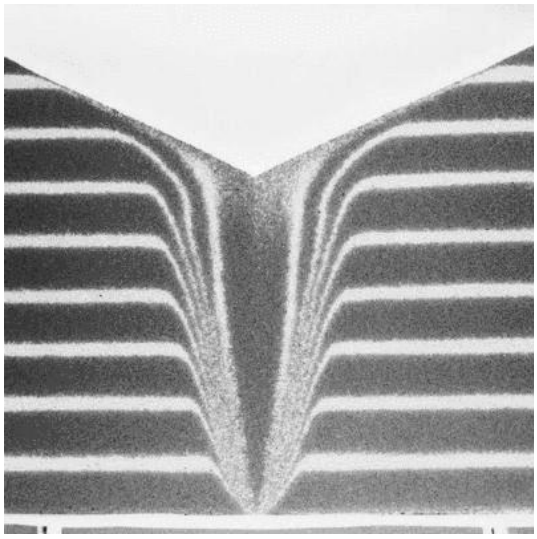

Figure 1.8: The draining from the bottom of a silo: it is clear the separation between a region where grain move downward and a region where grain do not move at all

Another configuration of granular flow under the force of gravity is the simple hopper geometry (a hopper is a funnel-shaped container in which materials, such as grain or coal, are stored in readiness for dispensation). The bottom of hopper is opened and the grains start to pour out. As already discussed the pressure (and therefore the flow rate) does not depend upon the height of the column of material. However the flux of grains leaving the container produces complex flow regions inside the container. Brown and Hawksley [47] identified four regions of density and velocity, most notably a tongue of dense motion just above the aperture and an area of no grain motion below a cone extending upwards from the opening (a similar can be observed in a silo, see Fig. 1.8). Baxter et al. [19] have showed that for large opening angles, density waves propagate upward from above the aperture against the direction of particle flow, but downwards for small angles. The flow can even stop due to "clogging", i.e. the grains can form big arches above the aperture and sustain the entire weight of the column.

More recent experiments have been performed on granular flows along inclined planes or chutes, evidencing other interesting phenomena:

- **Validations of kinetic theory** Azanza et al. [7] have recently repeated the experiment of grain flow along an inclined channel, studying the stationary profiles of velocity, solid fraction and granular temperature. They have verified that there is a limited range of inclinations of the channel that allow for a stationary flow. Moreover they have probed the validity of the kinetic theories developed in the previous years [194, 121, 152, 120, 150], based on the assumption of slight perturbation to the Maxwellian equilibrium. The profiles of hydrodynamic fields show two different regions: a collisional region (higher density) where the transport is mainly due to collisions, and a ballistic region (on the upper free surface) where the grains fly almost ballistically.
- **Clustering:** Kudrolli and Gollub [131, 133] have studied the formation of clusters measuring

the density distribution in an experiment consisting of steel balls rolling on a smooth surface which could or could not be inclined with a vibrating side. The experiment takes into account a monolayer (not completely covered) of grains, in order to study a true $2d$ setup. In both cases (inclined or horizontal), at high enough global densities, the distribution of density (going from Poissonian to exponential) indicates strong clustering.

- **Non-Gaussian velocity distributions:** Kudrolli and Henry [132] have studied the distributions of velocities in the same setup of the previous experiment, with varying angles of inclination, obtaining non-Gaussian statistics with enhanced high energy tails; moreover they have seen that increasing the angle of inclination the distributions tends toward the Maxwellian (see Fig. 1.9).

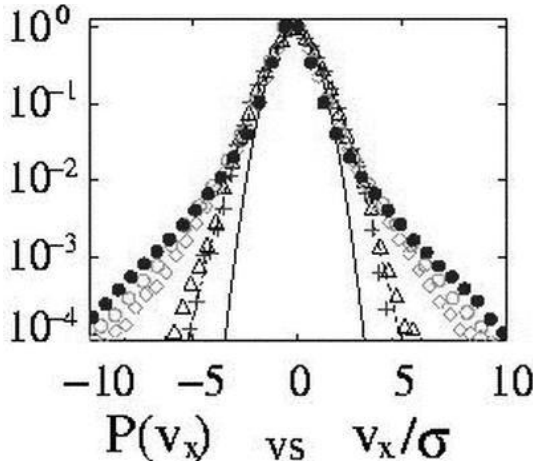

Figure 1.9: The experiment of Kudrolli and Henry [132]: distributions of horizontal velocities of grains rolling on an inclined plane, with the inferior wall vibrating.

- **Velocity correlations:** A very recent experiment of Blair and Kudrolli [71] with the same experimental setup of the previous ones has revealed strong correlations between velocity particles.
- **Size segregation in silo filling or emptying:** Samadani et al. [191] have recently studied the phenomena of size segregation in a quasi-two dimensional silo emptying out of an orifice. They [190] have also studied the effects of interstitial fluids.
- **Size segregation in rotating drums:** another typical experiment, inspired to many industrial situations, is the tumbling mixer, or rotating drum, i.e. a container with some shape that rotate around a fixed axis, usually used to mix different kind of granular materials (typically powders, in the pharmaceutical, chemical, ceramic, metallurgical and construction industry). Depending on the geometry of the mixer, the shapes of the grains, the parameters of the dynamics and so on, the grains can mix as well as separate. A very large literature exists on this phenomena (see a recent review of Ottino and Khakhar [177]). Usually segregation is strictly tied to convection: there is a shallow flowing layer on the surface of the material inside the rotating drum, the grains at the end of it are transported into the bulk and follow a convective path so that they emerge again in another point of the surface. Segregation happens in many different ways: segregated bands appear and slowly enlarge (like in a coarsening model), segregation can emerge in different directions, e.g. parallel to the rotation axis as well as transversal to it.

1.2.4 Vibrated grains

Many interesting observations can be done when the granular medium is subject to periodic vibration. As already discussed (see paragraph 1.1.2) the effect of slow vibration under of the bottom of a container filled of grains induces a very slow compaction of the material. When the amplitude of vibration is strong enough, i.e. when

$$\Gamma = \frac{a_{max}}{g} > 1 \tag{1.14}$$

(where a_{max} is the maximum acceleration of the vibrating plate, e.g. $a_{max} = A\omega^2$ if the plate is harmonically vibrating with A amplitude and ω frequency), then the granular shows several new phenomena.

- **Convection and segregation**: A large literature [87] exists on the convection and segregation phenomena observed in granular media contained in a box shaken from the bottom (or from the sides). Faraday [88] was perhaps the first to observe such a phenomenon. The geometry of the container can change dramatically the quality of the convection (e.g. in a cylinder may happen that the grains near the walls move downwards and the ones in the bulk move upwards, while inside an inverted cone the convection occurs in the opposite direction). Usually the larger grains (independent of their density) tend to move upwards (see Fig. 1.10), so that the material segregate (see for example [127, 79, 135, 125, 124]).

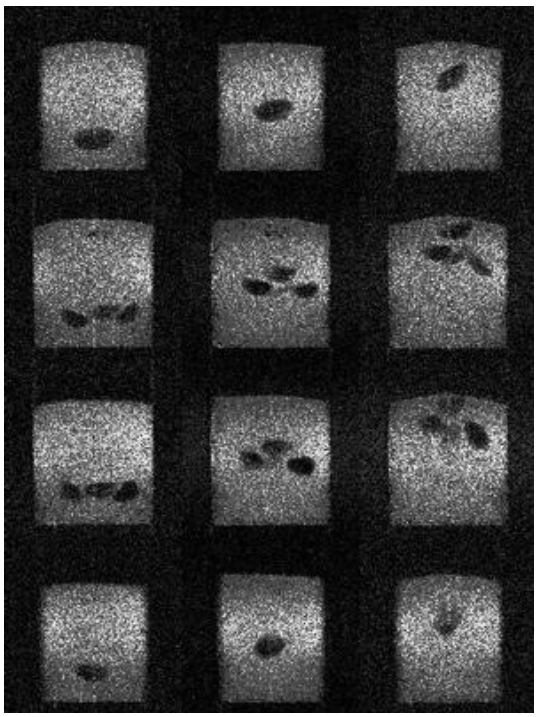

Figure 1.10: Segregation and convection in a vibrated mixture of grains of different sizes

- **Pattern formation in surface waves**: another problem that has been extensively studied in recent years is the formation of patterns on the surface of vibrated layers of grains. Depending on the whole set of parameters (amplitude and frequency of the vibration, shapes and sizes of the grains, size of the container, depth of the bed and so on) different qualities of standing waves can be observed, leading to unexpected and fascinating textures [161, 162, 209, 163] (see Fig. 1.11 on the following page and Fig. 1.12 on the next page).

- **Validations of kinetic theory**: a part of the experimental effort [147, 224, 223, 222] has also devoted to the study of hydrodynamic and kinetics fields (i.e. packing fraction profiles, granular temperature profiles, self-diffusion, velocity statistics) in vertically vibrated boxes (or vertical slices, that is 2d setups). The interest has also focused on the difficulties of imposing boundary conditions to the existing kinetics model, due to the existence of non-hydrodynamic boundary layers. This has also led to the formulation of hypothesis of scaling for the granular

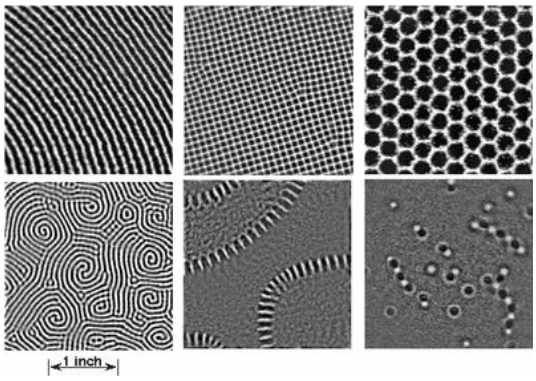

Figure 1.11: Different surface patterns obtained by vertical vibration of granular layers

Figure 1.12: The oscillon: a two-dimensional solitary standing wave on the surface of a granular monolayer

temperature as a function of the amplitude of vibration [134, 204]. For more recent experiments see [225].

- **Clustering**: the formation of high density clusters has also been studied in the same previous simple setup, i.e. in a vibrated cylindrical piston [84, 86, 85]. A transition has been observed with the increasing number of particles in the cylinder, from a gas-like behavior to a collective solid-like behavior. Such a transition has been also observed in the framework of fluidized beds [172], i.e. vertically shaken granular monolayers: the authors have observed a transition (with reducing the vibration amplitude) from a gas-like motion to a coexistence between a crystallized state (a pack of particles arranged in an ordered way) surrounded by gas.

- **Velocity distributions**: after the recent progresses in the numerical study of granular rapid dynamics, almost in the investigation of the limits of existing granular kinetic theories [42, 39, 211], the question of the true form of the velocity distributions has arisen and has induced many new experiments in order to give a realistic answer to it. The experiment of Olafsen and Urbach [172, 173] with a horizontal granular monolayer subject to a vertical vibration (and measuring horizontal velocities) has proven that, in the presence of clustering, the distributions are non-Gaussian, showing nearly exponential tails. The experiment of Losert et al. [144] on a similar monolayer with vertical vibration verify that both the predictions of van Noije and Ernst [211] on the high energy tails for cooling and driven granular gases are correct, measuring exponential tails for the former and $\exp(-v^{3/2})$ for the latter. Very recently Rouyer and Menon [189] have again measured the velocity fluctuations in a vertically vibrated vertical monolayer of grains, obtaining again a velocity distribution with $\exp(-v^{3/2})$ tails.

Chapter 2

Transport equations for elastic and inelastic gases

Granular systems are almost always out of thermodynamic equilibrium: they are open systems that need an external source to be kept in a steady state. This means that even in a homogeneous granular gas a flow of heat is present, from the environment into the bulk, to keep the gas in a stationary regime; more often the gas is unstable toward the formation of macroscopic flows, e.g. self-induced shear and vortices. In this chapter we review the basics of transport theory for elastic fluids in order to recall all the assumptions needed to follow its derivation. The general transport theory is the arrival point of a path that begins at the microscopic (we will say "molecular dynamics", MD) level and goes along through the definition of a space-time scale which separates equilibrium from non-equilibrium together with many other hypothesis. This chapter is a review of the many delicate passages which demand strong requirements usually not fulfilled by inelastic gases.

The main distinction between granular gases and the other "states" of granular matter comes from the fact that collisions are always considered binary. The so-called *inelastic collapse* observed in simulations is the signature of a departure from the gas behavior toward a solid-vapor coexistence (ordered clusters surrounded by the gas phase). This transition is usually avoided by means of a physical regularization (e.g. by assuming a velocity dependent restitution coefficient), or restricting the simulations to a limited region of the *parameter space* such that this instability cannot arise. We have observed that the presence of a randomizing source is sufficient to prevent the inelastic collapse.

In the first section a brief description of the elastic and inelastic binary collision event is given. Many widely known statistical concepts as mean free time, mean free path and collisional cross section will be defined in the case of elastic collisions. The derivation of the Boltzmann equation from the Liouville equation is sketched in the second section, going through the BBGKY hierarchy. We will put the accent on the assumption of *molecular chaos* which concerns correlations of pre-collisional velocities. Absence of pre-collisional correlations is a delicate assumption even for elastic systems. Molecular chaos, however, gives important simplification in numerical work, allowing the use of Monte Carlo methods which can be useful to catch qualitative pictures of granular physics. From the Boltzmann equation one can derive, by means of the Chapman-Enskog or the Grad methods the equations of transport for the out of equilibrium behavior of the gas. This derivation will be summarized in the third section. In the fourth section we review the existing closure theories for granular hydrodynamics (i.e. hydrodynamics of inelastic hard spheres). This program was begun in the early 80s and many exact results have been obtained in recent years: the renewal of interest is motivated by the speed up of computer simulations and by the consequent ease of testing the predictions of the theory. In section five, finally, we will present the criticism that has been put forward by different authors concerning the difficulties of an rigorous foundation of granular hydrodynamics: the path from microscopic to mesoscopic description is full of assumptions that could restrict the limits of validity of the existing kinetic theories. All of the concepts reviewed in the first three sections of this chapter will be of aid in order to establish the deep differences between elastic and inelastic gases.

2.1 The binary collision

We review the elementary theory of elastic binary collisions and the statistical concepts that can be derived from it (a very simple introduction to this concepts can be found on [98]). The case of inelastic binary collisions is finally considered, obtaining different reduced formulas for different modelizations of the collision event. In the rest of this work we use the simplest of them, the one for the instantaneous collision with a fixed restitution coefficient and no rotational degrees of freedom, that is Eq. (2.41).

2.1.1 Kinematics of the elastic collision

Let us consider two point-like particles with masses m_1 and m_2, coordinates $\mathbf{r}_1$ and $\mathbf{r}_2$ and velocities $\mathbf{v}_1$ and $\mathbf{v}_2$. One can introduce the center of mass vector $\mathbf{r}_c$:

$$\mathbf{r}_c = \frac{m_1\mathbf{r}_1 + m_2\mathbf{r}_2}{m_1 + m_2} \tag{2.1}$$

and the relative position vector:

$$\mathbf{r} = \mathbf{r}_1 - \mathbf{r}_2. \tag{2.2}$$

Their time derivatives are: the velocity of the center of mass:

$$\mathbf{v}_c = \frac{m_1\mathbf{v}_1 + m_2\mathbf{v}_2}{m_1 + m_2} \tag{2.3}$$

and the relative velocity:

$$\mathbf{V}_{12} = \mathbf{v}_1 - \mathbf{v}_2. \tag{2.4}$$

The forces between these two particles depends only on their relative position and are of equal magnitude and pointing in opposite directions:

$$\mathbf{F}_{12}(\mathbf{r}) = -\mathbf{F}_{21}(\mathbf{r}). \tag{2.5}$$

This is equivalent to say that the center of mass does not accelerate, i.e.:

$$\frac{d^2\mathbf{r}_c}{dt^2} = 0 \tag{2.6}$$

while the relative position obeys to the following equation of motion:

$$m^*\frac{d^2\mathbf{r}}{dt^2} = \mathbf{F}_{12}(\mathbf{r}) \tag{2.7}$$

where

$$m^* = \left(\frac{1}{m_1} + \frac{1}{m_2}\right)^{-1} \tag{2.8}$$

is the reduced mass of the system of two particles. If the collision is elastic an interaction potential can be introduced so that:

$$\mathbf{F}_{12} = -\frac{dU(r)}{dr}\hat{\mathbf{r}} \tag{2.9}$$

where $\hat{\mathbf{r}}$ is the unit vector along the direction of the relative position of the two particles. The force vector lies in the same plane where the relative position vector and relative velocity vector lie. The evolution of the relative position r is the evolution of the position of a particle of mass m^* in a central potential $U(r)$. The angular momentum of the relative motion $\mathbf{L} = \mathbf{r} \times m^*\mathbf{V}_{12}$ is conserved. This means that the particle trajectory, during the collision, will be confined to this plane. In Fig. 2.1

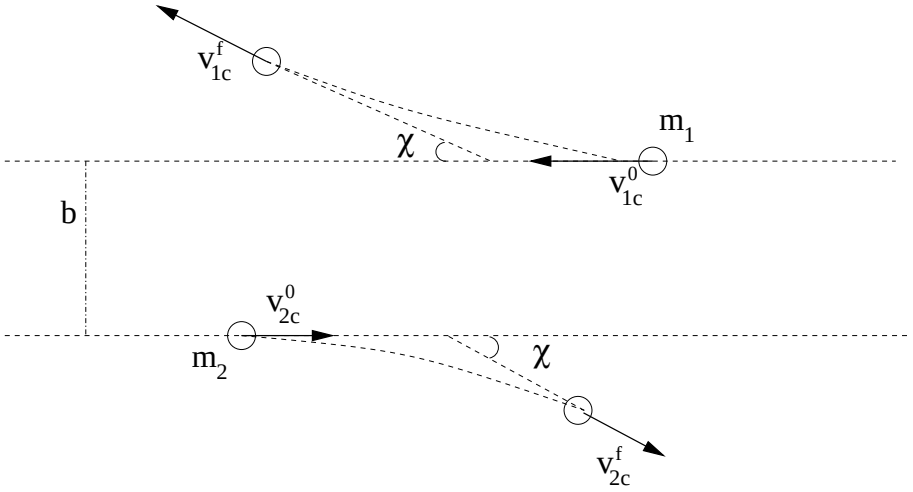

Figure 2.1: The binary elastic scattering event in the center of mass frame, with a repulsive potential of interaction

is sketched the typical binary scattering event when the interacting force is repulsive (monotonically decreasing potential), in the center of mass frame.

In the center of mass frame the elastic scattering has a very simple picture: the velocities of the particles are $\mathbf{v}_{1c} = \mathbf{V}_{12}m^*/m_1$ and $\mathbf{v}_{2c} = -\mathbf{V}_{12}m^*/m_2$. The elastic collision conserves the modulus of the relative velocity V_{12} and therefore also the moduli of the velocities of the particles in the center of mass frame. If one consider the collision event as a black box and observes the velocities of the particles "before" and "after" the interaction (i.e. asymptotically, when the interaction is negligible), then the velocity vectors are simply rotated of an angle χ called *angle of deflection*, which also represents the angle between asymptotic initial and final directions of the relative velocity. During the collision the total momentum is conserved (this happens also for inelastic collisions) but is redistributed between the two particles, i.e. the variation of the momentum of the particle 1 is $\delta(m_1\mathbf{v}_1) = m^*(\mathbf{V}'_{12} - \mathbf{V}_{12})$ where the prime indicates the post-collisional relative velocity. Obviously $\delta(m_1\mathbf{v}_1) = -\delta(m_2\mathbf{v}_2)$. Finally, one can calculate the components of the momentum transfer parallel and perpendicular to the relative velocity:

$$\delta(m_1 v_1)_\parallel = -m^* V_{12}(1 - \cos\chi) \tag{2.10a}$$

$$\delta(m_1 v_1)_\perp = m^* V_{12} \sin\chi. \tag{2.10b}$$

To calculate the angle of deflection χ one needs the exact form of the interaction potential, the asymptotic initial relative velocity V_{12}^0 (i.e. at a distance such that the interaction is negligible) and the *impact parameter* b that is the minimal distance between the trajectories of the particles if there were no interaction between them:

$$\chi = \pi - 2\int_{r_m}^{\infty} dr \frac{b}{r}\left[r^2 - b^2 - \frac{2r^2U(r)}{m^*(V_{12}^0)^2}\right]^{-1/2} \tag{2.11}$$

where r_m is the closest distance effectively reached by the two particles. From Eq. (2.11) it is evident that the angle of deflection decreases as the initial relative velocity increases.

The case of an inverse power potential is of physical interest:

$$\mathbf{F}_{12} = \frac{K_a}{r^a}\hat{\mathbf{r}} \tag{2.12a}$$

$$U(r) = \frac{K_a}{a-1} r^{-(a-1)} \tag{2.12b}$$

with $a > 1$ and K_a positive or negative in order to have respectively repulsive or attractive forces. In this case Eq. (2.11) can be explicitly calculated for some specific values of the power a. For example the gravitational or electrostatic interactions (in 3D) correspond to the case $a = 2$ for which

$$\chi = 2 \arcsin \left[\frac{1}{\sqrt{1 + x_0^2}} \right] \tag{2.13}$$

where $x_0 = b(m^*(V_{12}^0)^2/K_2)$. The case $a = 3$ is even simpler leading to the formula

$$\chi = \pi \frac{\sqrt{b_0^2 + b^2} - b}{\sqrt{b_0^2 + b^2}} \tag{2.14}$$

with $b_0 = (K_3/m^*(V_{12}^0)^2)^{1/2}$. The case $a = 5$ (in 3D) is of particular interest because for this special interaction the kinetic equation (Boltzmann equation, see section 2.2.3) is very simple. Particles interacting with this potential are called Maxwell molecules, discussed in more detail in paragraph 2.2.5. The deflection angle for this case is quite complicated:

$$\chi = \pi - \int_0^1 du \frac{2^{3/2} x_0 \sqrt{\sqrt{x_0^4 + 2} - x_0^2}}{\sqrt{(x_0^4 + 2) - \left\{ x_0^2 + u^2 \left[\sqrt{x_0^4 + 2} - x_0^2 \right] \right\}^2}} \tag{2.15}$$

with $x_0 = b(m^*(V_{12}^0)^2/K_5)^{1/4}$. For small values of x_0 (i.e. for small impact parameters or small initial relative velocities) the deflection angle approaches π linearly, i.e.:

$$\lim_{x_0 \to 0} \chi = \pi - 3.118 x_0. \tag{2.16}$$

2.1.2 Statistics of the elastic collision

The concept of *mean free path* was introduced in 1858 by Rudolf Clausius [65] and paved the road to the development of the kinetic theory of gas. For the sake of simplicity (and coherently with the rest of this work, as well as with the literature on granular gases) we consider a single species gas composed of hard spheres, all having the same diameter σ and mass m (see [62] or [98]).

The *mean free time* is the average time between two successive collisions of a single particle. We define νdt the probability that a given particle suffers a collision between time t and $t + dt$ (ν is called collision frequency) and assume that ν is independent of the past collisional history of the particle. The probability $f_{time} dt$ of having a free time between two successive collisions larger than t and shorter than $t + dt$ is equal to the product of the probability that no collision occurs in the time interval $[0, t]$ and the probability that a collision occurs in the interval $[t, t + dt]$:

$$f_{time}(t)dt = P_{time}(t)\nu dt \tag{2.17}$$

where $P_{time}(t)$ is the survival probability, that is the probability that no collisions happen between 0 and t, and can be calculated observing that $P_{time}(t + dt) = P_{time}(t)P_{time}(dt) = P_{time}(t)(1 - \nu dt)$ so that $dP_{time}/dt = -\nu P_{time}$, i.e. $P_{time}(t) = e^{-\nu t}$.

Finally one can calculate the average of the free time using the probability density $f_{time}(t)$:

$$\tau = \int_0^\infty dt t f_{time}(t) = \int_0^\infty dt t \nu e^{-\nu t} = \frac{1}{\nu}. \tag{2.18}$$

With the same sort of calculations an expression for the mean free path, that is the average distance traveled by a particle between two successive collisions, can be calculated. One again assumes that there is a well defined quantity (independent of the collisional history of the particle) αdl which is the probability of a collision during the travel between distances l and $l + dl$. The survival probability in terms of space traveled is $P_{path}(l) = e^{-\alpha l}$ and the probability density of having a free distance l is $f_{path}(l) = e^{-\alpha l}\alpha$ so that the mean free path is given by:

$$\lambda = \frac{1}{\alpha} \tag{2.19}$$

The other important statistical quantity in the study of binary collisions is the so-called *differential scattering cross section* s which is defined in this way: in a unit time a particle suffers a number of collisions which can be seen as the incidence of fluxes of particles coming with different approaching velocities $\mathbf{V}_{12}$ and scattered to new different departure velocities $\mathbf{V}'_{12}$. Given a certain approaching velocity $\mathbf{V}_{12}$ the incident particles arrive with slightly different impact parameters (due to the extension of the particles), and therefore are scattered in a solid angle $d\Omega'$. If I_0 denotes the intensity of the beam of particles that come with an average approaching speed $\mathbf{V}_{12}$, which is the number of particles intersecting in unit time a unit area perpendicular to the beam ($I_0 = nV_{12}$ with n the number density of the particles), then the rate of scattering dR into the small solid angle element $d\Omega'$ is given by

$$\frac{dR}{d\Omega'} = I_0 s(\mathbf{V}_{12}, \mathbf{V}'_{12}) \tag{2.20}$$

where s is a factor of proportionality with the dimensions of an area (in $3D$) which is called differential cross section and depends on the relative velocity vectors before and after the collisions. The total rate of particles scattered in all directions, R is the integral of the last equation:

$$R = I_0 \int\int_{4\pi} d\Omega' s(\mathbf{V}_{12}, \mathbf{V}'_{12}) = SI_0 \tag{2.21}$$

and defines the total scattering cross section S.

In the case of a spherically symmetric central field of force the differential cross section is a function only of the modulus of the initial relative velocity V_{12}, the angle of deflection χ, and the impact parameter b which in turn, once fixed the potential $U(r)$, is a function only of χ and V_{12}, that is $s = s(V_{12}, \chi)$. In particular it can be easily demonstrated that

$$s(V_{12}, \chi) = -\frac{b(V_{12}, \chi)}{\sin\chi}\frac{db}{d\chi}. \tag{2.22}$$

The case of inverse power interaction potential is of interest also for the study of cross sections: a very famous result in this framework is the Rutherford formula that concerns the differential cross section for the case $a = 2$ (scattering of an electron by an atomic nucleus):

$$s(V_{12}, \chi) = \frac{K_2^2}{(2V_{12}^2 m^*)^2}\frac{1}{sin^4(\chi/2)} \tag{2.23}$$

where $K_2 = e^2/4\pi\epsilon_0$ (for the electron charge e and the vacuum permittivity ϵ_0).

In addition to the differential and total scattering cross sections, in non-equilibrium transport theory several other cross sections are defined:

$$S_k(V_{12}) = \int_0^{2\pi} d\epsilon \int_0^{\pi} d\chi \sin\chi(1 - cos^k\chi)s(V_{12}, \chi) \tag{2.24}$$

where k is a positive integer (n=1,2,....). For instance, the transfer of the parallel component of the particle momentum is proportional to $1 - \cos\chi$ (see Eq. (2.10)) and therefore S_1 is related to the transport of momentum and plays an important role in the study of diffusion. Moreover, viscosity and heat conductivity depend on S_2.

To conclude this paragraph we recall that the collision frequency defined at the beginning is strictly tied to the total scattering cross section by the relation

$$\nu = nS\overline{V_{12}} \tag{2.25}$$

where n is the average density of the gas and $\overline{V_{12}}$ is an average of the relative velocities. Generally speaking (in the framework of a non-equilibrium discussion) n and $\overline{V_{12}}$ are averages taken in space-time regions in which equilibrium can be assumed. Assuming that in this region the distribution of velocities of the particle is the Maxwell-Boltzmann distribution:

$$f(\mathbf{v}) = \frac{m^{3/2}}{(2\pi k_B T)^{3/2}} e^{-\frac{mv^2}{2k_B T}} \tag{2.26}$$

the collision frequency can be calculated obtaining the formula:

$$\nu = \sqrt{2} n S \overline{v} \tag{2.27}$$

where $\overline{v}$ is the average of the modulus of the velocities and, in this case, is given by:

$$\overline{v} = \sqrt{\frac{8 k_B T}{\pi m}}. \tag{2.28}$$

In the same way the mean free path is given by

$$\lambda = \frac{1}{\sqrt{2} n S}. \tag{2.29}$$

2.1.3 Hard spheres

Hard spheres are one of the simplest models of molecular fluids and have represented for many years the testing ground for the predictions of the kinetic theory, thanks to the pioneering efforts of physicists who have developed hard spheres simulations on the old computers which were huge in encumbrance and very small in power (the work of Alder and Wainwright is considered the foundation of this subject [2, 3, 1, 4, 5]). Nowadays liquids and gases are almost always simulated with different tools and models (e.g. Lenard-Jones potentials or others), i.e. typically *soft spheres* models. Nevertheless the study of granular materials has again awakened the interest in hard spheres molecular dynamics, as the geometric character of the grain-grain interaction seems to be better modeled by an hard core interaction. Here we define the hard core potential and give expressions for the quantities calculated in the previous paragraphs.

Two hard spheres in 3D (hard disks in 2D, hard rods in 1D) of diameters σ_1 and σ_2 interact by means of a discontinuous potential $U(r)$ of the form:

$$U(r) = 0 \quad (r > \sigma_{12}) \tag{2.30a}$$
$$U(r) = \infty \quad (r < \sigma_{12}) \tag{2.30b}$$

where $\sigma_{12} = (\sigma_1 + \sigma_2)/2 = r_m$ is the distance of the centers of the spheres at contact. The potential in Eq. (2.30) can be taken as a definition of hard spheres systems. In this case the deflection angle is given by:

$$\chi = 2 \arccos\left(\frac{b}{\sigma_{12}}\right) \tag{2.31}$$

and the dependence from the initial relative velocity disappears (only geometry determines the deflection angle).

The differential scattering cross section for hard spheres is calculated from Eq. (2.22) obtaining a very simple formula: $s(V_{12}, \chi) = \sigma^2/4$ which can be integrated over the entire solid angle space giving an expression for the total cross section $S = \pi\sigma^2$. This result is consistent with the physical intuition of the cross section: it is the average of the areas of influence of the scatterer in the planes perpendicular to the approaching velocities of the incident particles.

Other interesting quantities to be easily calculated for hard spheres systems are the transport cross sections (see definition in Eq. (2.24)). The first two are given here:

$$S_1 = \pi\sigma^2 \tag{2.32a}$$
$$S_2 = \frac{2}{3}\pi\sigma^2 \tag{2.32b}$$

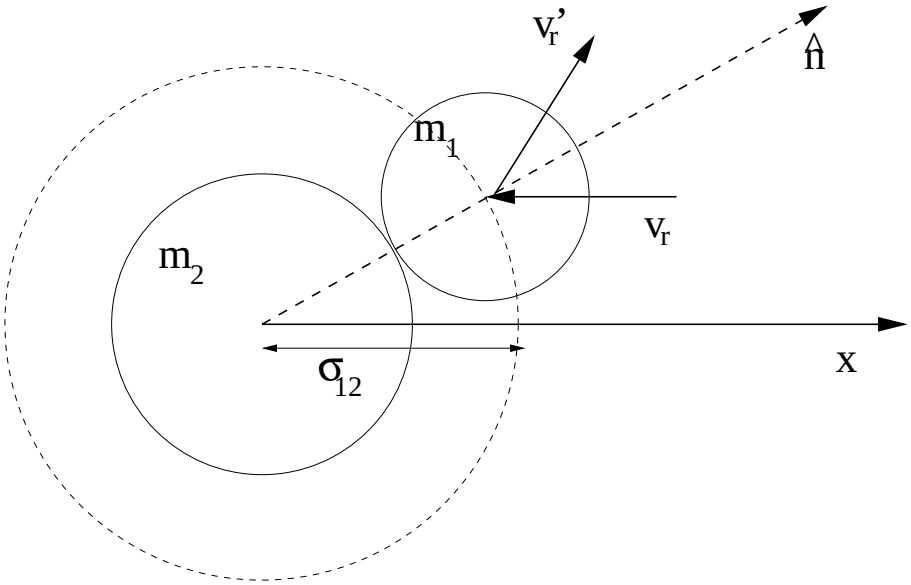

Figure 2.2: The collision between two elastic hard spheres

Finally we give a definition of *smooth hard spheres* (we consider this model as a paradigm for granular gases): smoothness is the absence of irregularities on the surface of the spheres, i.e. the instantaneous collision does not change the rotational degrees of freedom of the spheres at contact. Therefore, in the study of smooth hard spheres systems, a complete description of the dynamics requires only the positions of the centers $\mathbf{r}$ and their velocities $\mathbf{v}$. In particular the collision is an instantaneous transformation of the velocities of two particles i and j at contact which are "reflected" with the following rule (see Fig. 2.2):

$$\mathbf{v}_i' = \mathbf{v}_i - \frac{2m_2}{m_1+m_2}\hat{\mathbf{n}}[\hat{\mathbf{n}}\cdot(\mathbf{v}_i-\mathbf{v}_j)] \tag{2.33}$$

$$\mathbf{v}_j' = \mathbf{v}_j + \frac{2m_1}{m_1+m_2}\hat{\mathbf{n}}[\hat{\mathbf{n}}\cdot(\mathbf{v}_i-\mathbf{v}_j)] \tag{2.34}$$

$$\tag{2.35}$$

where $\hat{\mathbf{n}} = (\mathbf{r}_i - \mathbf{r}_j)/|\mathbf{r}_i - \mathbf{r}_j|$ and the primes denote the velocities after the collision. This collision rule conserves momentum and kinetic energy. It only changes the direction of the component of the relative velocity of the particles in the direction of $\hat{\mathbf{n}}$ (normal component), leaving unchanged the tangential component.

2.1.4 Elementary transport calculations

In the kinetic theory the condition of equilibrium is equivalent to the absence of macroscopic flows, i.e. absence of transport. The transport of the molecular quantity W along a particular direction $\hat{\mathbf{n}}$ is characterized by its net flux $\mathbf{j}_W(t,\mathbf{r})\cdot\hat{\mathbf{n}}$ which is defined as the net fraction of W crossing in the unit time a unit surface normal to the direction $\hat{n}$ in the point $\mathbf{r}$ of the space. If the quantity W is always transported by molecular motion or transferred from a particle to another via collision interactions that conserve the sum of W (i.e. W is said to be a *collisional invariant*), then the variation in time of the coarse grained field $W(t,\mathbf{r})$ (which is an average of W taken on particles in a well suited region of space-time centered in $(t,\mathbf{r})$) is simply expressed by a continuity formula:

$$\frac{\partial W}{\partial t} = -\nabla\cdot\mathbf{j}_W \tag{2.36}$$

In elastic gases the relevant conserved molecular quantities are: m, $m\mathbf{v}$ and $mv^2/2$, that is mass, momentum and energy.

Empirical observations show that, in situations *not too far from equilibrium* almost all the transport fluxes are proportional to the spatial gradient of the transported quantity:

$$\mathbf{j}_W = -C_W \nabla W \tag{2.37}$$

where C_W is called the *transport coefficient* for the quantity W. The most important transport coefficients are: the diffusion coefficient D (transport of mass or *self diffusion*), the viscosity η (transport of transversal momentum, e.g. transport of mv_x in the direction y or z) and the heat conductivity κ (transport of heat, that is internal energy). The flux of longitudinal momentum (e.g. mv_x in the direction x) is somewhat different as it is dominated by an order zero (in the spatial gradients) contribution which is given by the hydrostatic pressure p (in the Boltzmann-Grad limit $p = nk_BT$).

Starting from the basic concepts of mean free time and path, it is possible to derive heuristic expressions for the transport coefficients [62]. Such calculations, that take the name of *mean free path method* are meaningful in the limit of small Knudsen numbers:

$$\mathrm{Kn} = \frac{\lambda}{L} \ll 1 \tag{2.38}$$

where λ is the mean free path and L is the characteristic linear size of the problem (related to boundary conditions, e.g. in a shear experiment $L = \overline{v}/\gamma$ where $\overline{v}$ is the thermal velocity of the fluid and $\gamma = \Delta u_x/\Delta L_y$ is the shear rate). This condition corresponds to the necessity that the variation of all macroscopic quantities is small within a mean free path.

With this assumption, very rough calculations carry to good estimates of the main transport coefficients:

$$D = \frac{1}{3}\lambda\overline{v} = \left(\frac{2}{3S}\sqrt{\frac{k_B}{\pi m}}\right)\frac{\sqrt{T}}{n} \tag{2.39a}$$

$$\eta = \frac{1}{3}nm\lambda\overline{v} = \left(\frac{2}{3S}\sqrt{\frac{mk_B}{\pi}}\right)\sqrt{T} \tag{2.39b}$$

$$\kappa = k_B n\lambda\overline{v} = \left(\frac{2k_B}{S}\sqrt{\frac{k_B}{\pi m}}\right)\sqrt{T} \tag{2.39c}$$

In the last formulas the rightmost sides are calculated using the expressions for the mean free path and for the average velocity modulus obtained with the assumption of Maxwell-Boltzmann equilibrium. In the above equations one sees that the viscosity and the heat conductivity do not depend on the density, but only on the temperature of the gas. Apparently one expects that the viscosity depends upon the density (more particles carry more momentum) but in these approximated calculations the fluxes are assumed to be carried only by molecular motion (i.e. collisional transfer is negligible): for the viscosity for example this means the appearance of the product $n\lambda$ which does not depend on n (as λ is inversely proportional to n).

2.1.5 The effects of inelasticity and the reduced models

Granular particles collide dissipating relative kinetic energy. This is due to the macroscopic nature of the grains which leads to the presence of internal degrees of freedom. During the interaction, irreversible processes happen inside the grain and energy is dissipated in form of heat. All these processes conserve momentum, so that the velocity of the center of mass of the two grains is not modified.

Many modelizations of the binary inelastic collision have been proposed (soft spheres [221, 220, 52, 63, 107, 146] as well as hard spheres models [53, 112, 96, 159]): this is usually a difficult problem relatively to the information that can be gained from. Simplification often pays more, as very idealized models lead to interesting and physically meaningful results. The most used model in granular gas

literature is also the most simple one, that is the inelastic smooth hard spheres gas with the *fixed restitution coefficient rule* given by the following prescriptions:

$$m_1\mathbf{v}_1' + m_2\mathbf{v}_2' = m_1\mathbf{v}_1 + m_2\mathbf{v}_2 \tag{2.40a}$$
$$(\mathbf{v}_1' - \mathbf{v}_2')\cdot\hat{\mathbf{n}} = -r(\mathbf{v}_1 - \mathbf{v}_2)\cdot\hat{\mathbf{n}} \tag{2.40b}$$

where, as usual, the primes denote the postcollisional velocities, $\hat{\mathbf{n}}$ is the unity vector in the direction joining the centers of the grains, and $0 \leq r \leq 1$. In this model the collisions happen at contact and are instantaneous. When $r = 1$ the gas is elastic and the rule coincides with the collision description for hard spheres given in the paragraph 2.1.3. When $r = 0$ the gas is perfectly inelastic, that is the particles exit from the collision with no relative velocity in the $\hat{\mathbf{n}}$ direction.

As a matter of fact, the transformation that gives the (primed) postcollisional velocities from the precollisional velocities of the two colliding particles is

$$\mathbf{v}_1' = \mathbf{v}_1 - (1+r)\frac{m_2}{m_1+m_2}((\mathbf{v}_1 - \mathbf{v}_2)\cdot\hat{\mathbf{n}})\hat{\mathbf{n}} \tag{2.41a}$$
$$\mathbf{v}_2' = \mathbf{v}_2 + (1+r)\frac{m_1}{m_1+m_2}((\mathbf{v}_1 - \mathbf{v}_2)\cdot\hat{\mathbf{n}})\hat{\mathbf{n}} \tag{2.41b}$$

Sometimes it may be useful to have the reverse transformation that give precollisional velocities from postcollisional ones, with the primes exchanged:

$$\mathbf{v}_1' = \mathbf{v}_1 - \left(1+\frac{1}{r}\right)\frac{m_2}{m_1+m_2}((\mathbf{v}_1 - \mathbf{v}_2)\cdot\hat{\mathbf{n}})\hat{\mathbf{n}} \tag{2.42a}$$
$$\mathbf{v}_2' = \mathbf{v}_2 + \left(1+\frac{1}{r}\right)\frac{m_1}{m_1+m_2}((\mathbf{v}_1 - \mathbf{v}_2)\cdot\hat{\mathbf{n}})\hat{\mathbf{n}} \tag{2.42b}$$

As it can be seen, the inverse transformation is equivalent to a change of the restitution coefficient $r \to 1/r$. Obviously in the case of a perfectly inelastic gas ($r = 0$) there is no inverse transformation. We also note that in 1D and when $m_1 = m_2$ Eqs. (2.41) become:

$$v_1' = \frac{1-r}{2}v_1 + \frac{1+r}{2}v_2 \tag{2.43a}$$
$$v_2' = \frac{1+r}{2}v_1 + \frac{1-r}{2}v_2 \tag{2.43b}$$

which coincide to an exact exchange of velocities in the elastic ($r = 1$) case, and in a sticky collision in the perfectly inelastic ($r = 0$) case. In dimensions higher than *one* the $r = 0$ case is very different from the so-called *sticky gas*, which is defined as a gas of hard spheres that in a collision become stuck together. In one dimension, instead, the $r = 0$ case may be considered equivalent to a sticky gas but a further prescription of "stickiness" must be given in order to consider collisions among more than two particles.

Variants of this models have been largely used in the literature. The importance of tangential frictional forces acting on the grains at contact may be studied taking into account the rotational degree of freedom of the particles, i.e. adding a variable $\boldsymbol{\omega}_i$ to each grain. The most simplified model which takes into account the rotational degree of freedom of particles is the rough hard spheres gas ([120, 151, 150, 97, 156, 115, 148]). In this model the postcollisional translational and angular velocities are given by the following equations (where the bottom signs in $\pm$ are to be considered for particle 2):

$$\mathbf{v}_{1,2}' = \mathbf{v}_{1,2} \mp \frac{1+r}{2}\mathbf{v}_n \mp \frac{q(1+\beta)}{2q+2}(\mathbf{v}_t + \mathbf{v}_r) \tag{2.44a}$$
$$\sigma\boldsymbol{\omega}_{1,2}' = \sigma\boldsymbol{\omega}_{1,2} + \frac{1+\beta}{2q+2}[\hat{\mathbf{n}}\times(\mathbf{v}_t + \mathbf{v}_r)] \tag{2.44b}$$

where q is the dimensionless moment of inertia defined by $I = qm\sigma^2$ (with I the moment of inertia of the hard object), e.g. $q = 1/2$ for disks and $q = 2/5$ for spheres; $\mathbf{v}_n = ((\mathbf{v}_1 - \mathbf{v}_2) \cdot \hat{\mathbf{n}})\hat{\mathbf{n}}$ is the normal relative velocity component, $\mathbf{v}_t = \mathbf{v}_1 - \mathbf{v}_2 - \mathbf{v}_n$ is the tangential velocity component due to translational motion, while $\mathbf{v}_r = -\sigma(\boldsymbol{\omega}_1 - \boldsymbol{\omega}_2)$ is the tangential velocity component due to particle rotation. In Eqs. (2.44) the tangential restitution coefficient β appears: it may take any value between -1 and $+1$. When $\beta = -1$ tangential effects disappear, i.e. rotation is not affected by collision (rough spheres become smooth spheres). When $\beta = +1$ the particles are said to have perfectly rough surface. It can be easily seen that (when $r = 1$) energy is conserved for $\beta = \pm 1$.

Moreover, a new class of models for collisions has been recently introduced, justified by a deeper analysis of the collision process. In these models the restitution coefficient r (or the coefficients r and β in the more detailed description given above) depends on the relative velocity of the colliding particles. In particular it has been seen that the collision tends to become more and more elastic as the relative velocity tends to zero. This refined prescription, referred to as 'viscoelastic' model [108, 44], has relevance (usually quantitative rather than qualitative) in different issues of the statistical mechanics of granular gases. An important kinetic instability of the cooling (and sometimes driven) granular gases is the so-called *inelastic collapse* [157, 159], i.e. a divergence of the local collision rate due to the presence of a few particles trapped very close to each other: simulations of the gas with the viscoelastic model have shown that this instability is removed, suggesting that it is an artifact of the fixed restitution coefficient idealization.

Here we give an expression of the leading term for the velocity dependence of the normal restitution coefficient r in the viscoelastic model (the viscoelastic theory may be applied to give also a velocity dependent expressions for the tangential restitution coefficient):

$$r = 1 - C_1 |(\mathbf{v}_1 - \mathbf{v}_2) \cdot \hat{\mathbf{n}}|^{1/5} + ... \tag{2.45a}$$

where C_1 depends on the physical properties of the spheres (mass, density, radius, Young modulus, viscosity).

2.2 From the Liouville to the kinetic equations

In this section we outline the derivation of the equation for the probability density function in the one-particle phase space for the smooth elastic hard spheres gas, that is the Boltzmann equation. In the kinetic theory [98] framework the derivation of transport equations begins from the Boltzmann equation [61]. In view of the interesting issues of Chapter 5 and of last section of Chapter 3, where we will address the problem of formation of ordered structures [214, 213, 215, 212, 178], that is (short and long range) spatial correlations, here we sketch the key passages for the derivation of the *ring kinetic equation* which relaxes the Molecular Chaos constraint and takes into account the recollision events, relevant in dense situations [4, 83, 82, 74, 75]. This section is devoted to the elastic gases, but the mainstream of the derivation is the same for the inelastic gases, and here we point out all the assumptions used which lack of rigorous proofs. At the end we discuss the Boltzmann-Enskog equation and the ring kinetic equation for inelastic smooth hard spheres [41, 40, 210, 211], i.e. the main kinetic equations for granular gases.

2.2.1 The Liouville and the pseudo-Liouville equations

In order to discuss the behavior of a system of N identical hard spheres (of diameter σ and mass m) it is natural to introduce the phase space, i.e., a $6N-$dimensional space where the coordinates are the $3N$ components of the N position vectors of the sphere centers $\mathbf{r}_i$ and the $3N$ components of the N velocities $\mathbf{v}_i$. The state of the system is represented by a point in this space. We call $\mathbf{z}$ the $6N$-dimensional position vector of this point. If the positions $\mathbf{r}_i$ of the spheres are restricted in a space region Ω, then the full phase space is given by the product $\Omega^N \times \Re^{3N}$

If the state is not known with absolute accuracy, we must introduce a probability density $P(z,t)$ which is defined by

$$Prob(z \in \mathbf{D} \quad \text{at time } t) = \int_{\mathbf{D}} P(\mathbf{z},t)d\mathbf{z} \tag{2.46}$$

where $d\mathbf{z}$ is the Lebesgue measure in phase space and we implicitly assume that the probability is a measure absolutely continuous with respect to the Lebesgue measure.

The mean value of a dynamical observable $A(\mathbf{z})$ can be calculated from either the following expressions:

$$\int_\infty d\mathbf{z}P(\mathbf{z},0)A(\mathbf{z}(t)) = \int_\infty d\mathbf{z}P(\mathbf{z},t)A(\mathbf{z}) \tag{2.47}$$

which are respectively the Lagrangian and Eulerian averages (analogous to the Heisemberg and Schroedinger averages in quantum mechanics). In Eq. (2.47) the time dependence of the observable A and of the distribution P is due to the time evolution operator S_t (also called *streaming operator*, that is $A(\mathbf{z}(t)) \equiv S_t(\mathbf{z})A(\mathbf{z})$. Considering the equivalence in Eq. (2.47) as an inner product implies that

$$P(\mathbf{z},t) = S_t^\dagger P(\mathbf{z},0) \tag{2.48}$$

where $S_T^\dagger$ is the adjoint of S_t.

In a general system (not necessarily made of hard spheres) with conservative and additive interactions, the force between the particle pair (ij) is $\mathbf{F}_{ij} = -\partial V(r_{ij})/\partial \mathbf{r}_{ij}$ so that the time evolution operator is given by:

$$S_t(\mathbf{z}) = \exp[tL(\mathbf{z})] = \exp\left[t\sum_i L_i^0 - t\sum_{i<j}\Theta(ij)\right] \tag{2.49}$$

where the *Liouville operator* $L(\mathbf{z})... \equiv \{H(\mathbf{z}),...\}$ is the Poisson bracket with the Hamiltonian, so that

$$L_i^0 = \mathbf{v}_i \cdot \frac{\partial}{\partial \mathbf{r}_i} \tag{2.50a}$$

$$\Theta(ij) = \frac{1}{m}\frac{\partial V(r_{ij})}{\partial \mathbf{r}_{ij}} \cdot \left(\frac{\partial}{\partial \mathbf{v}_i} - \frac{\partial}{\partial \mathbf{v}_j}\right) \tag{2.50b}$$

and $S_t(\mathbf{z})$ is a unitary operator, $S_t^\dagger = S_{-t}$, while $L^\dagger = -L$. In Eq. (2.49) the evolution operator S_t has been divided into a free streaming operator $S_t^0 = \exp[t\sum_i L_i^0]$ which generates the free particle trajectories, plus a term containing the binary interactions among the particles.

Finally the Liouville equation is obtained writing explicitly Eq. (2.48):

$$\frac{\partial}{\partial t}P(\mathbf{z},t) = \left(-\sum_i L_i^0 + \sum_{i<j}\Theta(ij)\right) P(\mathbf{z},t) \tag{2.51}$$

which is an expression of the incompressibility of the flow in phase space.

In the specific case of identical hard spheres, the interaction among particles is defined by Eq. (2.30). It can be shown that this kind of interaction carries no contraction of phase space at collision, i.e.

$$P(\mathbf{z}',t) = P(\mathbf{z},t) \tag{2.52}$$

where $\mathbf{z}'$ and $\mathbf{z}$ are the phase space points before and after a collision. This can be considered a form of detailed balance law. It is important to stress that $\mathbf{z}' \neq \mathbf{z}$: a collision represents a time discontinuity in the velocity section of phase space. In particular we use the elastic collision model defined in this list of prescriptions (it coincides with the collision rule for smooth hard spheres, see Eq. (2.33)):

$$|\mathbf{r}_i - \mathbf{r}_j| = \sigma \tag{2.53a}$$

$$\hat{\mathbf{n}}_{ij} = (\mathbf{r}_i - \mathbf{r}_j)/\sigma \tag{2.53b}$$

$$\mathbf{V}_{ij} = \mathbf{v}_i - \mathbf{v}_j \tag{2.53c}$$

$$\mathbf{V}_{ij} \cdot \hat{\mathbf{n}}_{ij} < 0 \tag{2.53d}$$

$$\mathbf{z} \equiv (\mathbf{r}_1, \mathbf{v}_1, \mathbf{r}_2, \mathbf{v}_2, ..., \mathbf{r}_i, \mathbf{v}_i, ..., \mathbf{r}_j, \mathbf{v}_j, ..., \mathbf{r}_N, \mathbf{v}_N) \tag{2.53e}$$

$$\mathbf{z}' \equiv (\mathbf{r}_1, \mathbf{v}_1, \mathbf{r}_2, \mathbf{v}_2, ..., \mathbf{r}_i', \mathbf{v}_i', ..., \mathbf{r}_j', \mathbf{v}_j', ..., \mathbf{r}_N, \mathbf{v}_N) \tag{2.53f}$$

$$\mathbf{r}_i' = \mathbf{r}_i \tag{2.53g}$$

$$\mathbf{r}_j' = \mathbf{r}_j \tag{2.53h}$$

$$\mathbf{v}_i' = \mathbf{v}_i - \hat{\mathbf{n}}_{ij}(\hat{\mathbf{n}}_{ij} \cdot \mathbf{V}_{ij}) \tag{2.53i}$$

$$\mathbf{v}_j' = \mathbf{v}_j + \hat{\mathbf{n}}_{ij}(\hat{\mathbf{n}}_{ij} \cdot \mathbf{V}_{ij}) \tag{2.53j}$$

$$\tag{2.53k}$$

these relations conserve the total momentum and the total energy of the system.

To derive the Boltzmann equation, the collisions events $\mathbf{z} \to \mathbf{z}'$ are considered as boundary conditions and the Liouville Equation (2.51) is restricted to the interior of the phase space region $\Lambda \equiv \Omega^N \times \Re^{3N} - \Lambda_{ov}$ where

$$\Lambda_{ov} = \left\{\mathbf{z} \in \Omega^N \times \Re^{3N} \mid \exists\, i,j \in \{1,2,...,N\}\ (i \neq j) : |\mathbf{r}_i - \mathbf{r}_j| < \sigma\right\} \tag{2.54}$$

is the set of phase space points such that one or more pairs of spheres are overlapping. With this conditions, the Liouville equation reads:

$$\frac{\partial}{\partial t}P(\mathbf{z},t) = \left(-\sum_i \mathbf{v}_i \cdot \frac{\partial}{\partial \mathbf{r}_i}\right) P(\mathbf{z},t) \quad (\mathbf{z} \in \Lambda) \tag{2.55a}$$

$$P(\mathbf{z},t) = P(\mathbf{z}',t) \quad (\mathbf{z} \in \partial\Lambda) \tag{2.55b}$$

This version of the Liouville equation is time-discontinuous: this means that formal perturbation expansions used in usual many-body theory methods cannot be applied to it.

An alternative master equation for the probability density function in the phase space can be derived [83]. The streaming operator S_t for hard spheres is not defined for any point of the phase space $\mathbf{z} \in \Lambda_{ov}$. In the calculation of the average (2.47) of physical observables, this is not a problem, as the streaming operators appears multiplied by $P(\mathbf{z},0)$ which is proportional to the characteristic function $X(\mathbf{z})$ of the set Λ (the characteristic function is 1 for points belonging to the set and 0 for points outside of it). In perturbation expansions it is safer to have a streaming operator defined for every point of the configurational space. A standard representation, defined for all points in the phase space, has been developed for elastic hard spheres and is based on the binary collision expansion of $S_t(\mathbf{z})$ in terms of binary collision operators. The binary collision operator is defined in terms of two-body dynamics through the following representation of the streaming operator for the evolution of two particles:

$$S_t(1,2) = S_t^0(1,2) + \int_0^t d\tau S_\tau^0(1,2) T_+(1,2) S_{t-\tau}^0(1,2) \tag{2.56}$$

with $S_t^0 = \exp(tL_0)$ the free flow operator and a collision operator

$$T_+(1,2) = \sigma^2 \int_{\mathbf{V}_{12}\cdot\hat{\mathbf{n}}<0} d\hat{\mathbf{n}} |\mathbf{V}_{12}\cdot\hat{\mathbf{n}}| \delta(\sigma\hat{\mathbf{n}} - (\mathbf{r}_1 - \mathbf{r}_2))(b_c - 1) \tag{2.57}$$

where b_c is a substitution operator that replaces $\mathbf{v}_1, \mathbf{v}_2$ with $\mathbf{v}_1', \mathbf{v}_2'$ (see Eqs. (2.53)).

The Eq. (2.56) is a representation of the evolution of two particles as a convolution of free flow and collisional events. Noting that $T_+(1,2)S_\tau^0(1,2)T_+(1,2) = 0$ for $\tau > 0$ (two hard spheres cannot collide more than once), Eq. (2.56) can be put in the form

$$S_t(1,2) = \exp\{t[L_0(1,2) + T_+(1,2)]\} \tag{2.58}$$

that can be generalized to the N-particle streaming operator (here considered for the case of an infinite volume):

$$S_{\pm t}(\mathbf{z}) = \exp\left\{\pm t[L_0(\mathbf{z}) \pm \sum_{i<j} T_\pm(i,j)]\right\} \tag{2.59}$$

where

$$T_-(1,2) = \sigma^2 \int_{\mathbf{V}_{12}\cdot\hat{\mathbf{n}}>0} d\hat{\mathbf{n}} |\mathbf{V}_{12}\cdot\hat{\mathbf{n}}| \delta(\mathbf{r}_1 - \mathbf{r}_2 - \sigma\hat{\mathbf{n}})(b_c - 1) \tag{2.60}$$

Equation (2.59) defines the so-called *pseudo-streaming operator*. In order to write an analogue of the Liouville Equation (2.51), the adjoint of $S_{\pm t}$ is needed: its definition is identical to that in Eq. (2.59) but for the binary collision operators which must be replaced by their adjoints:

$$\overline{T}_\pm(1,2) = \sigma^2 \int_{\mathbf{V}_{12}\cdot\hat{\mathbf{n}} \lessgtr 0} d\hat{\mathbf{n}} |\mathbf{V}_{12}\cdot\hat{\mathbf{n}}| [\delta(\mathbf{r}_1 - \mathbf{r}_2 - \sigma\hat{\mathbf{n}})b_c - \delta(\mathbf{r}_1 - \mathbf{r}_2 + \sigma\hat{\mathbf{n}})] \tag{2.61}$$

Finally the pseudo-Liouville equation can be written:

$$\frac{\partial}{\partial t}P(\mathbf{z},t) = \left(-\sum_i L_i^0 + \sum_{i<j} \overline{T}_-(ij) \right) P(\mathbf{z},t). \tag{2.62}$$

This equation is the analogue of Eq. (2.51) for the case of hard core potential (hard spheres). In this sense it replaces Eq. (2.55) and will be used in the following, precisely in paragraph 2.2.7, to derive kinetic equations different from the ones discussed just below.

2.2.2 The BBGKY hierarchy

We define the reduced (marginal) probability densities P_s as

$$P_s(\mathbf{r}_1,\mathbf{v}_1,\mathbf{r}_2,\mathbf{v}_2,...,\mathbf{r}_s,\mathbf{v}_s,t) = \int_{\Omega^{N-s}\times\Re^{3(N-s)}} P(\mathbf{r}_1,\mathbf{v}_1,\mathbf{r}_2,\mathbf{v}_2,...,\mathbf{r}_N,\mathbf{v}_N,t) \prod_{j=s+1}^{N} d\mathbf{r}_j d\mathbf{v}_j \tag{2.63}$$

In order to derive an evolution equation for P_s the first step is to integrate Eq. (2.55) with respect to the variables $\mathbf{r}_j$ and $\mathbf{v}_j$ $(s+1 \le j \le N)$ over $\Omega^{N-s}\times\Re^{3(N-s)}$, obtaining:

$$\frac{\partial P_s}{\partial t} + \sum_{i=1}^{s}\int_{\Lambda_s} \mathbf{v}_i \cdot \frac{\partial P}{\partial \mathbf{r}_i} \prod_{j=s+1}^{N} d\mathbf{r}_j d\mathbf{v}_j + \sum_{k=s+1}^{N}\int_{\Lambda_s} \mathbf{v}_k \cdot \frac{\partial P}{\partial \mathbf{r}_k} \prod_{j=s+1}^{N} d\mathbf{r}_j d\mathbf{v}_j = 0 \tag{2.64}$$

where the integration space Λ_s extends to the entire $\Re^{3(N-s)}$ for the velocity variables, while it extends to Ω^{N-s} deprived of the spheres $|\mathbf{r}_i - \mathbf{r}_j| < \sigma$ $(i = 1,...,N, i \ne j)$ with respect to the position variables.

The typical term in the first sum contains the integral of a derivative with respect to a variable $\mathbf{r}_i$ over which one does not integrate, but in the exchange of order between integration and derivation one must take into account the domain boundaries which depend on $\mathbf{r}_i$, writing:

$$\int_{\Lambda_s} \mathbf{v}_i \cdot \frac{\partial P}{\partial \mathbf{r}_i} \prod_{j=s+1}^{N} d\mathbf{r}_j d\mathbf{v}_j = \mathbf{v}_i \cdot \frac{\partial P_s}{\partial \mathbf{r}_i} - \sum_{k=s+1}^{N}\int_{\Lambda_s} P_{s+1}\mathbf{v}_i \cdot \hat{\mathbf{n}}_{ik} d\sigma_{ik} d\mathbf{v}_k \tag{2.65}$$

where $\hat{\mathbf{n}}_{ik}$ is the outer normal to the sphere $|\mathbf{r}_i - \mathbf{r}_k| = \sigma$, $d\sigma_{ik}$ is the surface element on the same sphere and P_{s+1} has k as its $(s+1)-th$ index.

The typical term in the second sum in Eq. (2.64) can be immediately integrated by means of the Gauss theorem, since it involves the integration of a derivative taken with respect to one of the integration variables (and assuming that the boundary of Ω is a specular reflecting wall or a periodical boundary condition):

$$\int_{\Lambda_s} \mathbf{v}_k \cdot \frac{\partial P}{\partial \mathbf{r}_k} \prod_{j=s+1}^{N} d\mathbf{r}_j d\mathbf{v}_j$$
$$= \sum_{i=1}^{s}\int P_{s+1}\mathbf{v}_k \cdot \hat{\mathbf{n}}_{ik} d\sigma_{ik} d\mathbf{v}_k + \sum_{i=s+1, i\ne k}^{N}\int P_{s+2}\mathbf{v}_k \cdot \hat{\mathbf{n}}_{ik} d\sigma_{ik} d\mathbf{v}_k d\mathbf{r}_i d\mathbf{v}_i \tag{2.66}$$

The last term in the above equation, when summed over $s+1 \le k \le N$ vanishes: this fact directly stems from the equivalence (2.55b) (we do not enter in the few steps of this simple proof). Moreover, in both above equations the integral containing the term P_{s+1} is the same no matter what the value of the dummy index k is, so that we can drop the index and write $\mathbf{r}_*, \mathbf{v}_*$ instead of $\mathbf{r}_k, \mathbf{v}_k$.

As a matter of fact, Eq. (2.64) finally reads:

$$\frac{\partial P_s}{\partial t} + \sum_{i=1}^{s} \mathbf{v}_i \cdot \frac{\partial P_s}{\partial \mathbf{r}_i} = (N-s)\sum_{i=1}^{s}\int P_{s+1}\mathbf{V}_i \cdot \hat{\mathbf{n}}_i d\sigma_i d\mathbf{v}_* \tag{2.67}$$

where $\mathbf{V}_i = \mathbf{v}_i - \mathbf{v}_*$, $\hat{\mathbf{n}}_i = (\mathbf{r}_i - \mathbf{r}_*)/\sigma$ and the arguments of P_{s+1} are $(\mathbf{r}_1, \mathbf{v}_1, \mathbf{r}_2, \mathbf{v}_2, ..., \mathbf{r}_s, \mathbf{v}_s, \mathbf{r}_*, \mathbf{v}_*, t)$. Integrations in Eq. (2.67) are performed over the 1-particle velocity space $\Re^3$ and over the sphere S^i (given by the condition $|\mathbf{r}_i - \mathbf{r}_*| = \sigma$) with surface elements $d\sigma_i$.

Eq. (2.67) states that the evolution of the reduced probability density P_s is governed by the free evolution operator of the s-particles dynamics, which appears in the left hand side, with corrections due to the effect of the interaction with the remaining $(N - s)$ particle. The effect of this interaction is described by the right-hand side of this equation.

Usually Eq. (2.67) is written in a different form, obtained using some symmetries of the problem. In particular one can separate the sphere S^i of integration in the right-hand side, in the two hemispheres S^i_+ and S^i_- defined respectively by $\mathbf{V_i} \cdot \hat{\mathbf{n}}_i > 0$ and $\mathbf{V_i} \cdot \hat{\mathbf{n}}_i < 0$ (considering also that $d\sigma_i = \sigma^2 d\hat{\mathbf{n}}_i$):

$$\int P_{s+1} \mathbf{V}_i \cdot \hat{\mathbf{n}}_i d\sigma_i d\mathbf{v}_* = \sigma^2 \int_{\Re^3} \int_{S^i_+} P_{s+1} |\mathbf{V}_i \cdot \hat{\mathbf{n}}_i| d\hat{\mathbf{n}}_i d\mathbf{v}_* - \sigma^2 \int_{\Re^3} \int_{S^i_-} P_{s+1} |\mathbf{V}_i \cdot \hat{\mathbf{n}}_i| d\hat{\mathbf{n}}_i d\mathbf{v}_* \quad (2.68)$$

and observe that in the S^i_+ integration are included all phase space points such that particle i and particle $*$ (the $(s+1) - th$ generic particle) are coming out from a collision: this means that on the sphere S^i_+ we can write the substitution

$$P_{s+1}(\mathbf{r}_1, \mathbf{v}_1, ..., \mathbf{r}_i, \mathbf{v}_i, ...\mathbf{r}_s, \mathbf{v}_s, \mathbf{r}_i - \sigma\hat{\mathbf{n}}_i, \mathbf{v}_*)$$
$$\rightarrow P_{s+1}(\mathbf{r}_1, \mathbf{v}_1, ..., \mathbf{r}_i, \mathbf{v}_i - \hat{\mathbf{n}}_i(\hat{\mathbf{n}}_i \cdot \mathbf{V}_i), ...\mathbf{r}_s, \mathbf{v}_s, \mathbf{r}_i - \sigma\hat{\mathbf{n}}_i, \mathbf{v}_* + \hat{\mathbf{n}}_i(\hat{\mathbf{n}}_i \cdot \mathbf{V}_i)). \quad (2.69)$$

Moreover we can make the change of variable in the second integral (that on the sphere S^i_-) $\hat{\mathbf{n}}_i \rightarrow -\hat{\mathbf{n}}_i$ which only changes the integration range $S^i_- \rightarrow S^i_+$. Finally, replacing $\hat{\mathbf{n}}_i$ with simply $\hat{\mathbf{n}}$ (and therefore $S^i_+ \rightarrow S_+$) we have:

$$\frac{\partial P_s}{\partial t} + \sum_{i=1}^{s} \mathbf{v}_i \cdot \frac{\partial P_s}{\partial \mathbf{r}_i} = (N - s)\sigma^2 \sum_{i=1}^{s} \int_{\Re^3} \int_{S_+} (P'_{s+1} - P_{s+1}) |\mathbf{V}_i \cdot \hat{\mathbf{n}}| d\hat{\mathbf{n}} d\mathbf{v}_* \quad (2.70)$$

where we have defined

$$P'_{s+1} = P_{s+1}(\mathbf{r}_1, \mathbf{v}_1, ..., \mathbf{r}_i, \mathbf{v}_i - \hat{\mathbf{n}}_i(\hat{\mathbf{n}}_i \cdot \mathbf{V}_i), ...\mathbf{r}_s, \mathbf{v}_s, \mathbf{r}_i - \sigma\hat{\mathbf{n}}_i, \mathbf{v}_* + \hat{\mathbf{n}}_i(\hat{\mathbf{n}}_i \cdot \mathbf{V}_i)) \quad (2.71)$$

The system of equations (2.70) is usually called the BBGKY hierarchy for the hard sphere gas [60, 61].

2.2.3 The Boltzmann hierarchy and the Boltzmann equation

In a rarefied gas N is a very large number and σ is very small; let us say, to fix ideas, that we have a box whose volume is $1 \quad cm^3$ at room temperature and atmospheric pressure. Then $N \simeq 10^{20}$ and $\sigma \simeq 10^{-8} cm$ and (from Eq. (2.70)) for small s we have $(N - s)\sigma^2 \simeq N\sigma^2 \simeq 1m^2$; at the same time the difference between $\mathbf{r}_i$ and $\mathbf{r}_i + \sigma\hat{\mathbf{n}}$ can be neglected and the volume occupied by the particles ($N\sigma^3 \simeq 10^{-4} cm^3$) is very small so that the collision between two selected particles is a rather rare event. In this spirit, the Boltzmann-Grad limit has been suggested as a procedure to obtain a closure for Eq. (2.70): $N \rightarrow \infty$ and $\sigma \rightarrow 0$ in such a way that $N\sigma^2$ remains finite. We stress the fact that (as seen in section 2.1.2) the total number of collisions in the unit of time is given by the total scattering cross section multiplied by N, which for a system of hard spheres gives $N\pi\sigma^2$. The Boltzmann-Grad limit, therefore, states that the single particle collision probability must vanish, but the total number of collisions remains of order 1.

Within this limit, the BBGKY hierarchy reads:

$$\frac{\partial P_s}{\partial t} + \sum_{i=1}^{s} \mathbf{v}_i \cdot \frac{\partial P_s}{\partial \mathbf{r}_i} = N\sigma^2 \sum_{i=1}^{s} \int_{\Re^3} \int_{S_+} (P'_{s+1} - P_{s+1}) |\mathbf{V}_i \cdot \hat{\mathbf{n}}| d\hat{\mathbf{n}} d\mathbf{v}_* \quad (2.72)$$

where the arguments of P'_{s+1} and of P_{s+1} are the same as above, except that the position of the $(s+1)-th$ particle ($\mathbf{r}'_*$ and $\mathbf{r}_*$) is equal to $\mathbf{r}_i$ (as $\sigma \to 0$). Eq. (2.72) gives a complete description of the time evolution of a Boltzmann gas (i.e. the ideal gas obtained in the Boltzmann-Grad limit), usually called *the Boltzmann hierarchy*.

Finally the Boltzmann equation is obtained if the *molecular chaos assumption* is taken into account:

$$P_2(\mathbf{r}_1, \mathbf{v}_1, \mathbf{r}_2, \mathbf{v}_2, t) = P_1(\mathbf{r}_1, \mathbf{v}_1) P_1(\mathbf{r}_2, \mathbf{v}_2) \tag{2.73}$$

for particles that are about to collide (that is when $\mathbf{r}_2 = \mathbf{r}_1 - \sigma\hat{\mathbf{n}}$ and $\mathbf{V}_{12} \cdot \hat{\mathbf{n}} < 0$). This assumption naturally stems from the Boltzmann-Grad limit, as it is reasonable that, in the limit of vanishing single-particle collision rate, two colliding particles are uncorrelated. The lack of correlation of colliding particles is the essence of the molecular chaos assumption. We underline that nothing is said about correlation of particles that have just collided.

With the assumption (2.73) we can rewrite the first equation of the hierarchy (2.72), omitting the $_1$ subscript for simplicity:

$$\frac{\partial P(\mathbf{r}, \mathbf{v})}{\partial t} + \mathbf{v} \cdot \frac{\partial P(\mathbf{r}, \mathbf{v})}{\partial \mathbf{r}} = N\sigma^2 \int_{\Re^3} \int_{S_+} (P(\mathbf{r}, \mathbf{v}') P(\mathbf{r}, \mathbf{v}'_*) - P(\mathbf{r}, \mathbf{v}) P(\mathbf{r}, \mathbf{v}_*)) |\mathbf{V} \cdot \hat{\mathbf{n}}| d\mathbf{v}_* d\hat{\mathbf{n}} \tag{2.74}$$

with $\mathbf{v}' = \mathbf{v} - \hat{\mathbf{n}}(\mathbf{V} \cdot \hat{\mathbf{n}})$, $\mathbf{v}'_* = \mathbf{v}_* + \hat{\mathbf{n}}(\mathbf{V} \cdot \hat{\mathbf{n}})$, $\mathbf{V} = \mathbf{v} - \mathbf{v}_*$. This represents the Boltzmann equation for hard spheres. We also observe that the integral in Eq. (2.74) is extended to the hemisphere S_+ but could be equivalently extended to the entire sphere S^2 provided a factor $1/2$ is inserted in front of the integral itself, as changing $\hat{\mathbf{n}} \to -\hat{\mathbf{n}}$ does not change the integrand.

From a rigorous point of view [58], the molecular chaos has to be assumed and cannot be proved. However it has been demonstrated that if the Boltzmann hierarchy has a unique solution for data that satisfy for $t = 0$ a generalized form of chaos assumption:

$$P_s(\mathbf{r}_1, \mathbf{v}_1, ..., \mathbf{r}_s, \mathbf{v}_s, t) = \prod_{j=1}^{s} P_1(\mathbf{r}_j, \mathbf{v}_j, t) \tag{2.75}$$

than Eq. (2.75) holds at any time and therefore the Boltzmann equation is fully justified. Otherwise it has also been proved that if Eq. (2.75) is satisfied at $t = 0$ and the Boltzmann equation (2.74) admits a solution for the given initial data, then the Boltzmann hierarchy (2.72) has at least a solution which satisfy (2.75) at any time t.

2.2.4 Collision invariants, H-theorem and hydrodynamical limit

The integral appearing in the right-hand side of Eq. (2.74) is usually called collision integral:

$$Q(P, P) = \int_{\Re^3} \int_{S_+} (P'P'_* - PP_*) |\mathbf{V} \cdot \hat{\mathbf{n}}| d\mathbf{v}_* d\hat{\mathbf{n}} \tag{2.76}$$

where we have used an intuitive contracted notation (the prime or $*$ must be considered applied to the velocity vector in the argument of the function P). In the collision integral, the position $\mathbf{r}$ is the same wherever the function P appears, and therefore it can be considered a parameter of $Q(P, P)$.

Let us have a look to the integral

$$\int_{\Re^3} Q(P, P) \phi(\mathbf{v}) d\mathbf{v} = \int_{\Re^3} \int_{\Re^3} \int_{S_+} (P'P'_* - PP_*) \phi(\mathbf{v}) |\mathbf{V} \cdot \hat{\mathbf{n}}| d\mathbf{v}_* d\hat{\mathbf{n}} d\mathbf{v} \tag{2.77}$$

which can be transformed in many alternative forms, using its symmetries. In particular one can exchange primed and unprimed quantities, as well as starred and unstarred quantities. With manipulations of this sort, it is immediate to get the following alternative form of Eq. (2.77):

$$\int_{\Re^3} Q(P, P) \phi(\mathbf{v}) d\mathbf{v} = \frac{1}{8} \int_{\Re^3} \int_{\Re^3} \int_{S_+} (P'P'_* - PP_*)(\phi + \phi_* - \phi' - \phi'_*) |\mathbf{V} \cdot \hat{\mathbf{n}}| d\mathbf{v}_* d\hat{\mathbf{n}} \phi(\mathbf{v}) d\mathbf{v} \tag{2.78}$$

From this equation it comes that if

$$\phi + \phi_* = \phi' + \phi'_* \tag{2.79}$$

almost everywhere in velocity space, then the integral of Eq. (2.78) is zero independent of the particular function P. Many authors have proved under different assumptions that the most general solution of Eq. (2.79) is given by

$$\phi(\mathbf{v}) = C_1 + \mathbf{C}_2 \cdot \mathbf{v} + C_3|\mathbf{v}|^2 \tag{2.80}$$

Furtherly, if $\phi = \log P$, from Eq. (2.78) it follows that

$$\int_{\Re^3} Q(P,P)\phi(\mathbf{v})d\mathbf{v} = \frac{1}{8}\int_{\Re^3}\int_{\Re^3}\int_{S_+}(P'P'_* - PP_*)\log(PP_*/P'P'_*)|\mathbf{V}\cdot\hat{\mathbf{n}}|d\mathbf{v}_* d\hat{\mathbf{n}}\phi(\mathbf{v})d\mathbf{v} \leq 0 \tag{2.81}$$

which follows from the elementary inequality $(z-y)\log(y/z) \leq 0$ if $y, z \in \Re^+$. This becomes an equality if and only if $y = z$, therefore the equality sign holds in Eq. (2.81) if and only if

$$P'P'_* = PP_* \tag{2.82}$$

This is equivalent to two important facts:

- $\phi + \phi_* = \phi' + \phi'_*$ (taking the logarithms of both sides of Eq. (2.82)), so that we can use the result (2.80) obtaining $P = \exp(C_1 + C_2 \cdot \mathbf{v} + C_3|\mathbf{v}|^2) = C_0\exp(-\beta|\mathbf{v} - \mathbf{v}_0|^2)$ where we have defined $C_0 = \exp(C_1)$, $\beta = -C_3$ and $\mathbf{v}_0 = \mathbf{C}_2/2\beta$; this function is called Maxwell-Boltzmann distribution or simply Maxwellian;
- $Q(P,P) \equiv 0$, i.e. the collision integral identically vanishes.

Equation (2.81) is a fundamental result of the Boltzmann theory (it is often called Boltzmann Inequality) and can be fully appreciated with the following discussion: we rewrite the Boltzmann Equation (2.74) with a simplified notation:

$$\frac{\partial P}{\partial t} + \mathbf{v}\cdot\frac{\partial P}{\partial \mathbf{r}} = N\sigma^2 Q(P,P). \tag{2.83}$$

We multiply both sides by $\phi = \log P$ and integrate with respect to $\mathbf{v}$, obtaining a transport equation for the quantity ϕ:

$$\frac{\partial H}{\partial t} + \frac{\partial}{\partial \mathbf{r}}\cdot\mathbf{j}_H = S_H \tag{2.84a}$$

$$H = \int_{\Re^3} P\log P d\mathbf{v} \tag{2.84b}$$

$$\mathbf{j}_H = \int_{\Re^3} \mathbf{v}P\log P d\mathbf{v} \tag{2.84c}$$

$$S_H = N\sigma^2\int_{\Re^3}\log PQ(P,P)d\mathbf{v}. \tag{2.84d}$$

Then Eq. (2.81) states that $S_H \leq 0$ and $S_H = 0$ if and only if P is a Maxwellian. For example, if we look for a space homogeneous solution of the Boltzmann equation, it happens that

$$\frac{\partial H}{\partial t} = S_H \leq 0 \tag{2.85}$$

that is the famous H-Theorem. It simply states that there exists a macroscopic quantity (H in this case) that decreases as the gas evolves in time and eventually goes to zero when (if and only

if) the distribution P becomes a Maxwellian. When the homogeneity is not achievable (due to non-homogeneous boundary conditions) rigorous results are more complicated, but we are still tempted to say that the Maxwellian represents the local asymptotic equilibrium, with the spatial dependence carried by the parameters of this distribution function.

The H-Theorem shows that the Boltzmann equation, apparently obtained from microscopic reversible principles, has a basic feature of irreversibility: the trajectories in the phase space that corresponds to evolutions of the one-particle probability distribution that give place to an increase of H with time are not solutions of the Boltzmann equation, even if they are compatible with the given collision rules, i.e. with the laws of Newtonian mechanics. This paradox [207, 142] is nowadays discussed in the following way [61]: the assumption of Molecular Chaos is the source of irreversibility, the choice of factorization of probability for molecules that go *into* a collision induces correlations for the molecules that go *out of* a collision. If the velocity of all the molecules would be inverted at a certain time, the one particle probability distribution would no more satisfy the Molecular Chaos hypothesis and the Boltzmann equation could not describe the system. In general "no kind of irreversibility cam follow by correct mathematics from the analytical dynamics of a conservative system" (Cercignani et al. [61]). The other paradox often cited as a consequence of the H-Theorem is the so-called Zermelo's paradox [180, 227]: Zermelo noted that the "recurrence theorem" of Poincare [179] is in contrast with the H-Theorem. The recurrence theorem guarantees that the molecules of the gas, after a "recurrence time", can have positions and velocities so close to the initial ones that the one particle distribution would be practically the same, that is if it decreased initially, then it must have increased ad some later time. The answer of Boltzmann [35] to this objection is that the recurrence time is so large that, practically speaking, one would never observe a significant portion of the recurrence cycle. From a rigorous point of view, the Boltzmann-Grad limit ($N \to \infty$) guarantees that the Poincare recurrence theorem cannot be applied, as it works for a compact set: the recurrence time is expected to go to infinity.

Solutions of the Boltzmann equation in the form of a Maxwellian distribution with space dependent parameters (in the case of a steady solution, i.e. $\partial/\partial t = 0$) or space-time dependent parameters (in the dynamic case) can be found. The equations that govern the space-time evolution of the parameters of the Maxwellian are the Euler equations (see section 2.3.4). The Euler equations are based on a very important assumption, usually called *hydrodynamical limit*. If we solve the Boltzmann equation in a box of side ϵ^{-1} we obtain a solution $P_\epsilon(\mathbf{r}, \mathbf{v})$. If we enlarge the box (i.e. ϵ is reduced toward zero), while keeping the total number of particles proportional to the volume of the box, then the solution P_ϵ will assume a ϵ-dependent form. In order to regard the linear size of the box as being of order unity, we may rescale the space-time variables: $\rho = \epsilon\mathbf{r}$, $\tau = \epsilon t$, $\hat{P}(\rho, \mathbf{v}, \tau) = P(\mathbf{r}, \mathbf{v}, t)$. With this new variables, the mean free path (that is of order unity on the $\mathbf{r}$ scale) becomes of order ϵ. The distribution $\hat{P}$ solves a different Boltzmann equation in the new variables:

$$\frac{\partial \hat{P}}{\partial \tau} + \mathbf{v} \cdot \frac{\partial \hat{P}}{\partial \rho} = \epsilon^{-1} N\sigma^2 Q(\hat{P}, \hat{P}) \tag{2.86}$$

As the term $N\sigma^2$ is of order unity (Boltzmann-Grad limit, taken before) we must require that $Q(\hat{P}, \hat{P})$ is of order ϵ so that we can take the limit $\epsilon \to 0$. In other words, the hydrodynamical limit is a change of the level of description from the *microscopic* to the *macroscopic* one: at the macroscopic level the average number of collisions ($\epsilon^{-1}N\sigma^2$) diverges and therefore we ask that the average effect of a single collision (given by Q) is very small. Then taking the hydrodynamical limit, we expect that $\hat{P}$ is close to a Maxwellian (as it is the only solution of the equation $Q = 0$). In other words, the possibility of a macroscopic description is strictly tied to the possibility of a *separation of scales*: at the microscopic scale the phenomena are very rapid, i.e. the distribution function rapidly "thermalizes" coming toward the Maxwellian, while at the macroscopic scale the evolution of the gas is viewed as a slow evolution of the space-time dependent parameters of the Maxwellian, given by the hydrodynamic equations. If the "thermalization" stated above is so rapid that the distribution function P is *always* a Maxwellian, at any instant t, then the fluid is considered *ideal* and it is governed by the Euler equations (see paragraph 2.3.4). Otherwise, the evolution toward the Maxwellian is somewhat a dissipative process (in the sense of its irreversibility): it is the aim of the kinetic theory of transport to describe

its behavior. Assumptions on the "closeness" to the Maxwellian gives, in last analysis, the well known Navier-Stokes equations for non-ideal fluids (see paragraph 2.3.7).

2.2.5 The Maxwell molecules

The collisional integral of Boltzmann equation for hard spheres, Eq. (2.76), contains a term $g = |\mathbf{V} \cdot \hat{\mathbf{n}}|$ which multiplies the probabilities of particles entering or coming out from a collision. In general the collisional integral must contain the differential collision rate $dR/D\Omega$ for particle coming at a certain relative velocity (in modulus g and direction $\hat{\mathbf{n}}$, or equivalently scattering angle χ centered in the solid angle $d\Omega$), which may be expressed in terms of the scattering cross section s (see for example Eq. (2.20)):

$$\frac{dR}{d\Omega} = gs(g,\chi) P_2(\mathbf{r}, \mathbf{r} + \sigma\hat{\mathbf{n}}, \mathbf{v}_1, \mathbf{v}_2, t) d\mathbf{v}_2 \tag{2.87}$$

We discussed in paragraph 2.1.2 the fact that the scattering cross section depends strongly on the kind of interaction between the molecules of the gas. For power law repulsive interaction potential $V(r) \sim r^{-(a-1)}$, the scattering angle χ depends on the relative energy $g^2/2$ and on the impact parameter b only through the combination $(g^2 b^{a-1})$ (see for example [59]). This means that there exists a function $\gamma(\chi)$ such that:

$$b = g^{-2/(a-1)} \gamma(\chi) \tag{2.88}$$

and this means that from relation (2.22) one obtains:

$$gs(g,\chi) \sim g^{1-4/(a-1)} \frac{\gamma(\chi)}{\sin\chi} \frac{d\gamma}{d\chi} \tag{2.89}$$

which holds in $d = 3$. The extension to generic dimension of the last equation is:

$$gs(g,\chi) \sim g^{1-2(d-1)/(a-1)} \frac{\gamma^{d-2}}{(\sin\chi)^{d-2}} \frac{d\gamma}{d\chi} \sim g^{1-2(d-1)/(a-1)} \alpha(\cos\chi) \tag{2.90}$$

Therefore when $a = 1 + 2(d-1)$ (i.e. $a = 5$ for $d = 3$ and $a = 3$ for $d = 2$) the collision rate $gs(g,\chi)$ *does not depend upon* g. This property defines the so-called Maxwell molecules [81]. Interaction with $a < 1 + 2(d-1)$ are called soft interactions (e.g. the electrostatic or gravitational interaction). Interactions with $a > 1 + 2(d-1)$ are called hard interactions. Hard spheres ($a \to \infty$) belongs to this set of interactions, with $gs(g,\chi) \sim g$. It has been also studied the Very Hard Particles model, which is characterized by $gs(g,\chi) \sim g^2$, which is not attainable with an inverse power potential, as it requires an interaction harder than the hard sphere interaction.

The obvious advantage of Maxwell molecules is that the Boltzmann equation greatly simplifies, as g does not appear in the collision integral. A further simplification of the Boltzmann equation came from Krook and Wu [129], who studied the Boltzmann equation of Maxwell molecules with an isotropic scattering cross-section, i.e $\alpha = const$, often called Krook and Wu model. A very large literature exists for linear and non-linear model-Boltzmann equations (for a review see [81]). The importance of the Maxwell molecules model is the possibility of obtaining solutions for it: the general method (extended to other model-Boltzmann equations) is to obtain an expansion in orthogonal polynomial where the expansion coefficients are polynomial moments of the solution distribution function. For Maxwell molecules the moments satisfy a recursive system of differential equations that can be solved sequentially. Given an initial distribution, one can solve the problem if the series expansion converges. Bobylev [32] has shown that if one searches for *similarity* solutions (i.e. solutions with scaling form $P(\mathbf{v},t) \equiv e^{-\alpha t} F(e^{-\alpha t}\mathbf{v})$), then the solution can be found solving a recursive system of algebraic equation.

The Maxwell molecules model has been subject of study also in the framework of the kinetic theory of granular gases. In section 5.3 we discuss this issue.

2.2.6 The Enskog correction

The Boltzmann-Grad limit (see paragraph 2.2.3) restricts the validity of the Boltzmann equation to rarefied gases. This conditions is necessary to consider valid the *Molecular Chaos* which states the independence of colliding particles. In principle, in fact, two colliding particles can be correlated due to an intersection of their collisional histories: one simple possibility is that they may have collided some time before or, alternatively, they may have collided with particles that have collided before. Moreover, the spatial extension of particles (i.e. the fact that they are not really pointlike) restricts the possibilities of motion and as a consequence the degree of independence (this is the so called *excluded volume effect*). All these kinds of correlations become relevant when the gas is not in the situation considered by the Boltzmann-Grad limit, that is when the gas is not rarefied but (either moderately or highly) dense.

The first approach to the problem of not rarefied gases was introduced by Enskog [62]: he did not consider the effects of velocity correlations due to common collisional histories, but simply added to the Boltzmann equation an heuristic correction to take into account short range correlations on positions only. In general the two-body probability distribution function can be written in terms of the one-body functions:

$$P_2(\mathbf{r}_1, \mathbf{v}_1, \mathbf{r}_2, \mathbf{v}_2, t) = g_2(\mathbf{r}_1, \mathbf{v}_1, \mathbf{r}_2, \mathbf{v}_2) P_1(\mathbf{r}_1, \mathbf{v}_1) P_1(\mathbf{r}_2, \mathbf{v}_2) \tag{2.91}$$

where g_2 is the pair correlation function. The Molecular Chaos assumption states that $g_2(\mathbf{r}_1, \mathbf{r}_1 + \sigma\hat{\mathbf{n}}, \mathbf{v}_1, \mathbf{v}_2) \equiv 1$.

In the Enskog theory the Molecular Chaos assumption is modified in the following way:

$$P_2(\mathbf{r}_1, \mathbf{v}_1, \mathbf{r}_1 + \sigma\hat{\mathbf{n}}, \mathbf{v}_2, t) = \Xi(\sigma, n(\mathbf{r}_1)) P_1(\mathbf{r}_1, \mathbf{v}_1) P_1(\mathbf{r}_1 + \sigma\hat{\mathbf{n}}, \mathbf{v}_2) \tag{2.92}$$

i.e. $g_2 \equiv \Xi(\sigma, n)$ for particles entering or coming out from a collision, and the existence of a well defined coarse-grained density $n(\mathbf{r}_1)$ is assumed. The term $\Xi(\sigma, n)$ becomes a multiplicative constant in front of the collisional integral $Q(P, P)$, giving place to the so-called Boltzmann-Enskog equation. Of course, in a general non-homogeneous situation, the density is a spatially and temporally non-uniform quantity which can be described by a macroscopic field: one may assume (as it is in kinetic theory) that this field changes slowly in space-time, so that the Boltzmann-Enskog equation can be locally solved with constant n as it was a Boltzmann equation with an effective total scattering cross section $\Xi(\sigma, n) N \sigma^2$.

For elastic hard disks or hard spheres, spatial correlations are described by the formulas of Carnahan and Starling [56]:

$$\Xi(\sigma, n) = \frac{1 - 7\phi/16}{(1-\phi)^2} \; (d = 2) \tag{2.93a}$$

$$\Xi(\sigma, n) = \frac{1 - \phi/2}{(1-\phi)^3} \; (d = 3) \tag{2.93b}$$

$$\tag{2.93c}$$

where ϕ is the solid fraction ($\phi = n\pi\sigma^2/4$ in $d = 2$, $\phi = n\pi\sigma^3/6$ in $d = 3$). This formula is expected to work well with solid fractions below ϕ_c, where a phase transition takes place [3], with $\phi_c = 0.675$ in $d = 2$.

The Enskog correction produces, for example, important corrections to the transport coefficients and to the pressure term in the hydrodynamic description (see paragraph 2.3.9).

.

2.2.7 The ring kinetics equations for hard spheres

The BBGKY hierarchy for hard spheres can be obtained by integration of the Eq. (2.62). Here we report the first two equations of the hierarchy derived in this way:

$$\left(\frac{\partial}{\partial t}+L_1^0\right)P_1(1)=\int d\mathbf{r}_2\int d\mathbf{v}_2\overline{T}_-(1,2)P_2(1,2) \tag{2.94a}$$

$$\left[\frac{\partial}{\partial t}+L_1^0+L_2^0-\overline{T}_-(1,2)\right]P_2(1,2)=\int d\mathbf{r}_3\int d\mathbf{v}_3[\overline{T}_-(1,3)+\overline{T}_-(2,3)]P_3(1,2,3) \tag{2.94b}$$

This set of equations is an open hierarchy which expresses the time evolution of the s-particle distribution function in terms of the $(s+1)$-th function.

Using again the Molecular Chaos assumption (Eq. (2.73)), the Boltzmann Equation (2.74) is immediately recovered from Eq. (2.94a).

Using the Enskog correction to the Molecular Chaos, Eq. (2.92), the Boltzmann-Enskog Equation is obtained.

As the density increases, the contributions of correlated collision sequences to the collision term become more and more important. At moderate densities, a simple way to take these correlations into account has been found in a cluster expansion of the $s-$particle distribution functions, defined recursively as

$$P_2(1,2)=P_1(1)P_1(2)+g_2(1,2) \tag{2.95a}$$

$$P_3(1,2,3)=P_1(1)P_1(2)P_1(3)+P_1(1)g_2(2,3)+P_1(2)g_2(1,3)+P_1(3)g_2(1,2)+g_3(1,2,3) \tag{2.95b}$$

etc., where $g_2(1,2)=P_2(1,2)-P_1(1)P_1(2)$ accounts for pair correlations, $g_3(1,2,3)$ for triplet correlations, etc. The molecular chaos assumption implies $g_2(1,2)=0$. The basic assumption to obtain the ring kinetic equations is that the pair correlations are dominant and higher order ones can be neglected, i.e. $g_3=g_4=...=0$ in the above cluster expansion. The ring kinetic equations, obtained in this way, read:

$$\left(\frac{\partial}{\partial t}+L_1^0\right)P_1(1)=\int d\mathbf{r}_2\int d\mathbf{v}_2\overline{T}_-(1,2)(P_1(1)P_1(2)+g_2(1,2)) \tag{2.96a}$$

$$\left[\frac{\partial}{\partial t}+L_1^0+L_2^0-\overline{T}_-(1,2)\right]g_2(1,2)-\left[(1+\mathcal{X}(1,2))\int d\mathbf{r}_3\int d\mathbf{v}_3\overline{T}_-(1,3)(1+\mathcal{X}(1,3))P_1(3)\right]g_2(1,2)$$
$$=\overline{T}_-(1,2)[P_1(1)P_1(2)+g_2(1,2)] \tag{2.96b}$$

with $\mathcal{X}(i,j)$ the operator that interchanges the particle labels i and j. With further algebra and approximation one can derive the generalized Boltzmann equation in ring approximation. We do not give here this derivation, as it is not the aim of this work to review the entire ring kinetic theory in details, but just to give its basic ideas (which are the binary collision expansion Eqs. (2.56) and the cluster expansion, Eqs. (2.95)).

.

2.2.8 The Boltzmann equation for granular gases

The binary collision operator $\overline{T}_-(1,2)$, for inelastic particles, must be changed [210] according to the inelastic collision rules, Eqs. (2.41) and Eqs. (2.42). It must be noted that when $r=1$ (elastic collisions), the two set of equations coincide, i.e. the direct or inverse collision are identical transformation. This is not true if $r<1$. Therefore, in the definition of the inverse binary collision operators at the end of section 2.2.1, that is $T_-(1,2)$ and $\overline{T}_-(1,2)$, we have put the same operator b_c that appears in the direct binary collision operators $T_+(1,2)$ and $\overline{T}_+(1,2)$, while in general it must be used the operator b_c' that replaces velocities with precollisional velocities (using the transformation given in Eqs. (2.42)). The adjoint of inverse binary inelastic collision operator(the only one needed in the following) therefore reads:

$$\overline{T}_-(1,2) = \sigma^2 \int_{\mathbf{V}_{12}\cdot\hat{\mathbf{n}}>0} d\hat{\mathbf{n}} |\mathbf{V}_{12}\cdot\hat{\mathbf{n}}| \left[\frac{1}{r^2}\delta(\mathbf{r}_1 - \mathbf{r}_2 - \sigma\hat{\mathbf{n}}) b_c' - \delta(\mathbf{r}_1 - \mathbf{r}_2 + \sigma\hat{\mathbf{n}}) \right] \tag{2.97}$$

Deriving from this the BBGKY hierarchy (analogue of (2.94)) and putting in the first equation of it the Molecular Chaos assumption, the Boltzmann Equation for granular gases is obtained [41, 210]:

$$\left(\frac{\partial}{\partial t} + L_1^0\right) P(\mathbf{r}_1, \mathbf{v}_1, t) = \sigma^2 \int d\mathbf{v}_2 \int_{\mathbf{V}_{12}\cdot\hat{\mathbf{n}}>0} d\hat{\mathbf{n}} |\mathbf{V}_{12}\cdot\hat{\mathbf{n}}| \times \left[\frac{1}{r^2} P(\mathbf{r}_1, \mathbf{v}_1', t) P(\mathbf{r}_1, \mathbf{v}_2', t) - P(\mathbf{r}_1, \mathbf{v}_1, t) P(\mathbf{r}_1, \mathbf{v}_2, t) \right] \tag{2.98}$$

where the primed velocities are defined in Eqs. (2.42).

This equation has been studied in the spatially homogeneous case (no spatial gradients, $L_1^0 = 0$), with the Enskog correction (i.e. a multiplying factor $\Xi(\sigma, n)$ in front of the collision integral) by Goldshtein and Shapiro [97] and by Ernst and van Noije [211]. The equation is

$$\frac{\partial}{\partial t} F(\mathbf{v}_1, t) = \Xi(\sigma, n)\sigma^2 \int d\mathbf{v}_2 \int_{\mathbf{V}_{12}\cdot\hat{\mathbf{n}}>0} d\hat{\mathbf{n}} |\mathbf{V}_{12}\cdot\hat{\mathbf{n}}| \times \left[\frac{1}{r^2} F(\mathbf{v}_1', t) F(\mathbf{v}_2', t) - F(\mathbf{v}_1, t) F(\mathbf{v}_2, t) \right] \tag{2.99}$$

where $F(\mathbf{v}, t) = \int d\mathbf{r} P(\mathbf{r}, \mathbf{v}, t)$. Goldshtein and Shapiro [97] have shown that this equation admits an isotropic scaling solution which describes the so-called "Homogeneous Cooling State", depending on time only through the temperature $T(t)$ defined by the relation $\frac{3}{2} n T(t) = \int d\mathbf{v} \frac{1}{2} m v^2 F(\mathbf{v}, t)$:

$$F(\mathbf{v}, t) = \frac{n}{v_0^3(t)} \overline{F}\left(\frac{v}{v_0(t)}\right) \tag{2.100}$$

with v_0 defined by the relation $T(t) = m v_0^2(t)/2$.

The scaling function solves a complicated integro-differential equation. This can be studied using an expansion in Sonine polynomials:

$$\overline{F}(\overline{v}) = f_0(\overline{v})[1 + a_2 S_2(\overline{v}^2) + ...] \tag{2.101}$$

where $\overline{v} = v/v_0(t)$, $f_0(\overline{v}) = \pi^{-3/2} \exp(-\overline{v}^2)$ is the Maxwellian and $S_2(x) = x^2/2 - 5x/2 + 15/8$ is the second Sonyne polynomial. The calculations of Ernst and van Noije [211] have shown that for $0.6 \leq r < 1$ the coefficient a_2 is very near to zero, precisely $|a_2| \leq 0.04$ in three dimensions and $|a_2| \leq 0.024$ in two dimensions. The decay of the temperature has also been calculated:

$$T(t) = \frac{T(0)}{(1 + \gamma t/t_0)^2} \tag{2.102}$$

with $\gamma = \gamma_0(1 + 3a_2/16)$ (dimensionless damping rate), $\gamma_0 = (1 - r^2)/2d$, and the initial Maxwellian mean free time $t_0 = 1/\omega_0(T)$ ($\omega_0(T)$ is the collision frequency calculated with a Maxwellian with temperature T), while the true collision frequency reads $\omega(T) = \omega_0(T)(1 - a_2/16)$. Monte Carlo simulations (DSMC, see Appendix A) by Brey et al. [42] of the Eq. (2.99) have shown that the temperature decay and the fourth cumulant a_2 qualitatively agree with the results of Ernst and van Noije. Moreover the agreement between very dilute Molecular Dynamics simulations and Monte Carlo solutions of the Boltzmann equation in 2D have shown agreement up to moderate inelasticities ($r \geq 0.7$).

Ernst and van Noije [211] have also given estimates for the tails of the velocity distribution, using an asymptotic method employed by Krook and Wu [129]. This method assumes that for a fast particle

the dominant contributions to the collision integral come from collisions with thermal (bulk) particles and that the gain term of the integral can be neglected with respect to the loss term. They found an exponential behavior for the tails of the scaling distribution function of velocities:

$$\overline{f}(\overline{v}) \sim \exp(-\beta_1 c) \tag{2.103}$$

with β_1 a constant depending on r.

It is relevant that Ernst and van Noije have also studied Enskog-Boltzmann equation in the presence of a *random forcing*, i.e. a source of energy that acts randomly, uncorrelated and isotropically on all the particles. The homogeneous equation for this system reads:

$$\frac{\partial}{\partial t}F(\mathbf{v}_1,t) = \Xi(\sigma,n)\sigma^2 \int d\mathbf{v}_2 \int_{\mathbf{V}_{12}\cdot\hat{\mathbf{n}}>0} d\hat{\mathbf{n}}|\mathbf{V}_{12}\cdot\hat{\mathbf{n}}| \times \left[\frac{1}{r^2}F(\mathbf{v}_1',t)F(\mathbf{v}_2',t) - F(\mathbf{v}_1,t)F(\mathbf{v}_2,t)\right] + \frac{\xi_0^2}{2}\left(\frac{\partial}{\partial \mathbf{v}_1}\right)^2 F(\mathbf{v}_1,t) \tag{2.104}$$

where the velocity diffusion coefficient ξ_0^2 appears, which is proportional to the rate of energy input per unit mass $\frac{3}{2}\xi_0^2$. This equation admits a stationary homogeneous solution $F_S(\mathbf{v}) = (n/v_0^3)\overline{F}(v/v_0)$ with v_0 defined as above in terms of the granular temperature T. It is immediate to obtain a temperature balance

$$\frac{dT}{dt} = m\xi_0^2 - 2\gamma\omega_0 T. \tag{2.105}$$

From Eq. (2.105) follows the value for the stationary temperature (if the system remains homogeneous!). The authors have also given estimates for the coefficient a_2 of the Sonine expansion. Molecular dynamics by van Noije et al. [211] have shown that the predictions of the homogeneous Boltzmann equation work for $r \geq 0.7$ and low densities. The Krook and Wu method for the asymptotic behavior of the tails of the velocity distribution.function gives

$$\overline{f}(\overline{v}) \sim \exp(-\beta_2 c^{3/2}). \tag{2.106}$$

2.3 The hydrodynamical limit

The Boltzmann equation, when the gas is out of equilibrium, is an hard mathematical problem which is unresolved apart from very exceptional situations. The kinetic theory of non-uniform elastic gases near equilibrium, mainly due to Sydney Chapman and David Enskog [62], has been successful in establishing a method to derive the transport coefficients from the Boltzmann equation, obtaining closed hydrodynamic equations. It is interesting to mention that the first non-equilibrium solutions of the Boltzmann equation were presented by Enskog in his Ph.D thesis [80], defended in 1917 at the University of Uppsala, Sweden. In the late 40s H. Grad [99] developed an alternative mathematically equivalent method to obtain the same results. In this section we review the main passages of the kinetic theory of non-equilibrium elastic gases in order to have a reference frame for the next section, where the granular kinetics will be presented.

2.3.1 The phase space distribution function and its moments

We assume that a phase space distribution function can be defined:

$$N(t,\mathbf{r},\mathbf{v}) = P(t,\mathbf{r},\mathbf{v})d^3r d^3v \tag{2.107}$$

where $N(t,\mathbf{r},\mathbf{v})$ is the number of particles found at time t near the point $\mathbf{r},\mathbf{v}$ of the phase space. P is assumed to be the solution of the Boltzmann Equation (2.74).

The particle number density is defined as

$$n(t,\mathbf{r}) = \iiint_{\infty} d^3v P(t,\mathbf{r},\mathbf{v}) \tag{2.108}$$

The average molecular velocity is defined as

$$\mathbf{u}(t,\mathbf{r}) = \frac{1}{n(t,\mathbf{r})}\iiint_{\infty} d^3v \mathbf{v} P(t,\mathbf{r},\mathbf{v}) \tag{2.109}$$

and this allows to introduce the random velocity vector

$$\mathbf{c}(t,\mathbf{r}) = \mathbf{v} - \mathbf{u}(t,\mathbf{r}) \tag{2.110}$$

which depends on time and position (while $\mathbf{v}$ is independent of t and $\mathbf{r}$) and has zero average:

$$\iiint_{\infty} d^3c c_i P(t,\mathbf{r},\mathbf{c}) = 0 \tag{2.111}$$

The average fluxes of the molecular quantity $W(\mathbf{v})$ can be expressed as velocity moments of the phase space distribution function:

$$j^i_W(t,\mathbf{r}) = \iiint_{\infty} d^3v v_i W(\mathbf{v}) P(t,\mathbf{r},\mathbf{v}) \tag{2.112}$$

When $W = m$ one has the mass flux:

$$j^i_m = mn(t,\mathbf{r})u_i(t,\mathbf{r}). \tag{2.113}$$

When $W = mv_j$ one has the momentum flux:

$$j^i_{mv_j} = mn(t,\mathbf{r})\langle v_i v_j\rangle = mnu_iu_j + mn\langle c_ic_j\rangle \tag{2.114}$$

which is a 3×3 symmetric matrix. In the last form two contributions can be recognized, that is the flux due to the bulk (organized) motion and the flux resulting from the random (thermal) motion of the gas particles. This second term is usually called the *pressure tensor* $\mathcal{P}_{ij} = mn\langle c_ic_j\rangle$. One can

define, from this discussion, two quantities that are the *scalar pressure* p and the *vector temperature* T_i:

$$p = \frac{1}{3}(\mathcal{P}_{xx} + \mathcal{P}_{yy} + \mathcal{P}_{zz}) \tag{2.115}$$

$$\frac{1}{2}k_B T_i = \frac{1}{2}m\langle c_i^2 \rangle = \frac{1}{2}\frac{\mathcal{P}_{ii}}{n} \tag{2.116}$$

and in the isotropic case $T_i = T$ so that $p = nk_BT$. It can be also defined the stress tensor $\mathcal{T}$ as:

$$\mathcal{T}_{ij} = \delta_{ij}p - \mathcal{P}_{ij} \tag{2.117}$$

which expresses the deviation of the pressure tensor from the equilibrium Maxwellian case (for which $\mathcal{P}_{ij} = p\delta_{ij}$).

Finally, the flux of the quantity $W = mv_jv_k$ is given by:

$$j^i_{mv_jv_k} = mnu_iu_ju_k + u_i\mathcal{P}_{jk} + u_j\mathcal{P}_{ik} + u_k\mathcal{P}_{ij} + \mathcal{Q}_{ijk} \tag{2.118}$$

where $\mathcal{Q}_{ijk} = mn\langle c_ic_jc_k \rangle$ is the generalized heat flow tensor and describes the transport of random energy c_jc_k due to thermal motion c_i of the molecules (for all the permutations of i, j, k).

In equation (2.118) three contributions can be recognized: the first term describes the bulk transport of the bulk flux of momentum; the second, third and fourth terms describe the a combination of bulk and random momentum fluxes; the last term is the transport of random energy component due to the random motion itself. Often a "classical" heat flow vector is introduced, more intuitive than the generalized heat flow tensor:

$$q_i = \frac{\mathcal{Q}_{ikk}}{2} = n\left\langle c_i\frac{mc^2}{2}\right\rangle. \tag{2.119}$$

It is also of use to give the definition of the fourth velocity moment:

$$\mathcal{R}_{ijkl}(t, \mathbf{r}) = mn\langle c_ic_jc_kc_l \rangle \tag{2.120}$$

2.3.2 The Maxwell equation

The evolution of the quantity $W(\mathbf{v})$ is obtained by multiplying both sides of the Boltzmann equation, Eq. (2.74), by W and integrating over $\mathbf{v}$. Here we consider a molecular quantity that is function of the random velocity, i.e. $W(\mathbf{c})$, obtaining (after some algebra, mainly integrations by parts) the following equation [62, 98]:

$$\begin{aligned} &\frac{\partial(n\langle W\rangle)}{\partial t} + \frac{\partial(n\langle W\rangle u_i)}{\partial r_i} + \frac{\partial(n\langle c_iW\rangle)}{\partial r_i} \\ &+n\left\langle\frac{\partial W}{\partial c_i}\right\rangle\left(\frac{\partial u_i}{\partial t} + u_j\frac{\partial u_i}{\partial r_j}\right) + n\left\langle c_j\frac{\partial W}{\partial c_i}\right\rangle\frac{\partial u_i}{\partial r_j} - n\left\langle a_i\frac{\partial W}{\partial c_i}\right\rangle = \frac{\delta W}{\delta t} \end{aligned} \tag{2.121}$$

where $\mathbf{a}_i$ is the acceleration of particle i due to external force fields and where $n\langle\cdot\rangle = \iiint_\infty d^3c \cdot P$ and the quantity $\delta W/\delta t$ represents the change of W due to the collisions in the interval δt and is expressed by the formula of Eq. (2.77) with the substitutions $\phi \to W$ and $\mathbf{v} \to \mathbf{c}$:

We recall the intuitive fact that for every *summation invariant*, that is quantities whose sum is conserved during collisions, the collisional term (i.e. right hand side of Eq. (2.121)) is zero.

2.3.3 The moment equations

If one does not assume anything about the phase space distribution function P, then the Maxwell equation (2.121) calculated for the velocity moments from zero to third (1, v_k, $v_k v_l$, $v_k v_l v_h$) carries to the following set of equations [62, 98]:

$$\frac{\partial(mn)}{\partial t} + \frac{\partial(mnu_i)}{\partial r_i} = \frac{\delta(mn)}{\delta t} \tag{2.122a}$$

$$mn\left(\frac{\partial u_k}{\partial t} + u_j\frac{\partial u_k}{\partial r_j}\right) + \frac{\partial \mathcal{P}_{ik}}{\partial r_i} - mn\langle a_k\rangle = mn\frac{\delta u_k}{\delta t} \tag{2.122b}$$

$$\begin{aligned}\frac{\partial \mathcal{P}_{kl}}{\partial t} + \frac{\partial(\mathcal{P}_{kl}u_i)}{\partial r_i} + \mathcal{P}_{il}\frac{\partial u_k}{\partial r_i} + \mathcal{P}_{ik}\frac{\partial u_l}{\partial r_i} + \frac{\partial \mathcal{Q}_{ikl}}{\partial r_i} \\ -mn\langle a_k c_l + a_l c_k\rangle = \frac{\partial \mathcal{P}_{kl}}{\delta t}\end{aligned} \tag{2.122c}$$

$$\begin{aligned}\frac{\partial \mathcal{Q}_{klh}}{\partial t} + \left(\mathcal{Q}_{ilh}\frac{\partial u_k}{\partial r_i} + \mathcal{Q}_{ikh}\frac{\partial u_l}{\partial r_i} + \mathcal{Q}_{ikl}\frac{\partial u_h}{\partial r_i}\right) + \frac{\partial(\mathcal{Q}_{klh}u_i)}{\partial r_i} \\ -\frac{\mathcal{P}_{lh}\partial \mathcal{P}_{ik}}{mn\partial r_i} - \frac{\mathcal{P}_{kh}\partial \mathcal{P}_{il}}{mn\partial r_i} - \frac{\mathcal{P}_{kl}\partial \mathcal{P}_{ih}}{mn\partial r_i} + \frac{\partial \mathcal{R}_{iklh}}{\partial r_i} \\ +\langle a_k[\mathcal{P}_{lh} - mnc_l c_h]\rangle + \langle a_l[\mathcal{P}_{kh} - mnc_k c_h]\rangle + \langle a_h[\mathcal{P}_{kl} - mnc_k c_l]\rangle \\ = \frac{\delta \mathcal{Q}_{klh}}{\delta t} - \mathcal{P}_{lh}\frac{\delta u_k}{\delta t} - \mathcal{P}_{kh}\frac{\partial u_l}{\delta t} - \mathcal{P}_{kl}\frac{\delta u_h}{\delta t}\end{aligned} \tag{2.122d}$$

As it can be seen, the equation for the $n-th$ moment contains the $(n+1)-th$ moment. This means that some assumption must be introduced to close the Maxwell equations for the moments up to a given order.

2.3.4 The Euler equations

When the gas is elastic and very near to macroscopic equilibrium, it is reasonable to assume that at every spatial location the distribution function can be approximated with a Maxwell-Boltzmann distribution function, with parameters varying in time and spatial location. This is the so called assumption of local thermodynamic equilibrium.

If the particles of the gas have no internal degrees of freedom, then the first velocity moments m, $m\mathbf{c}$ and $mc^2/2$ (5 scalar quantities) are the only summation invariants that depend on the particle velocities. The Maxwell equations for these quantities (precisely Equations (2.122)) extremely simplify with this local equilibrium assumption:

$$\frac{\partial(mn)}{\partial t} + \frac{\partial(mnu_i)}{\partial r_i} = 0 \tag{2.123a}$$

$$mn\frac{\partial u_k}{\partial t} + mnu_j\frac{\partial u_k}{\partial r_j} + \frac{\partial p}{\partial r_k} - mn\langle a_k\rangle = 0 \tag{2.123b}$$

$$\frac{3}{2}\frac{\partial p}{\partial t} + \frac{3}{2}\frac{\partial(pu_i)}{\partial r_i} - mn\langle a_i c_i\rangle = 0 \tag{2.123c}$$

where it must be noted that for gravity or electromagnetic fields (as well for most external forces) the term $\langle a_i c_i\rangle$ vanishes.

The above three equations constitute the Euler equations for a perfect gas. They are the simplest form of fluid equations and are valid only when the assumption of local thermodynamic equilibrium can be assumed.

2.3.5 The Grad closure

Grad, in the late 1940s, introduced an assumption on the fourth moment [99]:

$$\mathcal{R}_{iklh} = \frac{1}{mn}(\mathcal{P}_{ik}\mathcal{P}_{lh} + \mathcal{P}_{il}\mathcal{P}_{kh} + \mathcal{P}_{ih}\mathcal{P}_{kl} - \mathcal{T}_{ik}\mathcal{T}_{lh} - \mathcal{T}_{il}\mathcal{T}_{kh} - \mathcal{T}_{ih}\mathcal{T}_{kl}) \tag{2.124}$$

The simple physical meaning of Grad's relation is that it is satisfied by relatively smooth distribution functions and it does not allow for 'spiky' distribution functions. This is the only requirement that the distribution function P must fulfill, no specific assumptions on the form of this distribution are needed. Using this assumption, the Maxwell equations for the first moments (2.122) become a closed set: it is a set of 20 equations for 20 unknown scalar functions. The unknown functions are n, $\mathbf{u}$ (3 components), $\mathcal{P}$ (6 components), $\mathcal{Q}$ (10 components). The equations are the first three groups of the set (2.122), which are $1+3+6=10$ scalar equations, plus the equation for the heat flow tensor that must be rewritten using the Grad relation:

$$\begin{aligned}
&\frac{\partial \mathcal{Q}_{klh}}{\partial t} + \left(\mathcal{Q}_{ilh}\frac{\partial u_k}{\partial r_i} + \mathcal{Q}_{ikh}\frac{\partial u_l}{\partial r_i} + \mathcal{Q}_{ikl}\frac{\partial u_h}{\partial r_i}\right) + \frac{\partial(\mathcal{Q}_{klh}u_i)}{\partial r_i} \\
&\quad + p(\delta_{ik}\delta_{lh} + \delta_{il}\delta_{kh} + \delta_{ih}\delta_{kl})\frac{\partial}{\partial r_i}\left(\frac{p}{mn}\right) - p\frac{\partial}{\partial r_i}\left(\frac{\delta_{ik}\tau_{lh} + \delta_{il}\tau_{kh} + \delta_{ih}\tau_{kl}}{mn}\right) \\
&- \tau_{lh}\frac{\partial}{\partial r_i}\left(\frac{\tau_{ik}}{mn}\right) - \tau_{kh}\frac{\partial}{\partial r_i}\left(\frac{\tau_{il}}{mn}\right) + \tau_{kl}\frac{\partial}{\partial r_i}\left(\frac{\tau_{ih}}{mn}\right) - (\delta_{lh}\tau_{ik} + \delta_{kl}\tau_{ih} + \delta_{kh}\tau_{il})\frac{\partial}{\partial r_i}\left(\frac{p}{mn}\right) \\
&\quad + \langle a_k[\mathcal{P}_{lh} - mnc_lc_h]\rangle + \langle a_l[\mathcal{P}_{kh} - mnc_kc_h]\rangle + \langle a_h[\mathcal{P}_{kl} - mnc_kc_l]\rangle \\
&\quad = \frac{\delta \mathcal{Q}_{klh}}{\delta t} - \mathcal{P}_{lh}\frac{\delta u_k}{\delta t} - \mathcal{P}_{kh}\frac{\partial u_l}{\delta t} - \mathcal{P}_{kl}\frac{\delta u_h}{\delta t}
\end{aligned} \tag{2.125}$$

2.3.6 The Chapman-Enskog closure

In elastic gases not so dense but not so rarefied the deviation from the Maxwell-Boltzmann equilibrium distribution is small and it can be treated as a perturbation. This is the main motivation of Chapman-Enskog method [62] to obtain transport equations more general than the Euler equations. The local distribution function is expanded around a reference unperturbed distribution, which is assumed to be a Maxwell-Boltzmann distribution with parameters depending on time and space: the local number density $n_0(t,\mathbf{r})$, local temperature $T_0(t,\mathbf{r})$ and local flow velocity vector $\mathbf{u}_0(t,\mathbf{r})$:

$$P_0(t,\mathbf{r},\mathbf{c}) = n_0(t,\mathbf{r})\left(\frac{m}{2\pi k_B T_0(t,\mathbf{r})}\right)^{3/2}\exp\left(-\frac{m(c_1^2+c_2^2+c_3^2)}{2k_BT_0(t,\mathbf{r})}\right) \tag{2.126}$$

with $\mathbf{c} = \mathbf{v} - \mathbf{u}_0$.
The series expansion around this reference distribution reads:

$$P(t,\mathbf{r},\mathbf{c}) = P_0(t,\mathbf{r},\mathbf{c})\left\{1 + \mathcal{A}_i(t,\mathbf{r})c_i + \mathcal{B}_{ij}(t,\mathbf{r})c_ic_j + \mathcal{D}_{ijk}(t,\mathbf{r})c_ic_jc_k + ...\right\} \tag{2.127}$$

where the expansion coefficient matrices are symmetric for the interchange of indexes.
The normalization conditions implies that

$$\begin{aligned}
\iiint_\infty d^3cP &= \iiint_\infty d^3cP_0 + \mathcal{A}_i\iiint_\infty d^3cc_iP \\
+\mathcal{B}_{ij}\iiint_\infty d^3cc_ic_jP_0 &+ \mathcal{D}_{ijk}\iiint_\infty d^3cc_ic_jc_kP_0 + ... = 0
\end{aligned} \tag{2.128}$$

which, noting that the averages of odds momenta of $\mathbf{c}$ are zero, becomes:

$$\mathcal{B}_{ii} + (\text{4th order term}) + ... = 0. \tag{2.129}$$

Using the fact that the average random velocity must be identically zero, another condition is obtained for the expansion coefficients:

$$\iiint_{\infty} d^3 c c_h P = 0 \tag{2.130}$$

which (as the odd order vanish) becomes:

$$\mathcal{A}_i \langle c_h c_i \rangle_0 + \mathcal{D}_{ijk} \langle c_h c_i c_j c_k \rangle_0 + ... = 0. \tag{2.131}$$

where $\langle\rangle_0$ are the averages weighted by the Maxwell-Boltzmann distribution P_0.

Assuming that the higher order terms of the expansion represent a decreasing series of perturbations, one can truncate the expansion to some low order. The zero order truncation gives, of course, a trivial approximation. First and second order truncations cannot be obtained as the condition of Eq. (2.131) requires the presence of at least two terms of odd orders (the first and the third). Therefore the lowest non-trivial possible expansion is the third order one, for which the above conditions (after having calculated the $\langle\rangle_0$ averages) read:

$$B_{ii} = B_{11} + B_{22} + B_{33} = 0 \tag{2.132a}$$

$$A_i + \frac{3 k_B T_0}{m} D_{ijk} = 0. \tag{2.132b}$$

The zero order expansion requires 5 independent parameters (that in transport equations become transported fields): density n_0, momentum $m\mathbf{u}_0$ and temperature T_0. The third order expansion requires $5 + 3 + 6 + 10 = 24$ parameters (it must be remembered that the coefficient matrices are symmetric) but the last couple of conditions (which are four) reduce the number of independent parameters to 20.

The Chapman-Enskog expansion is usually truncated to the first non-trivial order, that is the third, for which the first velocity moments read (with also the use of the above conditions):

$$m \iiint_{\infty} d^3 c P = m n_0 \tag{2.133a}$$

$$m \iiint_{\infty} d^3 c c_\alpha P = 0 \tag{2.133b}$$

$$m \iiint_{\infty} d^3 c c_\alpha c_\beta P = p_0 \left[\delta_{\alpha\beta} + 2 \left(\frac{k_B T_0}{m} \right) \mathcal{B}_{\alpha\beta} \right] \tag{2.133c}$$

$$m \iiint_{\infty} d^3 c c_\alpha c_\beta c_\gamma P = 6 p_0 \left(\frac{k_B T_0}{m} \right)^2 \mathcal{D}_{\alpha\beta\gamma} \tag{2.133d}$$

$$\tag{2.133e}$$

with $p_0 = n_0 k_B T_0$. From them one can immediately identify the macroscopic physical quantities introduced in the first paragraph of this section, mainly the stress and heat flow tensors:

$$\mathcal{T}_{\alpha\beta} = -2 p_0 \left(\frac{k_B T_0}{m} \mathcal{B}_{\alpha\beta} \right) \tag{2.134}$$

$$\mathcal{Q}_{\alpha\beta\gamma} = 6 p_0 \left(\frac{k_B T_0}{m} \right)^2 \mathcal{D}_{\alpha\beta\gamma} \tag{2.135}$$

coming to the conclusion that the third order Chapman-Enskog expansion of the phase space distribution function reads:

$$P = P_0 \left[1 - \frac{mn_0}{2p_0^2} \mathcal{T}_{ij} c_i c_j + \frac{(mn_0)^2}{6p_0^3} \left(\mathcal{Q}_{ijk} c_j c_k - \frac{3p_0}{mn_0} \mathcal{Q}_{ijj} \right) c_i \right] \tag{2.136}$$

With the third order truncation, it happens that the fourth moment $\mathcal{R}$ given in Eq. (2.120) is only a function of the parameters of the Maxwellian reference state P_0 (precisely only of n_0 and p_0) and of the second order tensor $\mathcal{B}$, or equivalently of the stress tensor $\mathcal{T}$. Again we have 20 free parameters: the 5 parameters of the Maxwellian n_0; $\mathbf{u}_0$ and p_0, the 5 elements of the traceless symmetric stress tensor $\mathcal{T}$, and the 10 elements of the symmetric heat flux matrix $\mathcal{Q}$. And again we obtain (as with the Grad closure method) $1 + 3 + 6 + 10 = 20$ transport equations, which we divide in two groups: the equations for the 5 parameters of the reference Maxwellian,

$$\frac{\partial (mn_0)}{\partial t} + \frac{\partial (mn_0 u_{0,i})}{\partial r_i} = \frac{\delta (mn_0)}{\delta t} \tag{2.137a}$$

$$mn_0 \left(\frac{\partial u_{0,k}}{\partial t} + u_{0,j} \frac{\partial u_{0,k}}{\partial r_j} \right) + \frac{\partial p_0}{\partial r_k} - \frac{\partial \mathcal{T}_{ik}}{\partial r_i} - mn_0 \langle a_k \rangle = mn_0 \frac{\delta u_{0,k}}{\delta t} \tag{2.137b}$$

$$\frac{\partial p_0}{\partial t} + \frac{\partial (p_0 u_{0,i})}{\partial r_i} + \frac{2}{3} p_0 \frac{\partial u_{0,i}}{\partial r_i} - \frac{2}{3} \mathcal{T}_{ih} \frac{\partial u_{0,h}}{\partial r_i} + \frac{2}{3} \frac{\partial h_i}{\partial r_i} = \frac{\delta p_0}{\delta t}, \tag{2.137c}$$

and the $5 + 10 = 15$ equations for the stress and heat tensors:

$$\begin{aligned} \frac{\partial \mathcal{T}_{kl}}{\partial t} - p_0 \left(\frac{\partial u_{0,k}}{\partial r_l} + \frac{\partial u_{0,l}}{\partial r_k} - \frac{2}{3} \delta_{kl} \frac{\partial u_{0,i}}{\partial r_i} \right) + \frac{\partial (\mathcal{T}_{kl} u_{0,i})}{\partial r_i} \\ + \left(\mathcal{T}_{ik} \frac{\partial u_{0,l}}{\partial r_i} + \mathcal{T}_{il} \frac{\partial u_{0,k}}{\partial r_i} - \frac{2}{3} \delta_{kl} \mathcal{T}_{ij} \frac{\partial u_{0,i}}{\partial r_j} \right) \\ - \frac{\partial}{\partial r_i} \left(\mathcal{Q}_{ikl} - \frac{2}{3} \delta_{kl} h_i \right) + mn_0 \langle a_k c_l + a_l c_k \rangle = \frac{\delta \mathcal{T}_{kl}}{\delta t} \end{aligned} \tag{2.138a}$$

$$\begin{aligned} \frac{\partial \mathcal{Q}_{klh}}{\partial t} + \frac{\partial (\mathcal{Q}_{klh} u_{0,i})}{\partial r_i} + \left(\mathcal{Q}_{ilh} \frac{\partial u_{0,k}}{\partial r_i} + \mathcal{Q}_{ikh} \frac{\partial u_{0,l}}{\partial r_i} + \mathcal{Q}_{ikl} \frac{\partial u_{0,h}}{\partial r_i} \right) \\ + p_0 (\delta_{ik}\delta_{lh} + \delta_{il}\delta_{kh} + \delta_{ih}\delta_{kl}) \frac{\partial}{\partial r_i} \left(\frac{p_0}{mn_0} \right) - p_0 \frac{\partial}{\partial r_i} \left(\frac{\delta_{ik}\mathcal{T}_{lh} + \delta_{il}\mathcal{T}_{kh} + \delta_{ih}\mathcal{T}_{kl}}{mn_0} \right) \\ - (\delta_{lh}\mathcal{T}_{ik} + \delta_{kl}\mathcal{T}_{ih} + \delta_{kh}\mathcal{T}_{il}) \frac{\partial}{\partial r_i} \left(\frac{p_0}{mn_0} \right) + \langle a_k [(p_0 \delta_{lh} - \tau_{lh}) - mn_0 c_l c_h] \rangle \\ + \langle a_l [(p_0 \delta_{kh} - \tau_{kh}) - mn_0 c_k c_h] \rangle + \langle a_h [(p_0 \delta_{kl} - \tau_{kl}) - mn_0 c_l c_k] \rangle \\ = \frac{\delta \mathcal{Q}_{klh}}{\delta t} - (p_0 \delta_{lh} - \mathcal{T}_{lh}) \frac{\delta u_{0,k}}{\delta t} - (p_0 \delta_{kh} - \mathcal{T}_{kh}) \frac{\delta u_{0,l}}{\delta t} - (p_0 \delta_{kl} - \mathcal{T}_{kl}) \frac{\delta u_{0,h}}{\delta t} \end{aligned} \tag{2.138b}$$

Keeping in mind the decomposition of the pressure tensor (2.117) it can be immediately seen that the first two equations in (2.137) (continuity and motion equations) are identical to that obtained by Grad. Moreover the last of (2.137) joined with the first of (2.138) are equivalent to (2.122c) which is the third equation of Grad's closure. The only difference between Grad and Chapman-Enskog method is in the equation for the heat flow tensor (Eqs. (2.138b) and (2.125)) and it appears to be a fourth order difference as it comes only from the appearance in Eq. (2.125) of terms containing $\mathcal{T}^2$ (which are related to the second order coefficients of the expansion $\mathcal{B}$, see Eq. (2.134)). We can conclude that the Chapman-Enskog expansion method and the Grad closure method are equivalent to third order accuracy.

Finally we must observe that the derivation of the transport equations is somewhat not complete, as (in both Grad and Chapman-Enskog formulas) the collision terms $\frac{\delta}{\delta t}$ remain unexpressed. The only

non-trivial collision terms are that for the stress and heat flow tensors (non-diagonal second order moments and third order moments of the Boltzmann collision terms), as the mass, velocity and energy are conserved during collisions, so that:

$$\frac{\delta(mn_0)}{\delta t} = 0 \tag{2.139a}$$

$$\frac{\delta u_k}{\delta t} = 0 \tag{2.139b}$$

$$\frac{\delta p_0}{\delta t} = 0 \tag{2.139c}$$

The collision terms for the last two equations (2.138) can be approximated with the well known *BGK approximation*, due to Bhatnagar, Gross and Krook [27], also known as *relaxation time approximation*. In a few word it states that

$$\frac{\delta P}{\delta t} = -\frac{P - P_0}{\tau_0}. \tag{2.140}$$

This means that as a consequence of the randomizing effect of collisions the distribution function tends to the equilibrium Maxwellian in an exponential way with a characteristic *relaxation time* τ_0 which remains a free parameter of the theory, to be calculated with other considerations. If one has a truncated expansion of P around the Maxwellian P_0, than Eq. (2.140) yields an expression for the collisional variations of all the needed velocity moments.

2.3.7 The Navier-Stokes approximation

The most complicated of the transport equations presented above is that for the general heat flow $\mathcal{Q}$. This set of 10 scalar quantities are tied to the fourth order corrections in the Chapman-Enskog expansion (see (2.135)). In most physical problems it is usually sufficient to know the evolution of the contracted quantity $\mathbf{q}$ defined in Eq. (2.119), which represents the transport of the total (modulus) random energy of the particles due to the random motion of the molecules (we lose accuracy on the transport of single random velocity components). Therefore we make the assumption:

$$Q_{ijk} = \frac{2}{3}(\delta_{ij}q_k + \delta_{ik}q_j + \delta_{jk}q_i), \tag{2.141}$$

reducing the set of 10 components to only 3 contracted components.

With this further assumption it is more easy to perform the BGK calculation of the collision terms that appear in the stress and heat tensor equations (2.138). Bypassing the details the final formula are:

$$\frac{\delta \mathcal{T}_{kh}}{\delta t} = -\frac{\mathcal{T}_{kh}}{\tau_0} \tag{2.142}$$

$$\frac{\delta q_k}{\delta t} = -\frac{q_k}{\tau_0}. \tag{2.143}$$

This last result is very important if inserted in equations (2.138). In fact it must be noted that the second and third order expansion coefficients (ultimately tied to $\mathcal{T}$ and $\mathbf{q}$) are usually negligibly small, except when they are multiplied by very large factors, in this case $1/\tau_0$. The Chapman-Enskog method can only be applied to gases which are not far from equilibrium: this means that very frequent collisions must nearly absorb all deviations from equilibrium. In other words the relaxation time τ_0 must be extremely short. Based on this argument, we can neglect all terms containing the stress tensor and the heat flow vector, except the ones which are multiplied by $1/\tau_0$, obtaining (for the case $\mathbf{a} = 0$):

$$\mathcal{T}_{kl} = \tau_0 p_0 \left(\frac{\partial u_{0,k}}{\partial r_l} + \frac{\partial u_{0,l}}{\partial r_k} - \frac{2}{3}\delta_{kl}\frac{\partial u_{0,i}}{\partial r_i} \right) \tag{2.144a}$$

$$q_k = -\frac{5}{2}\frac{k_B}{m}\tau_0 p_0 \frac{\partial T_0}{\partial r_k} \tag{2.144b}$$

which is the familiar linear relation between the flows and the gradients: momentum flow (non-diagonal) is proportional to the velocity gradient, heat flow is proportional to temperature gradient. Having recognized that, the hydrodynamic transport coefficients (viscosity and heat conductivity) can be expressed:

$$\eta = \tau_0 p_0 \tag{2.145a}$$

$$\kappa = \frac{5}{2}\frac{k_B}{m}\tau_0 p_0 \tag{2.145b}$$

that are equivalent (with slight differences in the numerical constants) with the mean free path calculations discussed in paragraph 2.1.4.

The 6 Navier-Stokes equations can be finally obtained:

$$\frac{\partial (m n_0)}{\partial t} + \frac{\partial (m n_0 u_{0,i})}{\partial r_i} = 0 \tag{2.146a}$$

$$m n_0 \left(\frac{\partial u_{0,k}}{\partial t} + u_{0,i}\frac{\partial u_{0,k}}{\partial r_i} \right) + \frac{\partial p_0}{\partial r_k} = \frac{\partial}{\partial r_i}\left[\eta \left(\frac{\partial u_{0,k}}{\partial r_i} + \frac{\partial u_{0,i}}{\partial r_k} - \frac{2}{3}\delta_{ik}\frac{\partial u_{0,j}}{\partial r_j} \right) \right] \tag{2.146b}$$

$$\frac{3}{2}\left(\frac{\partial p_0}{\partial t} + u_{0,i}\frac{\partial p_0}{\partial r_i} \right) + \frac{5}{2} p_0 \frac{\partial u_{0,i}}{\partial r_i} = \frac{\partial}{\partial r_i}\left(\kappa \frac{\partial T_0}{\partial r_i} \right) + \eta \left(\frac{\partial u_{0,k}}{\partial r_l} + \frac{\partial u_{0,l}}{\partial r_k} - \frac{2}{3}\delta_{kl}\frac{\partial u_{0,i}}{\partial r_i} \right) \frac{\partial u_{0,k}}{\partial r_l} \tag{2.146c}$$

These equations represent the most simple form of transport equations for a gas that is not in strict local thermodynamic equilibrium (which instead is described by Euler equations (2.123)). The deviation from equilibrium is slight but important, as irreversible (dissipative) processes emerge from it: these are taken into account by the linear transport coefficients (viscosity and heat conductivity) which represent the tendency of the gas to relax toward the Maxwellian equilibrium.

2.3.8 Burnett and super-Burnett orders

In this paragraph we briefly give a different scheme [62, 137] (which has somewhat a better formalization) of the Chapman-Enskog derivation and the definition of the Burnett and super-Burnett orders of the expansion, which will be useful in the discussion of the granular kinetic theories. The scheme includes the same fundamental passage, i.e. the individuation of a reference ("equilibrium") state which exactly solves the Boltzmann kinetic equation in the absence of perturbation, an expansion of the "perturbed" solution around this state in powers of the velocity and an expansion of all the transport equations in gradients of the hydrodynamical fields (above we have given it as a phenomenological fact, in Eq. (2.144)):

- it is observed that a probability density function P_0 with three global parameters (n_0, $\mathbf{u}_0$ and T_0) solves the Boltzmann equation if the external conditions impose as constant the density, average velocity and average square fluctuations of velocity: this solution is a Maxwellian;
- moreover, it is also observed that when different external conditions are imposed (e.g. specific boundaries or particular initial distributions) the same Maxwellian with space-time dependent parameters solves the Boltzmann equation if and only if those parameters satisfy the Euler equations; however this family of solutions is very particular, because it assumes an infinitely rapid relaxation to local equilibrium without any entropy production (i.e. irreversible processes);

- in general it is expected that the true solution P of the Boltzmann equation in situations not too far from mechanical equilibrium (i.e. absence of macroscopic flows) is similar to the space-time dependent Maxwellian, that is the space-time dependence all occurs through the local averages of the first velocity moments: $P(\mathbf{r},\mathbf{v},t) \equiv P(\mathbf{v}|n,\mathbf{u},T)$; this passage can be justified by means of the analysis of stability of the kinetic modes in the Boltzmann equations: it can be shown that the short wavelength (order mean free path) modes rapidly decay and only the long wavelength, slow, modes relative to the fluctuations of the conserved quantities (mass, momentum and energy) remains; this separation of scales is the justification of the hydrodynamical limit discussed above (see paragraph (2.2.4))

- then P is formally expanded as a series of powers of a "uniformity" parameter ϵ (which is set to 1 at the end):

$$P = P_0 + \epsilon P_1 + \epsilon^2 P_2 + ... \tag{2.147}$$

  and a factor ϵ is assigned to every gradient operator $\partial/\partial r_i \to \epsilon\partial/\partial r_i$ while different time scales are coupled to the different orders in the gradient expansion: $\partial/\partial t = \partial/\partial t_0 + \epsilon\partial/\partial t_1 + \epsilon^2\partial/\partial t_2 + ...$;

- finally this formal expansion of $P(\mathbf{v}|n,\mathbf{u},T)$ and of space-time coordinates is inserted into the Boltzmann equation: this results in a set of equations for the different orders terms P_0, P_1, etc.. At every order these equations contain space derivatives and different time derivatives (for different time scales) of the parameters n, $\mathbf{u}$, T plus an integration (due to the collisional term) in the velocity $\mathbf{v}$ (or in $\mathbf{c} = \mathbf{v} - \mathbf{u}$);

- the time derivatives of time scales different from the zero order time scale can be obtained putting the same formal expansion in the equation for the $\mathbf{c}$-moments (Maxwell Eqs. (2.122)) and comparing terms with the same order; in this passage the flux tensors ($\mathcal{P}$ and $\mathcal{Q}$) enter formally in the Boltzmann equation;

- in this way every ϵ^k-order of the Boltzmann equation becomes an integro-differential equation with first derivatives in the variables t_0 and $\mathbf{r}$ and integration in the velocity $\mathbf{v}$ of the P terms of order 0 through $k-1$, while the k-th order term (P_k) does not appear under space derivatives, so that a solution P_k can be searched in the form $P_k = \mathbf{A}(\mathbf{c})\cdot\nabla \ln T + \mathbf{B}(\mathbf{c})\cdot\nabla \ln n + \mathcal{C}_{ij}(\mathbf{c})\partial u_j/\partial r_i$;

- this approach leads finally to approximated expressions of the flux tensors as functions of the macroscopic fields n, $\mathbf{u}$, T, i.e. by truncating the expansion to some order; these expressions close the transport equations (2.122);

- the first order truncation (i.e. second and higher orders in ϵ are neglected) yields expressions for the flux tensors which are *linear* in the macroscopic fields, equivalent to Eq. (2.144); so that the transport equations become the Navier-Stokes equations (2.146); this is why the first order truncation of this Chapman-Enskog expansion is called Navier-Stokes order expansion;

- keeping the second order terms in the ϵ expansion yields the so-called Burnett equations, while adding the third order terms give the so-called super-Burnett equations; Bobylev has shown that the Burnett and super-Burnett hydrodynamics violates the basic physics behind the Boltzmann equation, i.e. sufficiently short acoustic waves are increasing with time instead of decaying, contradicting the H theorem; this remains a central open problem in the kinetic theory;

- the exact functional expression of the transport coefficients needs again a polynomial expansion in $\mathbf{c}$ of the unknown functions $\mathbf{A}(\mathbf{c})$, $\mathbf{B}(\mathbf{v})$ and $\mathcal{C}_{ij}(\mathbf{c})$ and consideration similar to the ones made above.

2.3.9 Corrections at high densities

If the Boltzmann-Enskog equation is used as the basic kinetic equation, the transport coefficients and the scalar pressure change. In principle the transport coefficients (and the scalar pressure) can be expanded in powers of the density [109]:

$$p = p_{dil}(1 + p_2 n + p_3 n^2 + ...) \tag{2.148a}$$
$$\eta = \eta_{dil}(1 + \eta_1 n + \eta_2 n^2 + ...) \tag{2.148b}$$
$$\kappa = \kappa_{dil}(1 + \kappa_1 n + \kappa_2 n^2 + ...) \tag{2.148c}$$
$$\eta' = \eta'_2 n^2 + \eta'_3 n^3 + ... \tag{2.148d}$$
$$\tag{2.148e}$$

where $p_{dil} = nk_BT$ is the scalar pressure in the dilute case $n \ll 1$, $\eta_{dil} \propto \sqrt{mk_BT}$ is the viscosity in the dilute case, $\kappa_{dil} \propto k_B\sqrt{k_BT/m}$ is the heat conductivity in the dilute case and η' is the *bulk viscosity* which has been neglected till now as it is of order $\sim n^2$. The bulk viscosity modifies the expression for the stress tensor, introduced in Eq. (2.144) i.e.:

$$\mathcal{T}_{kl} = \eta\left(\frac{\partial u_{0,k}}{\partial r_l} + \frac{\partial u_{0,l}}{\partial r_k} - \frac{2}{3}\delta_{kl}\frac{\partial u_{0,i}}{\partial r_i}\right) + \eta'\delta_{kl}\frac{\partial u_{0,k}}{\partial r_l} \tag{2.149}$$

The Enskog correction accounts for the appearance of position correlations at high densities: these correlations render the high n order terms important so that they must be included in analytical expressions.

In $d = 2$ the corrections are the followings:

$$p = \frac{4}{\pi\sigma^2}\phi T[1 + 2\phi\Xi(\sigma, n)] \tag{2.150a}$$
$$\eta = \frac{1}{2\sigma}\sqrt{\frac{mk_BT}{\pi}}\left[\frac{1}{\Xi(\sigma,n)} + 2\phi + \left(1 + \frac{8}{\pi}\right)\phi^2\Xi(\sigma,n)\right] \tag{2.150b}$$
$$\kappa = \frac{2}{\sigma}k_B\sqrt{\frac{k_BT}{\pi m}}\left[\frac{1}{\Xi(\sigma,n)} + 3\phi + \left(\frac{9}{4} + \frac{4}{\pi}\right)\phi^2\Xi(\sigma,n)\right] \tag{2.150c}$$
$$\eta' = \frac{8\phi^2\Xi(\sigma,n)}{\pi\sigma}\sqrt{\frac{mk_BT}{pi}} \tag{2.150d}$$

where ϕ is the solid fraction (see paragraph 2.2.6).

2.4 Granular hydrodynamics

This section is a brief review of the existing hydrodynamic theories for granular "fluids". The theories slightly differ in the constitutive relations that express the fluxes (e.g. stress tensor and heat flow) as functions of the fields (density, velocity and granular temperature). Nevertheless all the theories assume the hydrodynamical limit (see paragraph 2.2.4), i.e. a separation of scales between macroscopic slow changes and microscopic rapid relaxation to equilibrium: moreover almost all the authors, in order to obtain a *rigorous* derivation of the transport coefficients, work in the Boltzmann-Grad limit, so that the Boltzmann equation, i.e. the Molecular Chaos, can be considered valid. Other differences are in the intensity of dissipation considered (i.e. the range of values of the restitution coefficient), which is reflected in the limits of validity of certain perturbative expansions.

2.4.1 The energy sink

In the inelastic hard spheres model that we consider (see Eq. (2.41)), the total energy change in a collision between two particles with relative velocity $\mathbf{V}_{12}$ is $\Delta E = -(\mathbf{V}_{12}\cdot\hat{\mathbf{n}})^2(1-r^2)m/4$. It follows that in Eqs. (2.122c) the collisional term for the transport of pressure does not vanish (as in (2.139)). in particular it is straightforward to obtain the expression for the collisional change of the trace of the matrix $m<v_iv_j>/2$, i.e. the kinetic energy:

$$\int d\mathbf{v}\frac{1}{2}mv^2 Q_r(P,P) = -(1-r^2)\omega_c(P,P) \tag{2.151}$$

where

$$\omega_c(P,P) = \frac{m\pi\sigma^2}{16}\int d\mathbf{v}_1 d\mathbf{v}_2 |\mathbf{v}_1-\mathbf{v}_2|^3 P(\mathbf{r},\mathbf{v}_1,t)P(\mathbf{r},\mathbf{v}_2,t). \tag{2.152}$$

Recalling the composition (see Eqs. (2.115)-(2.117) in the isotropic term)

$$\mathcal{P}_{ij} = mn\langle c_i c_j\rangle = p\delta_{ij} - \left(\frac{1}{3}mn\langle c^2\rangle - mn\langle c_i c_j\rangle\right) \tag{2.153}$$

that defines the stress tensor $\mathcal{T}_{ij} = (mn/3)\langle c^2\rangle - mn\langle c_i c_j\rangle$ (which in the Chapman-Enskog expansions is seen to be related to the second order term, while the scalar pressure p is of order zero), and also the assumption (2.141) that neglects the differences between the generalized heat flow tensor $\mathcal{Q}$ and the classical heat flow vector $\mathbf{q}$, we can obtain an equation for the evolution of the (zero order) temperature field $T(\mathbf{r},t)$:

$$\frac{\partial T}{\partial t} + u_i\frac{\partial T}{\partial r_i} + \frac{2}{3nk_B}\left(\mathcal{P}_{ij}\frac{\partial u_i}{\partial r_j} + \frac{\partial q_i}{\partial r_i}\right) + (1-r^2)\frac{2}{3nk_B}\omega_c(P,P) = 0. \tag{2.154}$$

This equation, if compared to Eq. (2.122c) (with $p = nk_BT$), presents a very important difference, that is the presence of the last term in the left-hand side. This term is usually called *the energy sink*, as it yields the energy dissipation due to inelastic collisions. When $r = 1$ (elastic collisions) this term vanishes and the Maxwell equation for the energy transport is recovered.

Mean field considerations can be applied to have rough estimates of the energy sink:

$$\frac{\omega_c(P,P)}{n} \simeq \langle|\mathbf{c}|^3\rangle \simeq \langle c^2\rangle^{3/2} = \left(\frac{3k_BT}{m}\right)^{3/2} \tag{2.155}$$

consequently the energy sink can be written as

$$(1-r^2)\frac{2}{3nk_B}\omega_c(P,P) = 2(1-r^2)(3k_B)^{1/2}\left(\frac{T}{m}\right)^{3/2} \tag{2.156}$$

This mean field estimate assumes that the average of the squared relative velocity at collision is equal to the global average, and that the fractional powers of $\mathbf{c}$ can go in and out of this average.

This is the case when the granular gas is homogeneous, i.e. no correlations (in position and velocity) exist between particles. We will show in the following chapters that this situation is far from obvious in real situations. Nevertheless an important result can be obtained by means of Eq. (2.154) with the formula (2.156): in the absence of macroscopic flows Eq. (2.154) reads:

$$\frac{\partial T}{\partial t} = -C_{Haff} T^{3/2} \tag{2.157}$$

with $C_{Haff} = 2(1-r^2)(3k_B)^{1/2}/m^{3/2}$. The fact that the cooling rate (i.e. the temporal derivative of the temperature) is proportional to $T^{3/2}$ when correlations are absent can alternatively be understood with a simple consideration: the reduction of a velocity fluctuation due to an inelastic collision is proportional to the square of the fluctuation itself ($\sim T$), while the total number (per unit time) of collisions is proportional to the total scattering cross section multiplied by the mean velocity fluctuation ($\sim n\sigma^2\sqrt{T}$); this consideration results in the $T^{3/2}$ cooling rate. The solution of Eq. (2.157) yields the expression for granular temperature (which in this case is equal everywhere in the gas) decay [103]:

$$T(t) = \frac{T_0}{(1+\beta t)^2} \tag{2.158}$$

that is the widely known as "Haff law" for the *homogeneous cooling*, with β easily calculated from Eq. (2.157).

2.4.2 The first hydrodynamical models

In 1954 R. A. Bagnold [8] experimentally studied a suspension of wax spheres in a mixture of glycerin, water and alcohol, shearing the spheres in a coaxial cylinder rheometer. He found that at reasonably large concentrations and shear rates, the generated stresses depended on the square of the imposed shear rate and obeyed a relation of the form

$$\mathcal{T}_{ij} = \rho_p \sigma^2 \gamma^2 \mathcal{G}_{ij}(n) \tag{2.159}$$

where ρ_p is the density of a particle, σ is the radius of the particle, γ is the shear rate and $\mathcal{G}$ is a tensor-valued function of the solid fraction (which is the total volume occupied by the particles divided by the available volume in the container and is proportional to the number density n). Other experiments and computer simulations have confirmed this relation. This relation comes quite naturally from a dimensional analysis of the problem; moreover, as the granular temperature has units of squared velocity, it must be proportional to $\sigma^2\gamma^2$ and this means that the effective viscosity η (which in Eq. (2.159) is proportional to γ) varies as the square root of the granular temperature. This is not different from the expressions of the viscosity obtained in the framework of the kinetic theory of elastic hard spheres.(e.g. see Eq. (2.39b)). Moreover the experiment of Bagnold addressed the presence of "dispersive stresses": the shear work generates granular temperature which in turn generates normal stresses, in exactly the same way as the thermodynamic temperature generates thermodynamic pressure in a gas. These normal stresses tend to cause dilation of the material (i.e. they "disperse" the particles).

The analogy between the random motion of the granular particles and the thermal motion of molecules in the kinetic theory of gases was explicitly addressed by Ogawa [171] who coined the term "granular temperature" for the mean squared deviation of the velocity from the mean velocity, $T =< |\mathbf{c}_i|^2 >$ where $\mathbf{c}_i = \mathbf{v}_i - \mathbf{u}$.

One of the very first studies based on a complete continuum description of the granular rapid flow in terms of a Navier-Stokes-like equations is due to P. K.Haff [103]. He considered the several problems lying under a continuum description of granular flows and pointed out issues that are still debated in nowadays conferences. He firstly recognized that the granular temperature could be included in the list of macroscopic fields obeying to an energy balance equation analogous to the Eq. (2.146c) including dissipative term, i.e. Eq. (2.154). He also gave heuristic derivations of the transport coefficients $\eta \propto \sigma^2 n\sqrt{T}$ and $\kappa \propto \sigma^2\sqrt{T}$ and for the energy sink $\propto (1-r^2)nT^{3/2}$, stressing the assumption of homogeneity in this derivation. After having calculated these coefficients, Haff has shown qualitative behavior of the solutions of hydrodynamics in the most typical situations. He gave the form (2.158)

(with a slightly different constant β) as the solution of the hydrodynamics in absence of macroscopic flows. Then he studied the temperature profile in the steady state with or without gravity, obtaining solutions very similar to the ones obtained with rigorous analysis in the works of the successive twenty years. He realized the subtle problems posed by the boundary conditions: the effect of vibration of a wall driving the motion of the particles in the nearest layer (where the gas is strongly out of equilibrium) and also the behavior of the free surface in the presence of gravity in the most far layer (where the gas is too rarefied and grains are almost ballistic projectiles). He finally outlined the behavior of a granular gas in the steady-state Couette flow (shear in cylinder), the instabilities that could form in such an experimental setup and the problem of supersonic flow.

The attempt to derive expressions of the transport coefficients by means of the formalism of the kinetic theory of non-uniform dense gases, has begun with Savage and Jeffrey [194], who assumed a Maxwell distribution of velocities: they did not include the energy equation and therefore their theory was not complete. However they realized that in a situation of high shear rate it would be possible to observe an anisotropy of the distribution of angles at which collisions would occur (i.e. failure of Molecular Chaos assumption).

Lun et al. [152] studied the Couette flow obtaining closed hydrodynamic equations for arbitrary coefficients of restitution, imposing the anisotropic distribution of collision angles suggested by Savage and Jeffrey. Moreover they obtained, closed hydrodynamic equations for general situations for nearly elastic particles: in this framework they followed the Chapman-Enskog theory with the assumption of a slight correction to the Maxwell distributions.

Jenkins and Richman [119, 120] derived closed hydrodynamic equations for the dense gas of identical, rough, inelastic hard disks, by means of the expansion of distribution around the Maxwellian with two temperatures (translational and rotational).

In several computer simulations (see for example [51] and a references in [52]) it has also been addressed the problem of normal-stress differences: in a simple 2D shear flow with the velocity gradient in the y-direction, the $\mathcal{T}_{xx}$ normal stress is always larger than $\mathcal{T}_{yy}$, up to a ratio of order 10 in very rarefied or inelastic situations. This is due to an anisotropy of the mechanisms of momentum transport which relies on streaming transport (dominant at low densities and transporting only momentum in x direction) and collisional transport (dominant at high densities and transporting momentum isotropically).

It could be said that up to these contributions (and many others of 1980s) the approach to a continuum description of granular gases has been pursued on an engineeristic basis, with attention paid almost only to the "numbers" (refining and comparing the various expressions of transport coefficients) and not to the qualitative phenomena and to the physical problems. The pioneering contribution of Haff is surely an exception to this and should be read today with the same (or more) interest as many other very recent articles.

2.4.3 The new generation of granular hydrodynamics

Very recently a complete kinetic theory for granular gases has been proposed [42, 41, 210, 39]. The importance of this effort is in the possibility of the detailed evaluation of validity of the different truncations in the Chapman-Enskog expansion. Moreover this kinetic theory allows a better study of the linearization around a particular state (the so-called "Homogeneous Cooling State, HCS for further references) and therefore a complete derivation of a linear stability analysis. This is of capital importance to understand many of the results in Chapter V of this work.

The equations obtained by Brey et al. [39] are the following, for dimensions $d = 2$ or $d = 3$:

$$\frac{\partial n}{\partial t} + \frac{\partial n u_i}{\partial r_i} = 0 \tag{2.160a}$$

$$\frac{\partial u_j}{\partial t} + u_i \frac{\partial u_j}{\partial r_i} + \frac{1}{mn} \frac{\partial \mathcal{P}_{ij}}{\partial r_i} = 0 \tag{2.160b}$$

$$\frac{\partial T}{\partial t} + u_i \frac{\partial T}{\partial r_i} + \frac{2}{dnk_B} \left(\mathcal{P}_{ij} \frac{\partial u_j}{\partial r_i} + \frac{\partial q_i}{\partial r_i} \right) + T\zeta = 0 \tag{2.160c}$$

where $\zeta(\mathbf{r},t)$ is the cooling rate, while the pressure tensor and heat flux vector are decomposed and linearized in the following way:

$$\mathcal{P}_{ij} = nk_BT\delta_{ij} - \eta\left(\frac{\partial u_j}{\partial r_i} + \frac{\partial u_i}{\partial r_j} - \frac{2}{d}\delta_{ij}\frac{\partial u_l}{\partial r_l}\right) \tag{2.161}$$

$$q_i = \kappa\frac{\partial T}{\partial r_i} - \mu\frac{\partial n}{\partial r_i} \tag{2.162}$$

with η the shear viscosity, κ the thermal conductivity and μ a new transport coefficient which has non analogue in elastic gases, coupling the density gradient to the heat flux. The exact expressions for the transport coefficient and for the cooling rate as functions of the restitution coefficient r can be found in the literature [39, 43]. Here we note that - for consistency with the truncation of the transport fluxes up to the first order in the gradients, which gives contribution to the hydrodynamic equations, up to the second order in the gradients - the cooling rate ζ must be calculated with an expansion truncated up to the second order (Burnett order). It has been proved that this second order contribution can be neglected in most situations.

The importance of the novel transport coefficient μ (not present in previous formulation of granular hydrodynamics) has been studied by Soto et al. [203]: they have measured, in a numerical simulation, the heat flux in a 2D granular gas kept between two walls at different temperatures, in the presence of gravity, and have observed that this flux is not zero at the minimum of the temperature profile (where the gradient of temperature is zero); it depends upon the gradient of the density and its proportionality coefficient (μ in the above equations) depends upon r.

Brey et al. have also considered the linearization of Eqs. (2.160) around the Homogeneous Cooling State, that is the solution with no spatial gradients:

$$n(\mathbf{r},t) = n \tag{2.163a}$$

$$\mathbf{u}(\mathbf{r},t) = 0 \tag{2.163b}$$

$$T(\mathbf{r},t) = T_H(t) \tag{2.163c}$$

where $T_H(t)$ is the solution of the Eq. (2.157) with $C_{Haff} = -\zeta^* nk_B\sqrt{T}/\eta_0$, where ζ^* is a numerical coefficient (depending upon r) and $\eta_0 \propto \sqrt{T}$ is the value of shear viscosity for elastic molecular gases (both this coefficients can be found in [39]).

The analysis of the linear stability [39, 214] of solution (2.163) has shown that perturbations of the transversal component of the velocity (i.e. $u_y(x,0) = u_0\sin(q_0x)$ with $q_0 = 2\pi/L$) always decay in time, but following an algebraic decay. The details of the several studies on the linear stability analysis of hydrodynamics are discussed in the introduction to Chapter V of this work.

The authors [39] have also studied self-diffusion (i.e. evolution of the mean displacement of a tagged particle identical to the others) and Brownian motion (i.e. evolution of the mean displacement of a tagged particle more massive than the others of the gas) in the Homogeneous Cooling State. These situations can be studied by means of the Boltzmann-Lorentz equation that governs the one particle probability density function P_s of labeled particles. For granular gases this equation reads:

$$\frac{\partial P(\mathbf{r},\mathbf{v})}{\partial t} + \mathbf{v}\cdot\frac{\partial P(\mathbf{r},\mathbf{v})}{\partial \mathbf{r}} = \sigma^{d-1}\int_{\Re^3} d\mathbf{v}_*\int_{S_+} d\hat{\mathbf{n}}(r^{-2}P_s(\mathbf{r},\mathbf{v}')P(\mathbf{r},\mathbf{v}'_*) - P_s(\mathbf{r},\mathbf{v})P(\mathbf{r},\mathbf{v}_*))|\mathbf{V}\cdot\hat{\mathbf{n}}| \tag{2.164}$$

or otherwise (when the labeled particle has a mass very much greater than the mass of the other particles) to a Fokker-Planck equation (which has the advantage of being a linear equation in P_s).

The authors have verified that the self-diffusion coefficient obtained by a Chapman-Enskog solution of the Boltzmann-Lorentz equation is consistent with Molecular Dynamics and Direct Simulation Monte

Carlo solutions of the same equation. The study of the Brownian Motion has also indicated that, for a wide range of dissipation values ($r > 0.6$) the classical picture called "aging to hydrodynamics", i.e. microscopic modes decaying faster then the macroscopic ones and the long time evolution described by the hydrodynamic mode, is still valid.

The hydrodynamics contained in Eqs. (2.160) and in the closure relations (2.161) is limited to dilute situations, as can be also intuited observing that the scalar pressure has been kept in its dilute form ($p = nk_BT$) and that the bulk viscosity η' (see paragraph 2.3.9) is neglected. Even if in principle there are no restrictions in the inelasticity parameter, the equations of Brey and co-workers can become unreliable at high inelasticities because of strong density fluctuations: the total volume fraction, in fact, can become poorly representative of the local volume fraction, so that the diluteness in the initial condition may fail.

Some authors have given alternative closure relations, valid also in more dense regimes, in particular focusing on the equation of state of the gas that is the closure expression relating the scalar pressure p to the density and temperature fields (see for example [102, 149, 202]). One important result obtained for example is that the inelasticity parameter appears in these extended equations of state always to multiply a term of order $\sim n^2$, i.e. inelasticities corrections to the pressure are subleading terms and therefore negligible in dilute systems.

At the same time, another groups of authors [214] have investigated the physics of granular gases at a more basic levels, i.e. at the kinetic level. They have derived the ring kinetic equations as well as the Boltzmann-Enskog equation in a rigorous manner (as Brey et al. did in [41]) and have pursued a program of investigation of these equations. A brief outline of the results on the Boltzmann-Enskog equation has been given in paragraph 2.2.8. They have also addressed the emergence of ordered structures, i.e. short and long range correlations, proposing kinetic ordering equations for those processes. These results will be reviewed in the first section of Chapter V.

2.5 Granular gases without hydrodynamics

In this section we give a very brief review of the main criticisms toward hydrodynamics. Simulations and experiments employing minimal models (L. P. Kadanoff [77, 122]) and discussion of basic principles (I. Goldhirsch [96, 93]) have addressed the many "weak points" along the rigorous derivation of hydrodynamics. In terms of experiments, this means that the range of validity of the continuum descriptions given in the previous section is restricted to values of the restitution coefficient not too far from 1, low volume fractions and intensities of the external driving not too strong. In the rest of this work the use of hydrodynamics will be reduced to minimum, while concepts taken from the theory of stochastic processes, dynamical systems, phase ordering kinetics and linear response theory will become the relevant tools of theoretical interpretations for the results of computer simulations.

2.5.1 The break of equipartition

In 1995 Du, Li and Kadanoff [77] have published the results of the simulation of a minimal model of granular gas in one dimension. In this model N hard rods (i.e. hard particles in one dimension) move on a segment of length L interacting by instantaneous binary inelastic collisions with a restitution coefficient $r < 1$. To avoid the cooling down of the system (due to inelasticity) a thermal wall is placed at the one of the boundaries, i.e. when the leftmost particle bounces against the left extreme ($x = 0$) of the segment, it is reflected with a new velocity taken out from a Gaussian distribution with variance T. This particle carries the energy to the rest of the system. The main finding of the authors was that even at very small dissipation $1 - r << 1$ the profiles predicted by general hydrodynamic equations (they used constitutive relations of Haff [103] or Jenkins and Richman [120]) were not able to reproduce the essential features of the simulation. In particular the stationary state predicted by hydrodynamics is a flow of heat from the left wall to the right (it goes to zero at the right wall), with no macroscopic velocity flow ($u(x,t) = 0$), a temperature profile $T(x,t)$ which decreases from $x = 0$ to $x = L$, and a density profile inversely proportional to the temperature (as the pressure $p = nT$ is constant throughout the system). In Fig. 2.3 on the next page some snapshots of the system (i.e. the position of the grains at different instants) are shown. The system is in an "extraordinary" state with almost all the particle moving slowly and very near the right wall, while almost all the kinetic energy is concentrated in the leftmost particle. The system cannot be considered in a stationary state, even if its kinetic energy is statistically stationary (i.e. fluctuates around a well defined average which is time translational invariant). Moreover, reducing the dissipativity $1 - r$ at fixed N the cluster near the wall becomes smaller and smaller. If the heat bath is replaced by a sort of saw-tooth vibrating wall which reflects the leftmost particle always with the same velocity v_0, the evolution of the baricentrum changes in a stationary oscillation very near to the rightmost wall, so that this clustering instability does not disappear. The authors also point out the fact that the Boltzmann Equation can give a qualitative prediction of this clustering phenomena in the limit $N \to \infty$, $1 - r \to 0$ with $N(1 - r) \sim 1$. We have reproduced the results of Du et al. and have discovered the this model has no proper thermodynamic limit, i.e. when $N, L \to \infty$ with $N/L \sim 1$ the mean kinetic energy and the mean dissipated power reduce to zero. This is consistent with the scenario suggested by the authors: the equipartition of energy (i.e. local equilibration of the different degrees of freedom) is broken and the description of the system in terms of macroscopic (slowly varying) quantities no more holds. In this scenario, usual thermodynamic quantities such as mean kinetic energy or mean dissipated power, are not extensive quantities.

L. P. Kadanoff has also addressed, in a recent review article [122], a set of experimental situations in which hydrodynamics seems useless. We have already discussed a well known experiment by Jaeger, Knight, Liu and Nagel [117] where a container full of sand is shaken from the bottom, when the shaking is very rapid. The observations indicate that there is a boundary layer of a thickness of few grains near the bottom that is subject to a very rapid dynamics with sudden changes of motion of the particles. At the top of the container, instead, the particles move ballistically encountering very few collisions in their trajectory. Both the top and the bottom of the container cannot be described by hydrodynamics, as the assumption of slow variation of fields or that of scale separation between times (the mean free time must be orders of magnitude lower than the characteristic macroscopic times, as the vibration

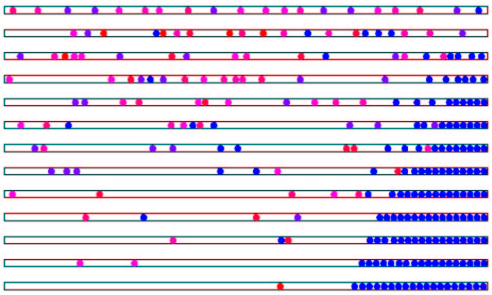

Figure 2.3: Some snapshots of the 1D system from the work of Du et al. [77]

period) are not satisfied. On the other hand, the slow dynamics regime has been studied, when the vibration is reduced to a rare tapping, so that the system reaches mechanical equilibrium (stop of motion) between successive tappings [126]. The equilibrium is reached at different densities, and - as the tapping is carried on - the "equilibrium" density slowly changes and its evolution depends on many previous instants and not on the very last tap, i.e. is history dependent. This non-locality in time cannot be described by a set of partial differential equations, therefore the hydrodynamic description here again fails.

The simulation of cooling granular gases have also interested L. P. Kadanoff in his excursus of the limits of hydrodynamics. The clustering instabilities and the inelastic collapse are clear signatures of the failure of macroscopic description. Moreover, in the inelastic collapse Kadanoff and Zhou [228] have pointed out (see Fig. 2.4) that there is a correlation between velocity directions of the particles involved in the collapse: in particular collapse is favored by parallel velocities (because they cannot escape in perpendicular directions). This situation implies a dramatic breakdown of Molecular Chaos assumption and gives evidence of the fact that Inelastic Collapse cannot be described even by a Boltzmann equation.

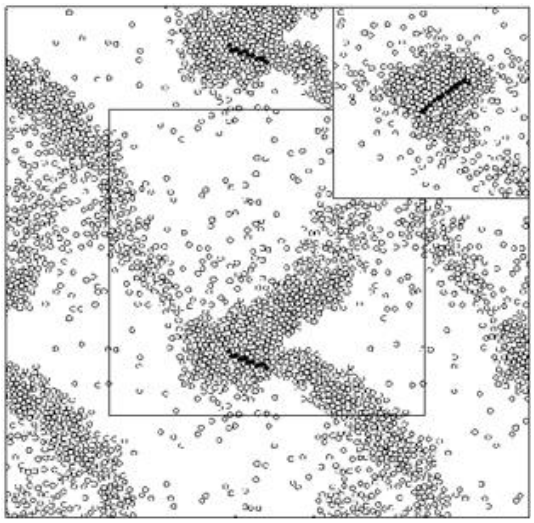

Figure 2.4: A snapshot from a MD simulation of cooling inelastic hard spheres [228]. The particles in black are those that have participated in the last collisions, just before a collapse

2.5.2 The problem of scale separation

The attack carried against granular hydrodynamics by I. Goldhirsch [96, 95, 94, 92, 93] is less hopeless, as he takes in consideration all the recent literature on rapid granular flows while he does not discuss the dense and quasi-static situations: the limits of hydrodynamics have been intensively probed by means of simulations and experiments, and it seems that a range of good validity can be found (perhaps it is more difficult to predict it!). However he points out that even these successes are somehow lacking a rigorous foundation, or using is words that "the notion of a hydrodynamic,or macroscopic description of granular materials is based on unsafe grounds and it requires further study". He addresses two fundamental issues:

1. in granular materials a reference equilibrium state is missing;
2. in granular materials the spatial and temporal scales of the dynamics of the particles are not well separated from the relevant macroscopic scales;

The first problem is more evident than the second. If a molecular gas is left to itself it comes to an equilibrium state given by the stationary solution of the corresponding kinetic equation (rarefied gases follow the Boltzmann equation, dense gases follow the Enskog-Boltzmann equation or better the ring kinetic equations). If such an equilibrium state is well defined, perturbations around it can be used as solutions of non-equilibrium problems. Moreover, if external time scales are much larger than the microscopic time scale of relaxation to equilibrium, most of the degrees of freedom of the gas are rapidly averaged and only a few variables are needed for the description of the out of equilibrium dynamics, which obey to macroscopic equations such as Euler or Navier-Stokes equations. If a granular gas is left to itself, instead, the only equilibrium state is an asymptotic death of the motion of all the particles, but before it different kinds of correlations arise leading to strong inhomogeneities (clustering, vortices, shocks, collapse, and so on). In this sense the relaxation to equilibrium has a characteristic time which is infinite and *many other characteristic times* given by different instabilities, due to the non-conservative nature of the collisions. What reference state can be used in a perturbative method like the Chapman-Enskog expansion? In the first derivations of granular hydrodynamics the Maxwell-Boltzmann equilibrium was used, in the latest derivations a more rigorous Chapman-Enskog expansion has been followed using solutions of the Enskog-Boltzmann equation by means of a Sonine expansion (which again must be performed around a Maxwell distribution). Goldhirsch has observed however that the limit $(1-r) \to 0$ and $Kn \to 0$ (the Knudsen number, indicating the intensity of the gradients, see Eq. (2.38)) is smooth and non singular for the granular Boltzmann equation, since the relaxation to local equilibrium takes place in a few collisions per particle, while the effect of (low) inelasticity is relevant on the order of hundreds or thousands of collisions. This means that a perturbative (in $1-r^2$ and Kn) expansion may be applied to the Boltzmann equation around a well suited "elastic" equilibrium, but it is expected to breakdown as $(1-r)$ or Kn are of order ~ 1.

In a stationary state the only hope is that the system fluctuates around a well defined "most probable state" (described by a well defined n-particles distribution function, hopefully $n=1$) and again an expansion around it can be performed. This program has not yet been realized: till now all hydrodynamic theories assume that the equilibrium reference state does not depend on the boundary conditions (e.g. the form of the external driving) and that both cooling and driven regimes can be described by the same set of equations.

The second issue raised by Goldhirsch stems from a more quantitative discussion. He stresses the fact that the lack of scales separation is not only a mere experimental problem: one can in principle think of experiments with an Avogadro number of grains and very large containers. Instead the lack of separation of scales is of fundamental nature in the framework of granular materials. This problem has been already recognized in molecular gases: indeed, when molecular gases are subject to large shear rates or large thermal gradients (i.e. when the velocity field or the temperature field changes significantly over the scale of a mean free path or the time defined by the mean free time) there is no scale separation between the microscopic and macroscopic scales and the gas can be considered mesoscopic. In this case the Burnett and super-Burnett corrections (and perhaps beyond) are of importance and the gas exhibits differences of the normal stress (e.g. $\mathcal{P}_{xx} \neq \mathcal{P}_{yy}$) and other properties characteristic of

granular gases. Even if clusters are not expected in molecular gases, strongly sheared gases do exhibit ordering which violates the molecular-chaos assumption. In granular gases this kind of *mesoscopicity* is generic and not limited to strong forcing. Moreover, phenomena like clustering, collapse (and of course avalanches or oscillon excitations) pertain only to granular gases. In mesoscopic systems fluctuations are expected to be stronger and the ensemble averages need not to be representative of their typical values. Furthermore, like in turbulent systems or systems close to second-order phase transitions, in which scale separation is non-existent, one expects constitutive relations to be scale dependent, as it happens in granular gases.

The quantitative demonstration of the intrinsic mesoscopic nature of (cooling) granular gases follows from the relation [96]

$$T = C\frac{\gamma^2 l_0^2}{1-r^2} \tag{2.165}$$

that relates the local granular temperature with the local shear rate γ and the mean free path l_0. The above relation holds until γ can be considered a slow varying (decaying) quantity in respect to the much more rapid decay of the temperature fluctuations (this can be observed by a linear stability analysis and also by the fact that shear modes decay slowly for small wave-numbers - a result of momentum conservation). From the Eq. (2.165) follows that the ratio between the change of macroscopic velocity over a distance of a mean free path $l_0\gamma$ and the thermal speed $\sqrt{T}$ is $\sqrt{1-r^2}/\sqrt{C}$, e.g. $\simeq 0.44$ for $r = 0.9$, that is not small. Thus, except for very low values of $1-r^2$, the shear rate is always large and the Chapman-Enskog expansion should therefore carried out beyond the Navier-Stokes order. The above consideration is a simple consequence of the supersonic nature of granular gases [93]. It is clear that a collision between two particles moving in (almost) the same direction reduces the relative velocity, i.e. velocity fluctuations, but not the sum of their momenta, so that in a number of these collisions the magnitude of the velocity fluctuations may become very small with respect to the macroscopic velocities and their differences over the distance of a mean free path. Also the notion of mean free path may become useless: l_0 is defined as a Galilean invariant, i.e. as the product between the thermal speed $\sqrt{T}$ and the mean free time τ; but in a shear experiment the average squared velocity of a particle is given by $\gamma^2 y^2 + T$ (y is the direction of the increasing velocity field), so when $y \gg \sqrt{T}/\gamma$, the distance covered by the particle in the mean free time τ is $l(y) = y l_0\gamma/\sqrt{T} = y\sqrt{1-r^2}/\sqrt{C}$ and therefore can become much larger that the "equilibrium" mean free path l_0 and even of the length of the system in the streamwise direction.

Furtherly, the ratio between the mean free time $\tau = l_0/\sqrt{T}$ and the macroscopic characteristic time of the problem $1/\gamma$, using expression (2.165), reads again $\sqrt{1-r^2}/\sqrt{C}$. This means that also the separation between microscopic and macroscopic time scales is guaranteed only for $r \to 1$. And this result is irrespective of the size of the system or the size of the grains. This lack of separation of time scales poses two serious problem: (a) the fast local equilibration that allows to use local equilibrium as zeroth order distribution function is not obvious; (b) the stability studies are usually performed linearizing hydrodynamic equations, but the characteristic times related to the (stable and unstable) eigenvalues must be of the order of the characteristic "external" time (e.g. $1/\gamma$) which, in this case, is of the order of the mean free time (as just derived), leading to the paradoxical conclusion that the hydrodynamic equations predict instabilities on time scales which they are not supposed to resolve.

Goldhirsch [93] has also shown that the lack of separation of space and time scales leads to scale dependence of fields and fluxes. In particular he has shown that the pressure tensor depends on the scale of the coarse graining used to take space-time averages. This is similar to what happens, for example, in turbulence, where the "eddy viscosity is scale dependent. Pursuing this analogy, Goldhirsch has noted that an intermittent behavior can be observed in the time series of experimental and numerical measures of the components pressure tensor: single collisions, which are usually averaged over in molecular systems, appear as "intermittent events" in granular systems as they are separated by macroscopic times.

Chapter 3

The randomly driven granular gas

Granular gases can be kept in a statistically stationary state by means of an external forcing. In experiments, this forcing is realized with shear strains, shaking, air fluidization, and so on. Usually it is not enough to simply give "energy" to the granular gas: for example a granular gas falling under the force of gravity (in the void) continues to cool, even if its kinetic energy increases as every grain accelerates. To obtain a stationary granular gas it is necessary to provide it with an "internal energy" input, i.e. a randomization (temperature) source. The stationary flow observed on inclined planes is due to the combined effect of gravity and random collisions with the inclined bottom. When a granular layer (monolayers are often used in experimental situation to reproduce a quasi-2d behavior) stays on a horizontal plate which is rapidly vibrated, the grains get random kicks (abrupt changes of moment) even if the vibration is periodic; moreover, while the vertical component of the kicks is not symmetrically distributed, the components parallel to the plate are isotropic. In all experimental situations the temperature source is also responsible for a systematic (non random) dissipation: in the examples given above this is simply understood as an effective friction due to collisions with the bottom. In such a situation, therefore, it is quite natural to model the evolution of velocity as a stochastic process composed of three ingredients:

- inelastic collisions between grains;
- random kicks;
- systematic dissipation;

It is important to keep separated the first two ingredients in this idealized picture, even if they seems similar in the sense that both are random changes of velocity: we impose all the statistical properties of the random kicks (i.e. distribution and spectral properties) but give very few constraints on the statistics of the collisions between grains. This situation is very different from that of the Brownian motion, where all the effects of the collisions between the observed particle and the fluid particles are embedded in the statistics of the random kicks (and in the form of the systematic dissipation). As a consequence of this, while the Brownian motion is essentially reduced to a one-particle problem, the randomly driven granular gas remains a many-body problem, where spatial correlations (in the density and in the velocity) can emerge.

3.1 The model

In this section the randomly driven granular gas is introduced in d dimensions and some issues about the characteristic times and the expected behavior (in different physical limits) are discussed. A physical interpretation of the random driving is proposed.

3.1.1 Equations of motion and collisions

The randomly driven granular gas that we have introduced (Puglisi et al. [183, 184]) consists of an assembly of N identical hard objects (spheres, disks or rods) of mass m and diameter σ. We put, for simplicity, $m = 1$ and $k_B = 1$ (the Boltzmann constant). Moreover, in dimension $d = 1$ the diameter (the length of the rods) is irrelevant because the objects are undeformable, therefore the only physical quantities that determine the dynamics of the gas are the lengths of the free spaces between the grains and their relative velocities: a system of infinitesimal grains of diameter $\sigma = 0$ is equivalent to a system with finite σ. Consequently, in dimension $d = 1$, we use the coordinate x to count only the free space (as the grains had $\sigma = 0$): at every instant t the true coordinates $X_i(t)$ of the centers of the grains with finite σ can be obtained from their fictitious coordinates $x_i(t)$ by the invertible mapping

$$X_i(t) = x_i(t) + (2i+1)\frac{\sigma}{2} \tag{3.1}$$

The grains move in a box (a square in $d = 2$, a segment in $d = 1$) of volume $V = L^d$ (L is the length of the sides of the box), with periodic boundary conditions, i.e. opposite borders of the box are identified. Therefore the topology of the ambient space is a d-dimensional torus (i.e. a circle in $d = 1$).

The mean free path (calculated exactly in Eq. (2.29) for the case of an homogeneous gas of 3D hard spheres with a Maxwellian distribution of velocities) can be roughly estimated as

$$\lambda^* = \overline{v}^* \tau_c^* = \frac{\overline{v}^*}{\nu^*} \simeq \frac{\overline{v}^*}{n^* \overline{v}^* S^*} = \frac{1}{n^* S^*} \tag{3.2}$$

where $\overline{v}^*$ is the typical velocity of the particles $\sqrt{\langle v^2 \rangle}$, τ_c^* is the mean collision time, ν^* is the mean collision rate (inverse of τ_c^*), $n^* = N/V$ is the mean number density and S^* is the total scattering cross section. We stress the fact that S^* has the dimensions of a surface in $d = 3$ ($S^* \sim \sigma^2$), of a line in $d = 2$ ($S^* \sim \sigma$) and no dimensions in $d = 1$ (this is consistent with the fact that the diameter, in $d = 1$ is irrelevant). The stars * indicate that all these quantities are *global* quantities: in this model we observe strong local fluctuations, that is the global quantities can be poorly representative of the effective dynamics.

The dynamics of the gas, as already discussed in the introduction to this chapter, is obtained as the byproduct of three physical phenomena: friction with the surroundings, random accelerations due to external driving, inelastic collisions among the grains. We model the first two ingredients in the shape of a Langevin equation with exact fulfillment of the Einstein relation (see for example[130]), for the evolution of the velocities of the grains in the free time between collisions. The inelastic collisions are, instead, considered at the kinetic level, i.e. they are instantaneous transformations of the velocities of two colliding particles (grains that are touching, with approaching relative velocity). The equations of motion for a particle i that is not colliding with any other particle, are:

$$\frac{d}{dt}\mathbf{v}_i(t) = -\frac{\mathbf{v}_i(t)}{\tau_b} + \sqrt{\frac{2T_b}{\tau_b}}\boldsymbol{\eta}_i(t) \tag{3.3a}$$

$$\frac{d}{dt}\mathbf{x}_i(t) = \mathbf{v}_i(t) \tag{3.3b}$$

We call the parameters τ_b and T_b *characteristic time of the bath* and *temperature of the bath* respectively. The function $\boldsymbol{\eta}_i(t)$ is a stochastic process with average $< \boldsymbol{\eta}_i(t) >= 0$ and correlations $< \eta_i^\alpha(t)\eta_j^\beta(t') >= \delta(t-t')\delta_{ij}\delta_{\alpha\beta}$ (α and β being component indexes) i.e. a standard white noise.

When two particles i and j satisfy the following conditions:

$$\mathbf{x}_i - \mathbf{x}_j = \sigma\hat{\mathbf{n}} \tag{3.4a}$$
$$(\mathbf{v}_i - \mathbf{v}_j)\cdot\hat{\mathbf{n}} < 0 \tag{3.4b}$$

they are said to be *colliding*. The unit vector $\hat{\mathbf{n}}$ is defined by Eq. (3.4a). When two particles are colliding, their velocities are instantaneously changed into new velocities according to the following collision rule:

$$\mathbf{v}_i' = \mathbf{v}_i - \frac{1+r}{2}((\mathbf{v}_i - \mathbf{v}_j)\cdot\hat{\mathbf{n}})\hat{\mathbf{n}} \tag{3.5a}$$
$$\mathbf{v}_j' = \mathbf{v}_j + \frac{1+r}{2}((\mathbf{v}_i - \mathbf{v}_j)\cdot\hat{\mathbf{n}})\hat{\mathbf{n}} \tag{3.5b}$$

These are the rules for inelastic collisions, for $0 \leq r < 1$ they reduce the longitudinal component of the relative velocity, while for $r = 1$ this component is only inverted. The parameter r is the normal restitution coefficient. After a collision, the two particles satisfy the following conditions:

$$\mathbf{x}_i - \mathbf{x}_j = \sigma\hat{\mathbf{n}} \tag{3.6a}$$
$$(\mathbf{v}_i - \mathbf{v}_j)\cdot\hat{\mathbf{n}} > 0 \tag{3.6b}$$

We say that two such particles are *anticolliding*.

3.1.2 Characteristic times, elastic limit, collisionless limit, cooling limit: the two stationary regimes

In the dynamics of the N particles, as defined in Eqs. (3.3), (3.4), (3.5), the most important parameters are:

- the coefficient of normal restitution r, which determines the degree of inelasticity;
- the ratio $\rho = \tau_b/\tau_c$ between the characteristic time of the bath and the "global" mean free time between collisions;

On the basis of these two parameters, we can define three fundamental limits of the dynamics of our model:

- the elastic limit: $r \to 1^-$;
- the collisionless limit: $\rho \to 0$ ($\tau_c \gg \tau_b$);
- the cooling limit: $\rho \to \infty$ ($\tau_c \ll \tau_b$);

The *elastic limit* is smooth in dimensions $d > 1$ (see for example the discussion in paragraph 2.5), so that we can consider it equivalent to put $r = 1$. In this case the collisions mix up the components leaving constant the energy (in the center of mass frame as well in the absolute frame). We can assume that, in this limit, the effect of the collisions is that of homogenizing the positions of the particles and making their velocity distribution relax toward the Maxwellian with temperature $T_g = \langle v^2\rangle/d = \langle v_x^2\rangle$ (this temperature is equal to the starting kinetic energy, but is modified by the relaxation toward T_b due to the Langevin Eqs. (3.3)). In one dimension this mixing effect (toward a "Maxwellian") is no more at work, as the elastic collisions exactly conserve the starting velocity distribution (the collisions can be viewed as exchanges of labels and the particles as non-interacting walkers).

In the *collisionless limit* we have $\tau_c \gg \tau_b$ and therefore, the collisions are very rare events with respect to the characteristic time of the bath. In this case we can consider the model as an ensemble

of non-interacting Brownian walkers, each following the Eqs. (3.3). Therefore, whatever r is, and in any dimension, the distribution of velocities relaxes in a time τ_b toward a Maxwellian with temperature $T_g = \langle v^2 \rangle / d = T_b$ with a homogeneous density.

Finally, in the *cooling limit*, the collisions are almost the only events that act on the distribution of velocities, while between collisions the particles move almost ballistically. In this limit (if $r < 1$) the gas can be considered stationary only on observation times very long with respect to the time of the bath τ_b, where the effect of the external driving (the Langevin equation) emerges. For observation times larger than the mean free time τ_c but shorter than τ_b, the gas appears as a *cooling granular gas*. This limit is considered in Chapter V of this thesis.

To conclude this brief discussion on the expected behavior of the randomly driven granular gas model, we sketch a scenario with the presence of two fundamental stationary regimes:

- the "collisionless" stationary regime: when $\rho \ll 1$, i.e. approaching the *collisionless* limit; in this regime we expect, after a transient time of the order of τ_b, the stationary statistics of an ensemble of non-interacting Brownian particles (homogeneous density and Maxwell distribution of velocities, absence of correlations);
- the "colliding" stationary regime: when $\rho \gg 1$, i.e. approaching the *cooling* limit, but observing the system on times larger than τ_b; here we expect to see anomalous statistical properties.

3.1.3 Interpretation of the random driving

We have introduced a Langevin equation as the most natural way to model the sum of external driving and external dissipation. In many experimental situations (see section 1.2) this fact has been recognized. One questionable issue is the decision of assume the validity of the fluctuation-dissipation relation (second kind in the Kubo terminology) between dissipation and random accelerations, disregarding the effect of collisions among the grains, i.e.:

$$< R(t_1)R(t_2) >= \frac{2T_b}{\tau_b}\delta(t_1 - t_2) \tag{3.7}$$

that is assumed from each component of Eq. (3.3a) if read as a Langevin equation of the form:

$$\frac{dv(t)}{dt} = -\frac{v_i(t)}{\tau_b} + R(t) \tag{3.8}$$

The validity of relation (3.7) cannot be guaranteed in a real system of particles kicked by random forces and in the presence of dissipative collisions, as the system is not in thermal equilibrium with the kicking bath. We are studying the possibility of a Langevin description of the whole system (external driving *plus* inelastic collisions) [16].

It is important to stress that *this is a model* and its main aim is not to reproduce quantitative details of a real system, but only to make qualitative predictions that can be verified in experiments or can be compared with other models.

To our knowledge, experimental measurements of velocity distributions have been performed only recently (and noticeably only for steady state granular systems under some sort of energy pumping), they have been discussed in section 1.2. We recall some of the real setups used, where non-Gaussian distribution have been observed:

- Vibration of the bottom of a 3D granular system (Losert et al. [144])
- Vertical vibration of an horizontal plate with a granular monolayer on the top of it (Olafsen and Urbach [172, 173])
- Vibration of the bottom side of an inclined plane with a very dilute granular monolayer rolling on it, under the presence of gravity (Kudrolli and Henry [132])
- Vibration of the bottom of a granular system confined in a vertical plane (Rouyer and Menon [189])

In paragraph 3.2.6 we discuss the possibility of checking the relevance of the viscous term: it is tied to the velocity correlations. A randomly driven granular gas with a relevant viscosity should not display velocity structures, while they can appear if this term is negligible.

3.2 MD and DSMC simulations: outcomes

We have performed Molecular Dynamics (event-driven) simulations in one dimension [183] and Direct Simulation Monte Carlo (Bird algorithm) in one and two dimensions [184]. We have checked the compatibility of the results between MD and DSMC in a wide range of parameters (restitution coefficient, number density, collision and driving times). We have computed the density and velocity distributions, the correlation dimension (fractal dimension D_2), the density entropy, the auto-correlation of velocity and the coefficients of self-diffusion.

3.2.1 Differences between MD and DSMC

In the next paragraph we give the results of the simulations of the randomly driven granular gas model. We have used *event driven* Molecular Dynamics simulations in $d = 1$: in these simulations the position of the particles are precisely known, the collisions happen if and only if the conditions (3.4) are verified, in other words the model is exactly reproduced by the simulator. In some of the *runs* performed, at low values of r and high values of the ratio $\rho = \tau_b/\tau_c$ (approaching the cooling limit) we have observed a dramatic increase of the collision rate resulting in very poor performances of the algorithm: we have discarded the results of these simulations considering them the evidence of a sort of inelastic collapse (this fact is reflected in the figures, where some points are missing). To simulate a larger number of particles in more than one dimension, we have performed a number of Direct Simulation Monte Carlo: this is an algorithm introduced (by Bird, see for example [30]) to reproduce the solution of the Boltzmann equation and assumes the Molecular Chaos, i.e. disregards correlations of colliding particles. In Appendix A we give a detailed description of Molecular Dynamics of hard spheres in $d = 1$ and of Direct Simulation Monte Carlo in $d = 1$ and $d = 2$. Here we just warn the reader to be careful and notice the captions of the figures. Where "DSMC" appears, it must be clear that an important assumption (Molecular Chaos) has been made. However the compatibility of the results with MD in $d = 1$ and also many agreements with experimental measurements has convinced us that the Bird algorithm is very well suited to study qualitatively dilute granular gases. Finally, we stress the fact that even if a granular gas is well described by the Boltzmann equation (this is the message/anticipation of this brief introduction), nothing is said about the hydrodynamic description, where further assumption are needed (e.g. low values of the gradients, scale separation, etc).

3.2.2 Kinetic energy and dissipated kinetic energy, stationarity, thermodynamic limit

We have studied the average kinetic energy ("granular temperature") and the average energy dissipated by the collisions of the system. These quantities are defined in the following way:

$$K = \frac{T_g}{2} = \frac{1}{2N}\sum_{i=1}^{N} v_i(t)^2 \tag{3.9a}$$

$$W_{\Delta t} = \frac{1}{\Delta t}\sum_{j:t_j\in[t-\Delta t/2,t+\Delta t/2]} (\Delta K)_j \tag{3.9b}$$

where $(\Delta K)_j$ is the kinetic energy loss during the j_{th} collision occurring at time t_j. These quantities reach a stationary value (i.e. are "constant") after a transient time of the order of the longest characteristic time (which may be τ_c or τ_b) and if they are time-averaged on an observation time of the same order (Δt is taken much smaller). The stationary values of kinetic and dissipated energy are shown in Fig. 3.1 on the next page for different choices of the restitution coefficients and of the characteristic time of the bath τ_b, in $d = 1$ Molecular Dynamics simulations.

In these MD simulations we can estimate the mean free time as

$$\tau_c \approx \frac{L}{2N\sqrt{T_g}} \tag{3.10}$$

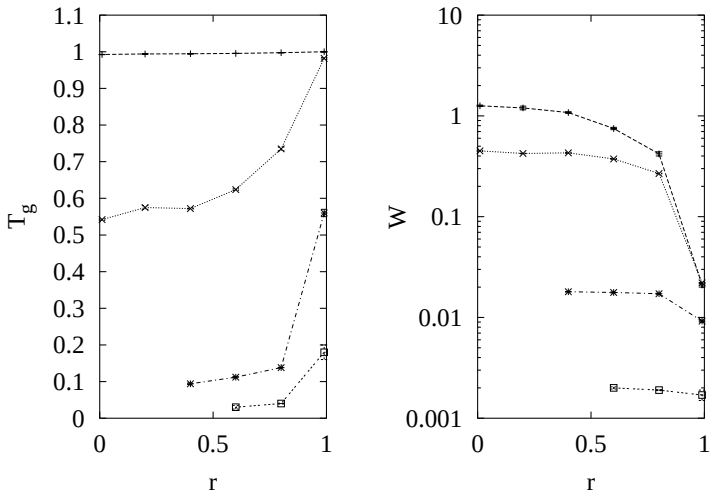

Figure 3.1: K and W vs r in $d = 1$ MD simulations, with τ_b that takes the values 0.01, 2, 100, 1000 (from top to bottom), while $\tau_c \in (0.5, 5)$, $N = L = 200$, $T_b = 1$. The values used for r are: 0, 0.2, 0.4, 0.6, 0.8 and 0.99. Missing data points are due to the appearance of strong density fluctuations: we have discarded these points assuming that the Bird algorithm is unreliable in these situations.

and, as T_g is observed to be almost always in the range $[T_b/10, T_b]$, using in all simulations $L/N = 1$ and $T_b = 1$, we expect $\tau_c \in [0.5, 2]$. Our observations confirm this expectation. The analysis of Fig. 3.1 are in agreement with the scenario proposed in the discussion of the previous paragraph. In the elastic limit $r \to 1^-$ the granular temperature tends toward the bath temperature (and the kinetic energy in collisions tends to zero). In the collisionless limit (upper curves) the granular temperature again tends toward the bath temperature and this happens for every value of r. In the "colliding" regime the system is sensible to inelasticity and the granular temperature drops under the bath temperature when $r < 1$.

A mean-field relation between granular temperature, bath temperature and dissipated energy in collisions can be calculated. We assume that in a small step of time of length Δt the dissipated energy in collisions is exactly equal to energy gained from the "bath" (i.e. the Langevin equation) $(\Delta K(t))_{Lang}$. This is of course a rough approximation: we have already noticed that the stationarity is strictly observed only for time-averages taken on the largest time of the problem, while on shorter times the values are fluctuating (in principle these fluctuations are physical and not statistical, i.e. they should not vanish if averaged on many realizations, because they are due to the different relaxation processes that have different characteristic times) and this equality is not guaranteed.

However, we try to verify this very rough relation, writing

$$(\delta K(t))_{Lang} = \frac{1}{2N}\sum_{i=1}^{N}(v_i(t) + \delta v_i(t))^2 - \frac{1}{2N}\sum_{i=1}^{N} v_i^2(t) = \\ = \frac{1}{2N}\sum_{i=1}^{N}(\delta v_i(t))^2 + \frac{1}{N}\sum_{i=1}^{N} v_i(t)\delta v_i(t) \quad (3.11)$$

where δv_i is the velocity variation during a time interval dt in Eq. (3.3a), from which we obtain the relations:

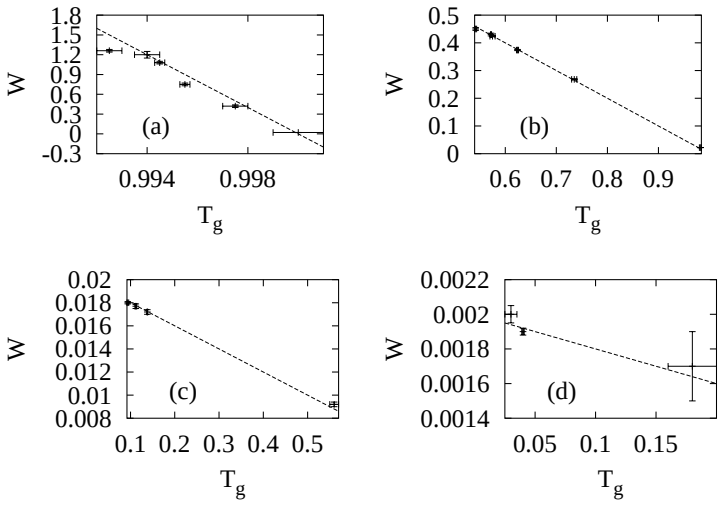

Figure 3.2: K vs. W in 1d, MD. (a) $\tau_b = 0.01$, (b) $\tau_b = 2$, (c) $\tau_b = 100$, (d) $\tau_b = 1000$. The other parameters take the same values as in Fig. 3.1 on the facing page

$$\lim_{dt\to 0} \left\langle \frac{\delta v_i(t))^2}{dt} \right\rangle = \frac{2T_F}{\tau} \tag{3.12}$$

$$\lim_{dt\to 0} \left\langle \frac{v_i(t)\delta v_i(t)}{dt} \right\rangle = -\frac{\langle v_i^2 \rangle}{\tau} \tag{3.13}$$

where the $< ... >$ average is taken over different realizations of the noise.

We then insert Eqs. (3.12) and (3.13) into Eq. (3.11), assuming the equivalence among time averages, particle averages and ensemble averages, obtaining:

$$W = \frac{T_F - T_g}{\tau} \tag{3.14}$$

The numerical check of such relation is shown in Fig. 3.2.

This relation is fairly verified, showing that in this model fluctuations have not dramatic effects on averages and that the model is not too far from ergodicity (we have identified time averages with realization averages) and from strict stationarity (we have assumed a perfect energy balance in a time step $dt \to 0$).

Finally, we have studied the thermodynamic limit of some physical observables, using Direct Simulation Monte Carlo (see Appendix A). The quantities under study are the granular temperature T_g, the mean collision rate ν and the correlation dimension d_2. The latter quantity will be exactly defined in the next paragraph. The number of particles has been increased keeping the ratio N/V fixed, in $d = 1$ and $d = 2$. We show the results of these simulations in Fig. 3.3 on the following page and Fig. 3.4 on the next page.

The results are at odds with the same study performed on the model proposed by Du, Li and Kadanoff. There it could be obtained a stationary state with no proper thermodynamic limit. Here the existence of a proper thermodynamic limit is well verified: moreover the results in the figures show that with a few particles the observed statistical properties are compatible with that measured in bigger systems.

3.2.3 Density correlations

We have studied (in $d = 1$ and $d = 2$) the arrangement of the grains inside the box and the correlations between their positions. The main feature observed in this study is the appearance of *spatial clustering*

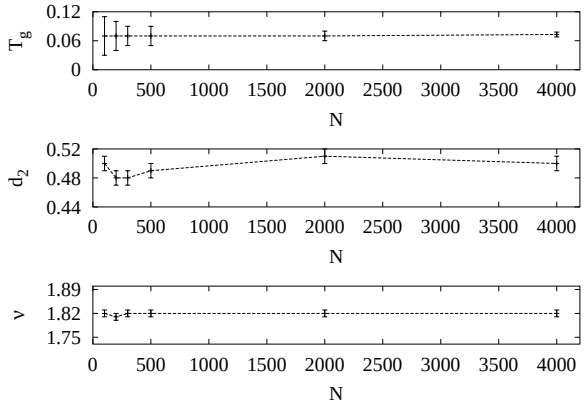

Figure 3.3: Thermodynamic limit in $d = 1$, using DSMC algorithm (see Appendix A). Here $\tau_b = 100$, $\tau_c = 0.5$, $r_B = 0.4$, $N/L = 1$, $r = 0.5$.

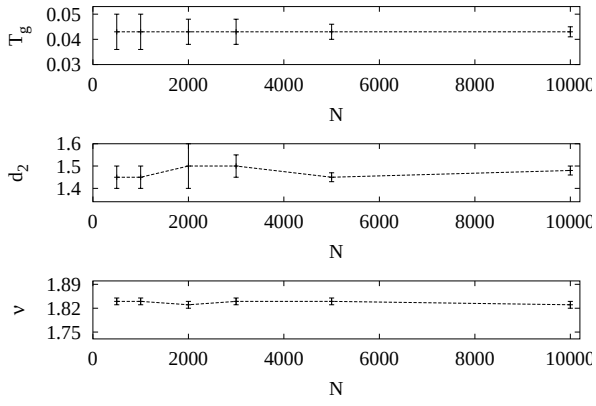

Figure 3.4: Thermodynamic limit in $d = 2$, using DSMC algorithm (see Appendix A). Here $\tau_b = 100$, $\tau_c = 0.5$, $r_B = 0.63$, $N/L^2 = 1$, $r = 0.5$.

for inelastic gases ($r < 1$) in the colliding regime ($\rho \gg 1$). We firstly give detailed results for $d = 1$ and, after, similar measurements for $d = 2$.

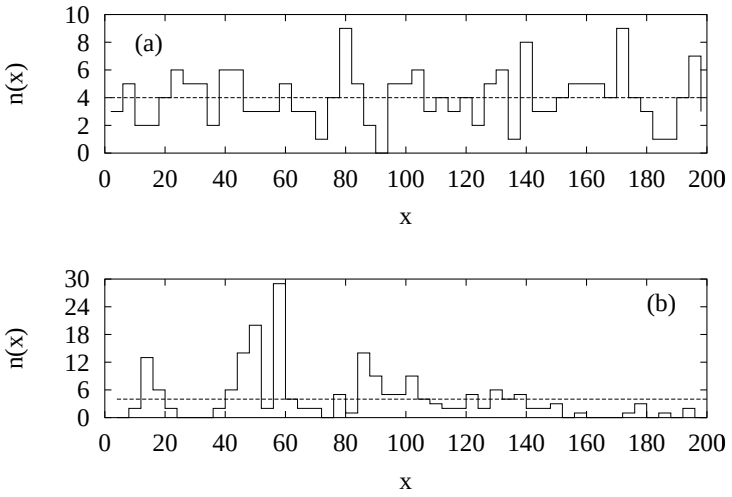

Figure 3.5: Density profiles in $d = 1$, obtained with MD simulations with $N = L = 200$ (and bins large $L_{bin} = 4$). Parameters in (a) are $\tau_b = 0.01$ and $r = 0.99$. In (b) instead are $\tau_b = 100$, $r = 0.6$.

In Fig. 3.5 we show a profile of the density (not normalized) of the gas obtained by means of a coarse graining. The pictures are taken for two different choices of the parameters: one in the collisionless regime (and near elasticity), the other in the colliding regime. A guideline indicates the average (uniform) density. The colliding regime is characterized by fluctuations of the density very much stronger than in the collisionless regime. We call these fluctuations "clusters".

In Fig. 3.6 on the next page and Fig. 3.7 on the following page we show the probability distribution of the "M-cluster mass" m_M defined as the number of particles found in a box of volume V/M. The two figures are similar in the choices of the parameters, but the first is taken from a MD simulation, while the second from a DSMC run. These figures are important because show an impressive qualitative agreement between the two algorithms used in this work: in the collisionless regime ($\tau_b \ll \tau_c$) the number of particle in a box is Poisson distributed, i.e.:

$$f(m_M) = \frac{\langle m_M \rangle^{m_M}}{m_M!} e^{-\langle m_M \rangle} \tag{3.15}$$

where $\langle m_M \rangle = N/M$ is the expected value of m_M. This distribution is the signature of the fact that the positions of the particles are independently distributed in the space, i.e. no correlations emerge from the dynamics in this regime. On the other side, in the colliding regime ($\tau_b \gg \tau_c$), the distribution is very different. In both the figures it can be fitted by a curve $m_M^{-\alpha_{cl}} \exp(-c_{cl} m_M)$. This curve is the product of a negative power law with a negative exponential cut-off. In most observed situations we have measured $\alpha_{cl} > 1$ and $1/c_{cl}$ slightly greater than N/M. The power law is the signature of self-similarity in the distribution of clusters: in the colliding regime structures emerge with no characteristic mass. The exponential cut-off is due to finite size effects (N is finite and is a normalizing constraint). We stress that the agreement between MD and DSMC results is striking: these observations suggest strong correlations between grains, a fact that cannot be considered obvious in a DSMC simulation (where some correlations are artificially removed).

We have characterized the departure from the Poisson distribution of the cluster masses by means of an h_M entropy functional which is defined as

$$h_M(t) = -\sum_{i=1}^{M} \frac{m_i}{N} \ln\left(\frac{m_i}{N}\right) \tag{3.16}$$

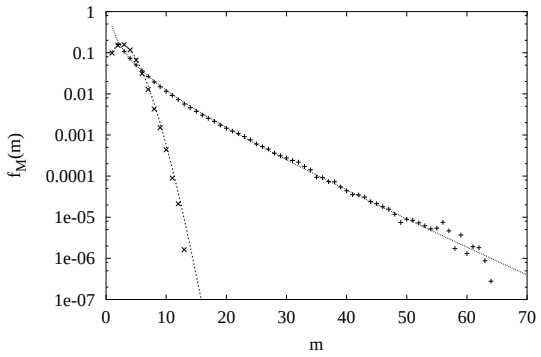

Figure 3.6: Distribution of cluster mass m_M, in $d = 1$, MD. With $N = L = 300$, $M = 100$, one set of data with $\tau_b = 0.01$ and $r = 0.99$, the other with $\tau_b = 100$ and $r = 0.7$. The first set is fitted by a Poisson distribution with average $\overline{m} = 3$, the other by a curve $m^{-1} \exp(-0.14m)$.

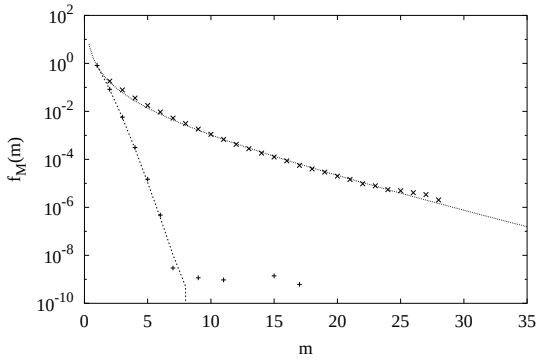

Figure 3.7: Distribution of cluster mass m_M, in $d = 1$, DSMC. With $N = L = 500$, $M = 12000$, one set of data with $\tau_b = 0.01$ and $r = 0.99$, the other with $\tau_b = 100$ and $r = 0.5$. The first set is fitted by a Poisson distribution with average $\overline{m} = N/M \approx 0.4$, the other by a curve $m^{-1.95} \exp(-0.26m)$.

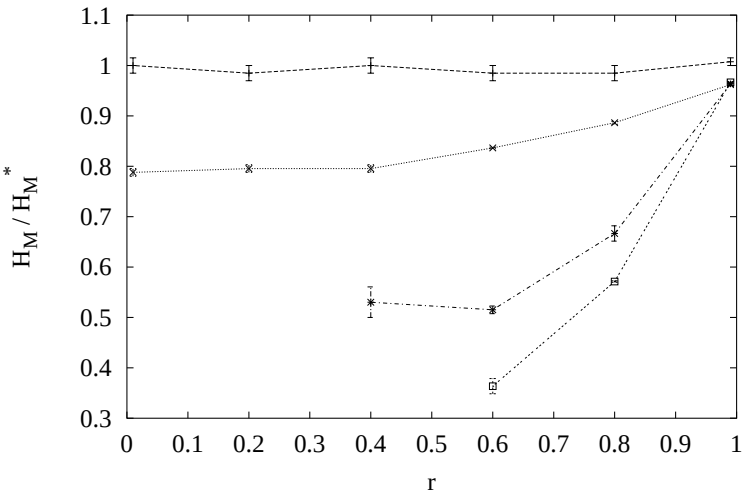

Figure 3.8: H_M/H_M^* vs. r in $d = 1$, MD simulations, with $N = 200$, $M = 80$ ($H_M^* \approx 63$), different values of τ_b: 0.01, 2, 100, 1000

where the system has been divided in M boxes of volume V/M and the quantity m_i is the number of particles in the i-th box. This quantity attains its maximum value $\ln M$ when the number of particle is the same, N/M, in every box and decreases as the density becomes more and more clusterized. As we have seen, the homogeneous regime is characterized by fluctuations of the quantity $m_i = m_M$, following the Poisson distribution of Eq. (3.15); in this case the value h_M can be numerically calculated. We call this "homogeneous" value h_M^*. The value h_M has the same properties of stationarity found for the kinetic energy or the dissipated energy. In Figure Fig. 3.8 it is shown the quantity H_M/H_M^*, where $H_M = \exp(h_M)$ and $H_M^* = \exp(h_M^*)$. We observe that the departure from the collisionless regime is accompanied by a sensible decrease of the entropy of the distribution of the masses, which is a signature of the organization in dense clusters and almost empty regions. The clusters are rapidly evolving, they break and form again, so that the entropy h_M is statistically stationary on large observation times (time averages).

Furtherly, to obtain more information on the kind of spatial correlations among grains, we have studied the correlation dimension (Grassberger and Procaccia [100]) d_2 that is defined in the following way. The cumulated particle-particle correlation function is:

$$C(t, R) = \frac{1}{N(N-1)} \sum_{i \neq j} \Theta(R - |\mathbf{x}_i(t) - \mathbf{x}_j(t)|) \tag{3.17}$$

After having checked that the system has reached a stationary regime, we have computed its time-average $C(R)$. In the Fig. 3.10 on page 77 and Fig. 3.11 on page 77 we show the $C(R)$ vs. R for different regimes and with different algorithm. We observe a power law behavior in both colliding and collisionless regimes, and with both algorithm, MD and DSMC (this is again a surprising agreement):

$$C(R) \sim R^{d_2} \tag{3.18}$$

This relation defines the correlation dimension d_2.

In the case of homogeneous density d_2 is expected to be the euclidean dimension $d_2 = d$. The case $d_2 < d$ is a definition of *fractal* density. We find a homogeneous density in the collisionless regime, and fractal density in the inelastic colliding regime ($\tau_b \gg \tau_c$ and $r < 1$). This is consistent with the power law distribution of cluster masses observed before in the same regime.

In Fig. 3.9 on the following page we show the stationary values of d_2 obtained for different choices of the parameters r and τ_b (keeping almost fixed τ_c). We stress the fact that the DSMC algorithm imposes the absence of correlations among colliding particles: this is observed in the plot of $C(R)$

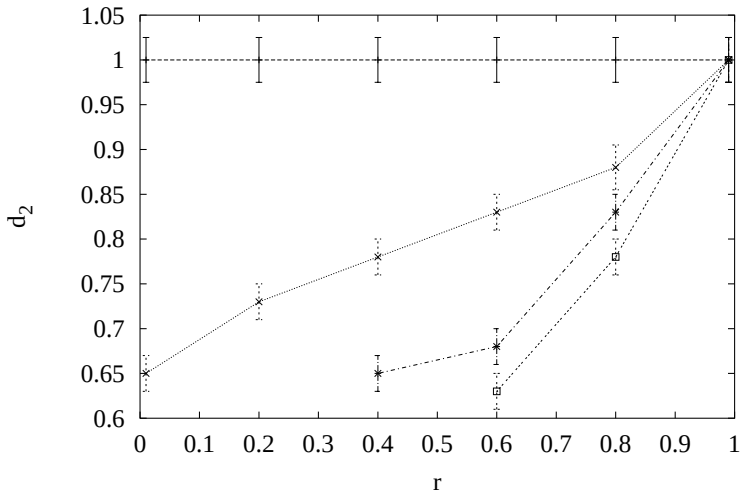

Figure 3.9: The correlation dimension d_2 vs r for different values of τ_b: 0.01, 2, 100, 1000 from top to bottom. $N = L = 200$ in all the simulations, with $d = 1$ MD

where, in the colliding regime, the slope $d_2 < d$ is observed only for $R > R_0$, with $R_0 \approx r_B$ (see Fig. 3.10 on the next page and Fig. 3.11 on the facing page) . For a discussion on the Bird radius r_B we refer to Appendix A.

We have repeated all the analysis of the density for the system in $d = 2$, using only DSMC simulations, and finding the same phenomena: homogeneous density in the case $\tau_b \ll \tau_b$ and clusterized fractal density when $\tau_b \gg \tau_c$ and $r < 1$. In Fig. 3.12 on page 78 we propose a "photography" of the system with the positions of the particles, in an instant of the simulation in the clusterized regime ($\tau_b \ll \tau_c$ and $r < 1$). In Fig. 3.13 on page 78 we show the probability distribution of cluster masses, as defined above, for the two different regimes: we observe again the Poisson distribution in the homogeneous situation and the power law (plus the finite size exponential cut-off) in the clusterized situation.

Finally, we have studied the correlation function defined in Eq. (3.17) and its power-law behavior characterized by the exponent d_2. The function is shown in Fig. 3.15 on page 79. In Fig. 3.14 on page 79 we have plotted a summary of the measurements of several quantities in $d = 2$: the granular temperature, the correlation dimension d_2, the collision rate ν and the diffusion coefficient D. The diffusion coefficient is discussed in a paragraph 5.66.

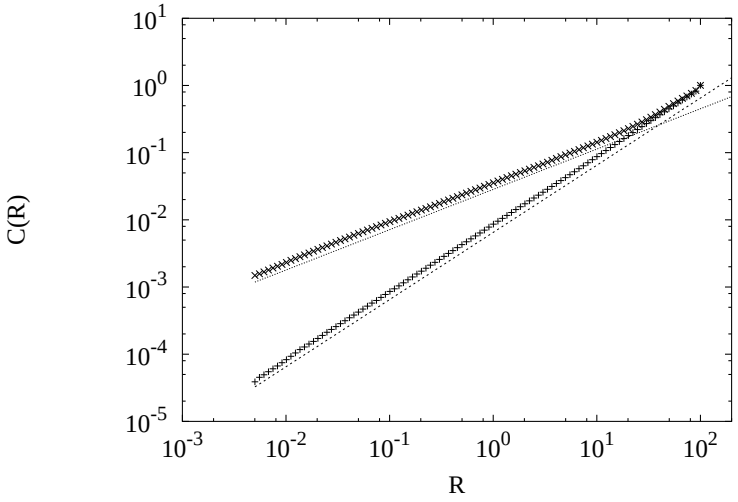

Figure 3.10: Density correlation function $C(R)$ vs R, in $d = 1$, with MD simulations with $\tau_b = 100$ and $r = 0.99$ (bottom) and $\tau_b = 100$ and $r = 0.6$ (top), $N = L = 200$; the measured d_2 takes respectively the values 1 and 0.59

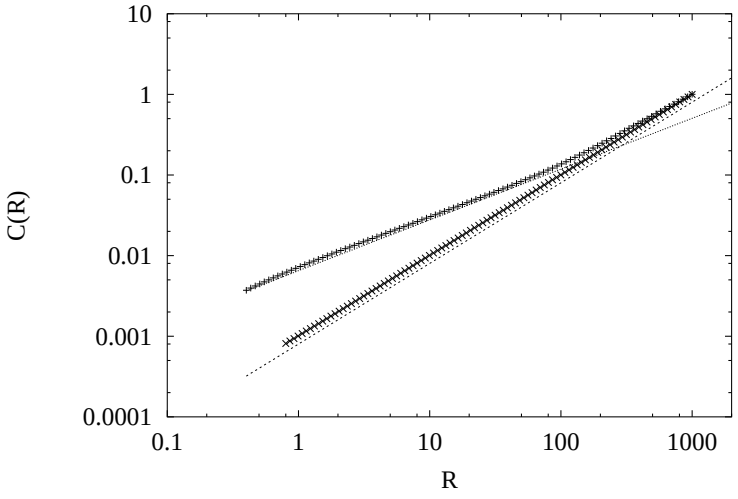

Figure 3.11: Density correlation function $C(R)$ vs R, in $d = 1$, with DSMC algorithm with $\tau_b = 0.01$ and $r = 0.99$ (bottom) and $\tau_b = 100$ and $r = 0.5$ (top), $N = L = 2000$, $\tau_c = 0.5$, $r_B = 0.4$; the measured d_2 takes respectively the values 1 and 0.55

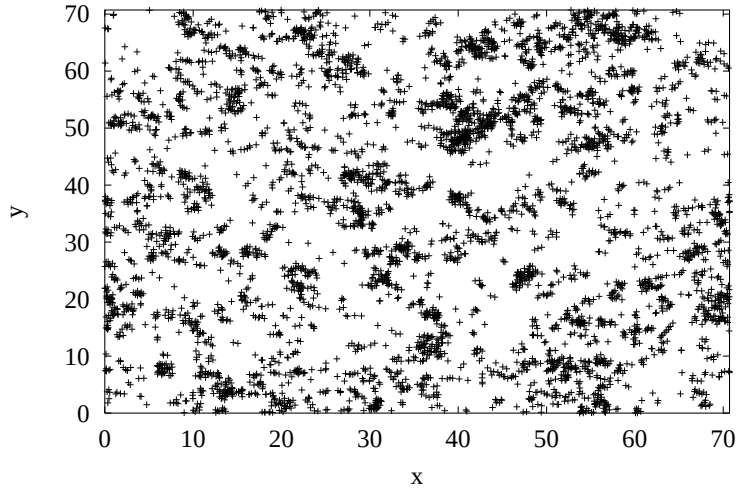

Figure 3.12: Snapshot of particle distribution in $d = 2$, in the clusterized regime ($\tau_b = 100$, $\tau_c = 0.01$, $r = 0.5$), with $N = L^2 = 5000$ and $r_B = 0.63$

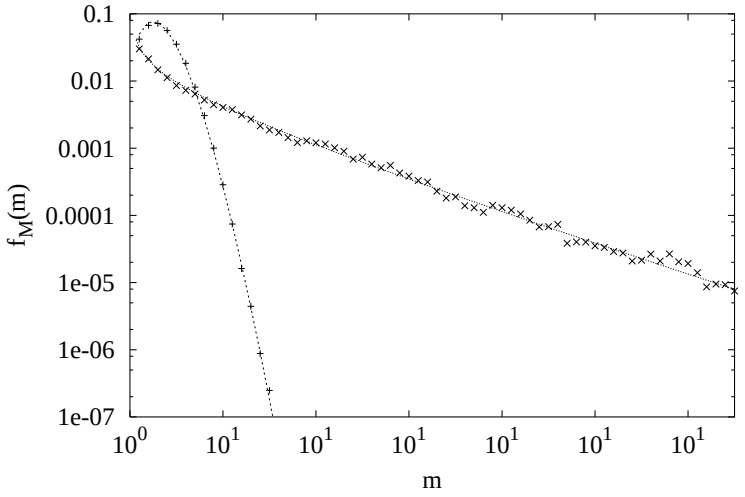

Figure 3.13: Distribution of cluster mass m_M, in $d = 2$, DSMC simulations. With $N = L^2 = 10000$, $M = 3200$, $\tau_c = 0.05$, $r_B = 0.22$, one set of data with $\tau_b = 0.01$ and $r = 0.99$, the other with $\tau_b = 100$ and $r = 0.5$. The first set is fitted by a Poisson distribution with average $\overline{m} = N/M = 3.125$, the other by a curve $m^{-0.5}\exp(-0.097m)$.

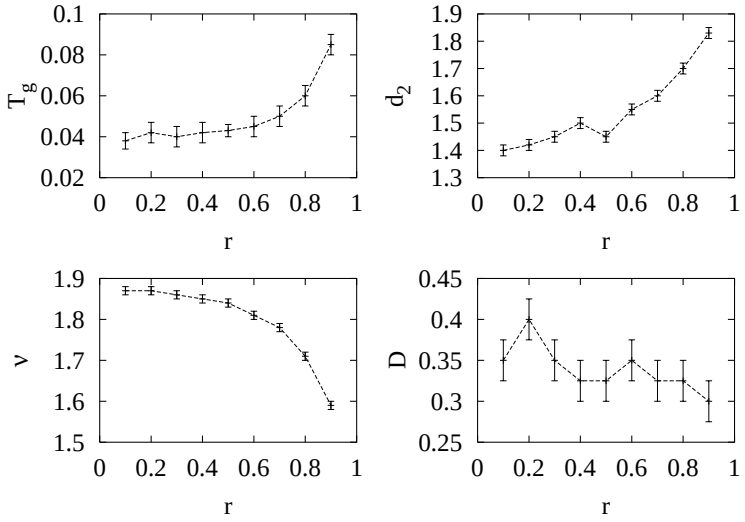

Figure 3.14: Granular temperature T_g, correlation dimension d_2, collision rate ν and diffusion coefficient D vs. r from DSMC simulations with $d = 2$, with $N = L^2 = 3000$, $\tau_c = 0.5$, $\tau_b = 100$ and $r_B = 0.5$

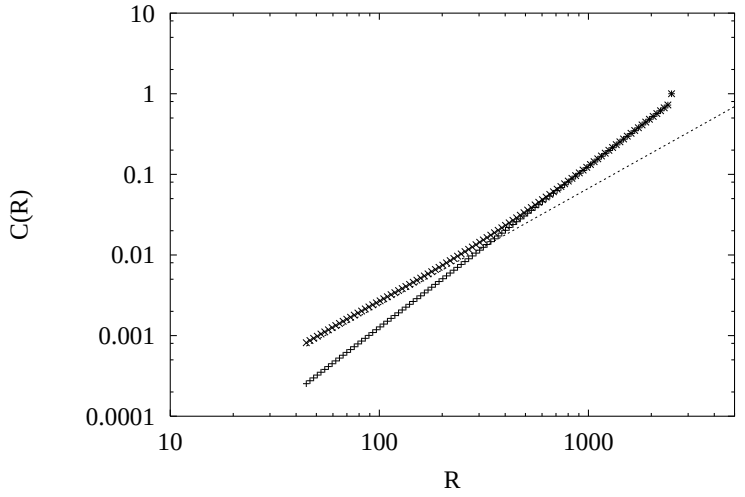

Figure 3.15: Density correlation function $C(R)$ vs R, in $d = 2$, with DSMC algorithm with $\tau_b = 0.01$ and $r = 0.99$ (bottom) and $\tau_b = 100$ and $r = 0.5$ (top), $N = L^2 = 5000$, $\tau_c = 0.5$, $r_B = 0.71$; the measured d_2 takes respectively the values 2 and 1.45

3.2.4 One-particle distribution of velocities

In the framework of a kinetic approach we are much interested in the behavior of the distribution of velocities $P(\mathbf{v})$, which is related to the one-particle probability density function $P_1(\mathbf{r}, \mathbf{v}, t)$ which appears in the kinetic equations of gases, i.e. the first equation of the BBGKY hierarchy (2.70), or the Boltzmann equation (2.74) if the Molecular Chaos can be reasonably assumed. In particular, in a stationary regime, after a transient time t_0 of the order of the maximum characteristic time of the problem (τ_b or τ_c), and using an observation time $T \gg t_0$, we have:

$$P(\mathbf{v}) = \frac{1}{V}\frac{1}{T-t_0}\int_V d\mathbf{r}\int_{t_0}^{T} dt P_1(\mathbf{r}, \mathbf{v}, t) \tag{3.19}$$

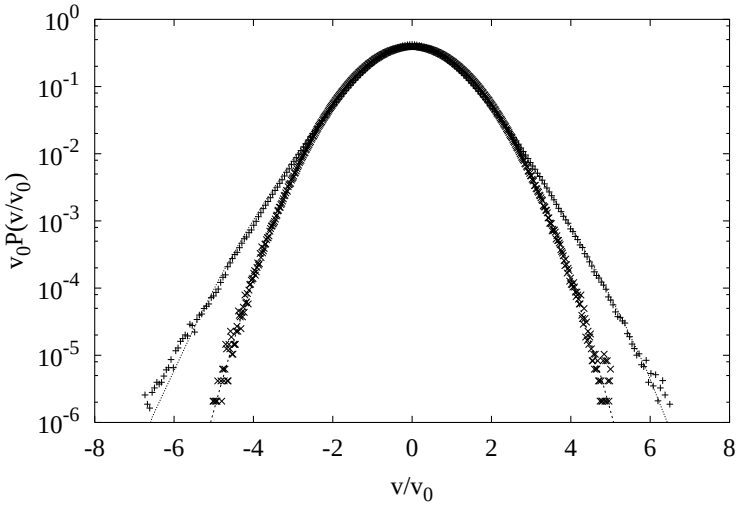

Figure 3.16: Rescaled distribution of velocities v/v_0 ($v_0 = \sqrt{T_g}$) in a Gaussian ($\tau_b = 0.01$, $r = 0.99$, crosses) and a non-Gaussian regime ($\tau_b = 100$, $r = 0.7$, pluses '+') for the MD simulations with $d = 1$. In both cases $N = L = 500$. The dot-dashed curve represents the Gaussian. The dashed line represents the fit discussed in paragraph 3.3

We have measured the distribution of velocities of the particles filling a histogram at many different times, after having verified the stationarity of the system. In Fig. 3.16 we show the results of these measurements for Molecular Dynamics in $d = 1$. Similar results are obtained in $d = 1$ with DSMC algorithm simulations, presented in Fig. 3.17 on the facing page. We find again a strong difference between the collisionless regime, $\tau_c \gg \tau_b$ and the colliding regime $\tau_c \ll \tau_b$: in this case the collisionless regime is characterized by a Gaussian distribution of velocities, while in the colliding regime a non-Gaussian behavior appears. The non-Gaussian distributions are characterized by enhanced high-energy tails.

We have repeated the measurements in $d = 2$, using DSMC simulations. The results, shown in Fig. 3.18 on page 82 are in fair agreement with the ones in $d = 1$, showing that this non-Gaussian behavior is robust not only against the Molecular Chaos, but also to the increase of dimensionality. Finally, to give a quantitative evaluation of the deviation from the Gaussian regime, we have fitted the tails of the observed distribution, in Fig. 3.19 on page 82. We have found evidence of $\sim \exp(-v^{3/2})$ tails, in agreement with the theoretical prediction of Ernst and van Noije [211] (which has been obtained with the assumption of spatial homogeneity and Molecular Chaos). We have also observed tails with a slower decay, e.g. $\sim \exp(-v)$ in a simulation with a very low restitution coefficient and a very high ratio $\rho = \tau_b/\tau_c$, i.e. when the system is approaching the "cooling limit" discussed in paragraph 3.1.2; we can consider it a stationary state because we measure time averages over very large time scales (larger than τ_b), but the statistics of velocities appears to be in agreement to the one predicted by

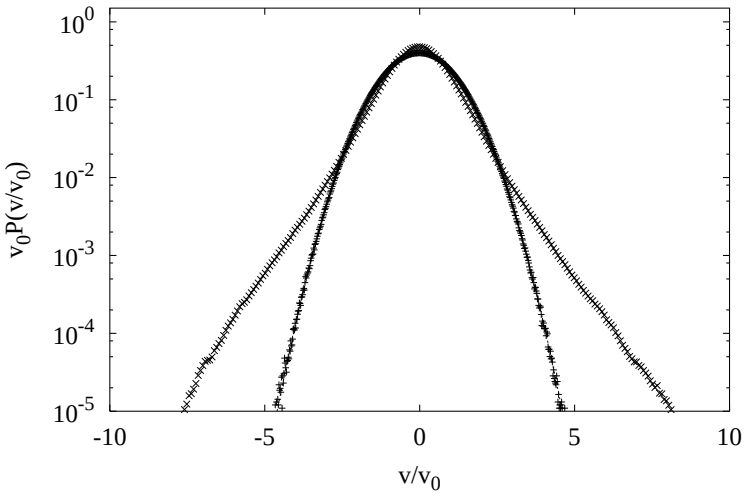

Figure 3.17: Rescaled distribution of velocities in a Gaussian ($\tau_b = 0.01$, $r = 0.99$) and a non-Gaussian regime ($\tau_b = 100$, $r = 0.5$) for the DSMC simulations with $d = 1$. In both cases $N = L = 2000$, $\tau_c = 0.5$, $r_b = 0.4$. The dashed curve represents the Gaussian. $v_0 = \sqrt{T_g}$

Ernst and van Noije for a cooling granular gas. Again we point out that the results of Ernst and van Noije were obtained with the assumptions of Molecular Chaos and absence of spatial gradients: in our clusterized regimes this is far from true, therefore we cannot rely on a direct comparison with the solutions of the homogeneous Enskog-Boltzmann equation. We can argue that the observed tails of the distributions of velocity are the sum of different effects: inelasticity as well as clusterization.

3.2.5 Self-diffusion and time self-correlation in 2D

In Fig. 3.20 on page 83 we report the results of the observation of the average square distance walked by a particle versus time:

$$L(t) = \langle |\mathbf{r}(t) - \mathbf{r}(t_0)|^2 \rangle \tag{3.20}$$

where t_0 is taken large enough ($t_0 > \max(\tau_c, \tau_b)$), in order to consider the system time translational invariant (i.e. the initial conditions have been forgotten).

From the figure it appears that the system presents normal diffusion in both the regimes (colliding and non-colliding), i.e.

$$L(t) \sim 2Dt. \tag{3.21}$$

The measurement of diffusion coefficients is more interesting. For *equilibrium* systems the Einstein relation is expected to be satisfied (fluctuation-dissipation relation):

$$D = \tau \langle v^2 \rangle \tag{3.22}$$

with τ the typical kinetic relaxation time of the system, $< v(t_1)v(t_2) > \sim \exp(-|t_1 - t_2|/\tau)$. For example, in the case of Brownian motion:

$$\frac{d\mathbf{v}}{dt} = -\frac{\mathbf{v}}{\tau_{visc}} + \mathbf{R}(t) \tag{3.23}$$

with Gaussian white noise $\mathbf{R}(t)$, it happens that $\tau \equiv \tau_{visc}$.

In the collisionless regime, where the heat bath dominates the dynamics, the diffusion coefficient D satisfies the Einstein relation with the bath temperature and $\tau = \tau_b$, as expected.

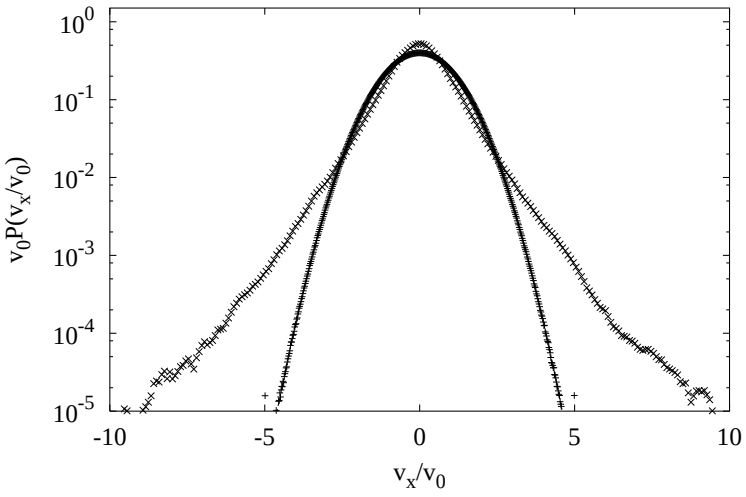

Figure 3.18: Rescaled distribution of velocities in a Gaussian ($\tau_b = 0.01$, $r = 0.99$) and a non-Gaussian regime ($\tau_b = 100$, $r = 0.5$) for the DSMC simulations with $d = 2$. In both cases $N = L^2 = 10000$, $\tau_c = 0.05$, $r_b = 0.22$. The dashed curve represents the Gaussian. $v_0 = \sqrt{T_g}$

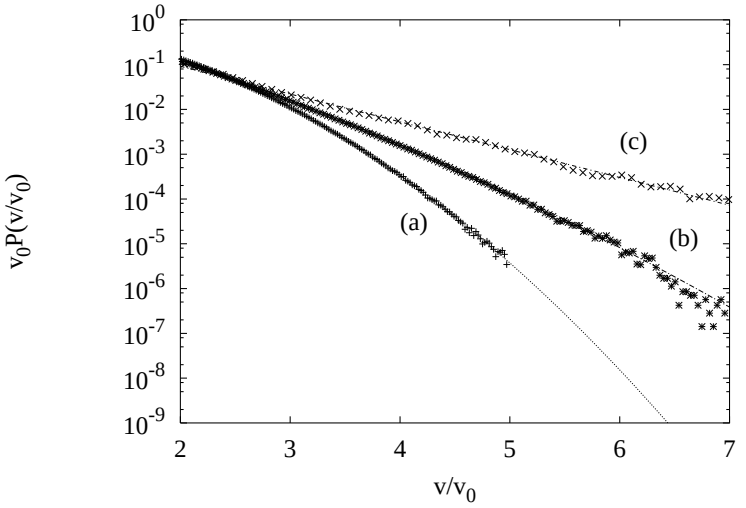

Figure 3.19: Rescaled distributions of velocities (particular) for three different choices of parameters, in DSMC simulations with $d = 2$: (a) $N = L^2 = 10000$, $\tau_b = 0.01$, $r = 0.99$, with Gaussian fit; (b) $N = L^2 = 3000$, $\tau_b = 5$, $r = 0.5$ with the fit $\sim \exp(-v^{3/2}/1.25)$; (c) $N = L^{=}10000$, $\tau_b = 100$, $r = 0.2$ with the fit $\sim \exp(-v/0.7)$. In the cases (a) and (c): $\tau_c = 0.05$, $r_B = 0.22$. In the case (b): $\tau_c = 0.5$ and $r_B = 0.63$. $v_0 = \sqrt{T_g}$

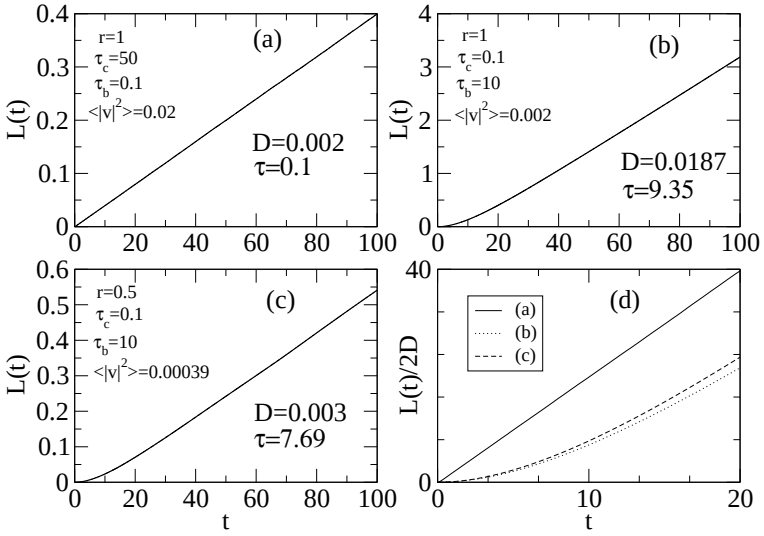

Figure 3.20: Averaged square distance $L(t)$ versus time t for different choices of the parameters in $d = 2$ DSMC simulations. In all simulations $N = L^2 = 500$ and $r_B = 0.5$. In (a) $T_b = 0.01$, in (b) and in (c) $T_b = 0.001$. In (d) the same data are rescaled and the initial transient is shown

One may expect that the characteristic relaxation time in the colliding regime ($\tau_c \ll \tau_b$) is τ_c, but the measurement of the diffusion coefficient shows that this is not the case. In general the diffusion coefficient is somehow very much larger than that expected from this prediction. For the case shown in Fig. 3.20, the time $\tau = D/\langle v^2 \rangle$ is compatible with $\tau_b \gg \tau_c$.

Furthermore the study of the *elastic* colliding regime, where $\tau_c \ll \tau_b$ but $r = 1$ shows that $\tau = \tau_b$.

These measurements are in agreement with the time self-correlation of velocity:

$$\Phi(t) = < v_x(t_1) v_x(t_1 + t) > \tag{3.24}$$

which is shown in Fig. 3.21 on the next page. In all the cases presented an exponential decay is observed:

$$\Phi(t) \sim \exp(-t/\tau) \tag{3.25}$$

The characteristic relaxation times τ for the various cases are compatible with the ones measured by means of the relation (3.22). Remarkably, the relaxation time of the colliding regime (elastic or inelastic) is almost equal to τ_b. The slight difference that distinguishes these regimes from the collisionless regime is in the short time behavior of $\Phi(t)$. The fit shown in the Figure is of the kind:

$$\Phi(t) = A \exp(-t/\tau_{short}) + B \exp(-t/\tau_{long}) \tag{3.26}$$

where $\tau_{long} \approx \tau_b$, while $\tau_{short} \approx \tau_b$. The long tails observed in the colliding case (elastic and inelastic) must not be regarded as equivalent to the well known long tails (which are algebraic) measured in elastic hard objects systems (Alder-Wainright, etc.), but as a consequence of the fact that the gas is not at equilibrium. In both elastic and inelastic cases, the particles have a collision rate which is far shorter than the relaxation time due to viscosity. On the other hand the viscosity has a far larger effect on the velocities, as it drags systematically the system toward the absence of flow. It happens that the viscous slow decay dominates the behavior of the self-correlation after a few collision times, while the very first decay is more rapid.

Finally we note that the differences between the relaxation time τ measured in diffusion and that measured in the self-correlation of velocity, appearing in the *inelastic colliding* regime, are due to some violation of fluctuation-dissipation relations, which are to be expected in systems out of equilibrium.

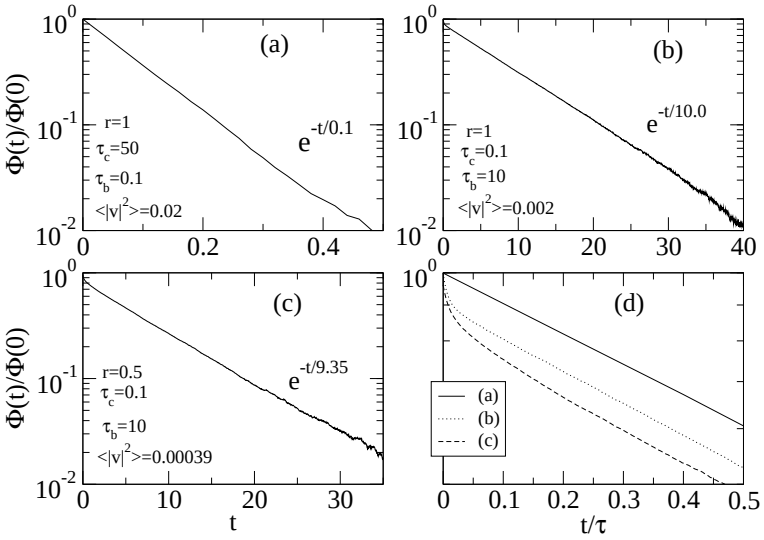

Figure 3.21: Rescaled self-correlation of velocity $\Phi(t)/\Phi(0)$ versus time t for different choices of the parameters in $d = 2$ DSMC simulations. In all simulations $N = L^2 = 500$ and $r_B = 0.5$. In (a) $T_b = 0.01$, in (b) and in (c) $T_b = 0.001$. In (d) the same data are rescaled and the initial transient is shown

3.2.6 Velocity structure factors in 2D

In a recent paper Trizac and coworkers [215] have studied the formation of structures in driven granular gases, using some statistical tools already developed for the case of cooling granular gases [212]. They have studied a different version of the randomly driven granular gas, as it does not take into account the systematic viscosity (that is: the grains follow Eq. (3.3) without the viscous term $v_i(t)/\tau_B$). The model without this term has been studied by many authors ([226, 67, 205, 211, 31, 178]. The absence of the viscous term arises many problems: typically it happens that total momentum has large fluctuations and, to avoid it, the simulations have artificial "re-scaling" mechanisms that keep the momentum constant. We have also evidence that in $d = 1$ the total kinetic energy logarithmically increases with time.

The study of large structures on this version of randomly driven granular gases has shown that there are no instabilities (all modes remain stable if linearly perturbed), at odds with the cooling case, where the existence of shear and cluster instabilities is well established (see Chapter V for a detailed discussion). The velocity correlators, for large distances, in $d = 2$ show a power law decay and in $d = 3$ a logarithmic decay:

$$G_{\parallel} \sim G_{\perp} \sim \frac{1}{|\mathbf{r}|} \; (d = 2) \tag{3.27a}$$

$$G_{\parallel} \sim G_{\perp} \sim \ln\left(\frac{L}{|\mathbf{r}|}\right) \; (d = 3) \tag{3.27b}$$

We have measured the sphericized structure factors and velocity correlators using our DSMC simulations for the randomly driven granular gas model, in $d = 2$, with and without viscosity, in order to make a comparison with the theoretical prediction of van Noije et al. [215]. The results are shown in Fig. 3.22 on the facing page. The choice of using the Direct Simulation Monte Carlo may affect the results of these numerical experiments, as certain structures expected to be originated at short scales are completely ruled out by the Molecular Chaos assumption. However we have already seen that large scale density structures appear and can be measured by means of Grassberger and Procaccia fractal dimension (see paragraph 3.2.3).

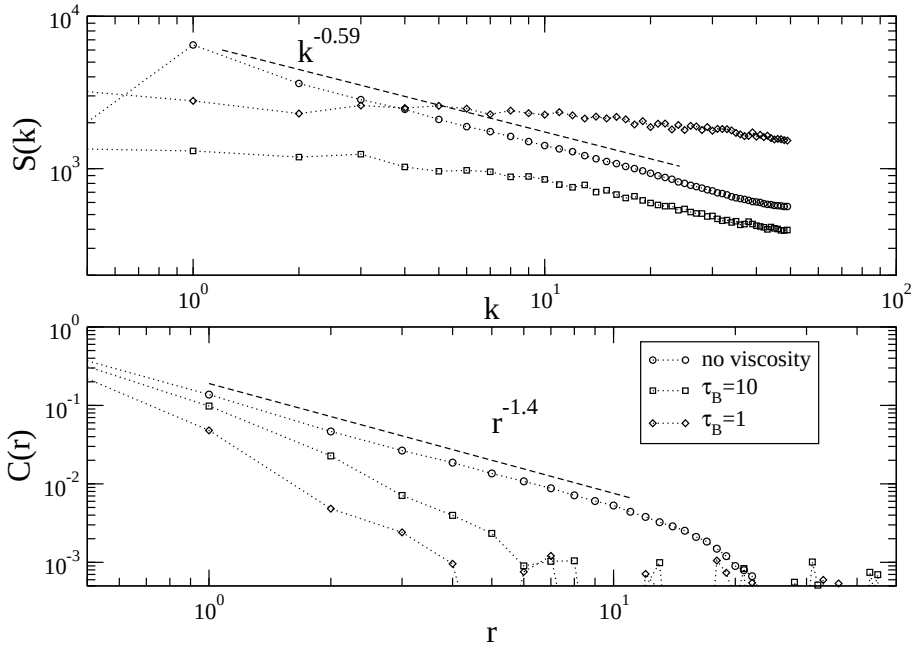

Figure 3.22: Velocity structure factors and correlators in randomly driven granular gases: DSMC simulations of the model introduced in this chapter without viscosity (circles) and with viscosity (squares $\tau_b = 10$ and diamonds $\tau_b = 1$). In all the simulations: $N = L^2 = 5000$, $T_b = 1$, $r = 0.5$, $\tau_c \approx 0.1$, and the coarse-graining boxes used to compute the structure factors are 100×100. The data for the case without viscosity have been fitted in the intermediate range with power laws

The main observation from Fig. 3.22 is about the effect of viscosity. When the viscous term is present, the structure factors are almost flat and the correlators have rapid decays. When the viscous term is suppressed (and the regularization of total momentum is implemented) we measure in an intermediate range for k or $|\mathbf{r}|$, for the sphericized factors and correlators:

$$S(k) \sim k^{-\beta} \tag{3.28a}$$

$$G(|\mathbf{r}|) \sim |\mathbf{r}|^{2-\beta} \tag{3.28b}$$

with $\beta \approx 0.59$ for a restitution coefficient $r = 0.5$ and absence of viscous term. This observation can be relevant to give a criterion for the choice of the correct model in particular experimental situations: the measure of velocity correlations can be of use to determine if the granular gas can be modeled neglecting viscosity or if viscosity (for example from the contact with the vibrating plate) plays any role.

3.3 Deviations from the homogeneous Boltzmann equation

The Homogeneous Boltzmann Equation describes the system in the absence of correlations between colliding particles. In the clusterized regime the recollision effect is enhanced and colliding particles are correlated. We give a tentative interpretation of the global distribution of velocities in terms of local Maxwellians with temperature that depends upon the density.

3.3.1 The scaling of the local temperature with the cluster mass

In paragraph 2.5 we have discussed the arguments of I. Goldhirsch against the possibility of a very general hydrodynamical description. One of the argument started by a heuristic estimate of the local temperature as a function of density and local shear rate (valid on time scales shorter than the time of decay of the shear rate), given in Eq. (2.165). In this formula it appeared that $T \propto l_0^2 \propto n^{-2}$, so that the local scalar pressure $p = nT \propto n^{-1}$: this is the reason of the clustering instability, i.e. in small regions an increase of the number of particles corresponds to a *decrease* of the local pressure, so that more particles can enter the region. We have studied, parametrically, the relation between local temperature and local density, plotting the mean square velocity in a box T_M as a function of the number of grains m in that box, after having divided the total volume in M boxes. As already discussed, the distribution of the cluster masses (i.e., the number of particles in a box) in the clusterized regime presents a power law decay with an exponential finite size cut-off. The plots of T_M vs. m are given in Fig. 3.23 on the facing page, Fig. 3.24 on the next page and Fig. 3.25 on page 88: these are $d = 1$ Molecular Dynamics, $d = 1$ DSMC simulations, and $d = 2$ DSMC simulations respectively.

In all the cases we have studied a collisionless situation ($\tau_b \ll \tau_c$) and a colliding situation ($\tau_b \gg \tau_c$), obtaining different results. In the collisionless situation the local temperature does not depend upon the cluster mass m. In the colliding situation the local temperature appears to be a power of the cluster mass, i.e. $T_M(m) \sim m^{-\beta}$ with $0 < \beta < 1$. This relation ensures that the scalar pressure $p = nT \propto n^{1-\beta} = n^{\beta^*}$ with $\beta^* > 0$: the clustering "catastrophe" (particles falling in an inverted pressure region) is absent. Moreover, we can give an estimate of the scale dependence of the temperature, using the previous result on the fractal correlation dimension d_2 (defined in Eq. 3.18) and assuming that the scaling relation for the temperature is valid at different scales replacing the density to the number of particles, i.e. $T(m) \sim n^{-\beta}$. The results on the fractal correlation dimension suggest that the local density has the following scale dependence $n(R) \sim R^{-(d-d_2)}$ so that the local temperature follows the law $T(R) \sim R^{\beta(d-d_2)}$ and the local pressure $p(R) \sim R^{-(1-\beta)(d-d_2)}$. The density and the pressure decrease with R, while the temperature increases. The scale dependence of the macroscopic fields is evidently at odds with the possibility of separating a mesoscopic scale from the microscopic one and therefore the hydrodynamical description cannot even be tempted.

3.3.2 The convolution model

Now, we can go a step further relating the clustering properties of the system to the velocity distribution. In order to do that we consider the following quantities: the distribution of boxes (of volume V/M), $f_M(m)$, containing a given number m of particles and the velocity variance $T_M(m)$, in a box occupied by m particles. We also observe that restricting the statistics of the velocities to boxes of volume V/M containing only a fixed number of particles, i.e. studying a sort of *fixed density velocity distribution*, the velocity distribution appears closer to a Maxwellian, even if the global distribution is strongly non-Gaussian. We show this measure in Fig. 3.26 on page 88

We consider first the non-clusterized case ($\tau \ll \tau_c$ and $r \simeq 1$). Within this regime we find from the simulations that:

$$T_m^{hom}(m) \simeq const \tag{3.29a}$$

$$f_M^{hom}(m) = \frac{\langle m \rangle^m e^{-\langle m \rangle}}{m!}. \tag{3.29b}$$

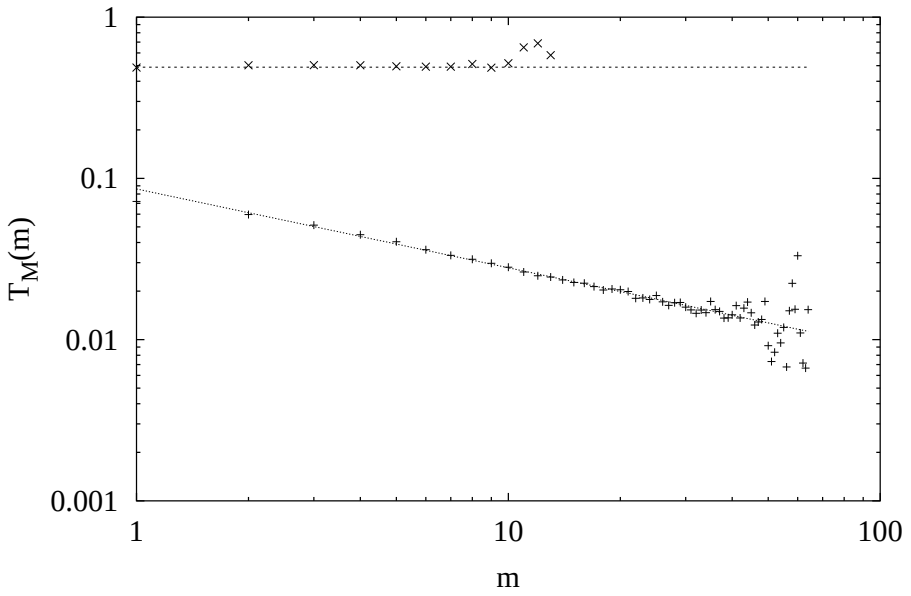

Figure 3.23: Granular temperature vs. cluster mass 1d, MD, with $r = 0.99$, $\tau_b = 0.01$, $\tau_c = 0.1$, and $r = 0.7$ and $\tau_b = 100$, $\tau_c = 0.1$ with $N = L = 300$ and $M = 100$. The Gaussian case is constant, while the non-Gaussian case is fitted by $\sim m^{-0.5}$

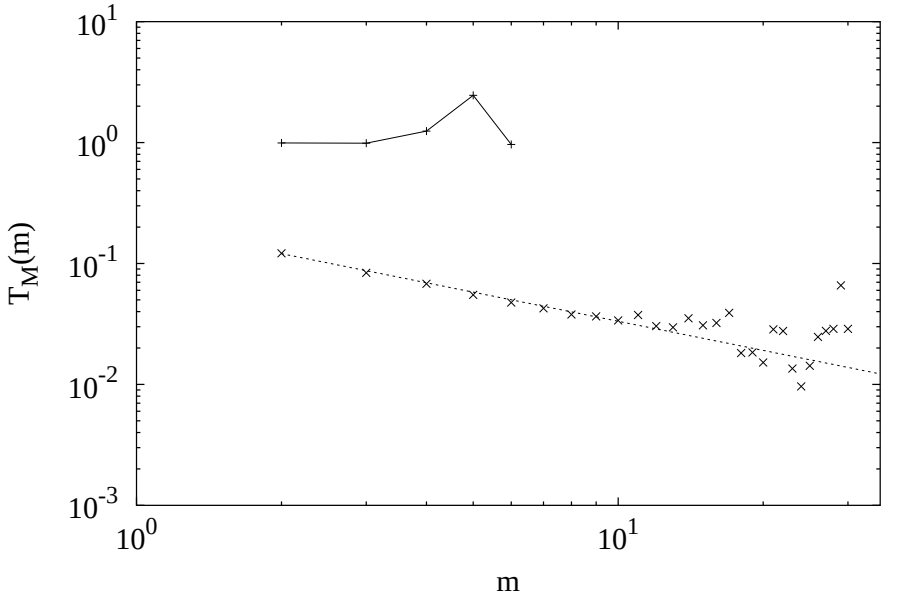

Figure 3.24: Granular temperature vs. cluster mass 1d, DSMC, with $r = 0.99$, $\tau_b = 0.01$, $\tau_c = 0.5$, and $r = 0.5$ and $\tau_b = 100$, $\tau_c = 0.5$ with $N = L = 500$ and $M = 12000$. The Gaussian case is constant, while the non-Gaussian case is fitted by $\sim m^{-0.8}$

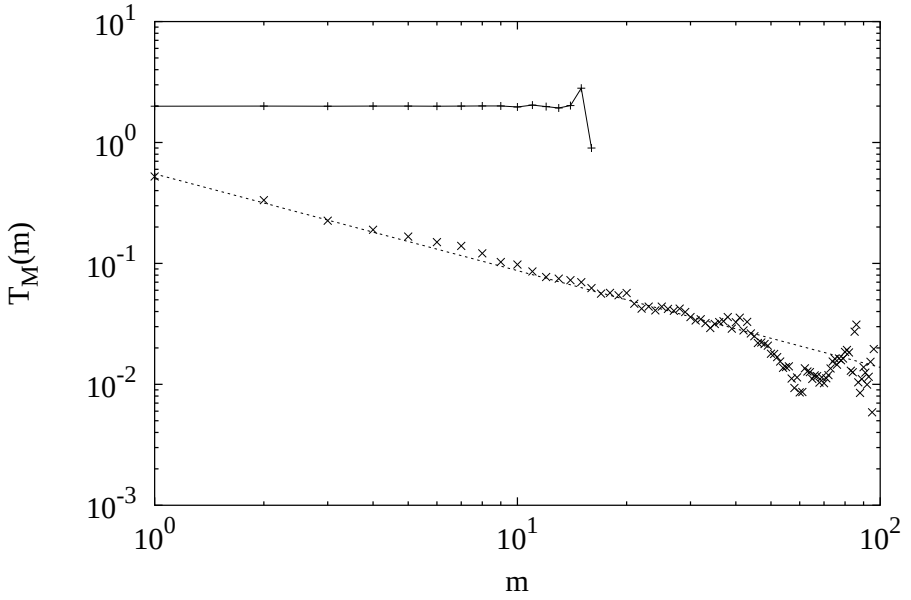

Figure 3.25: Granular temperature vs. cluster mass 2d, DSMC, with $r = 0.99$, $\tau_b = 0.01$, $\tau_c = 0.05$, and $r = 0.5$ and $\tau_b = 100$, $\tau_c = 0.05$ with $N = L^2 = 10000$ and $M = 3200$. The Gaussian case is constant, while the non-Gaussian case is fitted by $\sim m^{-0.8}$

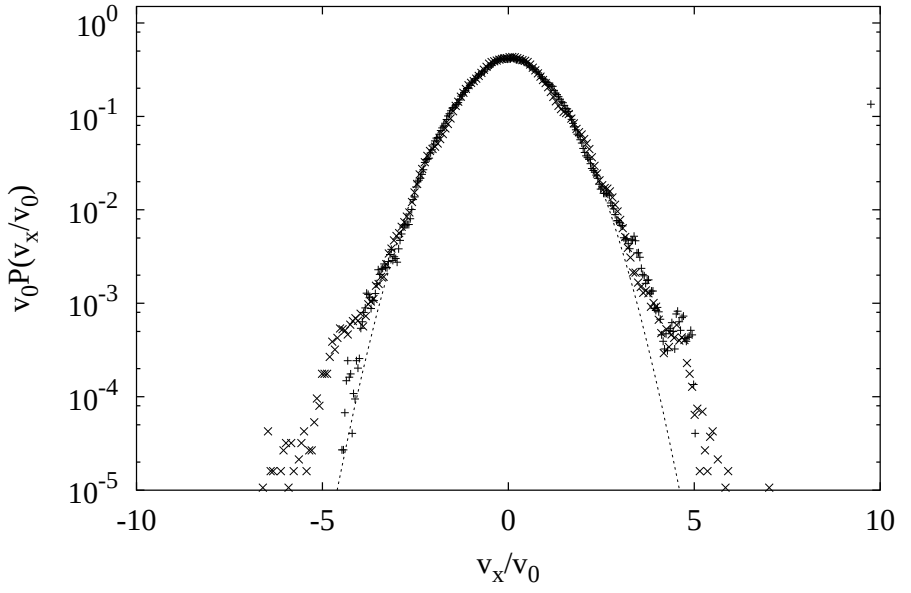

Figure 3.26: Velocity distribution in limited density 2d, DSMC: pluses (+) represent velocities only from boxes with $m = 1$, while crosses (×) represent velocities with $m = 5$, with $r = 0.5$, $N = L^2 = 10000$, $\tau_b = 100$, $\tau_c = 0.05$. $v_0 = \sqrt{T_g}$

By assuming in each box a Gaussian velocity distribution with a constant variance $T_M^{hom}(m)$ it turns out that the global velocity distribution $P^{hom}(v)$ is Gaussian. Let us recall that the Poisson distribution is the one associated with a process of putting independently $\langle m \rangle M$ particles into M boxes.

Let us turn to the clusterized case. If $\tau = 100$ and $r = 0.7$, in MD simulations with $d = 1$, considering only the occupied boxes ($m > 0$), we measure the following relations

$$T_M^{clust}(m) \sim m^{-\beta} \tag{3.30a}$$

$$f_M^{clust}(m) = \frac{e^{-c_{cl}m}}{m}, \tag{3.30b}$$

with $\beta \simeq 0.5$ and $c_{cl} \simeq 0.14$.

Let us compute from these scalings the global velocity distribution. Taking into account that the spatial probability distribution of the particles is $f_M^{clust}(m)$ and assuming that their local velocity distribution is Gaussian, but with a variance $T_M^{clust}(m) \simeq m^{-\beta}$ which depends on the occupancy, we obtain, for the global velocity distribution $P_{clust}(v)$, and in the continuum limit:

$$P_{inel}(v) \simeq \sum_{m=1}^{\infty} e^{(-\frac{v^2 m^\beta}{2})} e^{-c_{cl}m}. \tag{3.31}$$

We stress how the the distributions measured in the simulations are in very good agreement (see the dashed line in Fig. 3.16 on page 80) with the numerical computation of eq. (3.31), which, in summary, has been obtained under only the following hypothesis:

(i) non-Poissonian distribution for the box occupancy $f_M(m) \propto e^{-c_{cl}m}/m$;

(ii) Gaussian distribution of velocities in each box with a density-dependent variance $T_M(m) \propto m^{-\beta}$.

The hypothesis about the scaling relation between the velocity variance (i.e. $T_M(m)$) and the local density, apart from being justified numerically, can be understood in the following way. The stationarity and the scale-invariance of the cluster distribution, implies a certain distribution of lifetimes for the clusters. In particular each cluster has a lifetime which is inversely proportional to its size. The scale-invariant cluster-size distribution thus implies a scale-invariant distribution for the lifetimes. The cluster lifetime is strictly related to the variance of the velocity distribution inside the cluster itself. In order to ensure the stability of a cluster in a stationary state we have to require that the velocities of the particles belonging to it are not too different, or equivalently that the variance of the distribution is smaller the higher the density. So, given a scale-invariant distribution of clusters one would expect a scale-invariant distribution of variances, that is $T_M(m) \sim m^{-\beta}$.

3.4 Toy models for a mean field analysis

In this section two simple models are proposed to interpret the density and velocity distributions. The first is a hopping model with density-biased *in* and *out* probabilities, which reproduces the distribution of masses in the clusterized (as well as in the homogeneous) regime. The second is a mean field approximation of the effect of the collisions which predicts naturally a non-Gaussian distribution of velocities.

3.4.1 The hopping model

In this section we address the problem of the microscopic origin of the clusterization. In order to do that, we study a class of models in which the system is composed by M boxes and N particles assuming that the boxes have infinite connectivity (mean field hypothesis). One starts with a certain configuration and let the system evolve with an exchange dynamics in which, at each time step, one particle moves from one box to another, both boxes being chosen randomly. The probability for each single exchange is model-dependent and it will be our tuning-parameter to scan the different phenomenologies. Our goal is to understand in a quantitative way how the microscopic dynamics affects the clustering properties of the system. In particular we shall try to recover the results, obtained in the framework of the models previously introduced, for the density distributions in the clusterized and homogeneous cases (see Fig. 3.6 on page 74, Fig. 3.7 on page 74, Fig. 3.13 on page 78).

The models are defined in terms of master equations for the probability P_m of having a box with m particles, assigning transition rates for landing in a box with m particles $W_{in}(m)$ and for leaving a box with m particles $W_{out}(m)$. It must be

$$W_{in}(N) = W_{out}(0) = 0 \tag{3.32}$$

because no particles can be taken out of a box with 0 particles and a box with N particles cannot receive any more particle. Moreover the following conditions must be satisfied:

$$\sum_{m=0}^{\infty} P_m = 1 \tag{3.33a}$$

$$\sum_{m=0}^{\infty} m P_m = \frac{N}{M} = \langle m \rangle \tag{3.33b}$$

$$\sum_{m=0}^{\infty} W_{in}(m) M P_m = 1 \tag{3.33c}$$

$$\sum_{m=0}^{\infty} W_{out}(m) M P_m = 1 \tag{3.33d}$$

Eq.(3.33a) is the normalization condition for P_m, Eq. (3.33b) is a constraint on the first moment and Eqs. (3.33c) and (3.33d) are the normalization condition for W_{in} and W_{out} (a particle must be taken from somewhere and put somewhere).

The general question that we want give an answer to reads: given W_{in} and W_{out}, what is the asymptotic stationary distribution for the average number of boxes with m particles, $P(m)$?

The simplest case we can consider is the one in which each single movement is independent of the state of the departing and of the landing box. In this case there is no bias in the movements and $W_{in}(m)$ and $W_{out}(m)$ do not depend upon m:

$$W_{in}(m) = W_{out}(m) = \frac{1}{M} \tag{3.34}$$

(this automatically satisfies Eqs. (3.33c) and (3.33d)), so that the general master equation reads

$$\begin{aligned} M^2\frac{dP_m}{dt} &= P_{m-1}(P_{m-1}-\frac{1}{M})+2P_{m+1}P_{m-1}+P_{m+1}(P_{m+1}-\frac{1}{M})+ \\ &+P_{m+1}(1-P_m-P_{m+1}-P_{m-1})+(1-P_m-P_{m-1}-P_{m+1}-P_0)P_{m-1} \\ &-P_{m-1}P_m-2P_m(P_m-\frac{1}{M})-P_mP_{m+1}-P_m(1-P_{m-1}-P_m-P_{m+1}) \\ &-(1-P_m-P_{m+1}-P_{m-1}-P_0)P_m \qquad\qquad (0<m<N) \end{aligned} \tag{3.35a}$$

$$M^2\frac{dP_0}{dt} = P_1(1-P_0-\frac{1}{M})-(1-P_1-P_0)P_0 \tag{3.35b}$$

$$M^2\frac{dP_N}{dt} = P_1P_{N-1}-P_N(1-\frac{1}{M}) \tag{3.35c}$$

In the limit of $M >> 1$ one can neglect the $\frac{1}{M}$ terms in the right hand side of eq. (3.35) and easily get the stationary solution ($\frac{dP_m}{dt}=0$)

$$P_m = Ae^{-cm} \tag{3.36}$$

with $A = 1-e^{-c}$ corresponding to the normalization condition $\sum_0^\infty P_m = 1$ and where c is a constant depending on N and M: $c = ln(1+\frac{1}{\langle m\rangle})$ with $\langle m\rangle = \frac{N}{M}$.

This result has to be compared with the probability $f_M(m)$ in the non-clusterized cases of the previous sections. In order to do this it is necessary to recall that those results have been obtained with a small value of the number of boxes M. This means that one is very far from the limit $M >> 1$ and this situation corresponds to a sort of coarse graining in the system in which each box (big box) is actually composed by a certain number of small boxes (whose number is such that $M >> 1$). The problem can thus be formulated in the following way: given a system of N particles distributed in M_{small} boxes with the distribution P_m given by eq. (3.36), what is the distribution P_m^* for the particles in a system of M_{big} boxes each one composed by R ($R = M_{small}/M_{big}$) small boxes? The resulting distribution is easily written as

$$P_m^* = \sum^* \prod_{i=1}^R P_{m_i} = A^R e^{-cm} F(m,R), \tag{3.37}$$

where $\sum^*$ indicates the sum on the $\{m_1,...,m_R\}$ such that $\sum_{i=1}^R m_i = m$, $F(m,R)$ is the number of ways of distributing m particles in R boxes and it is given by:

$$F(m,R) = \binom{m+R-1}{m} \tag{3.38}$$

With the help of (3.38) and using the Stirling formula, the expression (3.37) becomes (for $R >> N >> 1$)

$$\begin{aligned} P_m^* = A^R e^{-cm}\frac{(m+R-1)!}{m!(R-1)!} &\approx A^R e^{-cm}\frac{(m+R-1)^m(m+R-1)^{R-1}}{m!(R-1)^{R-1}} \\ &\approx A^R e^{-cm}\frac{R^m}{m!} = \frac{A^R}{m!}e^{-m(\ln(1+\frac{M_{small}}{N})-\ln\frac{M_{small}}{N}-\ln\frac{N}{M_{big}})} \\ &\approx e^{-\langle m\rangle^*}\frac{(\langle m\rangle^*)^m}{m!} \end{aligned} \tag{3.39}$$

It has been used the definition of R, the fact that $c = \ln(1+M_{small}/N)$ and that $M_{small}/N >> 1$. In the last passage $\langle m\rangle^* = N/M_{big}$ has been introduced and A^R has become $e^{-\langle m\rangle^*}$, as can be verified when $\langle m\rangle^{-1} = M_{small}/N >> 1$. It has been shown, therefore, that the coarse grained version of the solution of (3.35) is exactly the Poisson distribution found in the simulations, in the non-clusterized regime (see Fig. 3.6 on page 74, Fig. 3.7 on page 74 Fig. 3.13 on page 78).

Let us consider now one case where the transition rates for the particle jumps depend on the contents of the departing and landing boxes. This corresponds to impose some sort of bias to the system that could well reproduce the situation one has in the clusterized cases due to the inelasticity. We consider in particular the following case, defined by the transition rates:

$$W_{in}(0) = \frac{1}{M} \tag{3.40a}$$

$$W_{in}(m) = (1 - P_0)\frac{m}{N} \qquad (0 < m < N) \tag{3.40b}$$

$$W_{out}(m) = \frac{m}{N} \qquad (0 < m \leq N) \tag{3.40c}$$

These transition rates, that satisfy the relations (3.33), have the following interpretation. The probability to land on a box containing already m particles is proportional to the number of particles in order to mimic the inelastic collision with a cluster of m particles. On the other hand the departure from a box containing already m particles has a probability proportional to m because the probability to select one particle in that particular box is proportional to m (in the homogeneous case this was also true, but the fluctuation of m were expected to be very small, as verified *a posteriori* by the Poissonian solution of the master equation).

Neglecting as usual the terms of order of $\frac{1}{M}$, and after simplifications, the stationary master equations write:

$$P_{m+1}(m+1) + (1 - P_0)(m-1)P_{m-1} - P_0 m P_m = 0 \tag{3.41a}$$

$$P_1 - \frac{N}{M}P_0 = 0 \tag{3.41b}$$

$$\frac{P_1}{N}P_{N-1}(1 - P_0)\frac{N-1}{N} - P_N(1 - \frac{1}{M})\frac{1}{M} = 0 \tag{3.41c}$$

The solution in this case is given by:

$$P_m = A\frac{1}{m}e^{-c_{cl}m} \tag{3.42a}$$

$$P_0 = 1 - e^{-c_{cl}} \tag{3.42b}$$

with $A = \langle m \rangle (e^{c_{cl}} - 1)$ and $\langle m \rangle = \frac{N}{M}$. A and c_{cl} are related by an implicit equation obtained imposing the condition $\sum_0^N P_m = 1$, that in the limit $N \to \infty$ becomes

$$1 - e^{-c_{cl}} - A * \ln(1 - e^{-c_{cl}}) = 1 \tag{3.43}$$

In the clusterized case we expect the solution to be self-similar, in the sense that P_m has the same behavior of P_m^*, and the coarse graining previously performed is expected not to change the solution (3.42), apart a renormalization of $\langle m \rangle$ and c_{cl}.

It must be noted that, as A must be finite, when $N \to \infty$ (and M is fixed) c_{cl} has to go to zero, while c_{cl} diverges when N/M goes to zero. It is natural to think to c_{cl} as to the inverse of the characteristic "mass" of a cluster, that is the typical number of particles in it. In this sense the term $\exp(-c_{cl}m)$ acts as a finite-size cut-off for the self-similar distribution $P_m \sim 1/m$, as already discussed.

The solution (3.42) is in excellent agreement with the numerical results obtained in the previous sections. In particular in the case $N = 300$ $M = 100$ of the MD simulations with $d = 1$ one recovers the density distribution with the correct value of $c_{cl} \simeq 0.14$ (see Fig. 3.6 on page 74).

To get the other observed behaviors of density distribution $P_m \sim e^{-c_{cl}m}/m^{\alpha_{cl}}$, it is enough to change the transition rates appearing in Eqs. (3.40a) into the following:

$$W_{in}(0) = \frac{1}{M} \tag{3.44a}$$

$$W_{in}(m) = \mu(1 - P_0)m^{\alpha_{cl}} \qquad (0 < m < N) \tag{3.44b}$$

$$W_{out}(m) = \mu m^{\alpha_{cl}} \qquad (0 < m \leq N) \tag{3.44c}$$

where μ is a normalizing constant:

$$\mu = \left(M \sum_i^N P_m m^{\alpha_{cl}} \right)^{-1} . \tag{3.45}$$

3.4.2 The mean field collision model

In order to shed some light on the relationship between the spatial clusterization and the anomalous velocity distributions observed above (Fig. 3.16 on page 80, Fig. 3.17 on page 81, Fig. 3.18 on page 82, Fig. 3.19 on page 82) we present a simplified theoretical model. For sake of notation simplicity, we discuss only the $d = 1$ case. Let us treat the collisions in a mean-field like fashion and modify the Langevin dynamics plus collision rules by the following set of coupled equations for the velocities ($i \in [1, N]$):

$$\frac{dv_i}{dt} = -\frac{v_i}{\tau_b} + \frac{1}{N} \sum_{j=1}^{N} g(v_i - v_j) + \sqrt{\frac{2T_b}{\tau_b}} f_i(t) \tag{3.46}$$

where the second term in the r.h.s. determines the velocity change of the particle i due to the collisions with the remaining particles and is chosen to mimic the inelastic behavior. This requirement poses some constraints about the form of the function $g(v - v')$:

- The momentum conservation dictates the antisymmetric property, $g(v - v') = -g(v' - v)$
- The inelasticity of the collision process requires $g(v - v')(v - v') \leq 0$

The Fokker-Planck equation of the process described by Eqs. (3.46) is

$$\begin{aligned} \frac{\partial}{\partial t} P_N(v_1, ..., v_N, t) - \frac{1}{\tau_b} \sum_{i=1}^{N} \frac{\partial}{\partial v_i} (v_i P_N(v_i, ..., v_N, t)) \\ - \frac{T_b}{\tau_b} \sum_{i=1}^{N} \frac{\partial^2}{\partial v_i^2} P_N(v_1, ..., v_N, t) \\ + \sum_{i=1}^{N} \frac{\partial}{\partial v_i} \left[\frac{1}{N} \sum_{j=1}^{N} g(v_i - v_j) P_N(v_1, ..., v_N, t) \right] = 0 \end{aligned} \tag{3.47}$$

From the above equation, using the fact that in the limit $N \to \infty$ the mean field approximation holds, assuming again Molecular Chaos, one can obtain a master evolution equation for the 1-body velocity probability distribution. We omit this derivation, and give directly the master equation:

$$\frac{\partial P(v,t)}{\partial t} - \frac{1}{\tau_b} \frac{\partial (v P(v,t))}{\partial v} - \frac{T_b}{\tau_b} \frac{\partial^2 P(v,t)}{\partial v^2} + \frac{\partial}{\partial v} \int dv' P(v,t) P(v',t) g(v - v') = 0 \tag{3.48}$$

From Eq. (3.48) one observes that the quantity:

$$\int dv' P(v',t) g(v - v') = G(v) = -\frac{\partial U(v)}{\partial v} \tag{3.49}$$

which is a function of v and a functional of $P(v)$, can be considered as an effective force acting on the particle generated by an effective potential U. Integrating once with respect to the velocity the stationary version of eq. (3.48) one can obtain the following equation:

$$\left(-\frac{v}{\tau_b} - \frac{T_b}{\tau_b}\frac{\partial}{\partial v} + G(v)\right) P(v) = 0 \tag{3.50}$$

The solution of Eq. (3.50) is:

$$P(v) \propto \exp\left(-\frac{\tau_b}{T_b}\left(\frac{v^2}{2\tau_b} + U(v)\right)\right) \tag{3.51}$$

In order to make some progress we consider the qualitative shape of $g(v_i - v_j)$. In eq. (3.46) the effect of collisions between the particles i and j in the unit of time is given by:

$$\frac{d}{dt}(v_i - v_j)|_{coll} = \frac{2}{N} g(v_i - v_j) \tag{3.52}$$

The variation of momentum in an interval dt can be rewritten as

$$\delta(v_i - v_j)|_{coll} = \delta q_{ij} \cdot (v_i - v_j) \tag{3.53}$$

where δq_{ij} is the analogue of $q = 1 - r$ in the randomly driven granular gas model defined in the paragraph 3.1.1. The important difference is that here δq_{ij} represents the effect of all the collisions during dt, and thus must be associated to an effective restitution coefficient. Eq. (3.53) may be rewritten as:

$$\frac{d}{dt}(v_i - v_j)|_{coll} = \chi_{ij} q \cdot (v_i - v_j) \tag{3.54}$$

where χ_{ij} is the number of collisions between the $i-th$ and the $j-th$ particles in the unit of time. Upon comparing Eqs. (3.52) and (3.54) one obtains an expression for $g(v_i - v_j)$:

$$g(v_i - v_j) = \frac{2\chi_{ij} q}{N}(v_i - v_j) \tag{3.55}$$

Now it is easy to understand that χ_{ij} is a decreasing function of $|v_i - v_j|$: indeed, a great number of collisions occurs when the pair i, j belongs to a cluster (where $|v_i - v_j|$ is small), whereas the two particles rarely collide when they are out of a cluster (and $|v_i - v_j|$ is high). We can, therefore, make a reasonable *ansatz* on $g(v_i - v_j)$, that is:

$$|g(v_i - v_j)| \sim \frac{|v_i - v_j|}{\tau_c} \qquad \text{inside clusters} \tag{3.56a}$$

$$|g(v_i - v_j)| \sim |v_i - v_j|^{\beta'} \qquad \text{outside clusters} \tag{3.56b}$$

with $\beta' < 1$. From Eq. (3.49) it appears that $G(v) \sim g(v - v')|_{v'=0}$ as the integration has to be performed with respect to the measure $P(v', t)dv'$ that is strongly peaked at $v' = 0$. Finally, one can conclude from the same Eq. (3.49) that

$$U(v) \sim \frac{v^2}{\tau_c} \qquad (v < \sqrt{T_g}) \tag{3.57a}$$

$$U(v) \sim v^{\beta} \qquad (v > \sqrt{T_g}) \tag{3.57b}$$

where $\beta = \beta' + 1 < 2$. It is clear now, looking at Eq. (3.51), that when $\tau_b < \tau_c$ (i.e., in the non-clusterized regime) the argument of the exponential is dominated by v^2/τ_b and therefore a Gaussian is expected for $P(v)$ with variance T_b. In the opposite regime, when $\tau_b > \tau_c$ the distribution is a Gaussian with variance $\frac{\tau_c}{\tau_b} T_b$ at low velocities, a simple exponential (if $\beta = 1$) at high velocities, and a Gaussian with variance T_b at extremely high velocities, but this very far tails practically cannot be observable. In Fig. 3.19 on page 82 in case (c), when $\tau_b >> \tau_c$ we observe a simple exponential tail, as we may expect from the argument presented above.

Chapter 4

The driven granular gas with gravity

Some recent experiments (see section 1.2) have investigated the effect of gravity on driven granular materials. Gravity is a uniform force field (obviously neglecting the differences of height), therefore it has no effect on the relative velocities, i.e. on the sequence of collisions, at the level of our simple modelization, that is the gas of inelastic hard spheres: it simply accelerates the baricentrum of the gas. Its effect becomes relevant when studied in the presence of particular boundary conditions that break the Galilean invariance, e.g. the walls of the box that contains the material. A wall has a relevant role in the randomization of granular material impinging on it: two particle coming parallel (in a direction not normal to the wall) are reflected in different times and may encounter thereafter; moreover, if the wall is active, i.e. it is vibrating with a random or harmonic movement, the randomization effect is still more efficient and not only internal energy but also total energy is gained. Gravity has eventually the role of driving the grains toward the randomization source (the standing or vibrating walls): in the Du, Li and Kadanoff model (see paragraph 2.5.1) the anomalous or "extraordinary" stationary state is observed in the absence of a force field that ensure the efficiency of the thermal wall, the particles are left in a cooling situation (far from the driving wall) for very long times, before the energetic particle come back with its fuel: in a word, almost the whole system is not in contact with the thermal bath for almost all the time, therefore it should not to be surprising to find that the equipartition of energy is violated. When the force of gravity is present, the temperature source is more efficient. However other problems arise, mainly related to the possibility of a hydrodynamic description: we and other authors have shown that the non homogeneity of the gas is essential for the description of the system in the presence of gravity, e.g. it is not true that the temperature is constant all over the system (the "isothermal atmosphere" hypothesis); furtherly, fractal clusters, and therefore scale invariance, are present in our measurements, posing doubts on the existence of a mesoscopic scale for hydrodynamic coarse graining. However the equations of hydrodynamics seem to work well in a range of low inelasticity and low density, they are in fair agreement with the density and temperature profiles obtained in DSMC simulations. In this framework, however, it is very difficult to find proper boundary conditions: the energy given to the gas from a vibrating wall depends on the density of the gas near this wall, and the layer near the wall is not correctly described by hydrodynamic equations, as strong spatio-temporal gradients are present. On the other side, at the top free surface of the granular assembly, the grains fly like projectiles, i.e. they rarely collide, and again the hydrodynamics description is useless: to obtain local equilibrium, a high collision rate is essential.

4.1 The models

Let us describe the **2D Inclined Plane Model** (IPM) and the **2D Inclined Channel Model** (ICM). These are two bi-dimensional models that mimic the behavior of a dilute granular gas in the presence of a gravity field, with different boundary conditions. We present the equations of the model and discuss the approximation used.

4.1.1 Equations of motion and collisions

We briefly resume the fundamental definitions of the model. We consider a granular gas in $d = 2$ consisting of N identical smooth hard disks of diameter σ and mass $m = 1$ subject to binary instantaneous hard-core inelastic collisions which conserve the total momentum

$$\mathbf{v}_1' + \mathbf{v}_2' = \mathbf{v}_1 + \mathbf{v}_2 \tag{4.1}$$

and reduce the normal component of the relative velocity

$$(\mathbf{v}_1' - \mathbf{v}_2') \cdot \hat{\mathbf{n}} = -r((\mathbf{v}_1 - \mathbf{v}_2) \cdot \hat{\mathbf{n}}) \tag{4.2}$$

where r is the normal restitution coefficient ($r = 1$ in the completely elastic case) and $\hat{\mathbf{n}} = (\mathbf{r_1} - \mathbf{r_2})/\sigma$ is the unit vector along the line of centers $\mathbf{r}_1$ and $\mathbf{r}_2$ of the colliding disks at contact. With these rules satisfied, the post-collisional velocities are:

$$\mathbf{v_1}' = \mathbf{v}_1 - \frac{1+r}{2}((\mathbf{v}_1 - \mathbf{v}_2) \cdot \hat{\mathbf{n}})\hat{\mathbf{n}} \tag{4.3a}$$

$$\mathbf{v}_2' = \mathbf{v}_2 + \frac{1+r}{2}((\mathbf{v}_1 - \mathbf{v}_2) \cdot \hat{\mathbf{n}})\hat{\mathbf{n}} \tag{4.3b}$$

In addition, the particles experience the external gravitational field and the presence of confining walls. With respect to the previous Chapter, the energy necessary to prevent the cooling of the system due to the inelastic collisions is not provided by a heat bath: in the present Chapter the energy feeding mechanism is of two types according to the two numerical experiments we perform.

4.1.2 The boundary conditions of the 2D Inclined Plane Model

The first model that we study is called "2D Inclined Plane Model". It is illustrated in Fig. 4.1 on the next page and inspired to recent laboratory experiments [132] and numerical simulations [116]. We have reviewed those experiments in section 1.2.We have shown that in many of them it has been used a closely packed array of grains (for example see [76, 181]). Our inspiration has come, instead, from the more dilute setup of Kudrolli and Henry [132], where the velocity distributions and the density correlations have been measured. We have considered that the dilute setup and the measurement performed where better suited to be investigated with our numerical tools, e.g. Direct Simulation Monte Carlo in two dimensions.

Similar models have been previously studied in the one-dimensional case, that is a vibrated column of grains under the force of gravity [147, 155] and the transition or the coexistence of different phases (gas, partially fluidized and condensed) was investigated. In two dimensions experiments [223], simulations [156] and theories [134, 204] have analyzed a vertical system of grains with gravity and a vibrating bottom wall (with different kinds of vibration) searching for a simple scaling relation between global variables as the global granular temperature T_g or the center of mass height h_{cm} as function of the size of the system N, the typical velocity of the vibrating wall V or the restitution coefficient r. In all these calculations the authors did not pay too much attention to the hydrodynamic profiles of the system, always assuming a constant granular temperature ("isothermal atmosphere") and a density profile exponentially decaying with the height, as in the case of a Boltzmann elastic gas under gravity.

The "apparatus" consists of a plane of dimension $L_x \times L_y$ inclined by an angle θ with respect to the horizontal. The particles are constrained to move in such a plane under the action of an

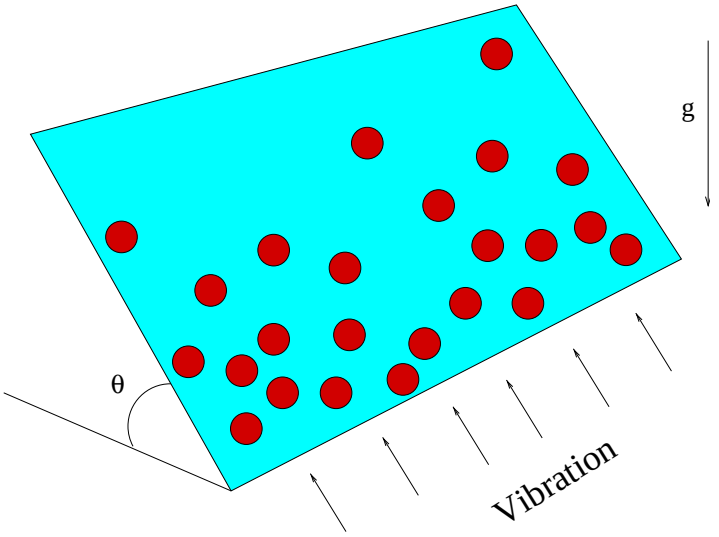

Figure 4.1: A sketch of the first model where the granular assembly is driven by gravity plus a (periodically or stochastic) vibrating wall

effective gravitational force $g_e = g\sin\theta$ pointing downward. In the horizontal direction there are periodic boundary conditions: each particle going out from the left or the right border enters at the same altitude and with the same velocity on the opposite border. The particles are confined by walls on top and bottom: both walls are inelastic with a restitution coefficient r_w. We use, in general, different restitution coefficients for the particle-particle interaction and the wall-particle interaction: this is reasonable also if the wall is covered by stuck grains (as often happens in experiments), because the microscopic dynamics of a collision with a stuck grain is completely different from that with a free grain.

The bottom wall vertically vibrates and therefore injects energy and momentum into the system. The vibration can have two different behaviors:

a) harmonic vibration (as in Kudrolli). In this case, the wall oscillates vertically with the law $Y_w(t) = A_w\sin(\omega_w t)$ ($Y_w(t)$ is the vertical position of the wall at time t) and the particles collide with it as with a body of infinite mass, so that the vertical component of their velocity after the collision is

$$v_y' = -r_w v_y + (1+r_w)V_w \tag{4.4}$$

where $V_w = A_w\omega_w\cos(\omega_w t)$ is the velocity of the vibrating wall.

b) stochastic vibration, with thermal properties (as in Isobe). In this case we assume that the vibration amplitude is negligible and that the particle colliding with the wall have, after the collision, new random velocity components $v_x \in (-\infty,+\infty)$ and $v_y \in (0,+\infty)$ with the following probability distributions:

$$P(v_y) = \frac{v_y}{T_w}\exp(-\frac{v_y^2}{2T_w}) \tag{4.5}$$

$$P(v_x) = \frac{1}{\sqrt{2\pi T_w}}\exp(-\frac{v_x^2}{2T_w}) \tag{4.6}$$

4.1.3 The boundary conditions of the 2D Inclined Channel Model

The second model that we study is sketched in Fig. 4.2. The "set-up" is a two dimensional channel of depth L_y and of length L_x, vertically confined by a bottom and a top inelastic wall, with periodic boundary conditions in the direction parallel to the flow. The channel is tilted up by an angle ϕ with respect to the horizontal so that gravity has both components $g_x = g\sin\phi$ and $g_y = g\cos\phi$.

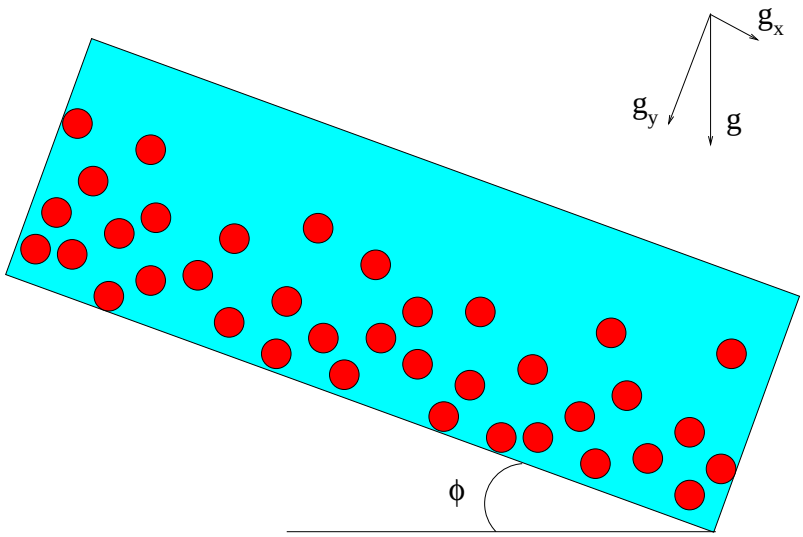

Figure 4.2: A sketch of the second model where the only energy source is gravity, with components in both directions

This model mimics the experiment performed by Azanza *et al.* [6], where a stationary flow in a two dimensional inclined channel was observed at a point far from the source of the granular material. The assumption of periodic boundary conditions in the direction of the flow is consistent with the observed stationarity, due to the balance between the gravity drift and the damping effect of inelastic collisions (for a discussion of the possible regimes that can be shown by one particle in presence of this balance, see [153]).

4.1.4 A discussion on the approximations: dilute density and absence of tangential forces

Under the assumption of *molecular chaos*, i.e. $P_2(\mathbf{x}, \mathbf{x}+\sigma\hat{\mathbf{n}}, \mathbf{v}_1, \mathbf{v}_2, t) = P(\mathbf{x}, \mathbf{v}_1, t)P(\mathbf{x}+\sigma\hat{\mathbf{n}}, \mathbf{v}_2, t)$ where P_2 and P are the probability density functions for two particles and one particle respectively, it is possible to write down the Boltzmann Equation (2.98), which can be solved by means of Monte Carlo methods. Here we used a simplified (but still efficient) version of the Direct Simulation Monte Carlo scheme proposed by Bird [30]. A detailed discussion of this method can be found in Appendix A. Here we briefly anticipate a difference with respect to the original version of the algorithm: the clock which determines the collision rate is replaced by an a-priori fixed collision rate via a constant collision probability p_c given to every disk at every time-step Δt of the simulation, in such a way that the single-particle collision rate is $\chi \sim p_c/\Delta t$. The colliding particle then seeks its collision partner among the other particles in a neighborhood of radius σ_B, choosing it randomly with a probability proportional to their relative velocities. Moreover in this approximation the diameter σ is no more explicitly relevant but it is directly related to the choices of p_c and σ_B in a non trivial way: in fact the Bird algorithm allows the particles to pass through each others, so that a precise diameter cannot be defined and estimated as a function of p_c and σ_B. The assumption of Molecular Chaos is reasonable at low densities and low inelasticities, when colliding particles can be considered uncorrelated. We have discussed what happens at medium and higher densities in elastic hard spheres gases (see section 2.2.7).

Furtherly the chosen collision rule excludes the presence of tangential forces [76, 181, 196], and hence the rotational degrees of freedom do not contribute to the description of the dynamics.

The agreement between our simulations and the inspiring experiments, justifies the simplifying assumptions considered for our model, i.e. assuming molecular chaos and neglecting tangential forces. Nevertheless, as a partial check, in section 4.3.2 we try a modified version of the 2D Inclined Channel Model where the tangential forces may affect the post-collisional velocities of the particles. As reported below, the introduction of such forces does not change the behavior of the measured quantities.

4.2 The 2D Inclined Plane Model

We have performed [15] Direct Simulation Monte Carlo for the 2D Inclined Plane Model (IPM). Here we report the measurements of the density, temperature and velocity profiles for different choices of the boundary conditions (different forms of the vibration of the bottom and inclination of the plane). In particular we have analysed the density correlations (*clustering*) and the distribution of velocities, observing interesting scaling features.

4.2.1 Macroscopic profiles (transport)

Simulations of the first model, the 2d Inclined Plane Model with a vibrating bottom wall, have been performed for different choices of the number of disks N, the normal restitution coefficient r, the dimensionless width of the plane $N_w = L_x/\sigma_B$ and the parameter measuring the rate of energy injection from the wall. This is the temperature T_w in the stochastic case and the amplitude and frequency A_w, ω_w in the periodic case.

Here we show how numerical simulations with the Molecular Chaos assumption reproduce the main results obtained in experiments [132] and in high performance computer simulations [116] of inelastic hard disks, in a wide range of values of the volume fraction (here represented by the parameter N_w) and of the restitution coefficient r.

Snapshots of the system and time-averaged density profiles are shown in Fig. 4.3 on the next page for the case of randomly vibrated wall. We are in the presence of a highly fluidized phase of the type Isobe and Nakanishi call granular turbulent: looking at the time evolution of the density distribution of the system and of the coarse-grained velocity field one observes an intermittency-like behavior with rapid and strong fluctuations of the density, sudden explosions (bubbles) followed by large clusters of particles traveling downward, coherently, under the action of gravity. Of course more dense and ordered phases (that one can expect at lower values of energy injection [116]) are not reproducible with the Direct Simulation Monte Carlo, as strong excluded volume effects appear and the assumption of negligible short range correlations fails.

In Fig. 4.4 on the following page it is shown the temperature profile $T_g(y)$. A minimum of the temperature can be observed not far from the bottom wall. From a certain height the strong temperature positive gradient abruptly changes into a very slow increase, which never becomes constant. It is interesting to look at the bottom frame in the same Figure: it shows a parametric plot of the granular temperature T_g versus the number density n, similar to those in Fig. 3.23 on page 87, Fig. 3.24 on page 87 and Fig. 3.25 on page 88 obtained with the Randomly Driven Granular Gas model. One of the data sets that we analyze is compatible with a power law $T_g \sim n^{-0.88}$ which resembles the algebraic fits in the Randomly Driven model. It must be noted that in a stationary fluid without the gravity field, the pressure is constant and therefore $T_g \sim n^{-1}$.

The case of periodically vibrated wall is illustrated in Fig. 4.5 on page 103 where one can see the density profile, together with a snapshot of the system, for a certain choice of the parameters of the model. The snapshot and the time-averaged profile is very similar to that shown for the case of the wall with stochastic vibrations. A rapid sequence of snapshots reproduces the same scenario discussed above, with very strong spatio-temporal gradients near the bottom wall and solitary particles in ballistic flight at the top of the container.

4.2.2 Density correlations

In order to characterize the spatial correlations, we have performed an analysis similar to that performed in section 3.2.3, where we observed a fractal clustering phenomena in the Randomly Driven model. In this case we have studied a cumulated particle-particle correlation function defined in this way:

$$C_{B(y,\Delta y)}(t,R) = \frac{1}{N_{B(y,\Delta y)}(N_{B(y,\Delta y)}-1)} \sum_{i\neq j:\mathbf{r}_i,\mathbf{r}_j\in B(y,\Delta y)} \Theta(R-|\mathbf{r}_i(t)-\mathbf{r}_j(t)|) \qquad (4.7)$$

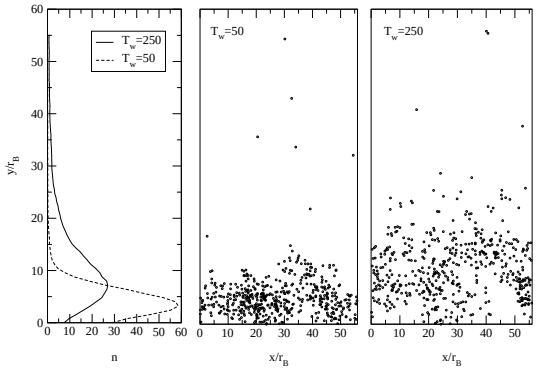

Figure 4.3: Snapshots of the 2D Inclined Plane Model with stochastic bottom wall at temperature $T_w = 50$ and $T_w = 250$. The leftmost inset displays the time-averaged number density profile for both cases. Values of other parameters: $N = 500$, $N_w \approx 56$, $r = 0.7$, $r_w = 0.7$,$g_e = -1$

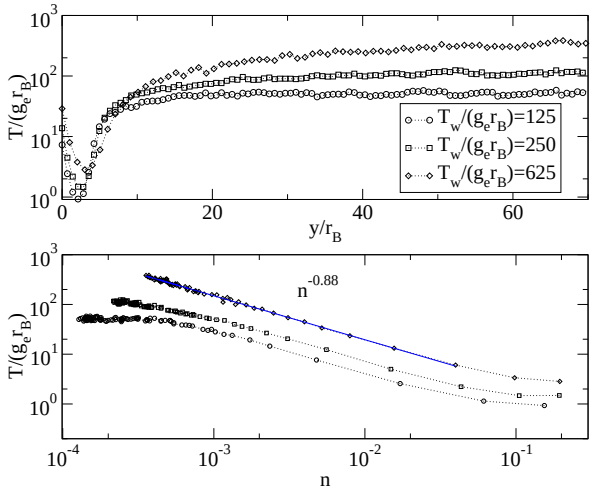

Figure 4.4: Granular (dimensionless) temperature $T_g/(g_e\sigma_B)$ versus dimensionless height y/σ_B (above) and versus number density n (bottom) for the for the 2D Inclined Plane Model with stochastic bottom wall, with $N = 5000$, $N_w \approx 180$, $r = 0.7$, $r_w = 0.7$, $g_e = -1$. The solid line is a power-law fit for $T(n)$.

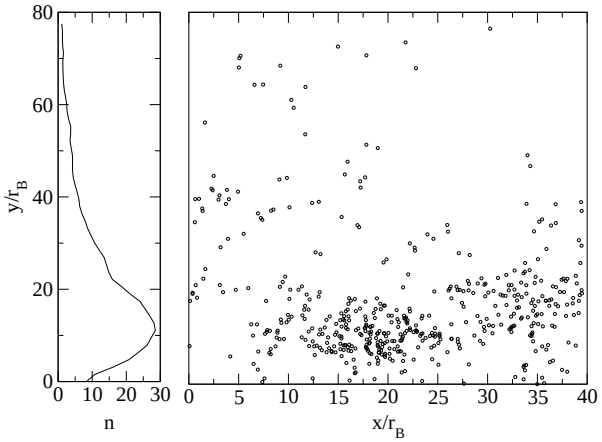

Figure 4.5: Snapshot of the 2D Inclined Plane Model with periodically vibrating wall (right) and time-averaged density profile (left) for the following choice of parameters: $N = 500$, $N_w \approx 56$, $r = 0.5$, $r_w = 0.7$, $g_e = -1$, $f_w = 400\pi$, $A_w = 0.1$

where $B(y, \Delta y)$ is a horizontal stripe defined by $y \in [y - \Delta y/2, y + \Delta y/2]$ and $x \in [0, L_x]$. After having checked that the system has reached a stationary regime, we have computed the time-average of the correlation function, that is

$$C_{B(y,\Delta y)}(R) = \frac{1}{T - t_0} \int_{t_0}^{T} dt C_{B(y,\Delta y)}(t, R) \tag{4.8}$$

which is independent on time if $T >> t_0$. In the Fig. 4.6 on the next page we show the correlation function $C(R)$ vs. R for different stripes $B(y, \Delta y)$. We observe a power law behavior

$$C_{B(y,\Delta y)}(R) \sim R^{d_2(y)} \tag{4.9}$$

In the case of homogeneous density d_2 is expected to be the topological dimension of the box $C_{B(y,\Delta y)}$. This dimension is $d_2 = 1$ if $R \gg \Delta y$, when the box appears as a "unidimensional" stripe and $d_2 = 2$ if $R \ll \Delta y$, because at close distance it appears as bidimensional.

Clustering, whose signature is a value of the correlation dimension d_2 lower than the topological dimension, appears in some of the analysed stripes: when the density is not too high an exponent smaller than 1 is measured (the fit is performed in the region $R \gg \Delta y$). Clusters are self similar arrangements of empty spaces alternated with filled spaces: when the particles are too packed (i.e. density is too high) the stripe is somehow *filled up* and the clustering phenomena disappears.

The evidence of clustering is at odds with the observation of Kudrolli and Henry [132]: they report, in fact, the absence of clustering by measuring the distribution of the number of particles in boxes of fixed dimensions spread all over the inclined plane. This observation is perhaps due to the fact that in the statistical analysis employed in the work of Kudrolli and Henry, the particles are counted in each box disregarding their heights, that is they may belong to regions of different densities which are more or less clusterized: therefore the convolution of different probability distributions with different averages (and different tails) hides the slow decaying tails, expected for the clusterized distributions of the stripes at lower densities. It is also true that, even from the global density distribution measured in their work, a tail decaying slower than a Poissonian cannot be clearly ruled out.

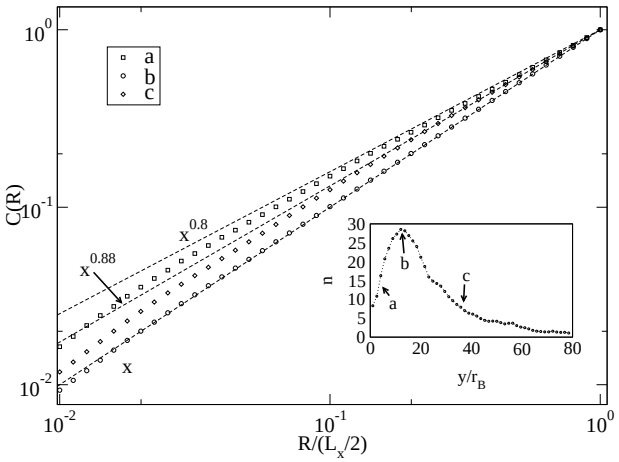

Figure 4.6: Cumulated correlation function C(R), as defined in the text, measured along stripes at different heights for the Inclined Plane Model, with periodically vibrating wall. In the inset is displayed the number density profile, with the position of the chosen stripes. Here $N = 500$, $N_w \approx 56$, $r = 0.5$, $r_w = 0.7$, $f_w = 400\pi$, $A_w = 0.1$ and $g_e = -1$

4.2.3 Distributions of velocity

In the Fig. 4.7 on the facing page and Fig. 4.8 on the next page we display the distributions of horizontal velocities for the 2D Inclined Plane Model with a bottom wall with stochastic vibrations. The first Fig. 4.7 on the facing page, shows the distributions taken from all over the system (i.e. counting particles independently of the height) for different T_w: the data collapse is obtained by rescaling the velocities by $\sqrt{T_w}$. The distributions are very different from a Gaussian.

Instead, in Fig. 4.8 on the next page we show the velocity distributions of particles contained in stripes at different heights from the wall, again rescaled by $\sqrt{T_g(y)}$ (their own variance) in order to obtain the data collapse. It again appears that the distributions are non-Gaussian and their broadening (that is the granular temperature $T_g(y)$) is height dependent. This dependence is shown in Fig. 4.4 on page 102.

The case of periodically vibrated wall is illustrated in Fig. 4.9 on the next page. One can see the distribution of horizontal velocities in two different regimes: for $g_e = -1$ a non-Gaussian distribution is obtained, while a distribution close to a Gaussian appears when $g_e = -100$. This trend toward a Gaussian, as the angle of inclination is raised up, reproduces exactly the experimental observation of Kudrolli and Henry [132] (where the angle of inclination of the plane was raised up from $\theta = 0.1^o$ to $\theta = 10^o$). This phenomena can be explained as an effect of the increase of the collision rate with the wall induced by the increase of the force of gravity: an higher collision rate "randomizes" the velocities in a more efficient way. If one accepts the analogy between the vibrating wall and the heating bath used to drive the granular gas in Chapter 3, the increase of collision rate with the wall is analogous to the decrease of the ratio τ_b/τ_c (an increase of the "heating rate"). In the Randomly Driven model the decrease of this ratio corresponds to the transition from the non-Gaussian regime to the Gaussian one.

In Fig. 4.10 on page 107 we show a log-log plot of the tails of the collapsed distributions presented in Fig. 4.8 on the next page. An algebraic fit $P(v) \sim v^{-2.8}$ is proposed.

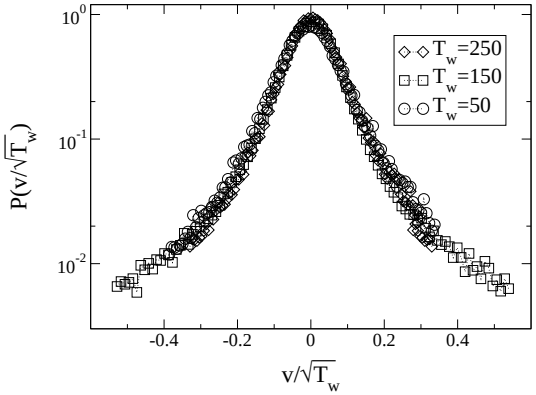

Figure 4.7: Distribution of rescaled horizontal velocities $v/\sqrt{T_w}$ for the 2D Inclined Plane Model with stochastic wall at different temperatures $T_w = 50$, $T_w = 100$, $T_w = 250$. The other parameters are $N = 5000$, $N_w \approx 180$, $r = 0.7$, $r_w = 0.7$, $g_e = -1$

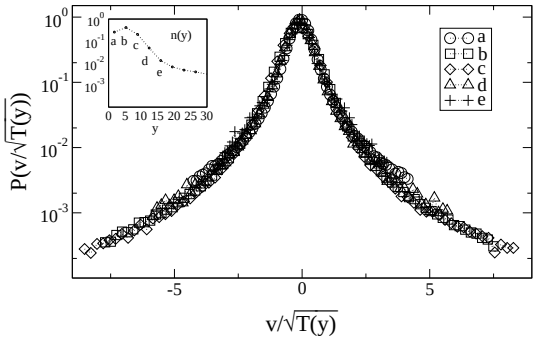

Figure 4.8: Distribution of horizontal velocities, for the 2D Inclined Plane Model with stochastic wall, measured on stripes at different heights and rescaled by the average granular temperature at that height. The inset shows the normalized number density profile with the position of the chosen stripes. $N = 5000$, $N_w \approx 180$, $r = 0.7$, $r_w = 0.7$, $g_e = -1$, $T_w = 100$

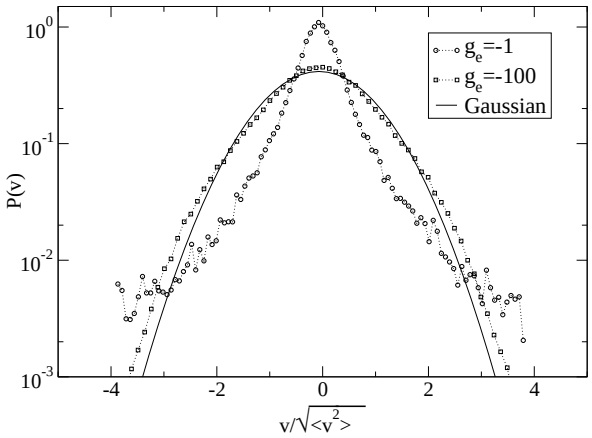

Figure 4.9: Distributions of horizontal velocities for the Inclined Plane Model with periodically vibrating wall for two different values of inclination, that is $g_e = -1$ and $g_e = -100$, while the other parameters are fixed: $N = 500$, $N_w \approx 56$, $r = 0.5$, $r_w = 0.7$, $f_w = 400\pi$, $A_w = 0.1$

4.3 The 2D Inclined Channel Model

Here we report the measurements [15] of the Direct Simulation Monte Carlo study of the Inclined Channel Model in $d = 2$. This study has again concentrated on the profiles of the macroscopic quantities (density, mean flow velocity, temperature), on the distribution of velocities and on the density correlations. The results have much in common with those presented in the previous section. Most noticeably, they are in fair agreement with experiments [6].

4.3.1 Macroscopic profiles (transport)

In Fig. 4.11 on the facing page and Fig. 4.12 on page 113 we show some profiles of mesoscopic coarse grained physical quantities: the hydrodynamical fields $n(y)$ (number density), $v_x(y)$ (velocity component parallel to the flow), $T_g(y)$ (granular temperature) are shown as functions of the distance from the bottom wall y. The velocity, the temperature and the height are made dimensionless dividing them by $\sqrt{g_x \sigma_B}$, $g_x \sigma_B$ and σ_B respectively. This means that we consider unitary the potential energy (in the gravity field) of a point of mass 1 at the height of a "Bird radius" σ_B.

The profiles well reproduce those measured experimentally by Azanza *et al.* [6]: they show a critical height H of about six times the radius σ_B which corresponds to the separation between two different regimes of the dynamics: under this critical height, the profiles are almost linear (in particular the density and velocity profiles); above this height H those profiles rapidly change and become almost constant.

This change of behavior can be explained studying the local dissipation rate due to inelastic collisions. In a mean field framework the local rate of dissipation due to the inelastic collisions (as already stated before) is $\zeta \propto n T_g^{3/2}$. This has been discussed in section 2.4.1 and can be simply understood noting that the collision rate is proportional to the local density and to the local relative velocity of the particles ($\sqrt{T_g}$), while the change in the granular temperature induced by every collision is proportional to the temperature T_g. The quantity $\tilde{\zeta} = n T_g^{3/2}$ as a function of y is shown in Fig. 4.13 on page 113. The cooling rate decreases exponentially and is reduced under $1/100$ of its maximum value at about the observed critical height $H \approx 6\sigma_B$. This means that under the critical height H the transport is mainly due to collisional exchange, while above H it is due to ballistic flights.

With respect to the velocity and temperature profiles in Fig. 4.11 on the next page, we note here that quite nonphysical features appear: in particular the strong slipping effect near the bottom wall is in contrast with the experimental findings. We check ahead the possibility that this could be due to a wrong modeling of the particle-wall collision events.

The restitution coefficient used in our model has to be considered as an effective parameter describing the energetics of collisions. It should depend on the details of the collision event, in principle even on the relative velocities of the colliding particles. In the experiment the bottom wall was covered with particles identical to the flowing ones with a spacing bounded between 0 and 0.8 mm: however the particles are stuck to the bottom wall so that the collision event is completely different from a two-particles collision.

Using a lower effective restitution coefficient for the wall r_w (see Fig. 4.11 on the facing page) we obtain a better agreement with the experimental profiles. In particular, both temperature and velocity profiles seems to go to zero near the bottom, although we cannot really rule out slipping effects ($v_x(y = 0) \neq 0$) (similar slipping effects are reported in other simulations, e.g. see [52]).

4.3.2 Profiles with tangential forces

We consider the comparison between our simplified model and the experimental profiles quite satisfactory: this seems to suggest that introducing further physical details should be irrelevant at this description level. However we briefly report the results obtained with a slightly modified version of the model, including the effects of tangential forces. Such forces play a key role in dense granular flows, e.g. being responsible for arching. On the other hand the present results suggest that in the case of diluted systems they act similarly to the normal forces without introducing noticeable effects.

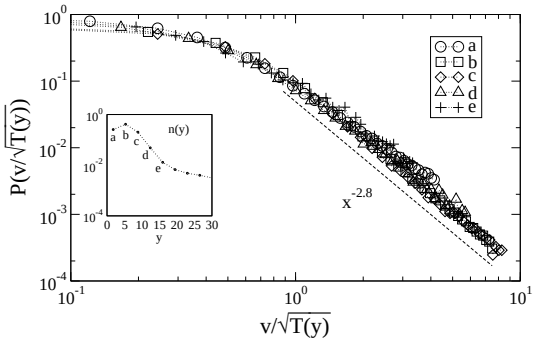

Figure 4.10: Zoom in log-log scale of the distribution of horizontal velocities, for the 2D Inclined Plane Model with stochastic wall, measured on stripes at different heights and rescaled by the average granular temperature at that height. The inset shows the normalized number density profile with the position of the chosen stripes. $N = 5000$, $N_w \approx 180$, $r = 0.7$, $r_w = 0.7$, $g_e = -1$, $T_w = 100$ (same as Fig. 4.8 on page 105). The fit indicates the power law behavior.

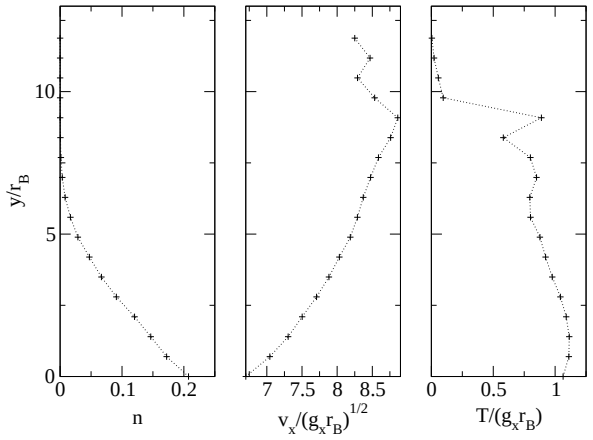

Figure 4.11: Normalized number density n, dimensionless horizontal velocity $v_x/\sqrt{g_x\sigma_B}$ and dimensionless granular temperature $T/\sqrt{g_x\sigma_B}$ versus dimensionless height y/σ_B for the 2D Inclined Channel Model: $N = 500$, $N_w \approx 56$, $g_x = 1$, $g_y = -2$ (i.e.: the inclination angle $\phi = \pi/6$), $r = 0.95$, $r_w = 0.95$

The introduction of tangential forces in the model studied accounts for a new collision rule:

$$(\mathbf{v}_1' - \mathbf{v}_2') \cdot \hat{\mathbf{n}} = -r^n((\mathbf{v}_1 - \mathbf{v}_2) \cdot \hat{\mathbf{n}}) \tag{4.10a}$$

$$(\mathbf{v}_1' - \mathbf{v}_2') \cdot \hat{\mathbf{t}} = -r^t((\mathbf{v}_1 - \mathbf{v}_2) \cdot \hat{\mathbf{t}}) \tag{4.10b}$$

where we replace the single restitution coefficient with a pair of parameters r^n and r^t, respectively due to the effect of normal and tangential collision forces ($\hat{t}$ is a unit vector perpendicular to $\hat{n}$). Analogously, the restitution coefficient r_w splits in two new parameters r_w^n and r_w^t. The results of simulations with several choices of the enlarged set of parameters do not show qualitative differences from the results previously presented: setting tangential restitution coefficients lower than one is equivalent to enhance the dissipation in the original model.

Just as an example of this, we show Fig. 4.14 on page 114, where the extremal case of a vanishing tangential restitution coefficient is reported. Note that the profiles are similar to those shown in Fig. 4.12 on page 113 where a low $r_w = 0.4$ was used.

4.3.3 Density correlations

We have investigated the homogeneity of the density, by means of the same tools already used (correlation functions for the measure of correlation dimension d_2): the Fig. 4.15 on page 114 shows the previously defined function $C_{B(y,\Delta y)}(R)$ for stripes at different density.

It appears again a clustering effect, with a correlation dimension ranging from 1 (homogeneous stripes) to 0.2 (highly clusterized stripes). In the figure it is also shown the very small distance region, $R < \sigma_B$, where homogeneity should be recovered. Since in our simulation, $\Delta y \approx \sigma_B$, we expect $d(y) = 2$ in this region.

4.3.4 Distributions of velocity

We have also studied the distribution of horizontal velocities in stripes at different heights (here the mean values are height dependent, as shown in the plots of the velocity profile). These distributions are displayed in Fig. 4.16 on page 115 showing the emergence of non-Gaussianity mainly in the case with $r_w < r$ and only in the stripes near the bottom wall. The authors of the experiment [6] claim that the distributions of velocity are very close to the Gaussian and try to fit their data with the rheological model proposed by Jenkins and Richman. This model postulates a quasi-Gaussian equilibrium to calculate the transport coefficients. Near the bottom wall the Gaussian approximation seems a very poor approximation of the real distribution, as shown by the results of our simulations: this is an effect of the inelasticity of the collisions but also of the proximity of the boundary, where high spatial gradients can put the gas out of Gaussian equilibrium.

4.4 A tentative hydrodynamic approach

Finally, in this section we discuss the hydrodynamic description of the Inclined Plane Model. We use the equations proposed by Brey et al. [39, 91], with the values of the transport coefficients that they have calculated. The problem can be solved but a close solution needs good boundary conditions. This is a non-trivial task, because the external parameters (e.g. the amplitude and frequency of the vibrating bottom, as well as the longitudinal size of the system) are connected to the bulk profiles through non-hydrodynamic layers (bottom and top).

4.4.1 The transport equations for the Inclined Plane Model

Let us quickly review the derivation of the hydrodynamic equations. The Boltzmann equation for the two models introduced in this paper (in two dimensions) reads:

$$\left(\frac{\partial}{\partial t}+\mathbf{v}\cdot\nabla+g_i\frac{\partial}{\partial v_i}\right)P(\mathbf{r},\mathbf{v},t)=Q(P,P) \tag{4.11}$$

where the collision integral reads, as usual:

$$Q(P,P)=\sigma\int d\mathbf{v}_1\int d\hat{\mathbf{n}}\Theta(\hat{\mathbf{n}}\cdot\mathbf{v}_r)(\hat{\mathbf{n}}\cdot\mathbf{v}_r) \times[r^{-2}P(\mathbf{r},\mathbf{v}',t)P(\mathbf{r},\mathbf{v}_1',t)-P(\mathbf{r},\mathbf{v},t)P(\mathbf{r},\mathbf{v}_1,t)] \tag{4.12}$$

Here $\hat{\mathbf{n}}$ is the unit vector along the line joining the centers of the colliding particles at contact, $\mathbf{v}_r=\mathbf{v}-\mathbf{v}_1$ is the relative velocity of the colliding disks, Θ is the Heaviside step function, $\mathbf{v}'$ and $\mathbf{v}_1'$ are the precollisional velocities leading after collision to velocities $\mathbf{v}$,$\mathbf{v}_1$.

The equation (4.11) must be completed with the boundary conditions in order to describe the microscopic evolution of the whole system.

The difficulty of solving the Boltzmann equation (4.11) can be bypassed substituting the microscopic description given by $P(\mathbf{r},\mathbf{v},t)$ with averages given by the hydrodynamic fields: the number density field $n(\mathbf{r},t)$, the velocity field $\mathbf{v}(\mathbf{r},t)$ and the granular temperature field $T(\mathbf{r},t)$. These quantities are given by

$$n(\mathbf{r},t)=\int d\mathbf{v}P(\mathbf{r},\mathbf{v},t) \tag{4.13}$$

$$\mathbf{u}(\mathbf{r},t)=\frac{1}{n(\mathbf{r},t)}\int d\mathbf{v}\mathbf{v}P(\mathbf{r},\mathbf{v},t) \tag{4.14}$$

$$k_BT(\mathbf{r},t)=\frac{1}{n(\mathbf{r},t)}\int d\mathbf{v}\frac{m(\mathbf{v}-\mathbf{u}(\mathbf{r},\mathbf{t}))^2}{2}P(\mathbf{r},\mathbf{v},t) \tag{4.15}$$

These quantities, in an elastic hard spheres gas, are collisional invariants and therefore are totally conserved during the dynamics: this property guarantees that - while the fluctuations of the microscopic degrees of freedom are rapidly absorbed at the time-scale of a few collisions per particle - these few macroscopic fields slowly relax on larger time-scales. Therefore on time-scales larger than the mean free time and on space-scales larger than the mean free path (if this distinction of scales is possible) the hydrodynamic fields can be described by the hydrodynamics equations discussed ahead, where a local pseudo-equilibrium is used to close the hierarchy of the Maxwell equations for the moments. This procedure has been discussed in Chapter 2.

Multiplying the Boltzmann equation (4.11) by 1 or $\mathbf{v}$ or $m(\mathbf{v}-\mathbf{u}(\mathbf{r},\mathbf{t}))^2/2$ and integrating over $\mathbf{v}_1$ one can derive the equations of fluid dynamics:

$$\frac{Dn}{Dt}+n\partial_i u_i=0 \tag{4.16}$$

$$mn\frac{Du_i}{Dt} = -\partial_j \mathcal{P}_{ij} + ng_i m \quad (i = 1, 2, 3) \tag{4.17}$$

$$n\frac{Dk_BT}{Dt} = -\partial_i q_i - \mathcal{P}_{ij}\partial_j u_i - \zeta n k_B T \tag{4.18}$$

where $\partial_i = \partial/\partial r_i$ (for the sake of compactness we use here the notation $x \to r_1$ and $y \to r_2$) and $D/Dt = \partial/\partial t + \mathbf{u}\cdot\nabla$ is the Lagrangian derivative, i.e.: $\frac{D}{Dt}F(\mathbf{r},t) = \frac{d}{dt}F(\phi(\mathbf{r}_0,t),t)$ with $\phi(\mathbf{r}_0,t)$ the evolution after a time t of $\mathbf{r}_0$ under the velocity field $\mathbf{u}$. In the above equations

$$\mathcal{P}_{ik} = n\int d\mathbf{v} m(v_i - u_i)(v_k - u_k)P(\mathbf{r},\mathbf{v},t) \tag{4.19}$$

is the stress tensor, $\mathbf{g}$ is the volume external force (gravity in our case),

$$q_i = n\int d\mathbf{v}\frac{m}{2}(v_i - u_i)|\mathbf{v}-\mathbf{u}|^2 P(\mathbf{r},\mathbf{v},t) \tag{4.20}$$

is the heat flux vector and

$$\zeta(\mathbf{r},t) = \frac{m(1-r^2)\pi^{1/2}\sigma}{8\Gamma(5/2)nk_BT}\int d\mathbf{v}_1\int d\mathbf{v}_2|\mathbf{v}_1-\mathbf{v}_2|^3 P(\mathbf{r},\mathbf{v}_1,t)P(\mathbf{r},\mathbf{v}_2,t) \tag{4.21}$$

is the cooling rate due to dissipative collisions.

The set of equations (4.16)-(4.18) become closed hydrodynamic equations for the fields n, $\mathbf{u}$ and T when $\mathcal{P}_{ij}$, $\mathbf{q}$ and ζ are expressed as functionals of these fields. This is obtained, for example, expressing the space and time dependence of P in terms of the hydrodynamic fields and then expanding P to first order (the so-called Navier-Stokes order) in their gradients, with the exception of ζ which requires an expression of P to the second order of gradients to be consistent with the other terms. With this approximation the equations (4.16)-(4.18) include the contributions up to the second order in the gradients of the fields.

We follow Brey et al. [39] and write down the hydrodynamics for the Inclined Plane Model presented in this paper (gravity in one direction and vibrating bottom wall, i.e. $\mathbf{g} = (0, g_e)$ and $g_e < 0$), with the following assumptions: the fields do not depend upon x (the coordinate parallel to the bottom wall), i.e. $\partial/\partial x = 0$, and the system is in a steady state, i.e. $\partial/\partial t = 0$. The continuity equation (4.16) then reads $\frac{\partial}{\partial y}(n(y)u_y(y)) = 0$ and this can be compatible with the bottom and top walls (where $nv_y = 0$) only if $n(y)v_y(y) = 0$, that is in the absence of macroscopic vertical flow. The equations are written for the dimensionless fields $\tilde{T}(\tilde{y}) = k_BT(y)/(-g_e m\sigma)|_{y=\sigma\tilde{y}}$ and $\tilde{n}(\tilde{y}) = n(y)\sigma^2|_{y=\sigma\tilde{y}}$, while the position y is made dimensionless using $\tilde{y} = y/\sigma$. Finally for the pressure we put $p(y) = \mathcal{P}_{22} = n(y)k_BT(y)$. With the assumption discussed above the equations of Brey et al read:

$$\frac{d}{d\tilde{y}}(\tilde{n}(\tilde{y})\tilde{T}(\tilde{y})) = -\tilde{n}(\tilde{y}) \tag{4.22}$$

$$\frac{1}{\tilde{n}(\tilde{y})}\frac{d}{d\tilde{y}}Q_r(\tilde{y}) - C(r)\tilde{n}(\tilde{y})\tilde{T}(\tilde{y})^{3/2} = 0 \tag{4.23}$$

where $Q_r(\tilde{y})$ is the granular heat flux expressed by

$$Q_r(\tilde{y}) = A(r)\tilde{T}(\tilde{y})^{1/2}\frac{d}{d\tilde{y}}\tilde{T}(\tilde{y}) + B(r)\frac{\tilde{T}(\tilde{y})^{3/2}}{\tilde{n}(\tilde{y})}\frac{d}{d\tilde{y}}\tilde{n}(\tilde{y}) \tag{4.24}$$

In the above equations $A(r)$, $B(r)$ and $C(r)$ are dimensionless monotone coefficients, all with the same sign (positive), explicitly given in the Appendix B. In particular $B(1) = 0$ and $C(1) = 0$, i.e. in the elastic limit there is no dissipation and the heat transport is due only to the temperature gradients, while when $r < 1$ a term dependent upon $\frac{d}{d\tilde{y}}\ln(\tilde{n}(\tilde{y}))$ appears in $Q_r(\tilde{y})$. The use of dimensionless fields eliminates the explicit $\mathbf{g}$ dependence from the equations, that remains hidden in their structure

(the right hand term of equation 4.22, that is due to the gravitational pressure gradient, disappears in the equation for $g = 0$).

The correct solution of Eqs. (4.22) *and* (4.23) *has been found and published by Brey et al. [43]. We have published [15], almost contemporaneously, a wrong solution (we have done a sign error in the starting equation, obtaining wrong final equations). The error was pointed out by Eggers and also by Brey and co-workers (private communications). In the following section the correct solution is sketched.*

4.4.2 The solution of the equations

A change of coordinate can be applied to Eqs. (4.22),(4.23) in order to obtain a simpler form:

$$\tilde{y} \to l(\tilde{y}) = \int_0^{\tilde{y}} \tilde{n}(y')dy' \tag{4.25}$$

It follows that when y spans the range $[0, L_y]$, the coordinate l spans the range $[0, \sigma/L_x]$. With this change of coordinate it happens that

$$\frac{d}{d\tilde{y}} \to \tilde{n}(l)\frac{d}{dl} \tag{4.26}$$

and the first equation (4.22) reads:

$$\frac{d}{dl}(\tilde{n}(l)\tilde{T}(l)) = -1 \tag{4.27}$$

from which is immediate to see that

$$H = \tilde{n}(l)\tilde{T}(l) + l \tag{4.28}$$

is a constant, i.e. $\frac{d}{dl}H = 0$. This is equivalent to observe that

$$p(y) - g\int_0^y n(y')dy' \tag{4.29}$$

is constant which is nothing more than the Bernoulli theorem for a fluid in the gravitational field with the density depending upon the height.

The relation (4.28) is verified by the model simulated in this work in the Fig. 4.17 on page 115 for almost all the height of the container, apart of the boundary layer near the bottom driving wall.

Using the coordinate l introduced in (4.25) and the elimination of $\tilde{n}(l)$ using the recognized constant, that is

$$\tilde{n}(l) = \frac{H - l}{\tilde{T}(l)} \tag{4.30}$$

the second equation (4.23), after some simplifications, and after a second change of coordinate $l \to s(l) = H - l$, becomes:

$$\frac{\alpha(r)s}{\tilde{T}(s)^{1/2}}\frac{d^2}{ds^2}\tilde{T}(s) - \frac{\alpha(r)s}{2\tilde{T}(s)^{3/2}}\left(\frac{d}{ds}\tilde{T}(s)\right)^2 + \frac{\beta(r)}{\tilde{T}(s)^{1/2}}\frac{d}{ds}\tilde{T}(s) - s\tilde{T}(s)^{1/2} = 0 \tag{4.31}$$

where $\alpha(r) = (A(r) - B(r))/C(r)$, $\beta(r) = (A(r) - \frac{1}{2}B(r))/(C(r))$ are numerically checked to be positive (α is positive for values of r not too low, about $r > 0.3$) and are divergent in the limit $r \to 1$.

The correspondence with the solution of Brey et al. [43] is given by:

$$k^* \to A \tag{4.32a}$$
$$\mu^* \to B \tag{4.32b}$$
$$\zeta^* \to \frac{C}{\pi} \tag{4.32c}$$
$$l \to 2\sqrt{2}s - p_L^* \tag{4.32d}$$
$$C \to 2\sqrt{2} \tag{4.32e}$$
$$a(r) \to \frac{1}{4\sqrt{2}\alpha} \tag{4.32f}$$
$$b(r) \to \frac{\beta}{\alpha} \tag{4.32g}$$
$$\xi \to \frac{s}{\sqrt{2\alpha}} \tag{4.32h}$$
$$\nu \to \frac{1}{2}\frac{\beta - \alpha}{\alpha} \tag{4.32i}$$

The equation (4.31) become a linear equation in $\tilde{T}(s)$ as soon as the change of variable $z(s) = \tilde{T}(s)^{1/2}$ is performed:

$$2\alpha(r)s\frac{d^2}{ds^2}z(s) + 2\beta(r)\frac{d}{ds}z(s) - sz(s) = 0 \tag{4.33}$$

giving the solution:

$$z(s) = \mathcal{A}s^{-\nu(r)}I_{\nu(r)}(s/\sqrt{2\alpha}) + \mathcal{B}s^{-\nu(r)}K_{\nu(r)}(s/\sqrt{2\alpha}) \tag{4.34}$$

where I_ν and K_ν are the modified Bessel functions of the first kind and the second kind respectively, $\nu(r) = B(r)/(4(A(r) - B(r)))$ is real and positive for all the values of r greater than the zero of the function $A(r) - B(r)$ (about $r \simeq 0.3$), with $\nu(1) = 0$, while $\mathcal{A}$ and $\mathcal{B}$ are constants that must be determined with assigning the boundary conditions.

Then we can derive the expressions for $\tilde{T}(l)$ and $\tilde{n}(l)$:

$$\tilde{T}(l) = (H-l)^{-2\nu(r)}(\mathcal{A}I_{\nu(r)}((H-l)/\sqrt{2\alpha(r)}) + \mathcal{B}K_{\nu(r)}((H-l)/\sqrt{2\alpha(r)}))^2 \tag{4.35}$$

$$\tilde{n}(l) = \frac{(H-l)^{1+2\nu(r)}}{(\mathcal{A}J_{\nu(r)}((H-l)/\sqrt{2\alpha(r)}) + \mathcal{B}N_{\nu(r)}((H-l)/\sqrt{2\alpha(r)}))^2} \tag{4.36}$$

To calculate the expressions of $\tilde{T}$ and $\tilde{n}$ as a function of the original coordinate $\tilde{y}$ one needs to solve the equation

$$\frac{d}{dl}\tilde{y}(l) = \frac{1}{\tilde{n}(l)} \tag{4.37}$$

putting in it the solution (4.36). However one can obtain a comparison with the numerical simulations using the new coordinate l. For a discussion of the boundary conditions needed to eliminate the constants H, $\mathcal{A}$ and $\mathcal{B}$ we refer the reader to the paper of Brey et al.[43]. In this paper the authors show that the solution fit very well a large region in the bulk but cannot work on the boundary regions near the vibrating bottom and near the open surface. The authors show also that the minimum of the temperature is compatible with the proposed equations.

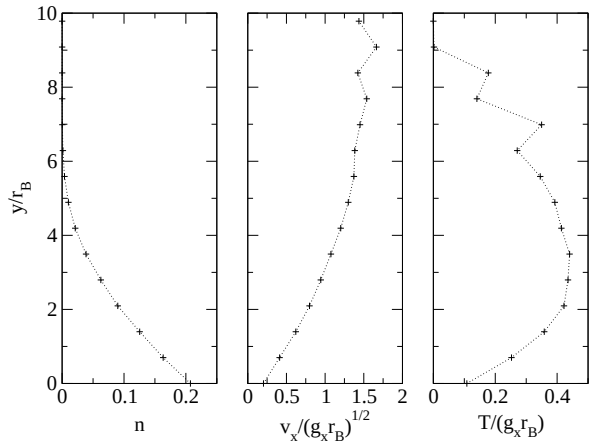

Figure 4.12: Normalized number density n, dimensionless horizontal velocity $v_x/\sqrt{g_x\sigma_B}$ and dimensionless granular temperature $T/\sqrt{g_x\sigma_B}$ versus dimensionless height y/σ_B for the 2D Inclined Channel Model: $N = 500$, $N_w \approx 56$, $g_x = 1$, $g_y = -2$ (i.e.: the inclination angle $\phi = \pi/6$), $r = 0.95$, $r_w = 0.4$

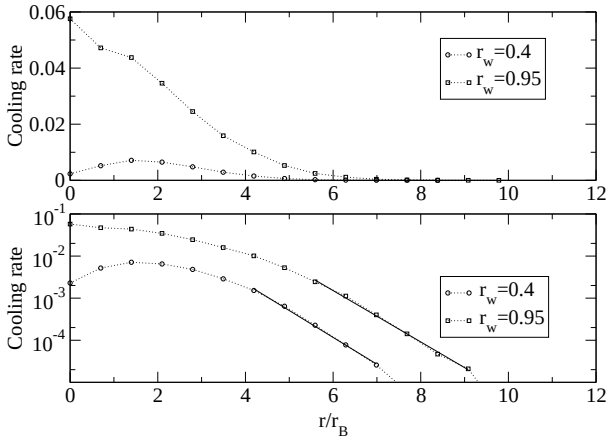

Figure 4.13: Cooling rate, as defined in the text, versus dimensionless height y/σ_B for the 2D Inclined Channel Model: $N = 500$, $N_w \approx 56$, $g_x = 1$, $g_y = -2$ (i.e.: the inclination angle $\phi = \pi/6$), $r = 0.95$, $r_w = 0.95$ or $r_w = 0.4$

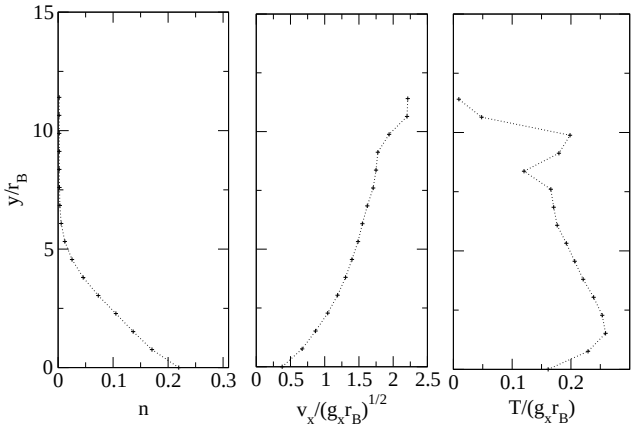

Figure 4.14: Normalized number density n, dimensionless horizontal velocity $v_x/\sqrt{g_x\sigma_B}$ and dimensionless granular temperature $T_g/(g_x\sigma_B)$ versus dimensionless height y/σ_B for the 2D Inclined Channel Model. Here tangential restitution coefficients smaller than one are considered (see text): $N = 500$, $N_w \approx 56$, $g_x = 1$, $g_y = -2$ (i.e.: the inclination angle $\phi = \pi/6$), $r^n = 0.95$, $r^t = 0$, $r_w^n = 0.95$,$r_w^t = 0$

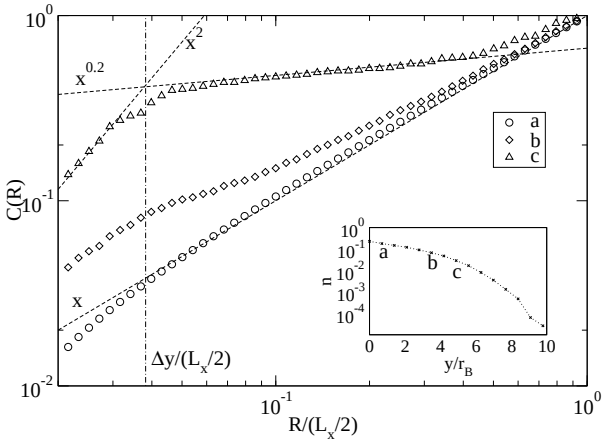

Figure 4.15: Cumulated correlation function C(R), as defined in the text, measured along stripes at different heights for the 2D Inclined Channel Model. In the inset is displayed the normalized number density profile with the position of the choose stripes. Here $N = 500$, $N_w \approx 56$, $r = 0.95$, $r_w = 0.95$, $g_x = 1$, $g_y = -2$ (i.e.: the inclination angle $\phi = \pi/6$). The dashed lines represent the power-law fits, the vertical dot-dashed line represent the width of the stripes Δy

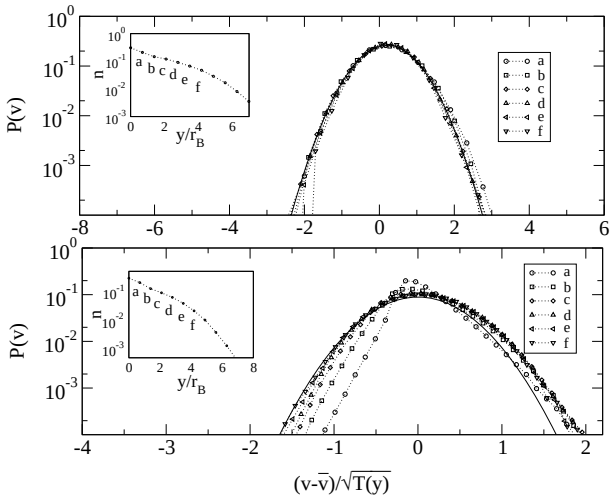

Figure 4.16: Distribution of horizontal velocities for the Inclined Channel Model, measured on stripes at different heights and rescaled in order to have the same mean and variance. The inset shows the normalized number density profile with the position of the chosen stripes. $N = 500$, $N_w \approx 56$, $r = 0.95$, $r_w = 0.95$ in the above frame and $r_w = 0.4$ in the bottom frame, $g_x = 1$, $g_y = -2$ (i.e.: the inclination angle $\phi = \pi/6$)

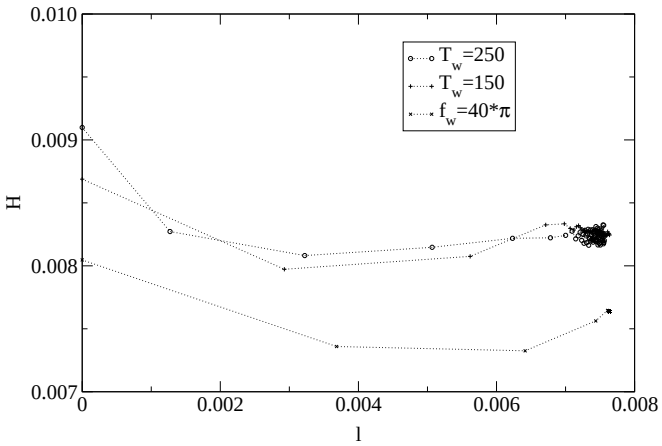

Figure 4.17: Plot of H, defined in the text, versus l, for three different simulations of the Inclined Plane Model: two cases are with the stochastic wall ($N = 5000$, $N_w \approx 180$, $r = 0.7$, $r_w = 0.7$, $g_e = -1$, $T_w = 150$ and $T_w = 250$), while the third case is with the periodic wall ($N = 5000$, $N_w \approx 180$, $r = 0.7$, $r_w = 0.7$, $g_e = -1$, $f_w = 80\pi$, $A_w = 0.1$

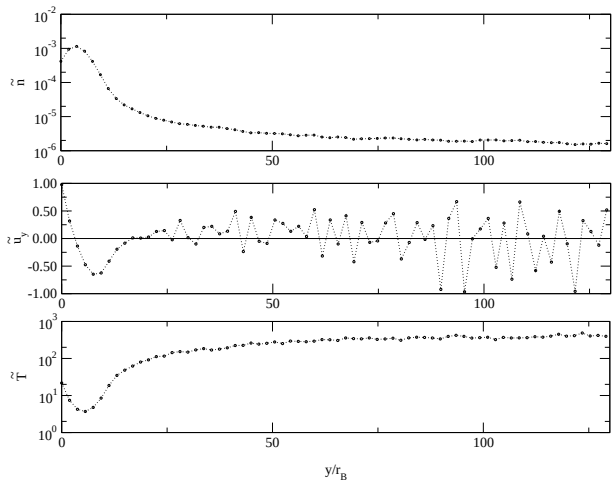

Figure 4.18: Profiles of dimensionless hydrodynamic fields $\overline{n}$, $\overline{v}_y$ and $\overline{T}$ versus the dimensionless height y/σ_B, for the Inclined Plane Model with the stochastic wall at temperature $T_w = 250$. $N = 5000$, $N_w \approx 180$, $r = 0.7$, $r_w = 0.7$, $g_e = -1$.

Chapter 5

Instability development in cooling granular fluids

The problem of granular gases becomes even more subtle when the energy input is suppressed and the system cools down due to dissipative collisions among particles. This is addressed as the problem of "cooling" granular gases and historically has preceded the problem of stationary granular gases with energy feeding mechanisms [103, 96, 157]. It is reasonable that a problem is investigated with a minimum set of ingredients (i.e.: free cooling, only collisions among particles) and then new physical ingredients (e.g: the energy input [77]) are added thereafter. Unfortunately, in this case the presence of an energy input changes drastically the behavior of the gas and in some sense reduces the difficulty of its investigation. A stationary granular gas, in fact, has only one regime to be studied (apart of a transient time necessary to forget initial conditions), while a cooling granular gas has several regimes intervening at different times, most of which are still lacking a complete comprehension.

Moreover, one can prepare a driven granular gas in such a way to obtain an ideal gas-like stationary regime [183] (simply chosing a not too high density or a not too high inelasticity or a strong energy input), while a cooling granular gas is unstable to the formation of liquid-like and solid-like phases, breaking in a non-trivial way the simmetries imposed by the initial condition.

The inelastic hard spheres model without energy input exhibits an initial regime characterized by homogeneous density and a probability distribution of velocities that depends on time only through the total kinetic energy (global granular temperature $T_g(t)$), i.e. a scaling velocity distribution. This is called the *Homogeneous Cooling State* or Haff regime [103]. It has been shown by several authors [96, 157, 73, 214] that this state is not stable towards shear and clustering instabilities: structures can form that seem to minimize dissipation, mainly in the form of velocity vortices and high density clusters. These instabilities grow on different space and time scales, so that one can investigate them separately. Several theories have been proposed to take into account the emergence of structures in granular gases. Some of them are more fundamental, obtaining the correlation functions from the kinetic equations [210]; others are more macroscopic (they have been called "mesoscopic" by the authors), involving the study of fluctuating hydrodynamics [212]; others are simply phenomenological theories that suggest analogies with Burgers equation [22] or spinodal decomposition models [219]. Some of these theories can grasp the behavior of the cooling granular gas far deeply into the correlated regime, giving predictions for the asymptotic decay of energy.

We review these recent theories in the first section of this chapter, focusing our attention on the results of Goldhirsch and Zanetti [96], those of Ernst and co-workers [214, 219], and finally to those of Ben-Naim and Redner [22] and some alternative models proposed by Ben-Naim and Krapivisky [24]. In the second section we study the behavior of the 1D cooling granular gas, comparing Molecular Dynamics simulations with a 1D inelastic lattice gas model proposed by us, which seems to reproduce very well the true (MD) phenomenology in the collisional (uncompressible) regime. In the third section we discuss this particular model, which is the inelastic mean-field version of the Maxwell molecules model (also known as Ulam model [208]), obtaining an exact scaling solution for its kinetic equation. In the fourth section we propose a 2D lattice gas model that well reproduces the behavior of the 2D cooling granular gas, providing a tool to study the diffusive character of the shearing instability and its statistical properties. The last section is devoted to a brief review of the results (analytical and numerical) known for 1d and 2d cooling granular gases, with different models considered.

5.1 Phenomenology and theory

Usually (in numerical or real experiments) granular gases are prepared in a **homogeneous** situation: uniform-random position of grains, Gaussian or uniform-random initial velocity with no preferred direction. It happens that, however the inelasticity of collisions be strong, the imposed homogeneity is broken after a certain time. The more accepted scenario is a two time symmetry breaking: at a time t_s the velocity field becomes unstable to the formation of shear bands, then at a time $t_c > t_s$ the density field becomes unstable toward the formation of high density clusters. After that, everything may happen.

5.1.1 The Homogeneous Cooling State

The Homogeneous Cooling State can be characterized at the kinetic or at the hydrodynamics level. We expose both the characterizations.

Kinetics of the Homogeneous Cooling State

We rewrite here the Boltzmann Equation for a 3D cooling granular gas [42, 210] (see paragraph 2.2.8):

$$\left(\frac{\partial}{\partial t}+L_1^0\right)P(\mathbf{r}_1,\mathbf{v}_1,t)=\sigma^2\int d\mathbf{v}_2\int_{\mathbf{V}_{12}\cdot\hat{\mathbf{n}}>0}d\hat{\mathbf{n}}|\mathbf{V}_{12}\cdot\hat{\mathbf{n}}| \times\left[\frac{1}{r^2}P(\mathbf{r}_1,\mathbf{v}_1',t)P(\mathbf{r}_1,\mathbf{v}_2',t)-P(\mathbf{r}_1,\mathbf{v}_1,t)P(\mathbf{r}_1,\mathbf{v}_2,t)\right] \quad (5.1)$$

The kinetic definition of Homogeneous Cooling State is given by the scaling ansatz for the state distribution function:

$$P(\mathbf{r},\mathbf{v},t)=nP(\mathbf{v},t)=\frac{n}{v_0^d(t)}\tilde{P}(\mathbf{c}) \quad (5.2)$$

where $\mathbf{c}=\mathbf{v}/v_0(t)$ and $v_0(t)$ is the thermal velocity defined by $T(t)=mv_0^2(t)/2$ with $T(t)$ the temperature (defined for example in Eq. (2.116)). If the Eq. (5.2) is inserted in the Boltzmann Equation (5.1), an equation for the temperature is obtained:

$$\frac{dT}{dt}=-\frac{\Omega_d}{\sqrt{2\pi}}mn\sigma^{d-1}v_0^3\gamma=-2\omega\gamma T \quad (5.3)$$

where $\Omega_d=2\pi^{d/2}/\Gamma(d/2)$ is the surface area of a d-dimensional unit sphere, ω is the time dependent collision frequency, while γ is the time independent cooling rate. These last two functions are defined by:

$$\omega=n\sigma^{d-1}v_0(t)\int d\mathbf{c}_1\mathbf{c}_2\int_{\mathbf{c}_{12}\cdot\hat{\mathbf{n}}>0}d\hat{\mathbf{n}}|\mathbf{c}_{12}\cdot\hat{\mathbf{n}}|\tilde{P}(\mathbf{c}_1)\tilde{P}(\mathbf{c}_2) \quad (5.4a)$$

$$\gamma=-\frac{\sqrt{2\pi}}{d\Omega_d}\int d\mathbf{c}_1c_1^2Q(\tilde{P},\tilde{P}) \quad (5.4b)$$

and can be approximated, using the Maxwellian approximation $\tilde{P}\approx\pi^{-d/2}\exp(-c^2)$, by ω_0 and γ_0 respectively, given by:

$$\omega_0=\Omega_dn\sigma^{d-1}\sqrt{\frac{T}{\pi m}} \quad (5.5a)$$

$$\gamma_0=\frac{1-r^2}{2d} \quad (5.5b)$$

The solution of the temperature equation (5.3) reads:

$$T(t) = \frac{T(0)}{(1+\gamma_0 t/t_0)^2} = T(0)\exp(-2\gamma_0\tau) \tag{5.6}$$

where $t_0 = 1/\omega(T(0))$ is the mean free time at the initial temperature $T(0)$ and

$$\tau = \frac{1}{\gamma_0}\ln(1+\gamma_0+t/t_0) \tag{5.7}$$

is the cumulated collision number obtained from the definition $d\tau = \omega(T(t))dt$. Eq. (5.6) is known as Haff's law [103] and has been discussed in paragraph 2.4.1.

Hydrodynamics of the Homogeneous Cooling State

The hydrodynamics for the Inelastic Hard Spheres model [39, 214] is described by the following equations (see section 2.4):

$$\frac{\partial n}{\partial t} + \frac{\partial (n u_i)}{\partial r_i} = 0 \tag{5.8a}$$

$$\frac{\partial u_j}{\partial t} + u_i \frac{\partial u_j}{\partial r_i} + \frac{1}{mn}\frac{\partial \mathcal{P}_{ij}}{\partial r_i} = 0 \tag{5.8b}$$

$$\frac{\partial T}{\partial t} + u_i \frac{\partial T}{\partial r_i} + \frac{2}{dnk_B}\left(\mathcal{P}_{ij}\frac{\partial u_j}{\partial r_i} + \frac{\partial q_i}{\partial r_i}\right) + T\zeta = 0 \tag{5.8c}$$

These equations are generally closed with constitutive relations obtained by means of expansions of kinetic equations. The results presented in this section have been obtained by van Noije, Ernst, Brito and Orza [212] and are based on the following (Navier-Stokes order) approximations:

$$\mathcal{P}_{ij} = nk_BT\left[1+\frac{\Omega_d\chi n\sigma^d}{2d}\right]\delta_{ij} - \eta\left(\frac{\partial u_j}{\partial r_i}+\frac{\partial u_i}{\partial r_j}-\frac{2}{d}\delta_{ij}\frac{\partial v_l}{\partial r_l}\right) - \eta'\delta_{ij}\frac{\partial v_l}{\partial r_l} \tag{5.9a}$$

$$q_i = -\kappa\frac{\partial T}{\partial r_i} \tag{5.9b}$$

$$\zeta = 2\gamma_0\omega_0 \tag{5.9c}$$

$$\omega_0 = \Omega_d\chi n\sigma^{d-1}\sqrt{\frac{T}{\pi m}} \tag{5.9d}$$

$$\gamma_0 = \frac{1-r^2}{2d} \tag{5.9e}$$

$$\chi = \begin{cases} \frac{2-\phi}{2(1-\phi)^3} \ (d=3) \\ \frac{1-7\phi/16}{(1-\phi)^2} \ (d=2) \end{cases} \tag{5.9f}$$

with η, η' and κ the shear viscosity, bulk viscosity and heat conductivity respectively. The expression for the pressure correction $p = nk_BT[1+...]$ and for the collision frequency correction (which both contains the pair distribution function of hard spheres or disks at contact $\chi = g_2(r=\sigma)$) are obtained from the Enskog theory (see paragraph 2.2.6), with ϕ the volume fraction ($\pi n\sigma^2/4$ if $d=2$ or $4\pi n\sigma^3/3$ if $d=3$).

The equations (5.8) are solved by the following homogeneous solution:

$$n(\mathbf{r},t) \equiv n \tag{5.10a}$$

$$\mathbf{u}(\mathbf{r},t) \equiv 0 \tag{5.10b}$$

$$T(\mathbf{r},t) = T(t) \tag{5.10c}$$

where $T(t)$ is the same as in Eq. (5.6).

An expansion of the kinetic equation in the inelasticity parameter $\epsilon = 1-r^2 \equiv 2d\gamma_0$ has shown [210, 198] that γ and ω are well approximated by γ_0 and ω_0 (their Maxwellian counterparts) for almost all values of r.

5.1.2 Linear stability analysis

A granular gas prepared with a homogeneous density and no macroscopic flow, at a given temperature $T(0)$, reaches the Homogeneous Cooling State in a few free times t_0. To study the behavior of small (macroscopic, i.e. for wave vectors of low magnitude $k \ll \min\{2\pi/l_0, 2\pi/\sigma\}$) fluctuations around this state, a linear stability study of hydrodynamics equations (5.8) has been performed by several authors (Goldhirsch and Zanetti [96], Deltour and Barrat [73], van Noije et al. [214]). We follow the detailed discussion of [212], reviewing their result for the linearized hydrodynamics of rescaled fields. The rescaled fluctuation fields are defined as

$$\delta\tilde{n}(\mathbf{r},\tau) = \delta n(\mathbf{r},t)/n \tag{5.11a}$$
$$\tilde{\mathbf{u}}(\mathbf{r},\tau) = \mathbf{u}(\mathbf{r},t)/v_0(t) \tag{5.11b}$$
$$\delta\tilde{T}(\mathbf{r},\tau) = \delta T(\mathbf{r},t)/T(t) \tag{5.11c}$$

Their Fourier transforms are given by $\delta\tilde{a}(\mathbf{k},\tau) = \int d\mathbf{r}\exp(-i\mathbf{k}\cdot\mathbf{r})\delta\tilde{a}(\mathbf{r},\tau)$, where a is one of $(n,\mathbf{u},T)$.

The vector $\tilde{\mathbf{u}}(\mathbf{k},\tau)$ can be decomposed in $(d-1)$ vectors perpendicular to $\mathbf{k}$, called indistinctly $\tilde{\mathbf{u}}_\perp$, and one vector parallel to $\mathbf{k}$, called $\tilde{\mathbf{u}}_\parallel$.

The linearized hydrodynamics for these fluctuations is given (in Fourier space) by the following equation:

$$\frac{\partial}{\partial\tau}\delta\tilde{\mathbf{a}}(\mathbf{k},\tau) = \tilde{\mathcal{M}}(\mathbf{k})\delta\tilde{a}(\mathbf{k},\tau) \tag{5.12}$$

where

$$\tilde{\mathbf{a}} = \begin{cases} (n, u_\perp, u_\parallel, T)\ (d=2) \\ (n, u_\perp, u'_\perp, u_\parallel, T)\ (d=3) \end{cases} \tag{5.13}$$

The matrix $\tilde{\mathcal{M}}$ is given (in $d=2$) by:

$$\tilde{\mathcal{M}} = \begin{pmatrix} 0 & 0 & -ikl_0 & 0 \\ 0 & \gamma_0(1-k^2\xi_\perp^2) & 0 & 0 \\ -ikl_0\left(\frac{1}{2nT\chi_T}\right) & 0 & \gamma_0(1-k^2\xi_\parallel^2) & -ikl_0\left(\frac{p}{2nT}\right) \\ -\gamma_0 g(n) & 0 & -ikl_0\left(\frac{2p}{dnT}\right) & -\gamma_0(1+k^2\xi_T^2) \end{pmatrix} \tag{5.14}$$

Here we have introduced the correlation lengths $\xi_\perp$, $\xi_\parallel$ and ξ_T that depend on the transport coefficients (shear and bulk viscosity and heat conductivity), on the isothermal compressibility $\chi_T = (\partial n/\partial p)_T/n$ and on the pair distribution function $g(n)$ already mentioned. We refer to [212] for detailed calculations of these correlation lengths.

We report in Fig. 5.1 on the following page a plot published in several articles from van Noije and co-workers [176], that displays the linear dispersion relations, i.e. the exponential growth rates of the modes as functions of the wave number.

Several facts must be noted. The first is that (in this linear analysis) the evolution of fluctuations of normal velocity components (shear modes, $\tilde{\mathbf{u}}_\perp$) are not coupled with any other fluctuating component. At the same time, all the other components are coupled together. The study of eigenvalues and eigenvectors confirms the fact that the shear modes are not coupled with the other modes. The eigenvectors of the matrix define, beyond the shear modes, three other modes: one heat mode and two sound modes, denoted in the following with the subscripts H and $+$ or $-$ respectively. The associated eigenvalues are $\zeta_\perp(k)$, $\zeta_H(k)$, $\zeta_+(k)$ and $\zeta_-(k)$. It is immediate to see that $\zeta_\perp(k) = \gamma_0(1-k^2\xi_\perp^2)$. At

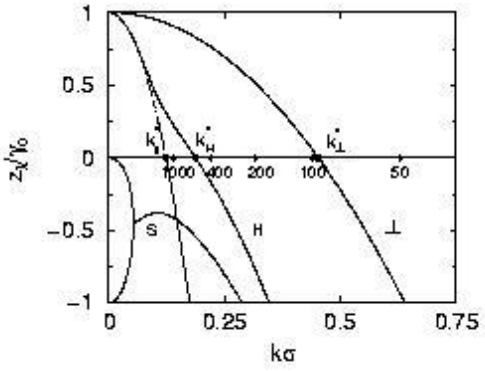

Figure 5.1: Growth rates ζ_λ/γ_0 for shear ($\lambda = \perp$), heat ($\lambda = H$) and sound ($\lambda = \pm$) modes versus $k\sigma$ for inelastic hard disks with $r = 0.9$ at a packing fraction $\phi = 0.4$. The dashed line indicate the imaginary parts of the sound modes that vanish for $k \ll \gamma_0/l_0$. (From Orza et al. [176])

low values of k (in the dissipative range defined below) also the heat mode is "pure", as it is given by the longitudinal velocity mode $\tilde{\mathbf{u}}_\parallel$ only, with eigenvalue $\zeta_H(k) \simeq \gamma_0(1 - \xi_\parallel^2 k^2)$; in this range the sound modes are combination of density and temperature fluctuations.

The most important result of this analysis is that $\zeta_\perp(k)$ and $\zeta_H(k)$ are *positive* below the threshold values $k_\perp^* = 1/\xi_\perp \sim \sqrt{\epsilon}$ and $k_H^* \simeq 1/\xi_\parallel \sim \epsilon$ respectively, indicating two linearly unstable modes with exponential (in τ) growth rates.

The shear and heat instabilities are well separated at low inelasticity, as $k_\perp^* \sim \sqrt{\epsilon}$ while $k_H^* \sim \epsilon$, so that $k_\perp^* \gg k_H^*$. It is also important to note that the linear total size L of the system can suppress the various instability, as the minimum wave number $k_{min} = 2\pi/L$ can be larger than k_H^* or even than $k_\perp^*$.

Moreover, the study of the eigenvalues of the linear stability matrix, shows that several regimes in the k-space are present:

- for $2\pi/L \ll k \ll \gamma_0/l_0$ (*dissipative range*), all the eigenvalues are real, so that propagating modes are absent;
- for $\gamma_0/l_0 \ll k \ll \sqrt{\gamma_0}/l_0$ (*standard range*), the eigenvalues corresponding to sound modes are complex conjugates, so that the sound modes propagate;
- for $\sqrt{\gamma_0}/l_0 \ll k \ll \min\{2\pi/l_0, 2\pi/\sigma\}$ (*elastic range*) the heat conduction become dominant; in this range the dispersion relations resemble those of an elastic fluid.

The above picture, of course, requires the scale separation $\gamma_0 \ll \sqrt{\gamma_0}$ (valid at low inelasticity).

5.1.3 Structure formations: vortices and clusters

When an instability arises, structures emerge. The characterization of structures is achieved by means of correlation functions or structure factors (their Fourier transforms):

$$G_{ab}(\mathbf{r}, t) = \frac{1}{V} \int d\mathbf{r}' \langle \delta a(\mathbf{r} + \mathbf{r}', t) \delta b(\mathbf{r}', t) \rangle \tag{5.15a}$$

$$S_{ab}(\mathbf{k}, t) = \frac{1}{V} \langle \delta a(\mathbf{k}, t) \delta b(-\mathbf{k}, t) \rangle = \int d\mathbf{r} e^{-i\mathbf{k}\cdot\mathbf{r}} G_{ab}(\mathbf{r}, t) \tag{5.15b}$$

where $V = L^d$ is the volume of the system.

If the quantities a and b in the above formulas are components i and j of a vector $\mathbf{a}$ (e.g. the components u_i and u_j of the velocity vector $\mathbf{u}$), then the functions G_{ij} and S_{ij} become isotropic tensor and can be decomposed in two scalar isotropic functions:

$$G_{ij}(\mathbf{r},t) = \hat{r}_i\hat{r}_j G_\parallel(r,t) + (\delta_{ij} - \hat{r}_i\hat{r}_j)G_\perp(r,t) \tag{5.16a}$$

$$S_{ij}(\mathbf{k},t) = \hat{k}_i\hat{k}_j S_\parallel(k,t) + (\delta_{ij} - \hat{k}_i\hat{k}_j)S_\perp(k,t) \tag{5.16b}$$

It is immediate to verify that, if the vector $\mathbf{a}$ is decomposed into $(d-1)$ components $a_\perp$ perpendicular to $\mathbf{k}$ and one component $a_\parallel$ parallel to $\mathbf{k}$, then

$$S_\parallel(k,t) = \frac{1}{V}\langle \delta a_\parallel(\mathbf{k},t)\delta a_\parallel(-\mathbf{k},t)\rangle \tag{5.17a}$$

$$S_\perp(k,t) = \frac{1}{V}\langle \delta a_\perp(\mathbf{k},t)\delta a_\perp(-\mathbf{k},t)\rangle \tag{5.17b}$$

or, if $\mathbf{a}$ is decomposed into $(d-1)$ components $a'_\perp$ perpendicular to $\mathbf{r}$ and one component $a'_\parallel$ parallel to $\mathbf{r}$, then

$$G_\parallel(r,t) = \frac{1}{V}\int d\mathbf{r}'\langle \delta a'_\parallel(\mathbf{r}+\mathbf{r}',t)\delta a'_\parallel(\mathbf{r}',t)\rangle \tag{5.18a}$$

$$G_\perp(r,t) = \frac{1}{V}\int d\mathbf{r}'\langle \delta a'_\perp(\mathbf{r}+\mathbf{r}',t)\delta a'_\perp(\mathbf{r}',t)\rangle \tag{5.18b}$$

$$\tag{5.18c}$$

We use in the rest of this section the subscript $\perp$ and $\parallel$ to indicate the structure factors and correlation functions relative to the velocity vector decomposed in parallel and perpendicular components, i.e. $\mathbf{a} = \mathbf{u}$.

In the isotropic tensor case (the one defined just above) it is often convenient to subtract the self-correlation equilibrium part from the correlation function and from the structure factor, i.e. defining:

$$G^+_{ij}(\mathbf{r},t) = G_{ij}(\mathbf{r},t) - A(t)\delta_{ij}\delta(\mathbf{r}) \tag{5.19a}$$

$$S^+_{ij}(\mathbf{k},t) = S_{ij}(\mathbf{k},t) - A(t)\delta_{ij} \tag{5.19b}$$

where $A(t) = (1/V)\int d\mathbf{r}'\langle (a_i(\mathbf{r}',t))^2\rangle$, e.g. if $\mathbf{a} \equiv \mathbf{u}$ then $A(t) \equiv T(t)/mn$.

The further assumption of incompressibility (which plays an important role in the following), states that $S^+_\parallel(k,t) = 0$ or, equivalently:

$$G^+_\perp(r,t) = G^+_\parallel(r,t) + \frac{r}{d-1}\frac{\partial}{\partial r}G^+_\parallel(r,t) \tag{5.20}$$

The study of correlation functions in cooling granular gases has been carried along by several authors. In particular the group of van Noije and co-workers has developed two lines of reasoning: a study of the ring kinetic theory [210] and a study of fluctuating hydrodynamics [212]. The first can be considered more fundamental, as it copes with kinetic degrees of freedom, while the second is based on the hydrodynamics description of the fluctuations, and therefore is less general.

Correlation functions from ring kinetic theory

The correlation function is directly related to the the pair correlation function $g_{12} = P_{12} - P_1P_2$ (discussed in paragraph 2.2.7), by the relation:

$$\begin{aligned} G^+_{ij}(\mathbf{r},t) &= G_{ij}(\mathbf{r},t) - T(t)\delta_{ij}\delta(\mathbf{r})/mn \\ &= \frac{1}{V}\int d\mathbf{r}'\frac{1}{n^2}\int d\mathbf{v}_1\int d\mathbf{v}_2 v_{1i}v_{2j}g_{12}(\mathbf{r}+\mathbf{r}',\mathbf{v}_1,\mathbf{r}',\mathbf{v}_2,t) \end{aligned} \tag{5.21}$$

The authors [210] have calculated, using the second of the ring kinetic equations 2.96, the structure factor for the correlation of shear mode fluctuations:

$$S_{\perp}^{+}(k,t) = \frac{T(t)}{mn} \frac{\exp[2\gamma_0 \tau(1-k^2\xi_{\perp}^2)]-1}{1-k^2\xi_{\perp}^2} \tag{5.22}$$

with $\xi_{\perp} = \sqrt{\eta/mn\omega\gamma_0}$ is the same correlation length appearing in the dispersion relations of the previous paragraph. This expression for the structure factor is identical to the energy spectrum $E(k)$ in the theory of $2D$ or $3D$ homogeneous turbulence in incompressible fluids.

The expression for the correlation functions indicates that $G_{\parallel}(r,t) \sim -(d-1)G_{\perp}(r,t) \sim 1/R^d$. The authors have performed 2D molecular dynamics simulations at low solid fraction ($\phi = 0.05$) obtaining a good verification of their results.

Correlation functions from fluctuating hydrodynamics

At the hydrodynamic level ($kl_0 \ll 1$) the correlation functions and structure factors can be obtained from the so-called fluctuating hydrodynamics [137]. This method consists in the study of coupled linear Langevin equations for the values of the hydrodynamic fields, obtained considering the linear transport of linearized hydrodynamics equation as the systematic (dissipative) part of the equations, while the noise is given by fluctuations of fluxes (momentum and heat):

$$\frac{\partial}{\partial \tau}\delta\tilde{\mathbf{a}}(\mathbf{k},\tau) = \tilde{\mathcal{M}}(\mathbf{k})\delta\tilde{\mathbf{a}}(\mathbf{k},\tau) + \tilde{\mathbf{f}}(\mathbf{k},\tau) \tag{5.23}$$

where the vector $\delta\tilde{\mathbf{a}}$ and the matrix $\tilde{\mathcal{M}}$ have been defined in the previous paragraph. The noise $\tilde{\mathbf{f}}$ is given by internal fluctuations of the fluxes. The fluxes (or currents) $\mathcal{P}$ and $\mathbf{q}$ are considered fluctuating around their average values:

$$\mathcal{P} \to \mathcal{P} + \tilde{\mathcal{P}} \tag{5.24a}$$

$$\mathbf{q} \to \mathbf{q} + \tilde{\mathbf{q}} \tag{5.24b}$$

where the fluctuating part of the currents is assumed to be a white Gaussian noise, local in space, with correlations given by appropriate fluctuation-dissipation relations (they can be found on the last chapter of [137]):

$$\langle \tilde{\mathcal{P}}_{ij}(\mathbf{r},t)\tilde{\mathcal{P}}_{kl}(\mathbf{r}',t)\rangle = 2T[\eta(\delta_{ik}\delta_{jl}+\delta_{il}\delta_{jk}) + (\eta' - \frac{2}{d}\eta)\delta_{ij}\delta_{kl}]\delta(\mathbf{r}-\mathbf{r}')\delta(t-t') \tag{5.25a}$$

$$\langle \tilde{\mathbf{q}}_i(\mathbf{r},t)\tilde{\mathbf{q}}_j(\mathbf{r}',t)\rangle = 2\kappa T^2\delta_{ij}\delta(\mathbf{r}-\mathbf{r}')\delta(t-t') \tag{5.25b}$$

(with η' the bulk viscosity, defined in paragraph 2.3.9) so that the (derived) fluctuation-dissipation relations for the noise $\tilde{\mathbf{f}}$ are given by:

$$\frac{1}{V}\langle \tilde{\mathbf{f}}_a(\mathbf{k},\tau)\tilde{\mathbf{f}}_b(-\mathbf{k},\tau')\rangle = \tilde{\mathcal{C}}_{ab}(k)\delta(\tau-\tau') \tag{5.26}$$

with

$$\tilde{\mathcal{C}} = \begin{pmatrix} 0 & 0 & 0 & 0 \\ 0 & \gamma_0 k^2\xi_{\perp}^2/n & 0 & 0 \\ 0 & 0 & \gamma_0 k^2\xi_{\parallel}^2/n & 0 \\ 0 & 0 & 0 & 4\gamma_0 k^2\xi_T^2/dn \end{pmatrix} \tag{5.27}$$

(as it can be seen, different components of noise are uncorrelated, and in the equation for the density there is no noise).

The results of the analysis is reviewed in the following table:

$$S_\perp(k,t) = \frac{T(t)}{mn}\left(1 + \frac{\exp[2\gamma_0\tau(1-k^2\xi_\perp^2)]-1}{1-k^2\xi_\perp^2}\right) \tag{5.28a}$$

$$S_\parallel(k,t) = \frac{T(t)}{mn}\left(1 + \frac{\exp[2\gamma_0\tau(1-k^2\xi_\parallel^2)]-1}{1-k^2\xi_\parallel^2}\right) \quad (kl_0 \ll \gamma_0) \tag{5.28b}$$

$$S_{nn}(k,t) = n^2 T\chi_T + \frac{nk^2l_0^2}{2\gamma_0^2}\left(\frac{\exp[2\gamma_0(1-\xi_\parallel^2k^2)\tau]-1}{1-\xi_\parallel^2k^2}\right) \quad (kl_0 \ll \gamma_0) \tag{5.28c}$$

$$\tag{5.28d}$$

The structure factor for the shear modes is identical to that derived from the ring kinetic equations (Eq. (5.22)). The factors calculated for the longitudinal velocity components and for the density fluctuations are obtained in the dissipative range ($kl_0 \ll \gamma_0$), in the absence of propagating modes (all eigenvalues of the linear stability matrix are real).

The above expressions for the structure factors yields the following important conclusions:

- The shear structure factor at the largest wavelength slowly decays as $S_\perp(k,t) \sim \exp(-2\gamma_0\xi_\perp^2k^2\tau)$ and this represents vorticity diffusion on the scale τ, with a diffusivity $\gamma_0\xi_\perp^2 = \eta/(\omega mn)$ and the typical length scales of vortices that grows like $L_v(t) \sim \sqrt{\tau}$, *independently of the degree of inelasticity*.

- The longitudinal (heat) structure factor at the largest wavelength follows a similar law, $S_\parallel(k,t) \sim \exp(-2\gamma_0\xi_\parallel^2k^2\tau)$, so that its diffusivity $\gamma_0\xi_\parallel^2$ is much larger than that of vorticity; the correlation length grows as $L_\parallel(t) \sim \xi_\parallel\sqrt{\gamma_0\tau} \sim \sqrt{\tau/\epsilon}$ (it depends on inelasticity).

- The structure factor relative to density fluctuations reveals that the density instability (clustering) is driven through a coupling to the unstable heat mode, which is, in the dissipative range, a pure longitudinal velocity mode. This coupling is rather weak, which explains why structures in the flow field appear long before density clusters appear; the initial growth of the typical cluster length scale is similar to that of the longitudinal fluctuations, i.e. $L_{cl} \sim L_\parallel \sim \sqrt{\tau/\epsilon}$.

Incompressible and compressible flows

An important assumption can be used to simplify the study of structures in cooling granular gases, that of *incompressibility*. This is a fairly realistic assumption for what concerns ordinary elastic fluids, so we can consider it applicable also to granular gases for small inelasticity.

In terms of hydrodynamics fields, it states that $\boldsymbol{\nabla}\cdot\mathbf{u} = 0$, and in terms of fluctuations modes it implies that $u_\parallel(\mathbf{k},t) \simeq 0$. The consequence of this is that $S_\parallel \equiv 0$, that the density structure factor S_{nn} does not evolve in time and that the temperature fluctuations $\delta T(\mathbf{k},t)$ simply decay as kinetic modes, staying spatially homogeneous. With this assumption is also easier to calculate the spatial correlation functions $G(\mathbf{r},t)$. It has been found that these correlation functions exhibits power law tails $G_\parallel(r,t) \sim G_\perp(r,t) \sim r^{-d}$ [212].

Moreover there is a difference between the two correlation functions: $G_\perp$ has a negative minimum in correspondence with $L_v(t)$ (this can be identified as the mean diameter of vortices), while $G_\parallel$ is always positive.

If the incompressibility assumption is relaxed (this is necessary at high inelasticity), the behavior of the correlation functions at large r changes. It happens that an exponential cut-off superimposes over the power law tail r^{-d}, at a typical distance $\xi_\parallel$. The power law behavior becomes an intermediate behavior, observable if $\xi_\parallel$ and $\xi_\perp$ are well separated. In the compressible regime [213], the correlation function of the density fluctuations shows a typical length scale $L_{cl} \sim \sqrt{\tau/\epsilon}$ which agrees with the prediction of the structure factor.

5.1.4 The asymptotic decay of energy

The initial energy decay, due to the dissipation in inelastic collisions in the homogeneous cooling regime, is very well described by the Haff law [103] $E(t) = E_{Haff}(t) \sim t^{-2} \sim \exp(-2\epsilon\tau)$. This law has largely been verified in numerical simulations. When correlations build up (in the velocity field, as well as in the density field), the energy decay changes: the shear instability (formation of vortices) discussed above slows it down because of the increased relevance of the *shear heating* term in the temperature balance. Shearing regions are heat sources that contrast the collisional cooling.

Analytical and numerical works on the energy decay in the correlated regime are very rare [96, 95, 45]. A mode-coupling analysis has been put forward by Brito and Ernst [45], for $d \geq 2$. They have studied the contribution to the energy decay due to unstable modes, obtaining that

$$E(T) = E_{Haff}(t) + E_{uu}(t) + E_{nT}(t) \tag{5.29}$$

where $E_{uu}(t)$ and E_{nT} are the contributions to the kinetic energy due to macroscopic velocity flow and to the $n - T$ fluctuations respectively. Brito and Ernst have calculated their contributions to the energy decay:

$$E_{uu} \sim \tau^{-d/2} \tag{5.30a}$$

$$E_{nT} \sim \tau^{-d/2-1} \tag{5.30b}$$

and therefore the $n - T$ term is sub-leading in respect to the $u - u$ term. As a consequence of (5.30), the decay of the kinetic energy after the homogeneous phase is predicted to be of the diffusive form $\sim \tau^{-d/2}$. The crossover (internal) time τ_{cross} is determined by the equality $E_{Haff}(\tau) = E_{uu}(\tau)$. To obtain the physical time t_{cross} is more difficult, as the relation $t(\tau)$ is not clear in the correlated phase. It must be stressed that in the homogeneous phase the main contribution to the energy decay is due to the short wavelengths, the standard-elastic range $kl_0 > \gamma_0$ (see paragraph 5.1.2), while the diffusive behavior of the non-homogeneous phase is due to the long wavelength of the dissipative range $kl_0 < \gamma_0$. The predictions of this theory have been checked in $d = 2$ [45, 175]: it seems difficult to have good tests of the prediction $\tau^{-d/2}$, MD simulations are quite demanding and rarely give a sufficient statistics. There is agreement in a window of values of the restitution coefficient r, of the volume fraction ϕ and of the time τ.

5.1.5 Burgers hypothesis, TDGL hypothesis and a note on pseudo-Maxwell molecules models

The Burgers hypothesis

In a recent paper, Ben-Naim et al. [22] have studied the cooling granular gas in $d = 1$, discovering that, after the homogeneous (Haff) phase, it asymptotically becomes independent of the value of inelasticity ϵ and maps onto the sticky gas model (that in $d = 1$ is equivalent to the cooling granular gas with $r = 0$, i.e. $\epsilon = \gamma_0/2 = 1$). For such a sticky gas the temperature decays as $t^{-2/3}$. Moreover, this gas shows instability in the density and velocity profiles: density clusters and velocity shocks form. The cooling gas in $d = 1$ become asymptotically equivalent to a sticky gas [57], for any value of ϵ, because of the formation of clusters: when the cluster size (number of particles belonging to it) has reached the critical value $N_c(\epsilon) \sim \epsilon^{-1}$, a particle colliding with the cluster is absorbed, i.e. never emerges from it. The $t^{-2/3}$ regime lasts until all the particles have fallen in one big cluster and the kinetic energy becomes constant. The authors have verified their idea with MD simulations, using a trick to avoid inelastic collapse: every time two particles collide with an absolute relative velocity lesser than δ, the collision is assumed to be elastic. They have verified that the results of MD simulations are independent of the value of δ. As the sticky gas is described by the inviscid (the kinematic viscosity $\nu = \eta/mn \to 0$) limit of the Burgers equation [199]:

$$\frac{\partial u}{\partial t} = -u\frac{\partial u}{\partial x} + \nu\frac{\partial^2 u}{\partial x^2} \tag{5.31}$$

the velocity profile can be predicted to be discontinuous, with shocks (i.e. asymmetric discontinuities shown in Fig. 5.3 on page 132) in correspondence with the clusters of the gas. The relation to the Burgers equation is useful also to establish an estimate of the tails of the asymptotic velocity distribution $P(v,t) \sim t^{1/3}\Phi(vt^{1/3})$ (independent of r), which reads $\Phi(z) \sim \exp(-|z|^3)$. The MD simulations have revealed very slight deviations from the Gaussian, and the authors have imputed the discrepancy from the expected behavior to the smallness of the constant in front of $|z|^3$. Finally, Ben-Naim et al. have conjectured that the Burgers equation describes the flow velocity $\mathbf{u}(\mathbf{r},t)$ of a cooling granular gas for arbitrary values of the inelasticity ϵ in generic d dimensions, i.e.:

$$\frac{\partial u_i}{\partial t} = -u_j \frac{\partial u_i}{\partial r_j} + \nu \frac{\partial^2 u_j}{\partial r_j^2} \tag{5.32}$$

where ν is the kinematic viscosity and the solutions are looked in the rotation-free class $\boldsymbol{\nabla} \times \mathbf{u} = 0$. This conjecture implies that the asymptotic behavior of the cooling inelastic gas is independent of ϵ (as it always falls in the universality class of the sticky gas) and that the upper critical dimension for the disappearance of the inelastic collapse is $d_c = 4$. The simplest objection to this conjecture comes from the consideration that in $d = 1$ the $r = 0$ case is equivalent to the sticky gas, while in $d > 1$ the $r = 0$ is not equivalent, as normal component of the relative velocity are in principle different from zero after a collision.

The TDGL hypothesis

In another interesting paper, Wakou et al. [219] have demonstrated that the evolution of the flow field of a granular fluid, neglecting the convective term $\mathbf{u} \cdot \boldsymbol{\nabla}\mathbf{u}$, can be cast in the form of a Time Dependent Ginzburg-Landau equation for a non-conserved order parameter

$$\frac{\partial \mathsf{S}}{\partial \tau} = (\gamma_0 + D\nabla^2)\mathsf{S} - \frac{2}{d} D \overline{|S|^2} S = -V \frac{\delta \mathcal{H}[\mathsf{S}]}{\delta \mathsf{S}^\dagger} \tag{5.33}$$

$$\mathcal{H}[\mathsf{S}] = -\frac{1}{2}\gamma_0 \overline{|\mathsf{S}|^2} + \frac{1}{2} D \overline{|\nabla \mathsf{S}|^2} + \frac{1}{2d} D \left(\overline{|\mathsf{S}|^2}\right)^2 \tag{5.34}$$

with $D = \nu/\omega$ independent of time, and the tensorial order parameter $\mathsf{S} = \boldsymbol{\nabla}\tilde{\mathbf{u}}$ (e.g. $\mathrm{tr}S = \nabla \cdot \tilde{\mathbf{u}} = 0$) $\tilde{\mathbf{u}} = \mathbf{u}/v_0(t)$ the rescaled velocity field.

It is useful to report Equation (5.33) in Fourier space:

$$\frac{\partial \mathsf{S}_{\mathbf{k}}}{\partial \tau} = \left\{ \gamma_0 - Dk^2 - \frac{2D}{dV^2} \sum_{\mathbf{q}} |\mathsf{S}_{\mathbf{q}}|^2 \right\} \mathsf{S}_{\mathbf{k}} = -V^2 \frac{\delta \mathcal{H}[\mathsf{S}]}{\delta \mathsf{S}^\dagger_{\mathbf{k}}} \tag{5.35}$$

$$\mathcal{H}[\mathsf{S}] = \frac{1}{2V^2} \sum_{\mathbf{k}} (-\gamma_0 + Dk^2)|S_{\mathbf{k}}|^2 + \frac{D}{2d} \left(\frac{1}{V^2} \sum_{\mathbf{k}} |\mathsf{S}_{\mathbf{k}}|^2 \right)^2 \tag{5.36}$$

The typical form of the Ginzburg-Landau equation of motion for a non-conserved order parameter can be recognized: $\partial_t \phi = \nabla^2 \phi - V'(\phi)$ with $V(\phi) = A(1 - B\phi^2)^2$. The Landau free energy functional $\mathcal{H}$ has a quartic term S^4 and a quadratic term S^2. It differs from the standard Landau free energy in that the quartic term contains summations over two totally independent wave numbers.

The energy functional has a *continuous* set of degenerate minima, having the shape of a Mexican hat. However the above considerations have been made neglecting the convective term of the hydrodynamics equations. When this term is added, only subsets of admissible solutions are selected out of this infinite set of minima. In two dimensions only *two* distinct minima survive: therefore the $d = 2$ cooling granular gas, during the formation of instabilities, greatly resembles the spinodal decomposition for a non-conserved order parameter (Model A universality class, in the Hohenberg-Halperin classification [110]).

The pseudo-Maxwell molecules model

Another approach to the study of cooling granular gas, as we have already discussed, is the study of the kinetic equation, assuming that some form of (Boltzmann or Boltzmann-Enskog) Molecular Chaos hypothesis holds. Some authors (Ben-Naim et al [24], Bobylev et al. [33]) have conjectured the possibility of get an insight on the kinetics of granular gas using a modification of the Boltzmann equation, i.e. using the Maxwell molecules model with inelasticity, usually referred to as the pseudo-Maxwell model. The connection between Maxwell model and granular kinetics has been conjectured by Bobylev et al. on the basis of heuristic considerations. We quote a passage from their article appeared on Journal of Statistical Physics [33]: the Equation (2.98) "is often considered as the basic kinetic equation for granular media. On the other hand, this equation is a fairly rough mathematical model of a real physical process. Even without mentioning rotational effects and deviations from spherical shape of particles, one can realize that the formula" (2.98) "is very rough outside of the Boltzmann-Grad limit. This formula certainly does not account for non-Markovian effects of repeating collisions. Moreover, the model of inelastic scattering based on empirical restitution coefficient is also a very rough approximation. Thus we have the equation" (2.98) "which is (a) a very rough approximation from physical point of view and (b) quite complicated equation from mathematical point of view. These obvious considerations lead to the idea of using a simplified version of Eq. " (2.98). It must be noted that Bobylev et al. refer to the Enskog-Boltzmann equation, i.e. to Eq. (2.98) with the Enskog corrections to the Molecular Chaos hypothesis (and with exact dependence on positions).

The simplification suggested is the following:

$$|v - v'| \simeq S\sqrt{T(\mathbf{r}, t)} \tag{5.37}$$

to be put in the Boltzmann (or Enskog-Boltzmann) equation (S is an appropriate constant). The assumption (5.37) leads to a dramatic simplification of the collisional integral $Q(P, P)$, which (in the absence of Enskog corrections) becomes:

$$\int d\mathbf{v}_2 \int_{\mathbf{V}_{12}\cdot\hat{\mathbf{n}}>0} d\hat{\mathbf{n}} \left[\frac{1}{r^2} P(\mathbf{r}_1, \mathbf{v}_1', t) P(\mathbf{r}_1, \mathbf{v}_2', t) - P(\mathbf{r}_1, \mathbf{v}_1, t) P(\mathbf{r}_1, \mathbf{v}_2, t)\right] \tag{5.38}$$

In the Boltzmann equation it appears multiplied by a factor $\sigma^2 S\sqrt{T(\mathbf{r}, t)}$. As discussed in section 2.2, this is analogous to the collisional integral of the Maxwell molecules model, as there is no dependence on the relative velocity in the scattering cross section. This model of kinetic equation is called pseudo-Maxwell model, as it concerns *inelastic* hard-core collisions.

Bobylev and co-workers have studied this model obtaining some theorems of existence and uniqueness of self-similar homogeneous asymptotic solutions and interesting relations among coefficients of Taylor expansion of the characteristic function for the asymptotic solution. They have also discussed the hydrodynamics (Euler) equations and their linear stability, finding again long wave-length instabilities. We discuss some of their result in paragraph 5.3.

It is also noticeable that the pseudo-Maxwell model with the (ideal) assumption of homogeneous density and perfectly uncorrelated colliding particles is analogous to another model, introduced some years ago by S. Ulam [208], in order to clarify the emergence of Maxwellian statistics in perfectly elastic gases. The model consists of a set of N "energies" with the following discrete evolution: at every time step a pair of energies is chosen at random and their kinetic energy is randomly re-distributed with the constraint that the sum is conserved. The asymptotic distribution of energies, independently of the starting distribution, is Maxwellian. The homogeneous pseudo-Maxwell model can be considered the inelastic counterpart of this Ulam model.

Ben-Naim and Krapivsky [24] have studied the same model considering scalar velocities (as in $d = 1$) in an infinitely connected topology (every particle can collide with every other particle, as in Ulam model), discovering that the asymptotic solution exhibits multiscaling, i.e. the moments of the solving distribution increase in time with different exponents, coming to the wrong conclusion that there is not a scaling solution $P(v, t) = \frac{1}{v_0(t)} P(\frac{v}{v_0(t)})$. We have found a correct scaling asymptotic solution for this model in $d = 1$ and verified, with numerical simulations, that it is reached by a very general class of initial distribution. This is discussed in the third section of the chapter.

5.2 Models in 1D

Hereafter we shall focus on the physics of rapid granular flows in one dimension [14, 12, 13], which in spite of its apparent simplicity shares many features with the physics of higher dimensions. We compare results of MD simulations of the Hard Rods model with those of the inelastic lattice gas model, and show that the latter reproduces many features of the real one-dimensional gas, in the homogeneous and, more remarkably, in the inhomogeneous regime.

5.2.1 The models

The Inelastic Hard Rods model

We introduce a system of hard rods (the length of the rods σ is not relevant, as already discussed in paragraph 3.1.1), confined to a ring and colliding inelastically. Two rods collide if and only if they are at contact and their relative velocity is of opposite sign with respect to the relative position, i.e. $(v_i - v_j)(r_i - r_j) < 0$.

After a binary collision the scalar velocities of the particles change according to:

$$v_i' = v_i - \frac{1+r}{2}(v_i - v_j) \tag{5.39a}$$

$$v_j' = v_j + \frac{1+r}{2}(v_i - v_j) \tag{5.39b}$$

where r is the restitution coefficient, which takes the value 1 for perfectly elastic systems and 0 for completely inelastic particles (in this case, $d = 1$, equivalent to the sticky gas model). Few years ago McNamara and Young [158], and Sela and Goldhirsch [197], simulated such a model and observed a universal algebraic decay of the kinetic energy, $E(t) \propto t^{-2}$ (Haff's Law [103]), together with an anomalous behavior for the global velocity distribution, even in the early homogeneous regime. Furthermore, strong inhomogeneities appeared as the precursor of a numerically catastrophic event, the inelastic collapse: particles perform an infinite number of collisions in finite time interval [157].

As already discussed, the renewal of interest on one-dimensional granular flows, has been generated by the recent work of Ben-Naim et al [22]. They have circumvented the inconvenience of the inelastic collapse, by means of a sort of "regularization": they assumed that when two particles collide with an absolute relative velocity lesser than an arbitrary cut-off $|v_i - v_j| < \delta$, the collision occurs elastically. This is not too different from the proposed visco-elastic model (see paragraph 2.1.5), where the restitution coefficient depends on the relative velocity of the colliding objects. Moreover, the authors have verified that the main results (e.g. the asymptotic energy decay) do not depend on the choice of the cut-off δ. Furtherly, we have checked that these (and other) results can be reproduced using the visco-elastic regularization, and they are quite independent from the details of the functional form $r(|v_i - v_j|)$. The choice of regularization, i.e. of the value of δ, of course is relevant for the length of the simulation: the system in fact behaves mostly as an elastic gas when a large part of the molecules have reached a velocity of the order of δ. This *quasi-elastic* final stage is δ-dependent.

However this regularizations allows the system to enter into a dynamical regime which was not investigated in the past (many authors, to prevent the collapse, chose smaller systems, but this prevented also the long wavelength instabilities). As discussed before, during such a regime, the kinetic energy decays as $E(t) \propto t^{-2/3}$, for any $r < 1$. A direct inspection of the hydrodynamic profiles, shows that such a regime is highly inhomogeneous, with density clusters and shocks in the velocity field. Accordingly, they suggest that inelastic systems behave asymptotically as a sticky ($r = 0$) gas [57] which is known to be described by the Burgers equation in the inviscid limit [199]. Such a behavior reflects the fact that the asymptotics is dominated by the dynamics of clusters of particles, which move through the system and coalesce, similarly to sticky objects. As already pointed out, one of the main predictions of the Burgers conjecture is the $\sim \exp(-|v/v_0(t)|^3)$ scaling distribution, which could not be verified in the work of Ben-Naim and co-workers.

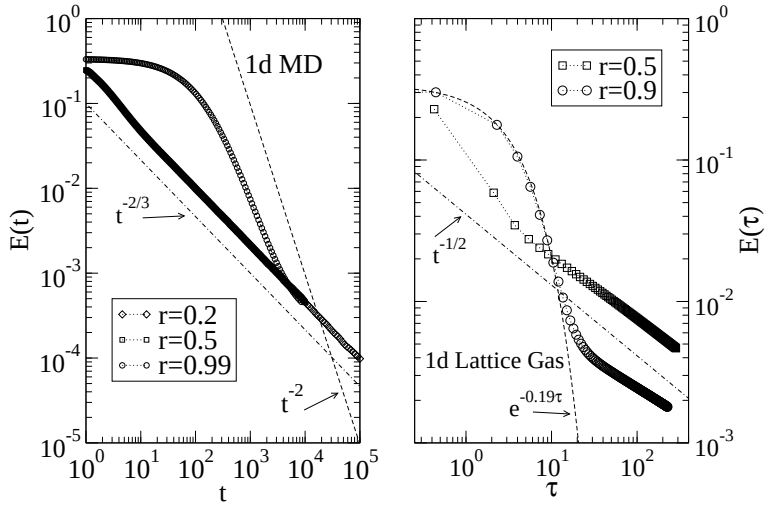

Figure 5.2: Time behavior of kinetic energy for the Inelastic Hard Rods (left) and for the Inelastic Lattice Gas (right). The homogeneous Haff stage is evident only for quasi-elastic system, whereas the more inelastic ones enter almost immediately in the correlated regime. Note the different time units used (t or τ). The Haff law $E \sim t^{-2} \sim \exp(-\tau)$ is verified for both systems. The correlated regime presents a behavior $t^{-2/3}$ independent of r for the Hard Rods, while appears diffusive (in collision units) $\tau^{-1/2}$ and r-dependent for the Lattice Gas.

The 1d Inelastic Lattice Gas model

Alternatively, one may attack the Boltzmann equation, by assuming a simpler form for the scattering cross section in the collision integral, i.e. taking the relative velocity of the colliding pair to be proportional to the average thermal velocity: $|v - v'| \sim \sqrt{E}$. This is the so called pseudo-Maxwell model [33], discussed in detail in paragraph 5.1.5.

The energy factor $\sqrt{E}$ can be eliminated via a time reparametrization, and one obtains a simpler equation:

$$\frac{\partial P(v,\tau)}{\partial \tau} + P(v,\tau) = \frac{1}{1-\gamma^*} \int du P(u,\tau) P\left(\frac{v-\gamma^* u}{1-\gamma^*}, \tau\right) \tag{5.40}$$

where $\gamma^* = (1-r)/2$ and the τ counts the number of collisions per particle. Eq. (5.40) is the master equation of the inelastic version of Ulam's scalar model: at each step an arbitrary pair is selected and the scalar velocities are transformed according to the rule of Eq. (5.39).

This model accounts for mean field behavior, i.e. disregards spatial correlation. Therefore it cannot give reliable results in the correlated phase that one expects after the end of the Homogeneous Cooling. Moreover, it does not reproduce the behavior of the Hard Rod model even in the homogeneous phase, as it is demonstrated in the next section (this in general means that the so-called "homogeneous" phase is not really homogeneous, even if it is characterized by a Haff-like decay of the energy which, in $d > 1$ is found only in a non-correlated system). To reinstate spatial correlation we considered the $d = 1$ version of the Inelastic Lattice Gas model introduced in the previous section. N sites disposed on a line with periodic boundary conditions have associated a "velocity" v_i. At every step of the evolution a pair of neighboring sites is chosen randomly and undergoes an inelastic collision according to Eq.(5.39) if $(v_i - v_j) \times (i - j) < 0$. The latter condition, which avoids collisions between particles "moving" far from each other, is to be be referred below as the *kinematic constraint* and plays a key role in the formation of structures during the inhomogeneous phase. A unit of time τ correspond to N collisions (i.e. to 1 collision per particle on average).

5.2.2 The decay of energy and the problem of the universal clock

In Fig. 5.2 on the facing page we report the time behavior of the total energy of the system

$$E = \frac{\sum v_i^2}{N} \tag{5.41}$$

We use the symbol t to indicate the physical time, while the symbol τ to indicate the time measured in number of collisions per particle. In the MD simulations the time can be measured in both units, while in the evolution of Inelastic Lattice Gas model the only measure of time is τ.

We observe that initially the energy $E(\tau)$ decreases exponentially in both the models: this corresponds to the law $E(t) \sim t^{-2}$ in the MD simulation, i.e. to the Haff regime, also called Homogeneous Cooling. In the following, we discuss how homogeneous is this first regime, studying its structure factor.

After the formation of long range velocity correlations, the decay slows down, and a power law decay appears for both the models. In the Hard Rods system the decay is of the form $E(t) \sim t^{-2/3}$, while in the Inelastic Lattice Gas the decay follows $E(\tau) \sim \tau^{-1/2}$, analogous to the decay of energy of a simple diffusion model.

Moreover, the asymptotic decay of the energy for the Hard Rod model, measured in terms of the number of collisions per particle, seems to depend on the regularization discussed above (the *elastic cut-off* δ), so that a reliable comparison between the observed behaviors is impossible.

It is interesting to note that the $E(t) \sim t^{-2/3}$ law is independent of r (as it is the law $E(\tau) \sim \tau^{-1/2}$ for the Inelastic Lattice Gas), while $E(\tau)$ changes with r. It should be explored the possibility if a sort of principle of minimum dissipation (with adequate constraints) governs the asymptotic dynamics: the system organizes itself in order to have a minimum dissipation rate independent of r, and do this changing its collision rate (which consequently depends upon r).

In general $\tau(t)$ (which makes sense only for the Hard Rod model) is a well defined "universal" function for the homogeneous regime only: in the inhomogeneous regime $\tau(t)$ diverges due to the inelastic collapse, or depends on the "regularization" of the restitution coefficient.

The problem can be circumvented in many situations, if one *assumes* the energy, instead of τ, as the physical clock of both dynamics. This allows a direct comparison of other physical measures, such as the structure factors or the velocity distributions. The surprising agreement in this comparison is a nice check of the validity of this "energy clock".

5.2.3 Velocity and density profiles

A comparison of velocity profiles at instants having the same energy in the two models is presented in Fig. 5.3 on the next page. The shocks in the velocity profile $v(x, \overline{t})$, correspond to high density clusters. The shocks are discontinuity of the velocity field, characterized by an almost continuous first derivative of the profile, which is averagely positive: this means that the particles in a shock are almost all non-colliding, as $(v_i - v_j) \times (x_i - x_j) > 0$ almost always. In this frame there are also the so-called pre-shocks, i.e. parts of the velocity profile that are going to become a shock in the near future, but are still continuous.

In the second frame, it is shown the profile $v(i, \overline{t}) \equiv v(x_i(\overline{t}))$ of the same Hard Rod model, where i is the particle label. The difference between $v(x, \overline{t})$ and $v(i, \overline{t})$ in the Hard Rod system is in the sign of large gradients: $v(x, \overline{t})$ displays large negative gradients, while $v(i, \overline{t})$ has large positive gradients. This happens because of the density profile: most of the particles are sitting near the *negative* discontinuity of the field, so that when the profile is "unrolled" as a function of the particle index, this negative discontinuity becomes a very large negative gradient, compared to the positive gradient which competes to few particles.

Finally, the bottom frame displays the $v(i, \overline{\tau})$ profile of the Inelastic Lattice Gas which fairly compares with the analogous profile for the Hard Rod system.

It is important to note that the presence of shocks in the lattice model is due to the kinematic constraint, since they disappear, together with the Porod's tails, relaxing the constraint.

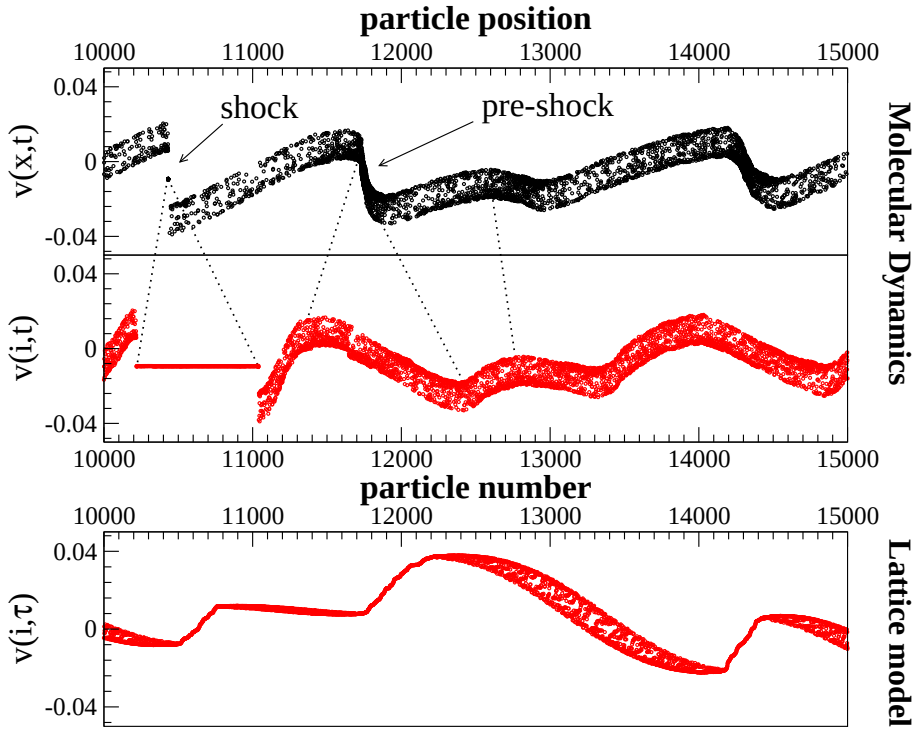

Figure 5.3: Portions of the instantaneous velocity profiles for the 1D MD (top $v(x,t)$, middle $v(i,t)$) and for the 1D lattice gas model (bottom, $v(i,\tau)$). In the middle frame we display the MD profile against the particle label in order to compare the shocks and preshocks structures with the lattice gas model (the dotted lines show how shocks and preshocks transform in the two representations for the MD). Data refers to $N = 2 \cdot 10^4$ particles, $r = 0.99$ (both models).

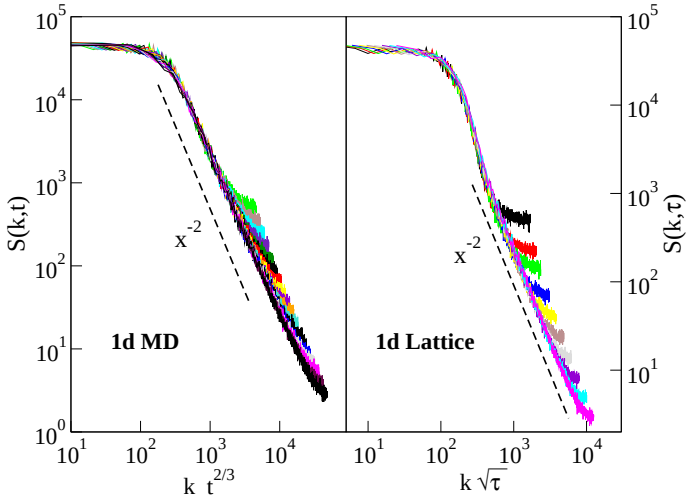

Figure 5.4: Structure factors $S(k,t)$ against $kt^{2/3}$ for the 1D MD and against $k\tau^{1/2}$ for the 1D lattice gas model, in the inhomogeneous phase. Times are chosen in the correlated regime, and in such a way that the two systems have the same energies (MD: $t = 15, ..., 316$, lattice model: $\tau = 11, ..., 601$). Data refers to system with more than $N = 10^5$ particles, $r = 0.5$ (both models).

5.2.4 Structure factors

The Gaussianity of the asymptotic field distribution, and the $\tau^{-1/2}$ asymptotic decay suggest that, in the lattice model, the scalar velocity field $v(i,\tau)$ is governed by a discretized version of the diffusion equation of the form:

$$\frac{\partial v(i,\tau)}{\partial \tau} = \nu \frac{\partial^2 v(i,\tau)}{\partial x^2} \tag{5.42}$$

This conjecture is analogous to the one made in the previous section for the $d = 2$ version of the same model.

We checked this possibility studying the structure factor $S(k,\tau) = \hat{v}(k,\tau)\hat{v}(-k,\tau)$ where $\hat{v}(k,\tau)$ is the Fourier transform of the field $v(i,\tau)$. In fact, at late times, $S(k,\tau) = f_1(k\tau^{1/2})$ scales similarly to a diffusive process as shown by the data collapse in Fig. 5.4 (right frame). However the form of the scaling function differs from the Gaussian shape predicted by the diffusion equation.

In the same figure (left) we report the *index structure factor* of the MD simulation of the Inelastic Hard Rod model, i.e. the Fourier transform of the correlation function in the index space

$$C(r,t) = \langle v(i,t)v(i+r,t)\rangle \tag{5.43}$$

where $v(i,t)$ is the velocity of the i-th particle. In this case a good data collapse, $S(k,t) = f_2(kt^{2/3})$, has been obtained.

The comparison between the two data collapses, i.e. between the two scaling forms obtained, suggests that for both models the correlation length grows as $L(t) \sim E(t)$ or $L(\tau) \sim E(\tau)$, confirming the idea that the physical clock of both system is the energy.

The algebraic tails of the structure factors observed in both models carry important information about the nature of the growing velocity correlations. In particular the power law behavior $S(k) \sim k^{-2}$ is due to the presence of short wavelength defects, viz. shocks, as predicted by Porod's law (for example see [38]).

5.2.5 Distribution of velocities

As discussed above, the conjecture that the Inelastic Hard Rod model falls, asymptotically, in the universality class of the inviscid Burgers equation (that describes the sticky gas), independently of r,

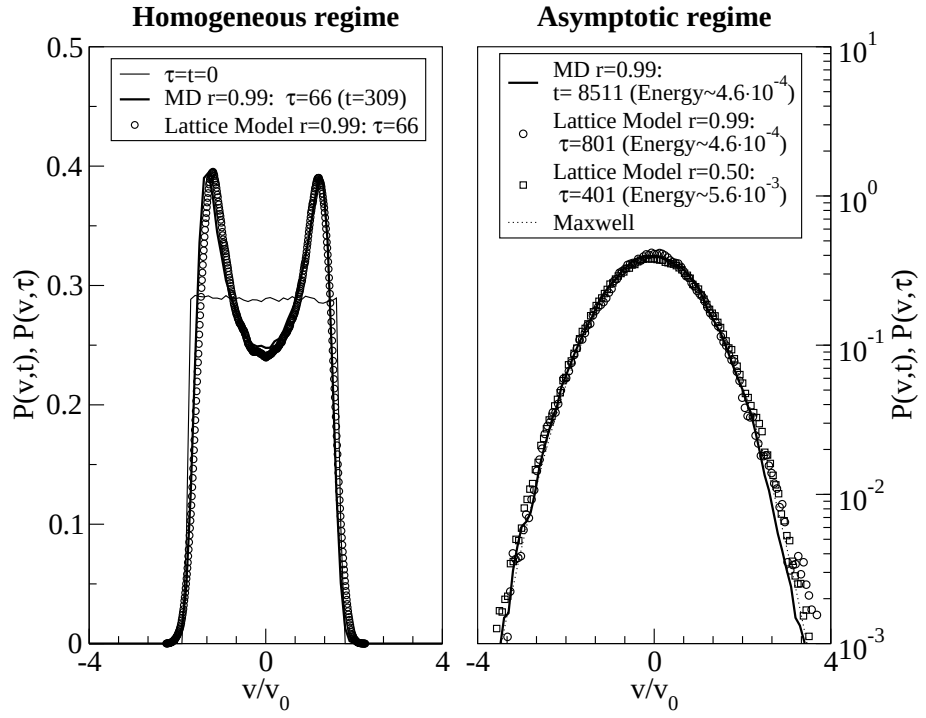

Figure 5.5: Rescaled velocity distributions for the 1D MD and in the 1D lattice gas, during the homogeneous (left) and the inhomogeneous phase (right). In the left frame is also shown the initial distribution (both models). The distributions refer to systems having the same energy. Data refer to $N = 10^6$ (both models) particles with $r = 0.99$ and $r = 0.5$ (for the lattice model in the inhomogeneous regime).

also predicts that the tails of the velocity distribution decay as $\exp(-(v/v_0(t))^3)$ [89]. On the other hand, an accurate numerical test of this prediction [22] seems problematic, whereas the bulk of the distribution does not deviate appreciably from a Gaussian. This can be seen in Fig. 5.5, right frame.

This Figure shows again (like in the discussion of the $d = 2$ Inelastic Lattice Gas) that the asymptotic velocity distribution is a Gaussian, whereas it deviates sensibly from a Gaussian in the first Haff regime.

To the best of our knowledge, exact analytic treatments of the Inelastic Hard Rod model are limited to the homogeneous regime, by means of asymptotic solutions of the Boltzmann equation. Caglioti et al. [25] have found analytic asymptotic solutions of the Boltzmann equation for a 1d inelastic hard rod gas in the limit $r \to 1^-$ and $\rho \to \infty$ (where ρ is the density), for general starting distributions. They obtained a distribution, invariant if v is rescaled with $v_0(t)$ which is the superposition of two delta functions. For MD numerical simulations, the observation of two distinct peaks in the rescaled velocity distribution was reported by Sela and Goldhirsch [197]. Our measurement agrees with this prediction, as evident in Fig. 5.5, left frame: it represents a precursor of that singular asymptotic distribution. However, the appearance of inhomogeneities and, eventually, the inelastic collapse prevent the approach to the expected limiting distribution.

5.3 The exact distribution of velocities for the 1D pseudo-Maxwell model

In this brief section we discuss the pseudo-Maxwell model, which disregards the exact kinetic kernel $|v - v'|$ in the Boltzmann equation and therefore accounts for a flat scattering cross section. We give an exact asymptotic scaling solution ("Baldassarri solution" [14, 12, 13]) of the model in $d = 1$. The problem in $d = 2$, has been discussed by Bobylev and co-workers [33]. The found solutions are compared with the granular models discussed before.

5.3.1 The pseudo-Maxwell molecules

The pseudo-Maxwell molecules model is defined through its Boltzmann-Enskog equation, and not in terms of a true particle dynamics. This equation reads:

$$\left(\frac{\partial}{\partial t} + v_i \frac{\partial}{\partial r_i}\right) P(\mathbf{r}, \mathbf{v}, t) = S(\mathbf{r}, t) \int d\mathbf{v}_2 \int_{(\mathbf{v}-\mathbf{v}_2)\cdot\hat{\mathbf{n}}>0} d\hat{\mathbf{n}} \times \left[\frac{1}{r^2} P(\mathbf{r}, \mathbf{v}', t) P(\mathbf{r}, \mathbf{v}_2', t) - P(\mathbf{r}, \mathbf{v}, t) P(\mathbf{r}, \mathbf{v}_2, t)\right] \quad (5.44)$$

The prefactor $S(\mathbf{r}, t)$ accounts for various terms, e.g. it can be taken proportional to $\Xi(\sigma, n(\mathbf{r}, t))\sqrt{T(\mathbf{r}, t)}$ if the derivation of Bobylev et al. is followed (see paragraph 5.1.5). In this case the Enskog correction $\Xi(\sigma, n)$ is the pair correlation function at distance σ and density n, which averagely takes into account correlations between the positions (scattering angle) of colliding particles.

The assumption of homogeneity changes the above equation in the following way:

$$\frac{\partial P(\mathbf{v}, t)}{\partial t} = S(t) \int d\mathbf{v}_2 \int_{(\mathbf{v}-\mathbf{v}_2)\cdot\hat{\mathbf{n}}>0} d\hat{\mathbf{n}} \times \left[\frac{1}{r^2} P(\mathbf{v}', t) P(\mathbf{v}_2', t) - P(\mathbf{v}, t) P(\mathbf{v}_2, t)\right] \quad (5.45)$$

When the velocities are scalar and the $S(t)$ dependence (e.g. the temperature) is absorbed by a time reparametrization $t \to \tau$, the equation simplifies:

$$\frac{\partial P(v, \tau)}{\partial \tau} + P(v, \tau) = \frac{1}{1 - \gamma^*} \int du P(u, \tau) P\left(\frac{v - \gamma^* u}{1 - \gamma^*}, \tau\right) \quad (5.46)$$

with $\gamma^* = (1 - r)/2$.

This equation is the master equation for the scalar Ulam model discussed at the end of the paragraph 5.1.5: at each step a pair of velocities v_i and v_j from a set of N velocities is chosen and transformed according to the usual rule of one-dimensional inelastic collisions. It should be noted that the time τ is proportional to the number of collisions per particles.

5.3.2 The "Baldassarri solution" in $d = 1$

In a stimulating paper, Ben-Naim and Krapivsky [24] considered such scalar model, and obtained the evolution of the moments of the velocity distributions. They found a multiscaling behavior, i.e.. at large times

$$\langle v^n \rangle \sim \exp(-\tau a_n) \quad (5.47)$$

and the decay rates $a_n \neq n a_2/2$ (they depend non-linearly on n). They argued that such a multiscaling behavior prevents the existence of a rescaled asymptotic distribution, i.e. that it was not possible to find a function f such that

$$P(v, \tau) \to \frac{f(v/v_0(\tau))}{v_0(\tau)} \quad (5.48)$$

for large τ, where

$$v_0^2(\tau) = \int v^2 P(v,\tau) dv = E(\tau). \tag{5.49}$$

On the contrary, we believe that such a "multiscaling" behavior only indicates the fact that the moments of the rescaled distribution

$$\int x^n f(x) dx = \langle v^n \rangle / v_0^n \tag{5.50}$$

diverge asymptotically for $n \geq 3$, and does not rule out the possibility of the existence of an asymptotic distribution with power law tails.

The Fourier transform of Eq. (5.46) reads

$$\partial_\tau \hat{P}(k,\tau) + \hat{P}(k,\tau) = \hat{P}[k/(1-\beta),\tau]\hat{P}[k/\beta,\tau] \tag{5.51}$$

It possesses several self-similar solutions of the kind

$$\hat{P}(k,\tau) = \hat{f}(k v_0(\tau)) \tag{5.52}$$

which correspond to the asymptotic rescaled distribution

$$P(v,\tau) = f(v/v_0(\tau))/v_0(\tau) \tag{5.53}$$

Many self-similar solutions do not correspond to physically acceptable velocity distributions. The divergence of the higher moments implies a non analytic structure of $\hat{f}$ in $k = 0$, since

$$\langle v^n \rangle / v_0^n = (-i)^n \frac{d^n}{dk^n} \hat{f}(k)|_{k=0} \tag{5.54}$$

and represents a guide in the selection of the physical solution.

As shown in Fig. 5.6 on the next page, our data collapse on the function

$$f(v/v_0(\tau)) = \frac{2}{\pi \left[1 + (v/v_0(\tau))^2\right]^2}. \tag{5.55}$$

corresponding to the self-similar solution [14]

$$\hat{f}(k) = (1 + |k|)\exp(-|k|) \tag{5.56}$$

Notice that (5.55) is a solution of Eq.(5.46) for every $r < 1$, i.e. this asymptotic velocity distribution does not depend on the value of $r < 1$, as shown in Fig. 5.6 on the facing page (left frame).

To conclude, we have checked numerically that the asymptotic scaling distribution in Eq. (5.55) is reached using general starting distributions. We have found that it is reached starting from a Gaussian distribution, from a uniform distribution and from an exponential distribution.

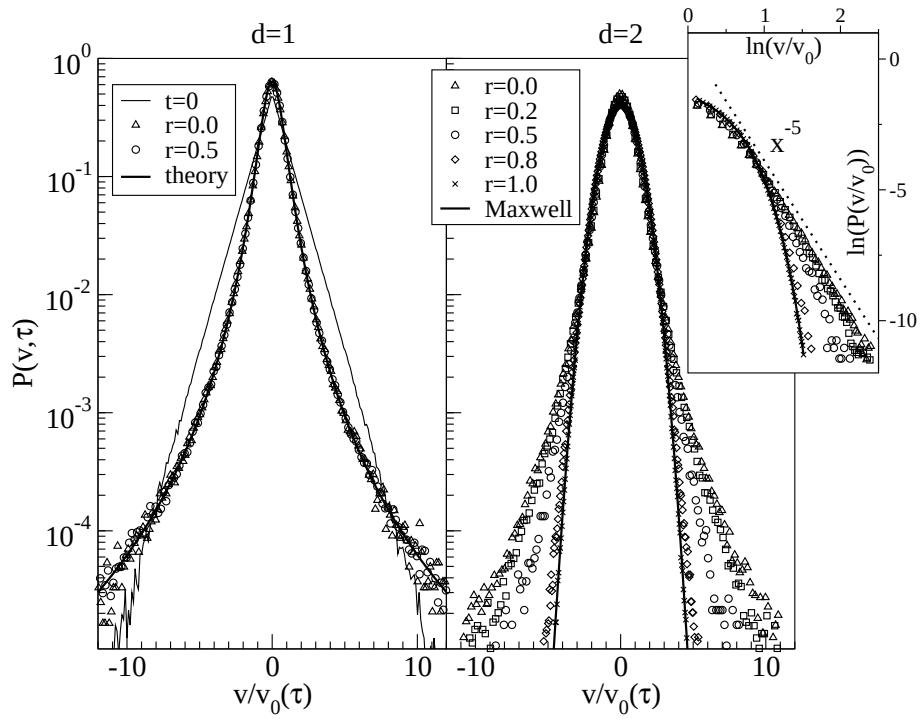

Figure 5.6: Asymptotic velocity distributions $P(v,\tau)$ versus $v/v_0(\tau)$ for different values of r from the simulation of the inelastic pseudo-Maxwell (Ulam's) model in 1D (left) and 2D (right). In 1D the asymptotic distribution is independent of r and collapse to the Eq.(5.55), that is "Baldassarri solution". The chosen initial distribution is drawn (same result with uniform and Gaussian initial distribution). In 2D the distributions still present power-law tails, but the power depends upon r, as shown in the inset: for $r = 0$ data are compatible with $\alpha = 5$, while for larger r, α increases and for $r \to 1$ tends to a Maxwell distribution. Data refers to more than $N = 10^6$ particles.

5.4 The Inelastic Lattice Gas: outcomes of 2D simulations

In this section we present a model of velocity vectors on a regular lattice [11, 14]: the vectors evolve by means of binary inelastic collisions. This model seems to reproduce the phenomenology of a granular gas in the homogeneous phase and, more remarkably, in the first correlated phase, that is when velocity correlations grow up (development of the shear instability). The further density instability (clustering) is prevented by the homogeneity of the density which is imposed in our model. Molecular dynamics simulations of inelastic hard objects are very demanding on space and time scales needed to observe the shear instability and usually are not satisfactory in terms of duration and statistics, so that information on structure factors, p.d.f. of physical quantities and energy decay are usually lacking. This lattice model is a formidable alternative to address all these problems.

5.4.1 The Inelastic Lattice Gas model

The model that we introduce is a lattice gas with constant density. It is constituted by the association of a d-dimensional velocity field $\mathbf{v}_i$ with every node of a d-dimensional lattice of linear extension L. N is the number of nodes in the lattice. The density of the "fluid" is considered constant and homogeneous throughout the whole system. In this way the dynamics of the gas consists of collisional events only. Hereafter we report the study performed in two dimensions on a triangular lattice [11, 14]. In the next chapter we will study the lattice in $d = 1$. We adopt periodic boundary conditions, so that finite size effects emerge if and only if the correlation lengths grow up to the size of the lattice, otherwise the system can be considered "without borders".

At each step of the dynamics a nearest neighbor pair of nodes (i, j) is randomly selected and the two velocities are updated according to the rule:

$$\mathbf{v}_i' = \mathbf{v}_i - \Theta(-(\mathbf{v}_i - \mathbf{v}_j)\cdot\hat{\mathbf{n}})\frac{1+r}{2}((\mathbf{v}_i - \mathbf{v}_j)\cdot\hat{\mathbf{n}})\hat{\mathbf{n}} \tag{5.57a}$$

$$\mathbf{v}_j' = \mathbf{v}_j + \Theta(-(\mathbf{v}_i - \mathbf{v}_j)\cdot\hat{\mathbf{n}})\frac{1+r}{2}((\mathbf{v}_i - \mathbf{v}_j)\cdot\hat{\mathbf{n}})\hat{\mathbf{n}} \tag{5.57b}$$

where $\hat{\mathbf{n}} = (\mathbf{r}_i - \mathbf{r}_j)/|(\mathbf{r}_i - \mathbf{r}_j)|$ represents the unit vector pointing from site $\mathbf{j}$ to $\mathbf{i}$, Θ is the Heaviside step function and $r \in [0, 1]$ is the normal restitution coefficient. We measure the time τ using the non dimensional number of collisions per particle, i.e. a time interval $\Delta\tau = 1$ represents N collisions. In each inelastic collision (Eq.(5.57)) the total linear and angular momentum are conserved, whereas a fraction $|(\mathbf{v}_i - \mathbf{v}_j)\cdot\hat{\mathbf{n}}|^2(1 - r^2)/4$ of the relative kinetic energy is dissipated. The inelasticity of the collisions has the effect of reducing the quantity $|(\mathbf{v_i} - \mathbf{v_j})\cdot\hat{\mathbf{n}}|$, inducing a partial alignment of the velocities. The presence of the Θ enforces the kinematic constraint that plays an important role in the development of structures, as shown below.

We note that when the velocity vectors are totally uncorrelated with each other, the evolution of the single-site probability $P(\mathbf{v}, t)$ should obey some kind of closed master equation similar to the Boltzmann equation. It is important to stress that in the dynamics proposed here, there is no dependence of the scattering cross section (or the collision rate) upon the relative velocity of the colliding sites. This means that the master equation should resemble the Boltzmann equation for the pseudo-Maxwell model introduced in the previous section (see paragraph 5.1.5).

Another consideration must be done, in order to make interesting connections with other fields of the physics of systems out of equilibrium. The cooling process exhibits striking similarities with the quench of a magnetic system from an initially stable disordered phase at a temperature T_0 to an ordered phase at a lower temperature T_{quench}. In a standard quench process [38] one usually considers the process by which a thermodynamic system, brought out of equilibrium by a sudden change of an external constraint, such as temperature or pressure, finds its new equilibrium state: this means that the typical processes of phase ordering (expected after the quench) happen while the external temperature is constant (often equal to zero). In the cooling of a granular fluid one wants to study the relaxation of a fluidized state after the external driving force (whose role is to reinject the energy dissipated by the collisions, keeping the system in a statistically steady state) is switched-off abruptly at some time

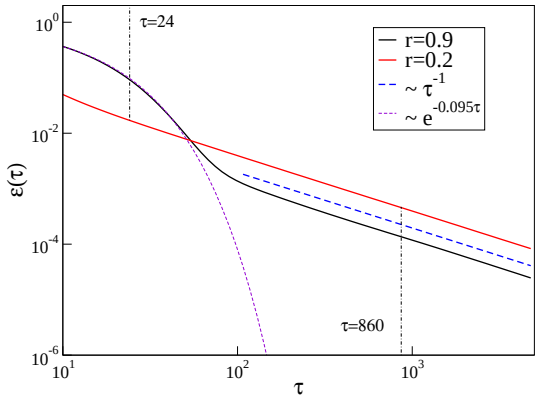

Figure 5.7: Energy decay for $r = 0.9$ and $r = 0.2$ (1024^2 sites). The bold dashed line $\sim 1/\tau$ is a guide to the eye for the asymptotic energy decay, while the light dashed line is the exponential fit corresponding to the Haff law $\exp(-2\gamma_0\tau)$. The Haff regime is too short to be observed in the system with $r = 0.2$. The two indicated times $\tau = 24$ and $\tau = 860$ correspond to the plots of Fig. 5.15 on page 148.

$\tau = 0$. Due to the competition of different configurations with comparable dissipation rates, the system does not relax immediately toward a motionless state, but displays a complex phenomenology similar to that observed in a coarsening process.

A last remark concerns the term *incompressibility*, which cannot be used rigorously in our model. In fact the continuity equation

$$\frac{\partial n}{\partial t} = \frac{\partial (n u_i)}{\partial r_i} \tag{5.58}$$

states that if the density is constant in space and time, then

$$\frac{\partial u_i}{\partial r_i} \equiv 0 \tag{5.59}$$

And this is equivalent, in Fourier space, to the equation

$$\mathbf{k} \cdot \mathbf{u} \equiv 0 \tag{5.60}$$

i.e.: there are no longitudinal velocity fluctuations, and therefore the correspondent structure factor vanishes, $S_{\parallel} \equiv 0$. This does not happen in our model, as the velocity is here only a passive mode, i.e. there is no coupling with the density (which actually does not exist). Longitudinal fluctuations can be present even if the fluid has constant density. Of course, we can consider our model as quasi-incompressible, i.e.: the longitudinal fluctuations of the velocity field are present but are much less important than the transverse fluctuations, so that the density transport can be neglected.

5.4.2 The decay of energy

One sees from Fig. 5.7 that during the initial stage, the total energy per particle

$$E(\tau) = \frac{\sum v_i(\tau)^2}{N} \tag{5.61}$$

is dissipated at an exponential rate

$$E(\tau) = E(0) \exp(-\tau/\tau_{Haff}) \tag{5.62}$$

with $\tau_{Haff}^{-1} = (1-r^2)/d$, as indicated in formulas 5.6 and 5.5b. The Haff law can be deduced from Eq.(5.57) imposing that each 'spin' fluctuates independently of the others. For times larger than τ_{cross},

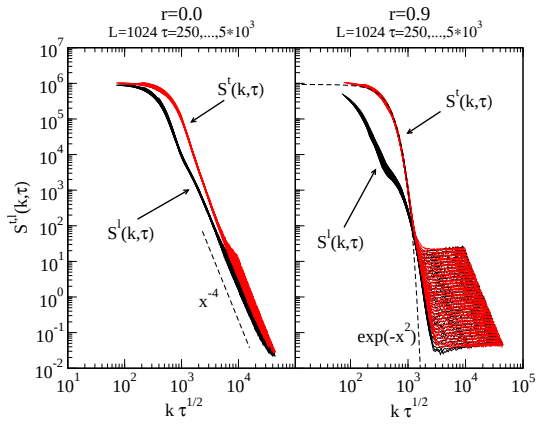

Figure 5.8: Data collapse of the transverse (S^t) and longitudinal (S^l) structure functions for $r = 0.$ and $r = 0.9$ (system size 1024^2 sites, times ranging from $\tau = 500$ to $\tau = 10^4$). The wave-number k has been multiplied by $\sqrt{\tau}$. Notice the presence of the plateaux for the more elastic system. For comparison we have drawn the laws x^{-4} and $\exp(-x^2)$.

of the order of τ_{Haff}, the system displays a crossover to a different regime, where the cooperative effects become dominant and the average energy per particle decay as $E(\tau) \sim \tau^{-1}$. Such a behavior agrees with the mode-coupling theory [45] discussed above (see paragraph 5.1.4) and with the behavior suggested by inelastic hard spheres simulations (IHSS) reported in various papers [175, 45]. As already discussed, and as shown below, the crossover from one regime to the other is due to the formation of a macroscopic velocity field, i.e. to the shear instability. This is analogous to the formation of domains in a standard quench processes of magnetic systems. After the formation stage these regions start to compete to homogenize: this causes a conversion of kinetic energy into heat by viscous heating. In the hydrodynamics description of Equation (5.8c), this is due to the third term, that is the term where the coupling between the stress tensor $\mathcal{P}_{ij}$ and the velocity gradients $\partial u_j/\partial r_i$ appear. The viscous heating acts against the collisional cooling and leads to a slower decay of the energy.

An interesting observation from Fig. 5.7 on the preceding page is that the smaller the inelasticity, the higher is the cumulated dissipated energy measured in the second (correlated) regime. This, a phenomenon observed in inelastic hard spheres simulations [158] and is due to the fact that the Haff regime (which is more rapid in dissipating energy) lasts more for less dissipative systems.

5.4.3 The structure factors and the self-correlation functions: more than diffusive behavior

The most relevant information about the spatial ordering process is contained in the equal-time structure functions, i.e. the Fourier transforms of the velocity correlation function:

$$S^{t,l}(k,\tau) = \sum_{\hat{k}} \mathbf{v}^{t,l}(\mathbf{k},\tau)\mathbf{v}^{t,l}(-\mathbf{k},\tau) \tag{5.63}$$

where the superscripts t, l indicate the transverse and longitudinal components of the field with respect to the wave vector $\mathbf{k}$ and the sum $\sum_{\hat{k}}$ is over a circular shell of radius k. Such structure factors, if rewritten in terms of the variable $(kt^{1/2})$ display fairly good data collapse, apart from the large k region.

This collapse identifies two characteristic lengths that grow with similar power laws:

$$L^t(t) \sim L^l(t) \sim \sqrt{\tau} \tag{5.64}$$

Considering the sum rule for the total kinetic energy

$$E(\tau) = \sum_k [S^t(k,\tau) + S^l(k,\tau)] \tag{5.65}$$

we observe that in the early Haff (exponential) regime the contribution from the two terms is approximately equal, whereas for times larger than τ_{cross} and r not too small, most of the kinetic energy remains stored in the transverse field, while the longitudinal component decays faster, with an apparent exponent τ^{-2}.

The diffusion scenario

The findings concerning the energy decay $E \sim \tau^{-1}$ and the growth of $L^{t,l}(t) \sim \sqrt{\tau}$, suggest that, if the observation time is longer than the time between two collisions and if the spatial scale is larger than the lattice spacing, the system behaves as if its evolution were governed by a diffusive dynamics [219]. Also the measure of velocity distributions (discussed ahead), which seem to be Gaussian in the correlated phase, encourages such a scenario.

To be more precise, we call *diffusive*, the following dynamics: let us consider a vector field $\boldsymbol{\phi}(\mathbf{r},\tau)$ which evolves according to the law

$$\frac{\partial \phi_i}{\partial \tau} = D \frac{\partial^2 \phi_i}{\partial r_j^2} \tag{5.66}$$

The explicit solution of this dynamics with a random uncorrelated initial condition shows that

- $\boldsymbol{\phi}(\mathbf{r},\tau)$ is asymptotically Gaussian distributed
- this field has a variance

$$\langle \boldsymbol{\phi}(\mathbf{r},\tau) \cdot \boldsymbol{\phi}(\mathbf{r},\tau) \rangle \propto \tau^{-d/2} \tag{5.67}$$

- the structure factors $S^{t,l}(k,\tau)$ assume a scaling form $S^{t,l}(k,\tau) = s(kL(\tau))$ where $L(\tau) = \sqrt{\tau}$.
- the two-time self-correlation of velocities

$$C_{\phi_i}(\tau_1,\tau_2) = \langle \phi_i(\mathbf{r},\tau_1)\phi_i(\mathbf{r},\tau_2) \rangle \tag{5.68}$$

assumes the following *aging* form

$$\frac{C_{\phi_i}(\tau_1,\tau_2)}{C_{\phi_i}(\tau_1,\tau_1)} = \frac{2}{(1+\frac{\tau_1}{\tau_2})} \tag{5.69}$$

In order to check our conjecture, we have compared the average self-correlation of the velocity components

$$C(\tau_1,\tau_2) = \frac{\sum_i v_i(\tau_1)v_i(\tau_2)}{N} \tag{5.70}$$

During a short time transient, the self-correlation function of our model differs from C_{ϕ_i}, since it depends on $\tau_1 - \tau_2$, i.e. it is time translational invariant (*TTI*). Later, $C(\tau_1,\tau_2)$ reaches the "aging" regime and depends only on the ratio $x = \tau_1/\tau_2$.

This *TTI* transient regime is similar to what occurs during the coarsening process of a quenched magnetic system: the self-correlation of the local magnetization $a(\tau_w, \tau_w + \tau)$ for $\tau \ll \tau_w$ shows a *TTI* decay toward a constant value $m^2_{eq}(T_{quench})$ that is the square of the equilibrium magnetization, indicating that the local magnetization is evolving in an ergodic-like fashion. Thereafter the self-correlation decays with the *aging* scaling law indicated above. Obviously, when $T_{quench} \to 0$, the *TTI* transient regime disappears. In our model the behavior of the self-correlation is even more subtle,

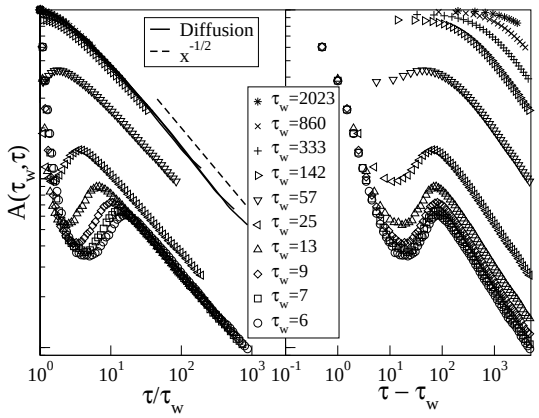

Figure 5.9: Angular auto-correlation function $A(\tau, \tau_w)$ for different values of the waiting time τ_w and $r = 0.9$ (1024^2 sites). The graph on the left shows the convergence to the τ/τ_w diffusive scaling regime, for large τ_w. For small τ_w, a local minimum is visible (for such a quasi elastic dynamics). In the graph on the right the same data are plotted vs $\tau - \tau_w$: note that the small τ_w curves tend to collapse. For higher τ_w the position of the local minimum does not move sensibly, but its value grows and goes to 1 for large τ_w

as the cooling process imposes a (slowly) decreasing "equilibrium" temperature $T_{quench} \to 0$: this progressively erodes the *TTI* regime and better resembles a finite rate quench.

The same dependence on the *TTI* manifests itself in the angular auto-correlation:

$$A(\tau, \tau_w) = \frac{1}{N} \sum_i \cos(\theta_i(\tau_w + \tau) - \theta_i(\tau_w)). \tag{5.71}$$

Again, for large waiting times τ_w this function assume the diffusive τ/τ_w scaling form, but for a (small) fixed τ_w, displays a minimum and a small peak before decreasing at larger τ (see Fig. 5.9). The non-monotonic behavior of $A(t, t_w)$ suggests that the initial direction of the velocity induces a change in the velocities of the surrounding particles, which in turn generates, through a sequence of correlated collisions, a kind of retarded field oriented as the initial velocity. As t_w increases the maximum is less and less pronounced.

Another check of the conjecture of a diffusive dynamics comes from the measure of the persistence exponent. In Fig. 5.10 on the facing page we show the decay $N_s \sim \tau^{-\theta}$ of the number N_s of sites where a velocity component never changed its sign up to time τ. The measure of the exponent $\theta = 0.18$ agrees with the theoretical prediction for the diffusive dynamics.

More than pure diffusion

In spite of these first results, that seem to give support to the idea that the model dynamics is purely diffusive, the model is more complex. The main evidence stems from the following facts:

- the Fourier modes interact and an initial single mode state, obtained assuming the initial configuration to be a plane wave, decays into shorter wavelength modes by a mechanism of period doubling; that is to say, contrary to the diffusion, plane waves are not eigenmodes (see Fig. 5.11 on page 144 and Fig. 5.12 on page 145). Interestingly, the time behavior of energy, for such peculiar initial conditions (only one mode, long wavelength, excited) is very different from the observed behavior in the case of a random initial condition: it is well fitted (apart from a quite short transient) by an exponential as expected in a diffusive system, but also like in the Haff law, but with a low exponent, i.e. with a very large characteristic time, compatible with an Haff law with an effective restitution coefficient near 1. This is the signature that this kind of mode interaction is almost elastic.

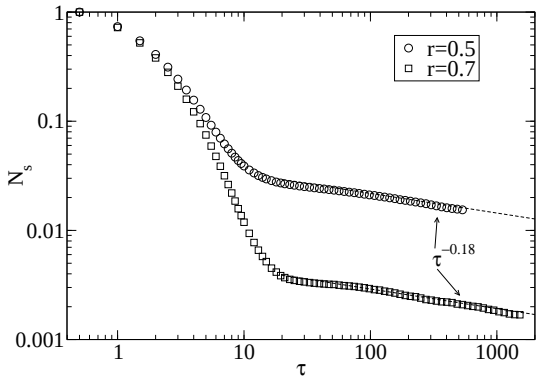

Figure 5.10: Measure of the persistence of the Inelastic Lattice Gas in $d = 2$, for two different values of the restitution coefficient. $N_s(\tau)$ counts the number of sites where the x velocity component never changed from the starting time of the dynamics up to time τ. The power-law regime corresponds to the correlated regime (see Fig. 5.7 on page 139). The measured exponent $\theta = 0.18$ is the persistence exponent predicted for the diffusive dynamics.

- the structure functions do not have the typical Gaussian tails of a diffusive system; this probably comes from the non-linearity represented by the kinematic factor in Eq.(5.57); the shapes of $S^{t,l}(k,\tau)$ display three different regions: a long-wavelength region which is diffusive in character; an intermediate region where the structure functions decay as $k^{-\beta}$ with $\beta \sim 4$; a plateau region where $S^{t,l}$ decay in time with a power law τ^{-2} but remain nearly constant with respect to k (for $r > 0$);

Let us discuss in more detail the different regions of the structure factors. They are in good agreement with the classification given in paragraph 5.1.2, with the difference that the homogeneous density enforced in our model changes the analysis of the modes (mainly for what concerns sound modes).

The diffusive region is in agreement with the *dissipative range*, where no macroscopic propagation is expected (diffusive transport is of course not macroscopic).

The existence of the quasi-elastic plateaux is the fingerprint of localized fluctuations which, for small inelasticity, propagate and are damped less than exponentially. A small r determines a rapid locking of the velocities of neighboring elements to a common value, while in the case of $r \to 1$, short range small amplitude disorder persists within the domains, breaking simple scaling of $S^{t,l}$ for large k and having the effect of a self induced noise. This range resembles the *elastic range* discussed in paragraph 5.1.2.

The existence of a $L^{-2}(\tau)k^{-4}$ region in the structure functions is consistent with Porod's law [38] and is the signature of the presence of topological defects, vortices in this $d = 2$ case, a salient feature of the cooling process. Vortices form spontaneously and represent the boundaries between regions which selected different orientations of the velocities during the quench and are an unavoidable consequence of the conservation laws which forbid the formation of a single domain (conservation of linear and angular momentum).

With the random initial conditions adopted, vortices are born at the smallest scales and subsequently grow in size by pair annihilation, conserving the total charge. In Fig. 5.13 on page 147 and Fig. 5.14 on page 147 we show a still shot of the velocity field, indicating the presence of vortices. By locating the vortex cores, we measured the vortex density $\rho_v(t)$, which represents an independent measure of the domain growth, and in fact it decays asymptotically ($\tau \gg \tau_{cross}$) as an inverse power of time, i.e.

$$L_v(\tau) = \rho_v^{-1/2} \propto \tau^{1/2} \tag{5.72}$$

This is analogous to the vortex diffusion studied in the fluctuating hydrodynamics framework by van Noije and coworkers [212].

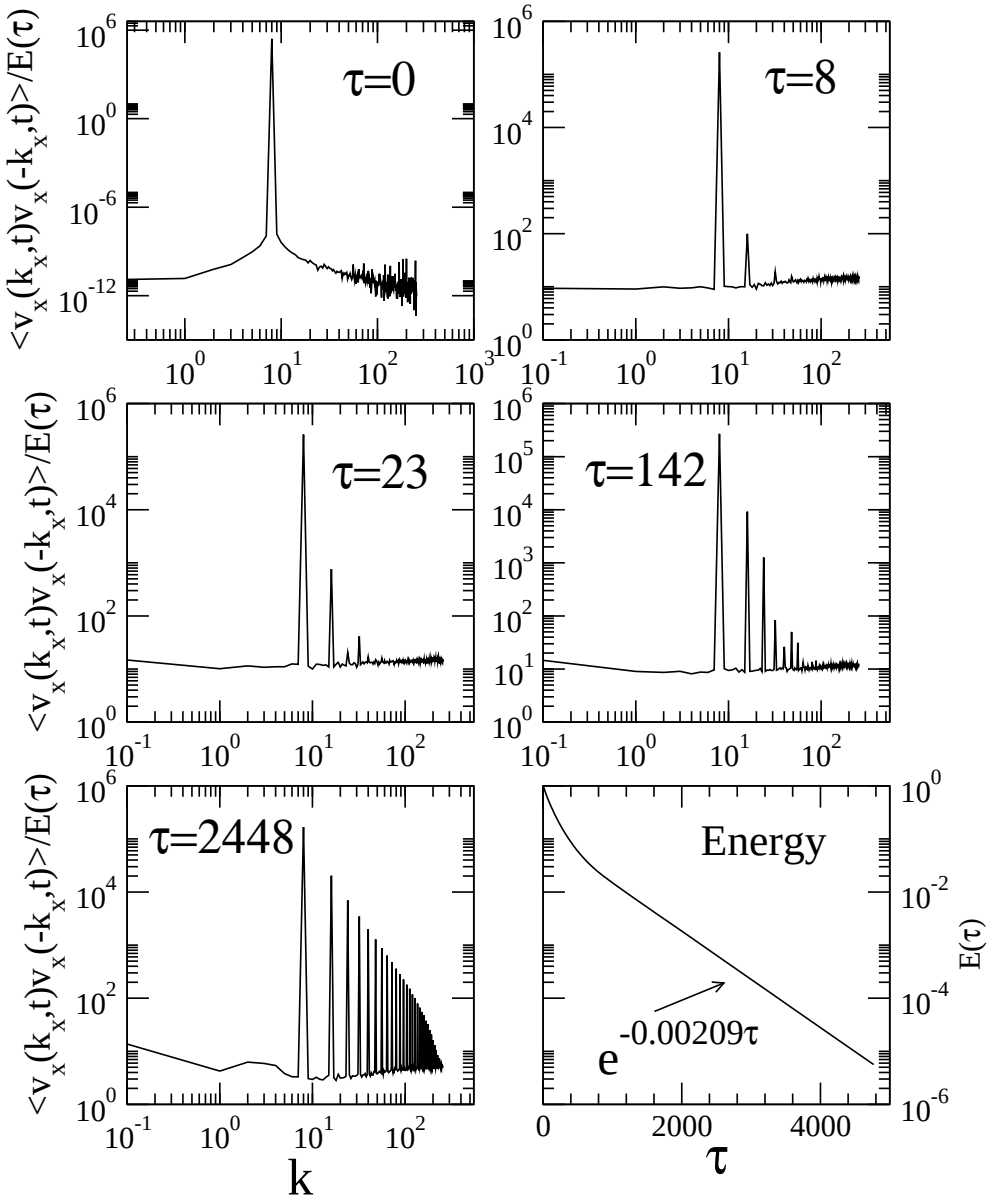

Figure 5.11: Evolution of longitudinal modes: a sequence of structure factors $\langle v_x(k_x,t)v_x(-k_x,t)\rangle$ at different times for a system of size $N = 512 \times 512$ and restitution coefficient $r = 0.5$. The initial condition for the velocity field is a plane wave $v_x(x,t) = \sin(K_0 x)$, $v_y = \sin(K_0 y)$ (i.e. all longitudinal modes), with $K_0 = 8k_0$ and $k_0 = 2\pi/L$ is the minimum vector number for this system. In the last frame there is the time behavior of the energy of the system, which is exponential. The exponent is compatible with the Haff law with an effective restitution coefficient $r = 0.998$.

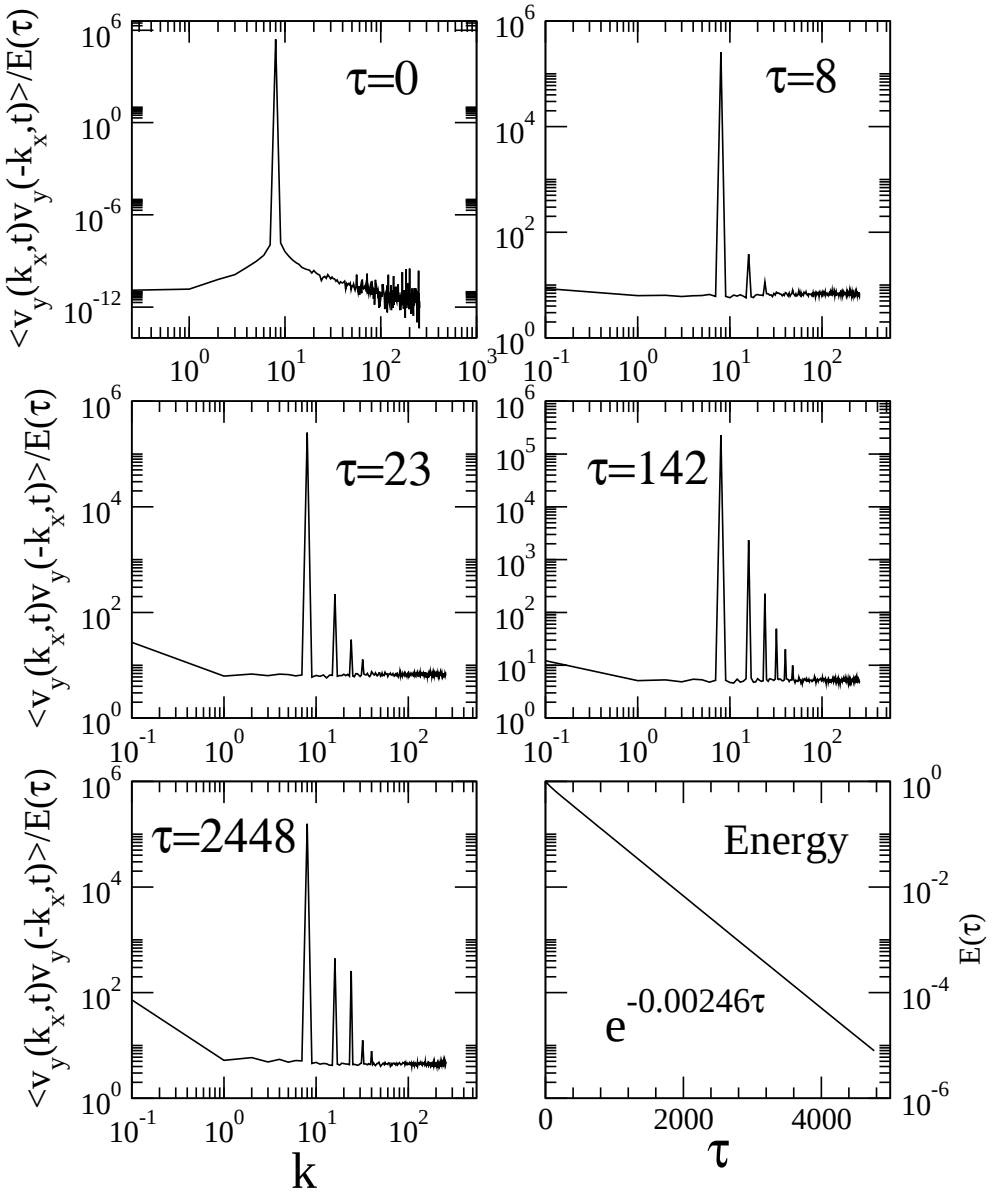

Figure 5.12: Evolution of shear modes: a sequence of rescaled structure factors $\langle v_y(k_x,t)v_y(-k_x,t)\rangle/E(\tau)$ at different times for a system of size $N = 512 \times 512$ and restitution coefficient $r = 0.5$. The initial condition for the velocity field is a plane wave $v_x(x,t) = \sin(K_0 y)$, $v_y = \sin(K_0 x)$ (i.e. all shear modes), with $K_0 = 8k_0$ and $k_0 = 2\pi/L$ is the minimum vector number for this system. In the last frame there is the time behavior of the energy of the system, which is exponential. The exponent is compatible with the Haff law with an effective restitution coefficient $r = 0.997$.

The vortex distribution turns out to be not uniform for r not too small. Its inhomogeneity is characterized by the correlation dimension d_2, defined through the definition of the cumulated correlation function:

$$H(R) = \frac{\sum_{i<j} \Theta(R - (\mathbf{r}_i - \mathbf{r}_j))}{N_v^2} \sim R^{d_2} \tag{5.73}$$

where $\mathbf{r}_i$ are the core locations. For $r \to 1$ the vortices are clusterized ($d_2 < 2$) i.e. do not fill homogeneously the space, whereas at smaller r their distribution turns to be homogeneous ($d_2 \to 2$).

5.4.4 Internal temperature and scale separation

The internal noise observed in the study of the longitudinal and transversal structure factor can be characterized by means of an average local granular temperature T_σ:

$$T_\sigma = \langle |\mathbf{v} - \langle \mathbf{v} \rangle_\sigma|^2 \rangle_\sigma \tag{5.74}$$

where $\langle ... \rangle_\sigma$ means an average on a region of linear size σ.

If we call $L(t)$ a characteristic correlation length of the system, since when $\sigma \gg L(t)$ the local average tends to the global (zero) momentum, then

$$\lim_{\sigma \to \infty} T_\sigma = E \tag{5.75}$$

For $\sigma < L(t)$, instead, $T_\sigma < E$. The behavior of T_σ in the uncorrelated (Haff) regime and in the correlated (asymptotic) regime for two different values of r is presented in Fig. 5.15 on page 148.

A very important observation is the following: for quasi elastic systems T_σ exhibits a plateau for $1 \ll \sigma \ll L(t)$ that identifies the strength of the internal noise and individuates the mesoscopic scale needed by a hydrodynamics description. The local temperature ceases to be well defined for smaller r: this clearly suggests the absence of scale separation between microscopic and macroscopic fluctuations in the strongly inelastic regime [93].

5.4.5 Distributions of velocities and velocity gradients

Within the early regime the velocity distribution deviates sensibly from a Maxwell distribution (corresponding to the same average kinetic energy), but displays fatter tails, a phenomenon which mirrors the behavior of the BK [24] model. The existence of these tails seems to be due to the lack of spatial correlations, intrinsically absent at all times in their model, whereas negligible in ours up to t_c. When the energy begins to decay as τ^{-1} the velocity distribution turns Gaussian.

Vortices are not the only topological defects of the velocity fields. In fact we observe shocks, similarly to recent experiments in rapid granular flows[186]. Shocks have a major influence on the statistics of velocity field, i.e. on the probability distributions of the velocity increments. The probability density function (p.d.f.) of the longitudinal increment

$$\Delta_l(\mathbf{R}) = \frac{1}{N} \sum_{\mathbf{i}} (\mathbf{v}_{i+R} - \mathbf{v}_i) \cdot \frac{\mathbf{R}}{R} \tag{5.76}$$

is shown in Fig. 5.17 on page 149 for $R = 1$ (longitudinal velocity gradient) in the main frame, and for $R = 40 > L(t)$ in the inset. For small $R \ll L(t)$ the longitudinal increment p.d.f. is skewed with an important positive tail, whereas for $R \gg L(t)$ it turns Gaussian. The distribution of transverse increments

$$(\mathbf{v}_{i+R} - \mathbf{v}_i) \times \hat{\mathbf{R}} \tag{5.77}$$

instead, is always symmetric, but non-Gaussian distributed for small R. A similar situation exists in fully developed turbulence [26].

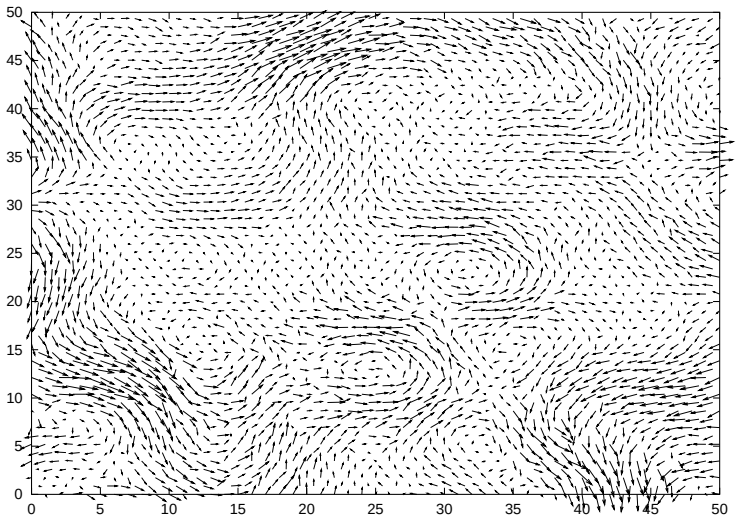

Figure 5.13: A (zoomed) snapshot of the velocity field at time $\tau = 52$ for the Inelastic Lattice Gas, $d = 2$, with $r = 0.7$ and size $N = 512 \times 512$. The time has been chosen at the beginning of the correlated regime. It is evident the presence of vortices. All the velocities have been rescaled to arbitrary units, in order to be visible.

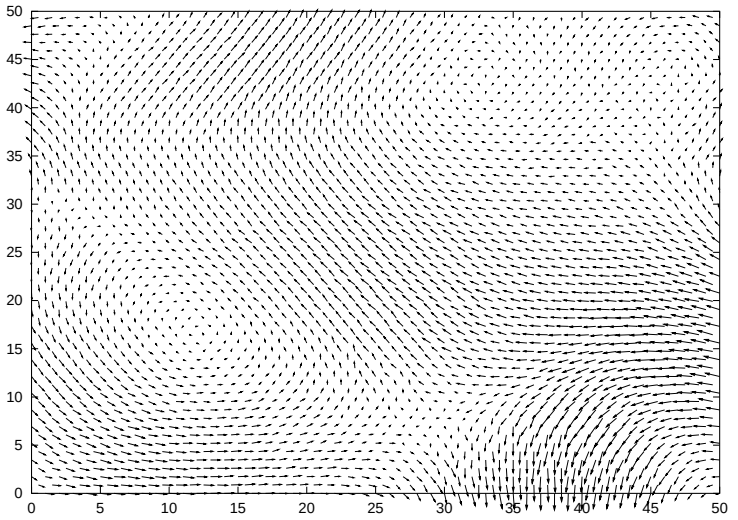

Figure 5.14: Another snapshot of the same system of Fig. 5.13 but at a later time $\tau = 535$. The diameter of the vortices has grown up. All the velocities have been rescaled to arbitrary units, in order to be visible.

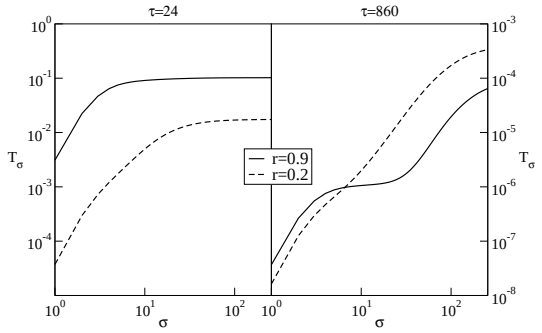

Figure 5.15: The scale dependent temperature, T_σ, defined in the text, as function of the coarse graining size σ for $\tau = 24$ (incoherent regime) and $\tau = 860$ (correlated regime for both choices of r). In the early incoherent regime the total energy per particle and T_σ remain nearly indistinguishable for a wide window of values of σ (length scales): for $\sigma < L(\tau)$ the thermal energy becomes much smaller than the kinetic energy, a clear indication of the onset of macroscopic spatial order. This becomes evident in the correlated regime. Furthermore, in the correlated regime the more elastic case presents a short wavelength plateau, indicating a well defined *mesoscopic* temperature, and therefore a clear separation between the microscopic scales (the first slope) and the macroscopic scales (the second slope).

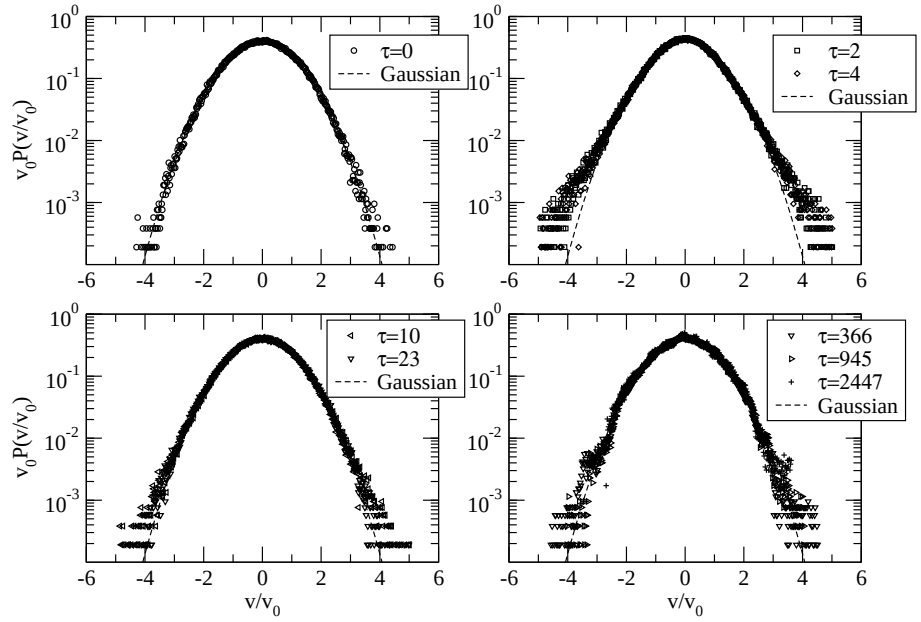

Figure 5.16: Distributions of x velocity at different times for the same system with $r = 0.2$ and $N = 512 \times 512$. The distributions are rescaled in order to have unit variance. The initial distribution is a Gaussian. The distribution becomes broader in the uncorrelated phase (first regime), and then turns back toward a Gaussian. At the late instants (when the correlation length has almost reached the finite size of the system) the distribution is still similar to a Gaussian, but presents asymmetries and peaks.

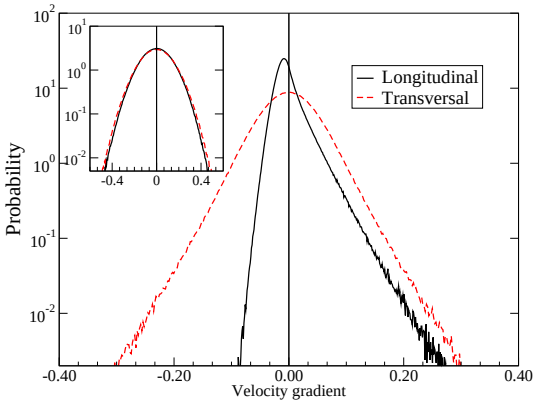

Figure 5.17: Probability densities of the longitudinal and transverse velocity increments. The main figure shows the p.d.f. of the velocity gradients ($R = 1$). The inset shows the Gaussian shape measured for $R = 40$ (larger than $L(t)$ for this simulation: $r = 0.2$, $t = 620$, system size 2048^2).

5.5 A synthesis of the cooling granular gas problem

In this section we want to offer a quick reference table on the existing results on the kinetics of cooling granular gas in $d = 1$ and $d = 2$. We review the results on energy decay, velocity distributions and spatial correlations, indicating if they have been obtained analytically or numerically and specifying the models used. In particular we have focused our attention on the usual Inelastic Hard Object Model in $d = 1$ (rods) and $d = 2$ (disks), the pseudo-Maxwell (Ulam) model and finally the Inelastic Lattice Gas models that we have introduced. We have also considered the diffusion model (Equation (5.66)) and the sticky gas model, i.e. the Burgers equation in the inviscid limit (Equation (5.32)).

The energy decay for $d = 1$

1d model	Homogeneous regime	Non-homog. regime
Hard Rods	$t^{-2} \equiv e^{-\tau}$	$t^{-2/3}$
Lattice Gas	$e^{-\tau}$	$\tau^{-1/2}$
Diffusion equation	/	$t^{-1/2}$
Sticky gas (Burgers)	/	$t^{-2/3}$

The Haff regime has been predicted analytically [103] and verified in all Hard Objects simulations. The energy decay for the correlated regime has been verified numerically by Ben-Naim et al. [22] and is consistent with the hypothesis of a sticky gas universality class. The fact that the inviscid Burgers equation and the sticky gas model are equivalent has been demonstrated [57]. The diffusion equation and the Burgers equation can of course have transient from the initial state to their correlated asymptotic regime.

The energy decay for $d = 2$

2d model	Homogeneous regime	Non-homog. regime
Hard Disks	$t^{-2} \equiv e^{-\tau}$	τ^{-1}
Lattice Gas	$e^{-\tau}$	τ^{-1}
Diffusion equation	/	t^{-1}
Sticky gas (Burgers)	/	t^{-1}

The τ^{-1} law has been predicted analytically [45], simulations of the Hard Disks model in the correlated regime are quite rare and have not verified this prediction in a satisfactory manner [45, 175].

The velocity distributions for $d = 1$

1d model	Homogeneous regime	Non-homog. regime
Hard Rods	2 peaks	Gaussian
Lattice Gas	2 peaks	Gaussian
Diffusion equation	/	Gaussian
Sticky gas (Burgers)	/	$\exp(-(v/v_0(t))^3)$
Boltzmann	2 peaks	/
Ulam	$\pi/(1+(v/v_0(t))^2)^2$	/

The velocity distribution for the Hard Rods system has been obtained numerically (in the homogeneous regime [158, 197], in the correlated regime [14, 12]). The velocity distribution for the Burgers equation has been predicted analytically [89]. The two peaks in the solution of the 1d Boltzmann equation have been predicted analytically by Caglioti et al [25], in the framework of an asymptotic solution for the quasi-elastic limit of this equation. An analytic asymptotic solution of the homogeneous pseudo-Maxwell (Ulam) scalar model has been obtained by us ("Baldassarri solution" [14, 12, 13]), and very well verified by numerical solutions with Gaussian or uniform initial conditions.

The velocity distributions for $d = 2$

2d model	Homogeneous regime	Non-homog. regime
Hard Disks	$\simeq \exp(-v/v_0(t))$	Gaussian ???
Lattice Gas	$\simeq \exp(-v/v_0(t))$?	Gaussian
Diffusion equation	/	Gaussian
Sticky gas (Burgers)	/	$\exp(-(v/v_0(t))^3)$
Boltzmann	$\simeq \exp(-v/v_0(t))$	/
Ulam	$\simeq (v/v_0(t))^{-\beta(r)}$	/

Numerical simulations of the Hard Disks model have not verified in a satisfactory manner the exponential tails of the velocity distributions (an interesting 3D experimental measurement of the

exponential tails has been obtained in [144]). These have been predicted solving the homogeneous Boltzmann equation [211]. The Gaussian asymptotic distribution is a pure conjecture, based on some evidence (e.g. Figure 9 of the article by Huthmann, Orza and Brito [114]). The asymptotic solution of the (vectorial) Ulam model has not been obtained analytically (calculation can be found in previous chapter, as well as in Bobylev et al. [33]).

The time behavior of the correlation length for $d = 1$ and $d = 2$, in the correlated stage

	1d	2d
Hard Objects	$\sim t^{-2/3}$	$\sim \tau^{-1}$?
Lattice Gas	$\sim \tau^{-1/2}$	$\sim \tau^{-1}$
Diffusion equation	$t^{-1/2}$	t^{-1}
Sticky gas (Burgers)	???	???

The growth of the correlation length for the Hard Rods has been obtained numerically [12, 14], while in 2d has been predicted analytically [214], with no reliable numerical checks.

Conclusions

In this thesis we have collected a panoramic of experiments, theories and models concerning the dynamics of granular systems. The rapid development in the study of granular gases in the last ten years has been made easier by the strong advancements in the kinetic theories of molecular systems achieved in the past decades. Many conclusions concerning correlations, breakdown of molecular chaos, the necessity of going beyond the Navier-Stokes order in hydrodynamics, finite size effects, scaling laws, boundary layers and so on, have been pointed out in the investigation of molecular systems under extreme conditions (high shear rates, high Reynolds number, etc.). Turbulence is another field of Physics where fluids show strong fluctuations, absence of scale separation and consequent scale dependent constitutive relations, and much more. The study of all these systems has put in evidence that standard tools of kinetic theory must be replaced by different kinds of analysis: often the study of stochastic processes or that of dynamical systems has led to important results. All techniques of statistical mechanics can be of relevance for granular gases: we have used Monte Carlo algorithms, as well as master equations for simple stochastic processes, probabilistic considerations, mean field models, kinetic or Fokker-Planck equations, coarsening models and diffusion equations, analysis of structure factors or persistence; even renormalization group (or mode-coupling) approaches have been used by other authors. More remarkably, the ability of reproduce essential features of a system with minimal models which can be more easily investigated (through analytical or numerical but also experimental efforts) has proven to have a key role in the approach to granular matter, as well as in the general scientific methodology.

The models that we have studied are in some case near to reality, in some other they must be considered first steps in a more general comprehension of physical mechanisms. We have probed the validity of some assumptions (Gaussian equilibrium and lack of short-range correlations) in the theory of driven granular fluids, using a model of hard objects with inelastic collisions coupled with an external heat bath. The analogy between the idealized heat bath and the more realistic driving plates or air fluidizations mechanisms should be understood better, but the agreement between the properties of the model and the experimental observation is not questioned: a real granular stationary flow presents a non-Gaussian equilibrium and short-range density correlations which can induce a lack of scale separation. We have obtained similar results using Molecular Dynamics as well as Direct Simulation Monte Carlo simulations: this means that the results are robust even if the short-range velocity correlations are ruled out by force. Measurement of large scale velocity correlations in real systems [71] have been obtained recently and could give hints on the correctness of some assumptions in the models: the randomly heated model with the external friction (as introduced by us) does not predict velocity structures, while the absence of friction induces structures but poses questions on the fluctuations of momentum and energy. Probably there is not a typical real situation and things can change from an experimental setup to another. Moreover, the inelastic hard object model with imposed Molecular Chaos (i.e. using DSMC) has proven to reproduce all the features of typical non-homogeneous steady granular flows, for example when driven by gravity: here again we have obtained a fair agreement with experiments, where non-Gaussian distributions of velocities and density correlations are found. The study of velocity correlations (which always suffer from the use of DSMC algorithm) is currently at work, in order to be compared with recent experiments. We have also checked the limits of hydrodynamic theories: there is usually, in the same setup, a region of the system that is well described by Navier-Stokes-like equations, and at the same time there are boundary layers that need different (more fundamental) approaches: ballistic flights or strong space-time gradients characterize these kinetic regions. The problem of boundary conditions is probably one of the more difficult and opened subjects of investigation in the physics of Granular Flows: it surely deserves more attention.

Cooling granular gases are apparently less connected to real situations, but in turns are more rich of intriguing phenomena and connections with other field of Physics (such as physics of systems quenched under the critical temperature, aging systems and so on). More remarkably, they are strongly connected with driven granular gases: a realistic steady flow should be understood as an alternation of cooling regions (in space-time) and driven regions, it is very rare that a granular system is subjected to a *truly continuous* and *truly homogeneous* external driving. Therefore some of the correlations expected in a cooling gas could be found also in a driven gas. As a matter of fact, the physics of cooling granular gases has still many things to understand: it happens that the homogeneous phase, early or later, ends and is substituted by a correlated regime. The positions and velocities of the grains

organize in structures that reduce dissipation. A serious conjecture that involves some kind of principle of minimum dissipation has not yet been proposed, but it seems a question that needs to be asked. Our main contribution in this field is the introduction of a lattice gas model with inelastic interactions, which in spite of its simplicity reproduces many properties of the inelastic hard objects model in its homogeneous phase as well as in its velocity correlated phase. The model is not capable of going through the density correlated phase but may be considered in good agreement with the predictions for the incompressible cooling gas. More remarkably, it shows the expected energy decay and the expected growth of structure factors by means of a microscopic dynamics, while the existing theories are based on stability analysis of hydrodynamics (i.e. they are mesoscopic approaches). We also put in evidence the appearance and disappearance of the separation between kinetic and hydrodynamic scales. This point deserves a deeper analysis: we could ask if such a scale separation is stationary and, in that case, if there is a transition in the parameter r (the restitution coefficient) from "quasi-elastic" systems that have it and "quasi-perfectly-inelastic" systems that do not have. Or otherwise, it could be that the later formation of new structures (in density), breaks this scale separation for every value of r. The study of pseudo-Maxwell models without spatial coordinates (where we have discovered an important analytical solution) perhaps can be useful for the Physics of granular gases, even if they have been given results different from MD simulations. The lattice model that we introduced, in fact, is a sort of lattice version of the pseudo-Maxwell kinetic kernel, that in the cross section disregards the relative velocity between colliding particles. The goodness of the latter in spite of the badness of the last could be explained as follows: in the lattice model the particles have the possibility of correlate, i.e. there can appear regions of neighboring particles with very similar velocities; this means that, apart from interfaces among these regions, the relative velocities of candidates for collisions are all very similar and therefore the kinetic term $|v - v'|$ of Boltzmann equation can be disregarded. In the pseudo-Maxwell model without spatial coordinates, instead, the colliding candidates can have very different velocities and the effect of disregarding their relative velocity is dramatic.

We are now considering some other issues of the physics of granular gases, a brief list of our actual studies follows:

- We are investigating the non-equilibrium stationary state of granular gases by means of linear response theory, probing the possibility of characterizing this state with an effective temperature that satisfies the Fluctuation-Dissipation theorem and that is different from the Granular Temperature. The necessity of coupling inelastic gases with a thermostat implies the impossibility of applying the *Zero Principle* of thermodynamics and therefore that of a standard definition of temperature as a thermalization parameter.

- We are looking to a better characterization of the Baldassarri solution (perhaps there exists an H-theorem for it that proves its asymptotic uniqueness), and to a possible analytical study of the same model in more than one dimensions. In this framework we are studying the connection between pseudo-Maxwell models and real granular gases.

- We are introducing polydispersity in driven and cooling models (using DSMC simulations): in this way segregation phenomena appear, as in real situations. The presence of different species of particles influences also the global properties of the gas.

- We are analyzing the velocity structure factors in the (homogeneously and non-homogeneously) driven granular gas and at the same time we are introducing a driving mechanism in the lattice gas model, in order to obtain a comparison between the systems. We are also interested in a better comprehension of the limits and possible variants of the DSMC algorithm in the context of granular gases: for example the DSMC algorithm (as it is not a molecular dynamics simulation, but a Monte Carlo algorithm of solution of the Boltzmann equation) does not take into account the fact that leaving particles cannot collide, but this seems crucial in the formation of some velocity structures (for example shocks).

Appendix A - The Direct Simulation Monte Carlo

The Direct Simulation Monte Carlo, also known as Bird algorithm, is a simulation scheme useful to solve the Boltzmann equation for gases. The Boltzmann equation is characterized by a linear partial differential operator plus the so-called collision integral (see paragraph 2.2.3):

$$Q(P,P) = \int_{\Re^3} \int_{S_+} (P'P'_* - PP_*)|\mathbf{V}\cdot\hat{\mathbf{n}}|d\mathbf{v}_* d\hat{\mathbf{n}} \tag{78}$$

It is a five-dimensional integral that makes difficult numerical approximations: if we want to approximate this integral by a quadrature formula, we need the evaluation of the integrand in N^5 points where N is the number of points necessary to well approximate a one-dimensional integral. For example, if $N = 20$, than we must evaluate the integrand in $3.2 \cdot 10^5$ points, at every time step of our integration algorithm. Particle simulation methods (like the Bird algorithm) avoid this problem by replacing the density distribution P by a discrete measure of test particles, the so-called "simulation gas". The number of test particles can be anything between 100 and several millions, depending on the capacity of the computer being used. The key idea of particle simulations stems from the consideration that the physical reality underlying the problem is a gas with, say, 10^{25} particles and that the Boltzmann equation is only a mathematical approximation to this reality: the use of this equation is a drastic reduction of the number of freedom degrees (even if it replaces a finite number of degrees with a six-dimensional infinite number of them, we can consider the Boltzmann equation the result of a *compression of information*), and therefore we can replace it with some other kind of approximation that reduces the number of freedom degrees. Therefore, in particle simulations we return to the particle level, but restrict the number of particles in order to make it tractable, and consequently change the interaction rules in order to make them reflect the influence of the collisions on the behavior of the gas.

The Bird scheme [29, 30] has been successfully employed for the simulation of rarefied gases for decades (for example in the calculations for the reentry of spacecrafts). Recently non constructive [218] and constructive [185] proofs of its convergence to the solution of the Boltzmann equation have been given.

The scheme consists of the following ingredients:

- **Time discretization**: time is discretized, i.e. $t = j \cdot \Delta t$ and the free flow operator S_t^0 (see paragraph 2.2.1) is approximated by $S_{\Delta t}^0 \sim 1 + L^0 \Delta t$ (Euler-type approximation).
- **Splitting**: the complete evolution of the gas in the time integration step Δt is divided in two sub-steps:

$$\tilde{P}(\mathbf{r},\mathbf{v},(j+1)\Delta t) = P(\mathbf{r},\mathbf{v},j\Delta t) + \Delta t Q(P,P) \tag{79a}$$

$$P(\mathbf{r},\mathbf{v},(j+1)\Delta t) = \tilde{P}(S^0_{-\Delta t}(\mathbf{r},\mathbf{v}),(j+1)\Delta t) \tag{79b}$$

  This means that the particles evolve independently for a time Δt and then the p.d.f. P is modified in order to take into account the collision, by evaluating the integral Q (this is the difficult part).

- **Local homogenization** (over space cells): the space domain is divided in non-overlapping cells C_k; the intermediate step in Eq. (79a) is performed on a p.d.f. $\bar{P}$ which is the spatial average of P on those cells, i.e.:

$$\bar{P}(\mathbf{r}, \mathbf{v}, j\Delta t) = \frac{1}{V(C_k)} \int C_k P(y, \mathbf{v}, j\Delta t) dy \tag{80}$$

and therefore also $\tilde{P}$ is homogeneous on the cells C_k of volume $V(C_k)$. The free flow step in Eq. (79b) will destroy the local homogeneity. We assume that all the cells C_k have the same diameter and call it r_B (B stays for Bird but also for Boltzmann, so that r_B is called Bird radius or Boltzmann radius indifferently). The local homogenization is important for both practical and conceptual reasons: it makes more easy (and rapid) to simulate the collisions among particles and, at the same time, fulfills the Boltzmann idea that the spatial variation of the particle density over a cell with volume $dxdydz$ could be neglected: it is the velocity dependence of the particles in such a cell that would make a difference.

.

Here follows the algorithm, step by step:

1. Evaluate the new positions at time $(j+1)\Delta t$ using the free flow operator, i.e. $x_i(j+1) = x_i(j) + v_i \Delta t$.
2. In every cell C_k (containing N_C particles and therefore $\binom{N_C}{2}$ collision pairs) do the following:
   (a) reset the "collision clock" $t_C = 0$.
   (b) Choose randomly a pair i_1, i_2 in the cell with probability $p_{i_1 i_2}$.

$$p_{i_1 i_2} = k \sigma_{i_1 i_2} \tag{81a}$$

$$\sigma_{i_1 i_2} = \int_{S^2} d\hat{\mathbf{n}} |(\mathbf{v}_{i_1} - \mathbf{v}_{i_2}) \cdot \hat{\mathbf{n}}| \tag{81b}$$

   with k a normalization constant.
   (c) Update the velocities of the particles i_1 and i_2 with the collision rule (for example the one in Eq. (2.33)), using a random choice of the collision parameter $\hat{\mathbf{n}}$.
   (d) Update the collision clock $t_C = t_C + \frac{2V(C_k)}{N_C^2 \sigma_{i_1 i_2}}$.
   (e) go to step 2b until $t_C > \Delta t$ (this guarantees an appropriate number of collisions, consistent with the collision integral)
3. repeat the step 2 for all the cells.
4. go to step 1 and advance the time $t = t + \Delta t$.

We have used a slight different scheme where the particles in the cells have a fixed *a-priori* probability p_c of colliding during a time step Δt: every particle is checked for collision, throwing a random number in the range $[0, 1)$; if the number is lesser than p_c then the particle is admitted for collision (it is particle i_1) and a collision mate i_2 is chosen in the cell with probability $p_{i_1 i_2}$. In a homogeneous situation with r_B of the order of the mean free path, this guarantees that the mean free time is about $\Delta t / p_c$.

To study more dense situations, alternative schemes have been proposed that take into account spatial density correlations in a way consistent with the Enskog correction to the Boltzmann equation [90, 165, 166].

Appendix B - Coefficients of granular hydrodynamics of 2D Inclined Plane Model

In section 4.4 the hydrodynamics of the first model is studied. The equations with the transport coefficients calculated by Brey et al. [43] are used. The coefficients needed in our case are the two thermal conductivities κ and μ appearing in the expression of the heat flux

$$\mathbf{q} = -\kappa \nabla T - \mu \nabla n \tag{82}$$

and the coefficient ζ of the dissipative term

$$-\zeta k_B T. \tag{83}$$

In reference [39] the coefficients are given for the case $d = 3$ (d is the dimension of the space). We have taken the coefficients for $d = 2$ from an unpublished (to our knowledge) work of Brey et al. They have been subsequently published it in [43] and we summarize their results here:

$$\kappa = \kappa^*(r)\kappa_0(T) \tag{84a}$$

$$\mu = \mu^*(r)\kappa_0(T)\frac{T}{n} \tag{84b}$$

$$\zeta = \zeta^*(r)\frac{nk_BT}{\eta_0(T)} \tag{84c}$$

where $\kappa_0(T)$ and $\eta_0(T)$ are the heat conductivity and viscosity coefficients respectively for elastic hard disks. In the limit $r \to 1$ the numerical coefficient κ^* tends to 1, while μ^* and ζ^* vanish. We have:

$$\kappa_0 = \frac{2k_B^{3/2}T^{1/2}}{\sigma\sqrt{m\pi}} \tag{85a}$$

$$\eta_0 = \frac{(mk_BT)^{1/2}}{2\sigma\sqrt{\pi}} \tag{85b}$$

The expression for the numerical coefficients are the following:

$$\kappa^* = \frac{1 + c^*(r)}{\nu_2^*(r) - 4\zeta^*(r)} \tag{86a}$$

$$\mu^* = \frac{2\zeta^*(r)\left(\kappa^*(r) + \frac{c^*(r)}{4\zeta^*(r)}\right)}{\nu_2^*(r) - 3\zeta^*(r)} \tag{86b}$$

$$\zeta^* = \frac{1}{2}(1 - r^2)\left(1 + \frac{3}{32}c^*(r)\right) \tag{86c}$$

$$\nu_2^*(r) = (1 + r)\left(\frac{19}{8} - \frac{15}{8}r + \frac{1}{1024}(14 - 6r)c^*(r)\right) \tag{86d}$$

$$c^*(r) = 32\frac{(1 - r)(1 - 2r^2)}{57 - 25r + 30r^2(1 - r)}. \tag{86e}$$

In section 4.4 we have used the following re-definitions of the above coefficients:

$$A(r) = \kappa^* \tag{87a}$$

$$B(r) = \mu^* \tag{87b}$$

$$C(r) = \zeta^* \pi \tag{87c}$$

Papers

- A. Puglisi, V.Loreto, U.Marini Bettolo Marconi, A.Petri, A.Vulpiani
  Clustering and Non-Gaussian Behavior in Granular Matter, Physical Review Letters, vol. 81, pag. 3848 (1998)
- A. Puglisi, V.Loreto, U.Marini Bettolo Marconi, A.Vulpiani
  A Kinetic Approach to Granular Gases, Physical Review E, vol. 59, pag. 5582 (1999)
- A. Baldassarri, U. Marini Bettolo Marconi, A. Puglisi, A. Vulpiani
  Granular gases under gravity, Physical Review E, vol 64, pag. 011601 (2001)
- A. Puglisi, V.Loreto, U.Marini Bettolo Marconi, A.Petri, A.Vulpiani
  Granular gases: where standard kinetic theory fails, INFM Highlights, vol. 1998-1999
- A. Baldassarri, U. Marini Bettolo Marconi, A. Puglisi
  Models of Freely evolving granular gases, to appear on Advances in Complex systems, Special Issue on "Frontiers in Granular Materials", A. Mehta and T. Halsey eds.
- A. Baldassarri, U. Marini Bettolo Marconi, A. Puglisi
  Cooling of a lattice granular fluid as an ordering process
  submitted to Physical Review Letters (2001), available on cond-mat/0105299
- A. Baldassarri, U. Marini Bettolo Marconi, A. Puglisi
  Influence of correlations on the velocity statistics of scalar granular gases
  submitted to Europhysics Letters (2001)
- A. Baldassarri, U. Marini Bettolo Marconi, A. Puglisi
  Maxwell granular gases in preparation
- A. Baldassarri, V. Loreto, A. Puglisi
  Fluctuation-dissipation relations in driven granular gases in preparation

Bibliography

[1] B. J. Alder. Triplet correlations in hard spheres. *Phys. Rev. Lett.*, 12(12):317–319, 1964.

[2] B. J. Alder and T. E. Wainwright. Studies in molecular dynamics. I. General method. *J. Chem. Phys.*, 31(2):459–466, 1959.

[3] B. J. Alder and T. E. Wainwright. Phase transition in elastic disks. *Phys. Rev.*, 127(2):359–361, 1962.

[4] B.-J. Alder and T. E. Wainwright. Velocity autocorrelations for hard spheres. *Phys. Rev. Lett.*, 18(23):988–990, 1967.

[5] B. J. Alder and T. E. Wainwright. Decay of the velocity autocorrelation function. *Phys. Rev. A*, 1(1):18–21, 1970.

[6] E. Azanza, F. Chevoir, and P. Moucheront. Experimental study of rapid granular flows in a two-dimensional channel. In R. P. Behringer and J. T. Jenkins, editors, *Powder & Grains 97*, page 455, Rotterdam, 1997. Proceedings of the 3rd International Conference on Powders and Grains, Durham, North Carolina, 18-23 May 1997, Balkema.

[7] E. Azanza, F. Chevoir, and P. Moucheront. Experimental study of collisional granular flows down an inclined plane. *J. Fluid Mech.*, 400:199–227, 1998.

[8] R. A. Bagnold. Experiments on a gravity-free dispersion of large solid spheres in a newtonian fluid under shear. *Proc. Royal Soc. London*, 225:49–63, 1954.

[9] P. Bak, C. Tang, and K. Wiesenfeld. Self-organized criticality: An explanation of $1/f$ noise. *Phys. Rev. Lett.*, 59(4):381–384, 1987.

[10] P. Bak, C. Tang, and K. Wiesenfeld. Self-organized criticality. *Phys. Rev. A*, 38(1):364–375, 1988.

[11] A. Baldassarri, U. M. B. Marconi, and A. Puglisi. Cooling of a lattice granular fluid as an ordering process. Submitted for publication, available on cond-mat/0105299.

[12] A. Baldassarri, U. M. B. Marconi, and A. Puglisi. Influence of correlations on the velocity statistics of scalar granular gases. Submitted for publication.

[13] A. Baldassarri, U. M. B. Marconi, and A. Puglisi. Maxwell granular gases. In preparation.

[14] A. Baldassarri, U. M. B. Marconi, and A. Puglisi. Models of freely evolving granular gases. In A. Mehta and T. Halsey, editors, *Advances in Complex systems, Special Issue on "Frontiers in Granular Materials"*.

[15] A. Baldassarri, U. M. B. Marconi, A. Puglisi, and A. Vulpiani. Granular gases under gravity. *Physical Review E*, 64:011601, 2001.

[16] A. Baldassarri, A. Puglisi, and V. Loreto. Fluctuation-dissipation relations in granular gases. In preparation.

[17] G. C. Barker and A. Metha. Transient phenomena, self-diffusion, orientational effects in vibrated powders. *Phys. Rev. E*, 47(1):184, 1993.

[18] A. Barrat, J. Kurchan, V. Loreto, and M. Sellitto. Edwards measures for powders and glasses. *Phys. Rev. Lett.*, 85:5034–5037, 2000.

[19] G. W. Baxter, R. P. Behringer, T. Fagert, and G. A. Johnson. Pattern formation in flowing sand. *Phys. Rev. Lett.*, 62(24):2825, 1989.

[20] M. Becker and W. Hauger. *Granular material - an experimental realization of a plastic Cosserat continuum*, pages 23–39. Warszawa - Poznan, Poland, 1982.

[21] M. Becker and H. Lippmann. Plane plastic flow of granular model material. experimental setup and results. *Archiv of Mechanics*, 29(6):829–846, 1977.

[22] E. Ben-Naim, S. Y. Chent, G. D. Doolent, and S. Redner. Shock-like dynamics of inelastic gases. *Phys. Rev. Lett.*, 83(20):4069–4072, 1999.

[23] E. Ben-Naim, J. B. Knight, and E. R. Nowak. Slow relaxation in granular compaction. *J. Chem. Phys.*, 100:6778, 1996.

[24] E. Ben-Naim and P. L. Krapivsky. Multiscaling in infinite dimensional collision processes. *Phys. Rev. E.*, 61:R5, 2000.

[25] D. Benedetto, E. Caglioti, and M. Pulvirenti. Kinetic equations for granular media. *Math. Mod. and Num. An.*, 31:615, 1997.

[26] R. Benzi, L. Biferale, G. Paladin, A. Vulpiani, and M. Vergassola. Multifractality in the statistics of the velocity gradients in turbulence. *Phys.Rev.Lett.*, 67:2299, 1991.

[27] P. L. Bhatnagar, E. P. Gross, and M. Krook. A model for collision processes in gases, I. *Phys. Rev.*, 94:511, 1954.

[28] K. Binder and A. P. Young. Spin glasses: experimental facts, theoretical concepts, and open questions. *Rev. Mod. Phys.*, 58:801–976, 1988.

[29] G. A. Bird. *Molecular gas dynamics*. Clarendon Press, Oxford, 1976.

[30] G. A. Bird. *Molecular Gas Dynamics and the Direct Simulation of Gas Flows*. Clarendon, Oxford, 1994.

[31] C. Bizon, M. D. Shattuck, J. B. Swift, and H. L. Swinney. Velocity correlations in driven two-dimensional granular media. In J. Karkheck, editor, *Dynamics: Models and Kinetic Methods for Nonequilibrium Many-Body Systems*, pages 361–371, Dordrecht, 2000. Kluwer Academic Publishers. cond-mat/9904135.

[32] A. V. Bobylev. Exact solutions of the nonlinear boltzmann equation and the theory of relaxation of a maxwellian gas. *Teoret. Mat. Fiz.*, 60:280–310, 1984.

[33] A. V. Bobylev, J. A. Carrillo, and I. M. Gamba. On some properties of kinetic and hydrodynamic equations for inelastic interactions. *J. Stat. Phys.*, 98:743–773, 2000.

[34] N. Bogdanova-Bontcheva and H. Lippmann. Rotationssymmetrisches ebenes Fließen eines granularen Modellmaterials. *Acta Mechanica*, 21:93–113, 1975.

[35] L. Boltzmann. Über das Wärmegleichgewicht von Gasen, auf welche äussere Kräfte wirken. *Sitzungsberichte der Akademie der Wissenschaften Wien*, 72:427–457, 1875.

[36] J.-P. Bouchaud, M. E. Cates, and P. Claudin. Stress distribution in granular media and nonlinear wave equation. *J. Phys. I*, 5:639–656, 1995.

[37] A. Brahic. Dynamical evolution of viscous discs. astrophysical applications to the formation of planetary systems and to the confinement of planetary rings and arcs. In T. Pöschel and S. Luding, editors, *Granular Gases*, volume 564 of *Lectures Notes in Physics*, Berlin Heidelberg, 2001. Springer-Verlag.

[38] A. Bray. Theory of phase-ordering kinetics. *Adv. Phys.*, 43:357–459, 1994.

[39] J. J. Brey, J. W. Dufty, C. S. Kim, and A. Santos. Hydrodynamics for granular flow at low density. *Phys. Rev. E*, 58(4):4638, 1998.

[40] J. J. Brey, J. W. Dufty, and A. Santos. Dissipative dynamics for hard spheres. *J. of Stat. Phys.*, 87(5/6):1051–1067, 1997.

[41] J. J. Brey, F. Moreno, and J. W. Dufty. Model kinetic equation for low-density granular flow. *Phys. Rev. E*, 54:445, 1996.

[42] J. J. Brey, M. J. Ruiz-Montero, and D. Cubero. Homogeneous cooling state of a low-density granular flow. *Phys. Rev. E*, 54:3664–3671, 1996.

[43] J. J. Brey, M. J. Ruiz-Montero, and F. Moreno. Hydrodynamics of an open vibrated granular system.

[44] N. V. Brilliantov, F. Spahn, J. M. Hertzsch, and T. Pöschel. Model for collisions in granular gases. *Phys. Rev. E*, 53(5):5382, 1996.

[45] R. Brito and M. H. Ernst. Extension of Haff's cooling law in granular flows. *Europhys. Lett.*, 43(15):497–502, 1998.

[46] R. Brockbank, J. M. Huntley, and R. Ball. Contact force distribution beneath a three-dimensional granular pile. *J. Phys. II France*, 7:1521–1532, 1997.

[47] R. L. Brown and P. G. W. Hawksley. The fundamental principles of segregation. *The Institute of Fuel*, 27:159, 1947.

[48] R. L. Brown and J. C. Richards. *Principles of Powder Mechanics*. Pergamon Press, Oxford, 1970.

[49] E. Caglioti and V. Loreto. Entropy for relaxation dynamics in granular media. *Phys. Rev. Lett.*, 83(21):4333–4336, 1999.

[50] E. Caglioti, V. Loreto, H. J. Herrmann, and M. Nicodemi. A "Tetris-like" model for the compaction of dry granular media. *Phys. Rev. Lett.*, 79(8):1575–1578, 1997.

[51] C. S. Campbell. The stress tensor for simple shear flows of a granular material. *J. Fluid Mech.*, 203:449–473, 1989.

[52] C. S. Campbell. Rapid granular flows. *Annu. Rev. Fluid Mech.*, 22:57, 1990.

[53] C. S. Campbell and C. E. Brennen. Computer simulation of granular shear flows. *J. Fluid. Mech.*, 151:167, 1985.

[54] C. S. Campbell and A. Gong. The stress tensor in a two-dimensional granular shear flow. *J. Fluid Mech.*, 164:107, 1986.

[55] H. Caram and D. C. Hong. Random-walk approach to granular flows. *Phys. Rev. Lett.*, 67(7):828, 1991.

[56] W. F. Carnahan and K. E. Starling. Equation of state for nonattracting rigid spheres. *J. Chem. Phys.*, 51:635, 1969.

[57] G. F. Carnevale, Y. Pomeau, and W. R. Young. Statistics of ballistic agglomeration. *Phys. Rev. Lett.*, 64(24):2913, 1990.

[58] C. Cercignani. On the Boltzmann equation for rigid spheres. *Theory Stat. Phys.*, 2:211–225, 1972.

[59] C. Cercignani. *Mathematical Methods in Kinetic Theory*. Plenum Press, New York, 1990.

[60] C. Cercignani. *The Boltzmann equation and its appplications*. Springer-Verlag, Berlin, 1994.

[61] C. Cercignani, R. Illner, and P. Pulvirenti. *The Mathematical Theory of Dilute Gases*. Springer-Verlag, New York, 1994.

[62] S. Chapman and T. G. Cowling. *The mathematical theory of nonuniform gases*. Cambridge University Press, London, 1960.

[63] S. Chen, Y. Deng, X. Nie, and Y. Tu. Clustering kinetics in granular media in three dimensions. *Phys. Lett. A*, 269:278, 2000.

[64] G. F. Chiarotti, F. Fermi, M. P. Tosi, and S. F. Edwards. Topics in statistical mechanics of disordered systems. volume 106 of *Proc. Int. Sched. Phys. "Enrico Fermi" Course, "Current Trends in the Physics"*, page 837, 1990.

[65] R. Clausius. Über die mittlere Länge der Wege, welche bei der Molecularbewegung gasförmigen Körper von den einzelnen Molecülen zurückgelegt werden, nebst einigen anderen Bemerkungen über die mechanischen Wärmetheorie. *Ann. Phys.*, 105:239, 1858.

[66] S. N. Coppersmith, C. Liu, S. Majumdar, O. Narayan, and T. A. Witten. Model for force fluctuations in bead packs. *Phys. Rev. E*, 53(5):4673–4685, 1996.

[67] S. J. Cornell, M. R. Swift, and A. J. Bray. Inelastic collapse of a randomly forced particle. cond-mat/9804229, 1998.

[68] C. A. Coulomb. *Acad. R. Sci. Mem. Math. Phys. par Divers Savants*, 7:343, 1773.

[69] M. Coulomb. Theorie des Machines Simples. *Academie des Sciences*, 10:166, 1781.

[70] K. Craig, R. Buckholz, and G. Domoto. An experimental study of the rapid flow of dry cohesionless metal powders. *J. Appl. Mech.*, 53:935, 1986.

[71] A. K. Daniel L. Blair. Velocity correlations in dense granular gases. cond-mat/0101015, 2001.

[72] P. G. de Gennes. Introduction a la physique des poudres, Course au Collège de France. 1995.

[73] P. Deltour and J.-L. Barrat. Quantitative study of a freely cooling granular medium. *J. Phys. I France*, 7:137–151, 1997.

[74] J. R. Dorfman and E. G. D. Cohen. Velocity correlation functions in two and three dimension. *Phys. Rev. Let.*, 25:1257–1260, 1970.

[75] J. R. Dorfman and H. van Beijeren. *The kinetic theory of Gases*. Plenum Press, New York, 1977.

[76] T. G. Drake. Structural features in granular flows. *J. of Geophysical Research*, 95(B6):8681–8696, 1990.

[77] Y. Du, H. Li, and L. P. Kadanoff. Breakdown of hydrodynamics in a one-dimensional system of inelastic particles. *Phys. Rev. Lett.*, 74(8):1268–1271, 1995.

[78] S. F. Edwards and P. W. Anderson. Theory of spin glasses. *J. Phys. F: Metal Phys.*, 5:965–974, 1975.

[79] E. E. Ehrichs, H. M. Jaeger, G. S. Karczmar, J. B. Knight, V. Kuperman, and S. R. Nagel. Granular convection observed by magnetic resonance imaging. *Science*, 267:1632–1634, 1995.

[80] D. Enskog. *Theorie der Vorgänge in massing verdumten Gasen*. PhD thesis, University of Uppsala,Sweden, 1917.

[81] M. H. Ernst. Nonlinear model-Boltzmann equations and exact solutions. *Phys. Rep.*, 78:1–171, 1981.

[82] M. H. Ernst and J. R. Dorfman. *Physica*, 61:157, 1972.

[83] M. H. Ernst, J. R. Dorfman, W. R. Hoegy, and J. M. J. van Leeuwen. Hard-sphere dynamics and binary-collision operators. *Physica*, 45:127, 1969.

[84] E. Falcon, S. Fauve, and C. Laroche. Cluster formation, pressure and density measurements in a granular medium fluidized by vibrations. *European Physical Journal B*, 9:183–186, 1999.

[85] E. Falcon, S. Fauve, and C. Laroche. An experimental study of a granular gas fluidized by vibrations. In T. Pöschel and S. Luding, editors, *Granular Gases*, volume 564 of *Lectures Notes in Physics*, Berlin Heidelberg, 2001. Springer-Verlag.

[86] É. Falcon, R. Wunenburger, P. Evesque, S. Fauve, C. Chabot, Y. Garrabos, and D. Beysens. Cluster formation in a granular medium fluidized by vibrations in low gravity. *Phys. Rev. Lett.*, 83:440–443, 1999.

[87] L. T. Fan, Y.-M. Chen, and F. S. Lai. Recent developments in solids mixing. *Powder Technol.*, 61:255, 1990.

[88] M. Faraday. On a peculiar class of acoustical figures; and on certain forms assumed by groups of particles upon vibrating elastic surfaces. *Philos. Trans. R. Soc. London*, 52:299, 1831.

[89] L. Frachebourg and P. A. Martin. Exact statistical properties of the burgers equation. *J. Fluid Mech.*, 417:323, 2000.

[90] A. Frezzotti. A particle scheme for the numerical solution of the Enskog equation. *Phys. Fluids*, 9:1329–1335, 1997.

[91] V. Garzó and J. W. Dufty. Dense fluid transport for inelastic hard spheres. *Phys. Rev. E*, 59(5):5895–5911, 1999.

[92] I. Goldhirsch. Kinetics and dynamics of rapid granular flows. In H. J. Herrmann, J.-P. Hovi, and S. Luding, editors, *Physics of dry granular media - NATO ASI Series*, page 371, Dordrecht, 1998. Kluwer Academic Publishers.

[93] I. Goldhirsch. Scales and kinetics of granular flows. *Chaos*, 9:659–672, 1999.

[94] I. Goldhirsch and M.-L. Tan. The single-particle distribution function for rapid granular shear flows of smooth inelastic disks. *Phys. Fluids*, 8(7):1752–1763, 1996.

[95] I. Goldhirsch, M.-L. Tan, and G. Zanetti. A molecular dynamical study of granular fluids I: The unforced granular gas in two dimensions. *Journal of Scientific Computing*, 8:1–40, 1993.

[96] I. Goldhirsch and G. Zanetti. Clustering instability in dissipative gases. *Phys. Rev. Lett.*, 70(11):1619–1622, 1993.

[97] A. Goldshtein and M. Shapiro. Mechanics of collisional motion of granular materials. Part 1. General hydrodynamic equations. *J. Fluid Mech.*, 282:75–114, 1995.

[98] T. I. Gombosi. *Gaskinetic theory*. Cambridge University Press, Cambridge, 1994.

[99] H. Grad. On the kinetic theory of rarefied gases. *Comm. Pure Appl. Math.*, 2:331, 1949.

[100] P. Grassberger and I. Procaccia. Characterization of strange attractors. *Phys. Rev. Lett*, 50:346, 1983.

[101] G. Grinstein. In A. McKane, editor, *Scale Invariance, Interfaces and Non-Equilibrium Dynamics*, volume 344 of *NATO Advanced Study Institute, Series B: Physics*, New York, 1995. Plenum.

[102] E. L. Grossman, T. Zhou, and E. Ben-Naim. Towards granular hydrodynamics in two-dimensions. *Phys. Rev. E*, 55:4200, 1997.

[103] P. K. Haff. Grain flow as a fluid-mechanical phenomenon. *J. Fluid Mech.*, 134:401–430, 1983.

[104] Hagen. Über den Druck und die Bewegung des trockenen Sandes. *Monatsberichte der königlich, preußischen Akademie der Wissenschaften zu Berlin*, page 35, 19. Jan. 1852.

[105] D. M. Hanes and D. L. Inman. Observations of rapidly flowing granular-fluid materials. *J. Fluid Mech.*, 150:357, 1985.

[106] J. Hemmingsson. A sandpile model with dip. *Physica A*, 230:329–335, 1995.

[107] H. J. Herrmann. Simulation of granular media. *Physica A*, 191:263, 1992.

[108] J.-M. Hertzsch, F. Spahn, and N. V. Brilliantov. On low-velocity collisions of viscoelastic particles. *J. Phys. II*, 5:1725–1738, 1995.

[109] J. O. Hirschfelder, C. F. Curtiss, and R. B. Bird. *Molecular Theory of Gases and Liquids*. John Wiley and Sons, New York, 1954.

[110] P. C. Hohenberg and B. I. Halperin. Theory of dynamic critical phenomena. *Rev.Mod.Phys*, 49(3):435, 1977.

[111] D. C. Hong, S. Yue, J. K. Rudra, M. Y. Choi, and Y. W. Kim. Granular relaxation under tapping and the traffic problem. *Phys. Rev. E*, 50:4123–4135, 1994.

[112] M. A. Hopkins and M. Y. Louge. Inelastic microstructure in rapid granular flows of smooth disks. *Phys. Fluids A*, 3(1):47, 1991.

[113] D. Howell and R. P. Behringer. Fluctuations in a 2d granular Couette experiment: A critical transition. *Phys. Rev. Lett.*, 82:5241, 1999.

[114] M. Huthmann, J. A. G. Orza, and R. Brito. Dynamics of deviations from the gaussian state in a freely cooling homogeneous system of smooth inelastic particles. pages 189–199, 2000.

[115] M. Huthmann and A. Zippelius. Dynamics of inelastically colliding rough spheres: Relaxation of translational and rotational energy. *Phys. Rev. E*, 56(6):R6275–6278, 1997.

[116] M. Isobe and H. Nakanishi. Phase changes in inelastic hard disk systems with a heat bath under the weak gravity for granular fluidization. *J. Phys. Soc. Jap.*, 68:2882, 1999.

[117] H. M. Jaeger, J. B. Knight, C. Liu, and S. R. Nagel. What is shaking in the sandbox? *MRS Bulletin May 1994*, XX(5):25–31, 1994.

[118] H. A. Janssen. Versuche über Getreidedruck in Silozellen. *Zeitschr. d. Vereines deutscher Ingenieure*, 39(35):1045–1049, 1895.

[119] J. T. Jenkins. Grad's 13-moment system for a dense gas of inelastic spheres. *Arch. Rat'l. Mech. Anal.*, 87:355, 1985.

[120] J. T. Jenkins and M. W. Richman. Kinetic theory for plane flows of a dense gas of identical, rough, inelastic, circular disks. *Phys. of Fluids*, 28:3485–3494, 1985.

[121] J. T. Jenkins and S. B. Savage. A theory for the rapid flow of identical, smooth, nearly elastic, spherical particles. *J. Fluid Mech.*, 130:187–202, 1983.

[122] L. P. Kadanoff. Built upon sand: Theoretical ideas inspired by granular flows.

[123] R. Khosropour, J. Zirinsky, H. K. Pak, and R. P. Behringer. Convection and size segregation in a couette flow of granular material. *Phys. Rev. E*, 56(4):4467–4473, 1997.

[124] J. B. Knight. External boundaries and internal shear bands in granular conveciton. *Phys. Rev. E*, 55(5):6016–6023, 1997.

[125] J. B. Knight, E. E. Ehrichs, V. Kuperman, J. K. Flint, H. M. Jaeger, and S. R. Nagel. Experimental study of granular convection. *Phys. Rev. E*, 54(5):5726–5738, 1996.

[126] J. B. Knight, C. G. Fandrich, C. N. Lau, H. M. Jaeger, and S. R. Nagel. Density relaxation in a vibrated granular material. *Phys. Rev. E*, 51(5):3957–3962, 1995.

[127] J. B. Knight, H. M. Jaeger, and S. R. Nagel. Vibration-induced size separation in granular media: The convection connection. *Phys. Rev. Lett.*, 70(24):3728–3731, 1993.

[128] T. M. Knowlton, J. W. Carson, G. E. Klinzing, and W.-C. Yang. The importance of storage, transfer, and collection. *Chem. Eng. Prog.*, 90:44–54, 1994.

[129] M. Krook and T. T. Wu. Formation of maxwellian tails. *Phys. Rev. Lett.*, 36:1107–1109, 1976.

[130] R. Kubo, M. Toda, and N. Hashitune. *Statistical Physics II: nonequilibrium statistical mechanics*. Springer-Verlag, Berlin, 1978.

[131] A. Kudrolli and J. P. Gollub. Studies of cluster formation due to collisions in granular material. In *Powders & Grains 97*, page 535, Rotterdam, 1997. Balkema.

[132] A. Kudrolli and J. Henry. Non-gaussian velocity distributions in excited granular matter in the absence of clustering. *Phys. Rev. E*, 62(2):R1489–R1492, 2000.

[133] A. Kudrolli, M. Wolpert, and J. P. Gollub. Cluster formation due to collisions in granular material. *Phys. Rev. Lett.*, 78(7):1383–1386, 1997.

[134] V. Kumaran. Temperature of a granular material "fluidized" by external vibrations. *Phys. Rev. E*, 57(5):5660–5664, 1998.

[135] V. Kuperman, E. E. Ehrichs, H. M. Jaeger, and G. S. Karczmar. A new technique for differentiating between diffusion and flow in granular media using magnetic resonance imaging. *Rev. Sci. Instrum.*, 66(8):4350–4355, 1995.

[136] L. Landau and E. M. Lifschitz. *Theory of elasticity*. MIR, Moscow, 1967.

[137] L. Landau and E. M. Lifschitz. *Physique théorique - Mécanique des fluides*. MIR, Moscow, 1971.

[138] C. Liu. Spatial patterns of sound propagation in sand. *Phys. Rev. B*, 50, 1994.

[139] C. Liu and S. R. Nagel. Sound in sand. *Phys. Rev. Lett.*, 68(15):2301–2304, 1992.

[140] C. Liu and S. R. Nagel. Sound in a granular material: Disorder and nonlinearity. *Phys. Rev. B*, 48:15646, 1993.

[141] C. Liu, S. R. Nagel, D. A. Schecter, S. N. Coppersmith, S. Majumdar, O. Narayan, and T. A. Witten. Force fluctuations in bead packs. *Science*, 269:513, 1995.

[142] J. Loschmidt. Über den Zustand des Wärmegleichgewichtes eines Systems von Körpern mit Rücksicht auf die Schwerkraft". *Wien. Ber.*, 73:128, 1876.

[143] W. Losert, L. Bocquet, T. C. Lubensky, and J. P. Gollub. Particle dynamics in sheared granular matter. *Phys. Rev. Lett.*, 85:1428, 2000.

[144] W. Losert, D. G. W. Cooper, J. Delour, A. Kudrolli, and J. P. Gollub. Velocity statistics in excited granular media. *Chaos*, 9:682, 1999.

[145] W. Losert, J.-C. Géminard, S. Nasuno, and J. Gollub. Mechanisms for slow strengthening in granular materials. *Phys. Rev. E*, 61:4060, 2000.

[146] S. Luding, E. Clément, A. Blumen, J. Rajchenbach, and J. Duran. Anomalous energy dissipation in molecular dynamics simulations of grains: The "detachment effect". *Phys. Rev. E*, 50:4113, 1994.

[147] S. Luding, E. Clément, A. Blumen, J. Rajchenbach, and J. Duran. Studies of columns of beads under external vibrations. *Phys. Rev. E*, 49(2):1634, 1994.

[148] S. Luding, M. Huthmann, S. McNamara, and A. Zippelius. Homogeneous cooling of rough dissipative particles: Theory and simulations. *Phys. Rev. E*, 58:3416–3425, 1998.

[149] S. Luding and O. Strauß. The equation of state of polydisperse granular gases. In T. Pöschel and S. Luding, editors, *Granular Gases*, Berlin, 2000. Springer-Verlag.

[150] C. K. K. Lun. Kinetic theory for granular flow of dense, slightly inelastic, slightly rough spheres. *J. Fluid Mech.*, 233:539–559, 1991.

[151] C. K. K. Lun and S. B. Savage. A simple kinetic theory for granular flow of rough, inelastic, spherical particles. *J. Appl. Mech.*, 54:47, 1987.

[152] C. K. K. Lun, S. B. Savage, D. J. Jeffrey, , and N. Chepurniy. Kinetic theories for granular flow: inelastic particles in couette flow and slightly inelastic particles in a general flowfield. *J. Fluid. Mech.*, 140:223–256, 1984.

[153] U. M. B. Marconi, M. Conti, and A. Vulpiani. Motion of a granular particle on a rough line. *Europhysics Letters*, 51:685, 2000.

[154] U. M. B. Marconi, A. Petri, and A. Vulpiani. Janssen's law and stress fluctuations in confined dry granular materials. *Physica A*, 280:279–288, 2000.

[155] R. Mazighi, B. Bernu, and F. Delyon. Steady state of a column of shaked inelastic spheres. *Phys. Rev. E*, 50:4551, 1994.

[156] S. McNamara and S. Luding. Energy nonequipartition in systems of inelastic, rough spheres. *Phys. Rev. E*, 58:2247–2250, 1998.

[157] S. McNamara and W. R. Young. Inelastic collapse and clumping in a one-dimensional granular medium. *Phys. Fluids A*, 4(3):496, 1992.

[158] S. McNamara and W. R. Young. Kinetics of a one-dimensional granular medium in the quasielastic limit. *Phys. Fluids A*, 5(1):34, 1993.

[159] S. McNamara and W. R. Young. Inelastic collapse in two dimensions. *Phys. Rev. E*, 50(1):R28–R31, 1994.

[160] A. Mehta and S. F. Edwards. Statistical mechanics of powder mixtures. *Physica A*, 157:1091, 1989.

[161] F. Melo, P. B. Umbanhowar, and H. L. Swinney. Transition to parametric wave patterns in a vertically oscillated granular layer. *Phys. Rev. Lett.*, 72(1):172–175, 1994.

[162] F. Melo, P. B. Umbanhowar, and H. L. Swinney. Hexagons, kinks, and disorder in oscillated granular layers. *Phys. Rev. Lett.*, 75(21):3838–3841, 1995.

[163] T. H. Metcalf, J. B. Knight, and H. M. Jaeger. Standing wave patterns in shallow beds of vibrated granular material. *Physica A*, 236:202–210, 1997.

[164] M. Mézard, G. Parisi, and M. Virasoro. *Spin glass theory and beyond*. World Scientific, Singapore, 1987.

[165] J. M. Montanero and A. Santos. Monte Carlo simulation method for the Enskog equation. *Phys. Rev. E*, 54:438–444, 1996.

[166] J. M. Montanero and A. Santos. Simulation of the Enskog equation 'à la Bird'. *Phys. Fluids*, 8:2057–2060, 1997.

[167] D. M. Mueth, G. F. Debregeas, G. S. Karczmar, P. J. Eng, S. R. Nagel, and H. M. Jaeger. Signatures of granular microstructure in dense shear flows. *Nature*, 406:385, 2000.

[168] D. M. Mueth, H. M. Jaeger, and S. R. Nagel. Force distribution in a granular medium. *Phys. Rev. E.*, 57(3):3164–3169, 1998.

[169] S. R. Nagel. Instabilities in a sandpile. *Rev. of Mod. Phys.*, 64(1):321, 1992.

[170] M. Nicodemi and A. Coniglio. Aging and multiscaling in out of equilibrium dynamical processes in granular media. *Phys. Rev. Lett.*, 82:916–919, 1999.

[171] S. Ogawa. Multitemperature theory of granular materials. In S. C. Cowin and M. Satake, editors, *Proc. of US-Japan Symp. on Continuum Mechanics and Statistical Approaches to the Mechanics of Granular Media*, page 208, Fukyu-kai, 1978. Gakujutsu Bunken.

[172] J. S. Olafsen and J. S. Urbach. Clustering, order and collapse in a driven granular monolayer. *Phys. Rev. Lett.*, 81:4369, 1998.

[173] J. S. Olafsen and J. S. Urbach. Velocity distributions and density fluctuations in a 2d granular gas. *Phys. Rev. E*, 60:R2468, 1999.

[174] G. Y. Onoda and E. G. Liniger. Random loose packings of uniform spheres and the dilatancy onset. *Phys. Rev. Lett.*, 64(22):2727–2730, 1990.

[175] J. A. G. Orza, R. Brito, and M. H. Ernst. Asymptotic energy decay in inelastic fluids. Available only on cond-mat/0002383, 2000.

[176] J. A. G. Orza, R. Brito, T. P. C. van Noije, and M. H. Ernst. Patterns and long range correlations in idealized granular flows. *Int. J. of Mod. Phys. C*, 8:953, 1997.

[177] J. M. Ottino and D. V. Khakhar. Mixing and segregation of granular materials. *Annu. Rev. Fluid Mech.*, 32:55–91, 2000.

[178] I. Pagonabarraga, E. Trizac, T. P. C. van Noije, and M. H. Ernst. Randomly driven granular fluids: collisional statistics and short scale structure. 2001. cond-mat/0107570.

[179] H. Poincaré. Sur le problème des trois corps et les équation de la dynamique. *Acta Mathematica*, 13:1–270, 1890.

[180] H. Poincaré. Le mécanisme et l'expérience. *Revue de Metaphysique et de Morale*, 1:534–537, 1893.

[181] T. Pöschel. Granular material flowing down an inclined chute: A molecular dynamics simulation. *J. Phys. II France*, 3:27, 1993.

[182] T. Pöschel and S. Luding. *Granular Gases*. Springer Verlag, Berlin, 2000.

[183] A. Puglisi, V. Loreto, U. M. B. Marconi, A. Petri, and A. Vulpiani. Clustering and non-gaussian behavior in granular matter. *Phys. Rev. Lett.*, 81:3848, 1998.

[184] A. Puglisi, V. Loreto, U. M. B. Marconi, and A. Vulpiani. A kinetic approach to granular gases. *Phys. Rev. E*, 59:5582–5595, 1999.

[185] M. Pulvirenti, W. Wagner, and M. B. Zavelani. Convergence of particle schemes for the boltzmann equation. *Eur. J. Mech. B/Fluids*, 3:339–351, 1994.

[186] E. Rericha, C. Bizon, M. Shattuck, and H. L. Swinney. Shocks in supersonic sand. cond-mat/0104474.

[187] O. Reynolds. On the dilatancy of media composed of rigid particles in contact. *Philos. Mag. Ser. 5*, 50-20:469, 1885.

[188] K. Ridgway and R. Rupp. Flow of granular material down chutes. *Chem. Proc. Eng.*, 51:82, 1970.

[189] F. Rouyer and N. Menon. Velocity fluctuations in a homogeneous 2d granular gas in steady state. *Phys. Rev. Lett.*, 85:3676–3679, 2000.

[190] A. Samadani and A. Kudrolli. Segregation transitions in wet granular matter. *Phys. Rev. Lett.*, 85:5102–5105, 2000.

[191] A. Samadani, A. Pradhan, and A. Kudrolli. Size segregation of granular matter in silo discharges. *Phys. Rev. E*, 60(6):7203–7209, 1999.

[192] S. B. Savage. Gravity flow of cohesionless granular materials in chutes and channels. *J. Fluid Mech.*, 92:53, 1979.

[193] S. B. Savage. The mechanics of rapid granular flows. *Adv. Appl. Mech.*, 24:289, 1984.

[194] S. B. Savage and D. J. Jeffrey. The stress tensor in a granular flow at high shear rates. *J. Fluid. Mech.*, 110:255, 1981.

[195] S. B. Savage and M. Sayed. Stresses developed by dry cohesionless granular materials sheared in an annular shear cell. *J. Fluid Mech.*, 142:391–430, 1984.

[196] J. Schäfer, S. Dippel, and D. E. Wolf. Force schemes in simulations of granular materials. *J. Phys. I France*, 6:5–20, 1996.

[197] N. Sela and I. Goldhirsch. Hydrodynamics of a one-dimensional granular medium. *Phys. Fluids*, 7(3):507–525, 1995.

[198] N. Sela and I. Goldhirsch. Hydrodynamic equations for rapid flows of smooth inelastic spheres, to Burnett order. *J. Fluid Mech.*, 361:41–74, 1998.

[199] S. F. Shandarin and Y. B. Zeldovich. The large-scale structure of the universe: Turbulence, intermittency, structures in a self-gravitating medium.

[200] D. Sherrington and S. Kirkpatrick. Solvable model of a spin glass. *Phys. Rev. Lett.*, 35:1792–1796, 1975.

[201] D. Sornette, A. Johansen, and I. Dornic. *J. Phys. I (France)*, 5:325, 1995.

[202] R. Soto and M. Mareschal. Statistical mechanics of fluidized granular media: Short-range veocity correlations. *Phys. Rev. E*, 63:041303, 2001.

[203] R. Soto, M. Mareschal, and D. Risso. Departure from Fourier's law for fluidized granular media. *Phys. Rev Lett.*, 83(24):5003–5006, 1999.

[204] P. Sunthar and V. Kumaran. Temperature scaling in a dense vibrofluidized granular material. *Phys. Rev. E*, 60(5):1951–1956, 1999.

[205] M. R. Swift, M. Boamfa, S. J. Cornell, and A. Maritan. Scale invariant correlations in a driven dissipative gas. *Phys. Rev. Lett.*, 80:4410–4413, 1998.

[206] C. Tang and P. Bak. Critical exponents and scaling relations for self-organized critical phenomena. *Phys. Rev. Lett.*, 60(23):2347–2350, 1988.

[207] W. Thomson. The kinetic thoery of the dissipation of energy. *Proc. Royal Soc. Edinburgh*, 8:325–334, 1874.

[208] S. Ulam. *Adv.Appl.Math.*, 1:7, 1980.

[209] P. B. Umbanhowar, F. Melo, and H. L. Swinney. Localized excitations in a vertically vibrated granular layer. *Nature*, 382:793–796, 1996.

[210] T. P. C. van Noije and M. H. Ernst. Ring kinetic theory for an idealized granular gas. *Physica A*, 251:266–283, 1998.

[211] T. P. C. van Noije and M. H. Ernst. Velocity distributions in homogeneously cooling and heated granular fluids. *Granular Matter*, 1(2):57–64, 1998.

[212] T. P. C. van Noije and M. H. Ernst. Cahn-Hilliard theory for unstable granular flows. *Phys. Rev. E*, 61:1765, 2000.

[213] T. P. C. van Noije, M. H. Ernst, and R. Brito. Spatial correlations in compressible granular flows. *Phys. Rev. E*, 57:R4891, 1998.

[214] T. P. C. van Noije, M. H. Ernst, R. Brito, and J. A. G. Orza. Mesoscopic theory of granular fluids. *Phys. Rev. Lett.*, 79:411, 1997.

[215] T. P. C. van Noije, M. H. Ernst, E. Trizac, and I. Pagonabarraga. Randomly driven granular fluids: large scale structures. *Phys. Rev. E*, 59:4326–4341, 1999.

[216] A. Vespignani and S. Zapperi. Order parameter and scaling fields in self-organized criticality. *Phys. Rev. Lett.*, 78:4793–4796, 1997.

[217] J. Šmid and J. Novosad. Pressure distribution under heaped bulk solids. *I. Chem. E. Symposium Series*, 63:D3/V/1–12, 1981.

[218] W. Wagner. A convergence proof for bird's direct simulation monte carlo method for the boltzmann equation. *J. Stat. Phys.*, 66, 1992.

[219] J. Wakou, R. Brito, and M. H. Ernst. Towards a Landau-Ginzburg-type Theory for Granular Fluids. cond-mat/0103086.

[220] O. R. Walton and R. L. Braun. Stress calculations for assemblies of inelastic spheres in uniform shear. *Acta Mechanica*, 63:73, 1986.

[221] O. R. Walton and R. L. Braun. Viscosity, granular-temperature, and stress calculations for shearing assemblies of inelastic, frictional disks. *Journal of Rheology*, 30(5):949–980, 1986.

[222] S. Warr and J. M. Huntley. Energy input and scaling laws for a single particle vibrating in one dimension. *Phys. Rev. E*, 52(5):5596–5601, 1995.

[223] S. Warr, J. M. Huntley, and G. T. H. Jacques. Fluidization of a two-dimensional granular system: Experimental study and scaling behavior. *Phys. Rev. E*, 52(5):5583–5595, 1995.

[224] S. Warr, G. T. H. Jacques, and J. M. Huntley. Tracking the translational and rotational motion of granular particles: use of high-speed photography and image processing. *Powder Technol.*, 81:41–56, 1994.

[225] R. D. Wildman, J. M. Huntley, and J.-P. Hansen. Experimental studies of vibro-fluidised granular beds. In T. Pöschel and S. Luding, editors, *Granular Gases*, volume 564 of *Lectures Notes in Physics*, Berlin Heidelberg, 2001. Springer-Verlag.

[226] D. R. M. Williams and F. C. MacKintosh. Driven granular media in one dimension: correlations and equations of state. *Phys. Rev. E*, 54(1):R9–R12, 1996.

[227] E. Zermelo. Über einen Satz der Dynamik und die mechanische Warmetheorie. *Annalen der Physik*, 54:485–494, 1896.

[228] T. Zhou and L. P. Kadanoff. Inelastic collapse of three particles. *Phys. Rev. E*, 54:623, 1996.

Credits for pictures

Some of the pictures used in the first, second and fifth chapters have been taken from some on-line resources and published articles. We have not asked for authorization to the authors, as this work is not meant to be published or sold. However we cite here their sources:

- The picture in the title page of Chapter 1 comes from the web site of Bob Behringer
  `http://www.phy.duke.edu/~bob/`
- Fig. 1.1 on page 4 comes from the web site of Bob Behringer
  `http://www.phy.duke.edu/~bob/`
- Fig. 1.2 on page 5 comes from the web site of the Chicago Group
  `http://arnold.uchicago.edu/~jaeger/granular2/`
- Fig. 1.3 on page 7 comes from the article of Knight et al. [126]
- Fig. 1.4 on page 7 comes from the web site of Vittorio Loreto
  `http://pil.phys.uniroma1.it/~loreto/science2.html`
- Fig. 1.5 on page 9 comes from the Nature website
  `http://www.nature.com/nature/debates/earthquake/equake_5.html`
- Fig. 1.6 on page 9 comes from the article of Nagel [169]
- Fig. 1.7 on page 11 comes from the web site of Bob Behringer
  `http://www.phy.duke.edu/~bob/`
- Fig. 1.8 on page 13 comes from the page of Arshad Kudrolli
  `http://physics.clarku.edu/~akudrolli/silo.html`
- Fig. 1.9 on page 14 comes from the page of Arshad Kudrolli
  `http://physics.clarku.edu/~akudrolli/nls.html`
- Fig. 1.10 on page 15 comes from the web site of the Chicago Group
  `http://arnold.uchicago.edu/~jaeger/granular2/`
- Fig. 1.11 on page 16 comes from the web site of Paul B. Umbanhowar
  `http://www.aps.org/mar96/vpr/Q5.02.html`
- Fig. 1.12 on page 16 comes from the web site of Paul B. Umbanhowar
  `http://www.aps.org/mar96/vpr/Q5.02.html`
- Fig. 2.3 on page 59 comes from the web site of the Chicago Group
  `http://arnold.uchicago.edu/~jaeger/granular2/`
- Fig. 2.4 on page 59 comes from the web site of the Chicago Group
  `http://arnold.uchicago.edu/~jaeger/granular2/`
- Fig. 5.1 on page 122 comes from the article of Orza et al. [176].

A brief note on the opening citation

The phrase "In girum imus nocte et consumimur igni" is a fascinating latin phrase whose origin is not clearly known. It means "We go making circles in the night and are consumed by fire". It is a palindrome: in fact it is equal if read from the end to the beginning. It has been used by Guy Debord as a title for one of his movies. Guy Debord (1931-1994) is the author of *La société du Spectacle* (1967). He has been a theorist of total criticism. He has criticized modern urbanization, inventing psycho-geography and the theory of *derive* (i.e. "inspired random walk"). He has criticized art and all its conventions conceiving the *détournement* (i.e. free use of everybody's art to create new art, with the demolition of the concept of author and that of intellectual property, let's say "open art" well before "open source"...). He has criticized cinema, making some movies (his cinematographic corpus amounts to seven works, almost all shorts) composed by *collages* of pieces of other movies, photographies, and his own melancholic shootings, with his voice as the only comment, expressing his own political, artistic and philosophical ideas of total destructuration. He has criticized whole life at every level for its passive spectacularization that can absorb and make inoffensive any form of revolution, founding the movement of Situationism. In 1953 he has written on a wall of rue de Sein, in Paris, the phrase "Ne travaillez jamais", that is "Never work". He has committed suicide on the 30h of November, 1994.

What has to do this phrase (and Guy Debord) with this thesis? It is a habit that physicists, feeling in debt with literature and art in general, open their works with duct citations that have "something" to do with their research. Of course someone can find that this phrase contains the principles of granular systems: there is movement and dissipation (someone else could even assert that "circularity" has something to do with vortices). I prefer to think that this citation has *nothing* to do with this thesis.